

Physiologische Konsequenzen eines
gestörten Ceramid Stoffwechsels durch
Aktivitätsveränderungen von
Ceramidsynthase 3 und saurer
Ceramidase

Dissertation
zur Erlangung des Grades
"Doktor der Naturwissenschaften"
im Promotionsfach analytische Chemie
am Fachbereich Chemie, Pharmazie und Geowissenschaften
der Johannes Gutenberg-Universität
in Mainz

Vorgelegt von
Aline Bayerle
Geboren in Mainz, 30. Juni 1985
Heidelberg, den 20.12.14

Mündliche Prüfung: 13.02.2015

Gutachter:

Prof. Dr. XX

Prof. Dr. XX

Prüfungskomitee: Prof. Dr. XX, Prof. Dr. XX

Die vorliegende Doktorarbeit wurde vom Februar 2011 bis zum Dezember 2014 am Deutschen Krebsforschungszentrum in der Abteilung Zelluläre und Molekulare Pathologie und Pathobiochemie, sowie am Institut für Anorganische und Analytische Chemie der Johannes Gutenberg-Universität Mainz, unter der Betreuung von Prof. Dr. XX und Prof. Dr. XX angefertigt.

DFG Förderung **SA 1721/2-1**

D77 Dissertation der Universität Mainz

Physiological consequences of a
disturbed ceramide metabolism due to
altered activities of ceramide synthase 3
and acidic ceramidase

Dissertation
for the degree of
„Doctor of natural sciences”
submitted to the
Faculty of Chemistry, Pharmacy and Geosciences,
of the Johannes Gutenberg-University of Mainz, Germany

Presented by
Aline Bayerle
born in Mainz, 30th of June 1985
Heidelberg, the 20th of December 2014

Zusammenfassung

Sphingolipide (SL) zeigen eine große strukturelle Vielfalt auf und erzeugen dadurch spezifische Expressionsmuster in Abhängigkeit von Zelltyp und Grad der Zelldifferenzierung. Ultra langkettige (ULC)-SL, die sich durch N-Acylsubstituenten mit Kettenlängen von 26 und mehr C-Atomen auszeichnen, sind vor allem in differenzierenden Keratinozyten der Epidermis und reifenden männlichen Keimzellen der Testis zu finden. In Säugetieren sind die Ceramidsynthasen (CerS1–6) für die Bildung von (Dihydro)Ceramiden verantwortlich. CerS3-Defizienz in Mäusen führte zu einem kompletten Verlust der Ceramide mit einer Kettenlänge von mehr als 24 Kohlenstoffatomen, einschließlich aller ω -Hydroxy-ULC Ceramide. Dies führt zu einer starken Beeinträchtigung der Wasserpermeabilitätsbarriere (WPB) der Epidermis und letztlich zum neonatalen Tod. Die in ihrer Funktion kompromittierte Haut der CerS3 Mutanten erleichterte mikrobiologisches Wachstum von Pathogenen auf der Haut (*Candida albicans*) und anschließende Kolonisierung in tiefere Schichten. Daher ist eine fundierte Kenntnis des Ceramid Stoffwechsels für unser Verständnis zur Pathophysiologie der Haut (z.B. bei Ichthyosis, atopischer Dermatitis oder Psoriasis) unabdingbar und ist Voraussetzung für gezielte Therapieansätze.

In dieser Arbeit wurde massenspektrometrisch eine Methode zur Quantifizierung von Sphingosin, welches ein wichtiges Abbauprodukt von Ceramiden ist, entwickelt. Sphingosin wurde als antimikrobieller Wirkstoff identifiziert, indem es das Wachstum von Pathogenen auf der Hautoberfläche inhibiert, jedoch konnte seinem Folgeprodukt Sphingosin 1-phosphat, keine pro-chemotaktische Wirkung auf dendritische Zellen nachgewiesen werden. Ebenso wurde eine neue Klasse von Ceramiden, die 1-O-Acylceramide, entdeckt. Ich konnte zeigen, dass die CerS3, die neutrale Glucosylceramidase und die Glycosylceramide Synthase die homeostatischen Konzentrationen der 1-O-Acylceramide beeinflussen. Enzyme der Diacylglycerol-1-O-acyltransferase Familie könnten diese Cer-Subgruppe bilden. In ersten Untersuchungen konnte die Verantwortung aber keinem einzelnen Enzym zugewiesen werden. Untersuchungen des Farber-Krankheit-Mausmodells, in welchem Ceramide intrazellulär gespeichert werden, weisen weitere Gewebe, möglicherweise Makrophagen, als 1-O-AcylCer-Syntheseorte auf. Zusammenfassend zeigte ich den Einfluss des Ceramid Metabolismus auf die Immun-Barriere auf und konnte zum Verständnis eines bisher nicht völlig verstandenen SL Stoffwechselweges durch Untersuchungen an CerS3-defizienten Mäusen und Farber-Mäusen mit limitierter saurer Ceramidase Aktivität beitragen.

Summary

Sphingolipids (SLs) exhibit a broad structural diversity and generate unique expression patterns according to cell type and degree of cell differentiation. Ultra long chain (ULC)-SLs possess an N-acyl moiety of 26 or more C-atoms and are primarily expressed in epidermal keratinocytes and testicular adluminal male germ cells. In mammals, the ceramide synthases (CerS 1-6) are responsible for fatty acid incorporation into SLs yielding in (dihydro)ceramides. One family member, the CerS3, is fundamental for the synthesis of ULC-SLs and a deficiency in mice resulted in a complete loss of epidermal ULC-SLs, including all ω -hydroxy-ULC-ceramides (Cers). This led to severe impairment of the epidermal water permeability barrier (WPB) and to premature neonatal death. The damaged skin integrity of mutant mice facilitated growth and invasion of pathogens shown by colonization of *Candida albicans* on cultured skin biopsies. This highlights that a detailed knowledge of ceramide metabolism is necessary for the understanding of skin pathophysiology (e.g. ichthyosis, atopic dermatitis or psoriasis) and hence is prerequisite for targeted therapy of skin disorders.

In this work a mass spectrometric method for quantification of sphingosine (So), which is an important degradation product of Cers, was successfully established. So was identified as an antimicrobial agent that reduces growth of pathogens on the skin surface, but its downstream product sphingosine 1-phosphate (S1P) could not be verified as pro-chemoattractant for dendritic cells. Also a novel class of ceramides, the 1-O-acylceramides, was discovered. Due to highly hydrophobic properties they could contribute to a functional WPB. I showed that CerS3, neutral glucosylceramidase, glycosylceramide synthase and diacylglycerol acyltransferase 2 (DGAT2) influence the homeostatic level of 1-O-acylceramides. Members of the DGAT2 family could be able to synthesize this Cer subgroup, but initial analysis did not point to a single essential member. The investigation of Farber mutant mice, which accumulate ceramides intracellularly, suggested additional tissues, eventually macrophages, as further site of 1-O-acylceramide production, which could also influence the course of the disease. Finally CerS3 could be localized in the stratum granulosum of the skin and stage specifically in testicular germ cells. Hence, like in epidermis where the lamellar bodies are required for CerS3-derived lipid transport, also in testis special organellar structures may direct the corresponding SLs. In summary, I demonstrated the contribution of ceramide metabolism to an intact immune barrier and shed light on the enzymatic regulations of a yet not well recognized mammalian SL pathway through the investigations of CerS3-deficient mice and a Farber disease mouse model with limited acidic ceramidase activity.

List of Abbreviations

1-O-AcylCers	1-O-acylceramides
ACAT	Acyl CoA acyl transferase
ACD	Allergic contact dermatitis
ACDase	Acid ceramidase
AD	Atopic dermatitis
AJCs	Apical junction complexes
AJs	Adherens junctions
APCs	Antigen presenting cells
ARCI	Autosomal recessive congenital ichthyoses
AS	α -hydroxy FAs
BTB	Blood-testis barrier
CB	Chromatoid body
CDs	Corneodesmosomes
CE	cornified envelope
CerS	Ceramide synthase
Cers	Ceramides
CFU	colony forming units
CHS	Contact hypersensitivity
CI	Congenital ichthyosis
CLE	cornified lipid envelope
CoA	Coenzyme A
CSHTM	Charged Surface Hybrid
DAG	Diacylglycerol
DCs	Dendritic cells
DES1	Desaturase enzyme
Dga1p	Yeast Diacylglycerol O-acyltransferase
DGAT2	Diacylglycerol O-acyltransferase 2
ECM	Extracellular matrix
ELL	Extracellular lipid lamellae
Elovl	elongation of very long chain fatty acids
ER	Endoplasmic reticulum
ESI	Electrospray ionization
eST	Elongated spermatids
EX	Prenatal dayX
FA	Fatty acid
FD	Farber disease
FGSL	Fucosylated GSL
Gb2a	nGlcCerase
GPCRs	G-protein coupled receptors
GSLs	Glycosohingolipids
HI	Harlequin ichthyosis
HILIC	Hydrophilic interaction chromatography
Ht	Heterozygous

Ko	Knock out
LBs	Lamellar bodies
LCs	Langerhans cell
LC	Long chain
LCAT	Lecithin cholesterol acyl transferase
LI2	Lamellar ichthyosis type II
Lin	Linoleic acid
LOD	Limit of detection
LOQ	Limit of quantification
LPLA 2	Group XV lysosomal phospholipase A 2
Lro1p	Phospholipid:diacylglycerol acyltransferase
LSDs	Lysosomal storage disorders
MBOAT	Membrane-bound O-acyltransferases
MRM	Multiple reaction monitoring
nGSL	Neutral GSLs
NS	Nonhydroxylated FAs
OS	ω -hydroxy FAs
PHS	4-hydroxysphinganine (t17:0)
PKC	Protein kinase C
PLA2	Phospholipase A2
pISC – ISC	Preleptotene and leptotene spermatocytes
pISC and ISC	preleptotene and leptotene spermatocytes
PM	Plasma membranes
POS	Protein amino acid sidechain
pSC	Pachytene SC
PX	Postnatal day X
rb	residual body
rRF	Relative response factor
rST	Round spermatids
S/N	Signal to noise ratio
S1P	Sphingosine-1-phosphate
SB	Stratum basale
SC	Stratum corneum
SG	Stratum granulosum
SLs	Sphingolipids
SM	Sphingomyelin
So	Sphingosine
SphK	Sphingosine kinases
sPLA2	Secretory phospholipase A2
SPT	Serine C-palmitoyltransferase
SRM	Selected reaction monitoring
SS	Stratum spinosum
Sza	Spermatozoa
TAGs	Triacylglycerols
TEWL	Transepidermal water loss
TJs	Tight junctions
Ugcg	UDP-glucose:ceramide glucosyltransferase

ULC	Ultra long chain
UPLC-ESI-MS/MS	Ultra performance liquid chromatography coupled-electrospray ionization-tandem mass spectrometry
VLC	Very long chain
WB	Western blot
WPB	Water permeability barrier
Wt	wild type
XRI	X-linked recessive ichthyosis
ωh	ω-hydroxy

Table of contents

Zusammenfassung	i
Summary	iii
1. Basics	1
Sphingolipids	2
Sphingolipid biosynthesis	4
2. Hypothesis and aim	7
3. Materials and Methods	8
3.1. Materials	9
Chemicals	9
Buffers and solutions	9
DNA and Protein ladders	11
Mouse lines	12
Primer	12
Antibodies	13
Cell lines and Plasmids	14
Media for cell culture	14
Kits and standards	15
Instrumentation	16
3.2. Methods	17
Animal care	17
Genotyping	18
Cloning	18
Cell culture	19
Immunohistochemistry	20
Pathogenic growth experiments	22
Western blot	23
Lipid analysis	25
Statistics	31
I. Sphingosine in antimicrobial defense of the skin	34
I.1 Introduction	35
I.1.1 Skin topology and Epidermis	35

I.1.2	Skin barrier defects.....	43
I.1.3	Antimicrobial barrier.....	45
I.2	Results	48
I.2.1	Method development for quantification of sphingoid bases	48
I.2.2	Quantification of sphingoid bases in epithelial tissue.....	61
I.2.3	Dendritic cells and immune barrier.....	66
I.2.4	Sphingosine and antimicrobial barrier	69
I.3	Discussion.....	72
II.	1-O-acylceramides	76
II.1	Introduction	77
II.1.1	1-O-acylceramides	78
II.1.2	Farber disease and the lysosomal acid ceramidase	80
II.2	Results	82
II.2.1	Epidermal 1-O-acylceramide production.....	82
II.2.2	Farber disease and the lysosomal acid ceramidase	97
II.3	Discussion.....	102
III.	CerS3 localization.....	108
III.1	Introduction	109
III.1.1	Testis	109
III.1.2	Epithelial tissue	112
III.2	Results	114
III.2.1	Localization of CerS3.....	114
III.2.2	Antibody establishment in cell culture.....	114
III.2.3	Localization of CerS3 in skin.....	116
III.2.4	Localization of CerS3 in testis	120
III.3	Discussion.....	125
IV.	Conclusions.....	129
V.	References.....	133
VI.	Appendix.....	152

1. Basics

Sphingolipids

Sphingolipids (SLs) are the major components of cell membranes and were originally discovered in 1884 as natural constituents of the brain (Thudichum, 1884). In contrast to phosphoglycerides that have glycerine as core structure, SLs derive from the unsaturated aminoalcohol sphingosine. As amphiphatic molecules with a polar and unpolar side, SLs and their derivatives the glycosphingolipids (GSLs) organize into a lipid bilayer and form the main component of plasma membranes. SLs and their derivatives play a role in many biological processes, such as in cell signaling, proliferation and differentiation. Biochemically SLs can be divided into three main types: Ceramides (Cers), glycosylceramides (GlcCers) and sphingomyelin (SM). Ceramide is composed of a sphingoid base and an amide-linked fatty acid (FA) moiety, whereas for GSLs or SM the hydroxyl head group is exchanged with a sugar or a phosphorylcholine group, respectively.

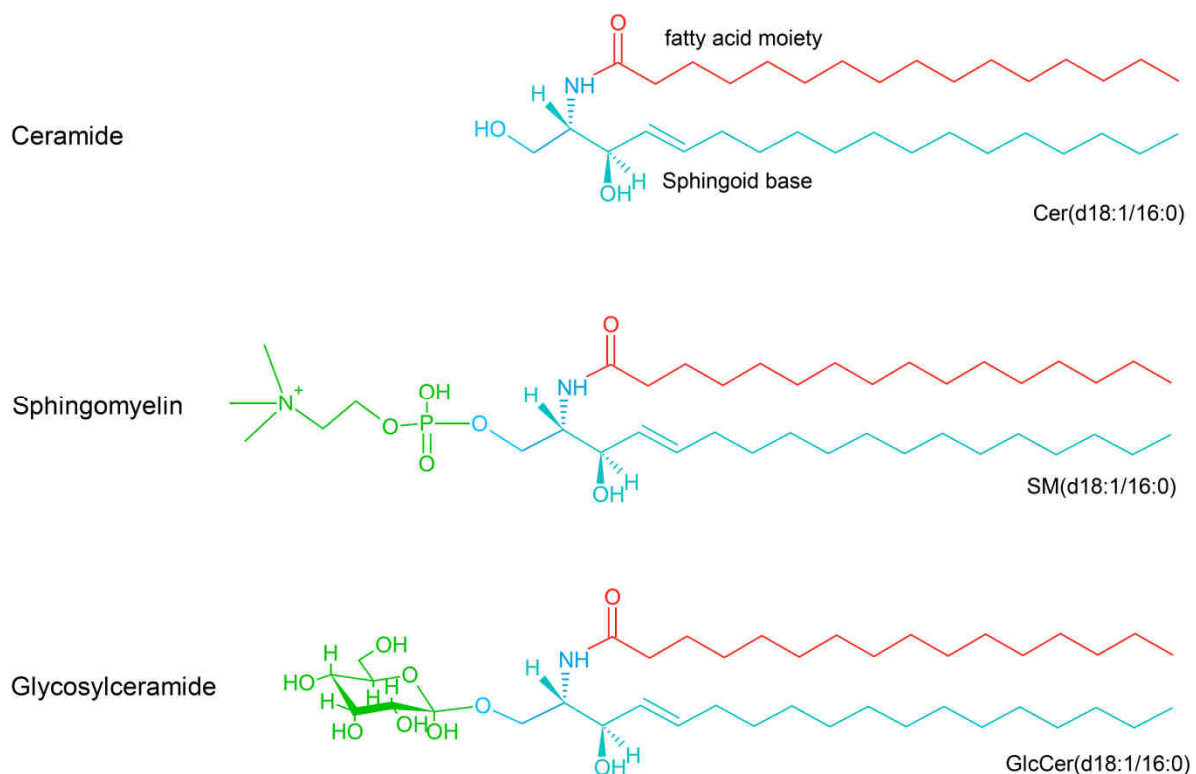


Figure 1 Structure of major sphingolipid classes. Sphingolipids are synthesized via condensation of the amine group of a sphingoid molecule with an activated fatty acid (acyl CoA). The sphingoid base shown here corresponds to sphingosine (blue; designated d18:1 in the short-hand notation). The amide-linked fatty acid at position 2 is represented by a 16:0 palmitoyl moiety (red). The substituent (green) at the sphingoid carbon 1 determines the SL class and can be the original hydroxy group (as in sphingosine), a phosphocholine moiety or a mono- or oligosaccharide group.

The amide linkage and the hydroxyl group at the Carbon atom C2 and C3 of the sphingoid base together form the amphiphatic character of SLs. For more complex SLs polarity results from the combination out of (1) the hydrophobic sphingoid base, (2) its amide-linked FA, and (3) the hydrophilic region of the head group. These three parts of SLs also create a broad structural diversity and are therefore prerequisite for their functional specialization in different tissues or cell types. The FA moiety can tissue-specifically differ in chain length and in degree of saturation and hydroxylation. FAs are mostly bound to sphingosine (4E-sphingenine, or in short-hand notation 4E-d18:1 or simply d18:1), as in the SLs in Figure 1, but also to sphinganine (4,5-dihydrosphingosine; d18:0), 4E-6-hydroxy-sphingosine (6-t18:1), to phytosphingosine (4-hydroxysphinganine; 4-t18:0) or other sphingoid bases (Kendall and Nicolaou, 2013; Pruett et al., 2008). Possible head groups are for example phosphocholine in SMs or carbohydrates in GSLs (e.g., monosaccharide in cerebroside, oligosaccharide in globosides and gangliosides) leading to thousands of different structures (Kolter et al., 2002).

Expression patterns of SLs are determined by many factors as for example the cellular differentiation state, degeneration or cell cycle and can therefore regulate different cell fates (Hakomori, 1981; Majoul et al., 2002; Muramatsu, 2000). GSLs can for example function as recognition molecules for toxins, viruses and bacteria at the outer cell surface by their complex oligosaccharide chain as binding site (Schnaar, 1991). More simple SLs such as ceramide, sphingosine (So) and sphingosine-1-phosphate (S1P), have been shown to act as bioactive molecules in multiple signaling cascades (Lahiri and Futerman, 2007). Cer works antagonistic to S1P and can induce apoptosis by elevation upon various external or internal stress signals. These signals lead to intracellular Cer synthesis and activation of enzymes such as protein kinases (e.g., janus kinase, protein kinase C (PKC)), phosphatases (e.g., ceramides activated protein phosphatase, or phospholipase A2 (PLA2), phospholipase D) (Bourbon et al., 2000; Huwiler et al., 2001; Perry and Hannun, 1998; Westwick et al., 1995).

Current lipid research is focusing on the role of SLs in inherited and acquired human diseases such as sphingolipidoses and cancer progression (Kannagi et al., 2004; Raffaghello et al., 2003). Furthermore, SLs also contribute to the development of a multitude of diseases including neurodegeneration (Grimm et al., 2005), inflammatory skin diseases (Macheleidt et al., 2002) and pathogen invasion (Arikawa et al., 2002; Bibel et al., 1992).

Sphingolipid biosynthesis

De novo SL biosynthesis takes place at the cytosolic leaflet of the endoplasmic reticulum (ER) and is initiated by the condensation of L-serine and palmitoyl-CoA (CoA = Coenzyme A) to form 3-keto-sphinganine (Figure 2) catalyzed by the enzyme complex serine C-palmitoyltransferase (SPT) (Hanada, 2003; Mizukoshi et al., 2011). The reduction of 3-keto-sphinganine yields in sphinganine (dihydro-sphingosine), which is subsequently amide-linked to a particular FA to give dihydroceramide. This step is performed by an acyl-CoA-specific ceramide synthase (CerS) (Pewzner-Jung et al., 2006). In mammals a family of six homologue enzymes is responsible for the synthesis of ceramides, the CerS1–6. Then a desaturase enzyme (DES1) introduces the 4,5-trans-double bond to result in Cer, which can later be cleaved again to give sphingosine by a ceramidase. Sphingosine in turn, can be either derivatized to S1P, recycled for Cer synthesis or it can serve as a precursor for more complex SMs or GSLs.

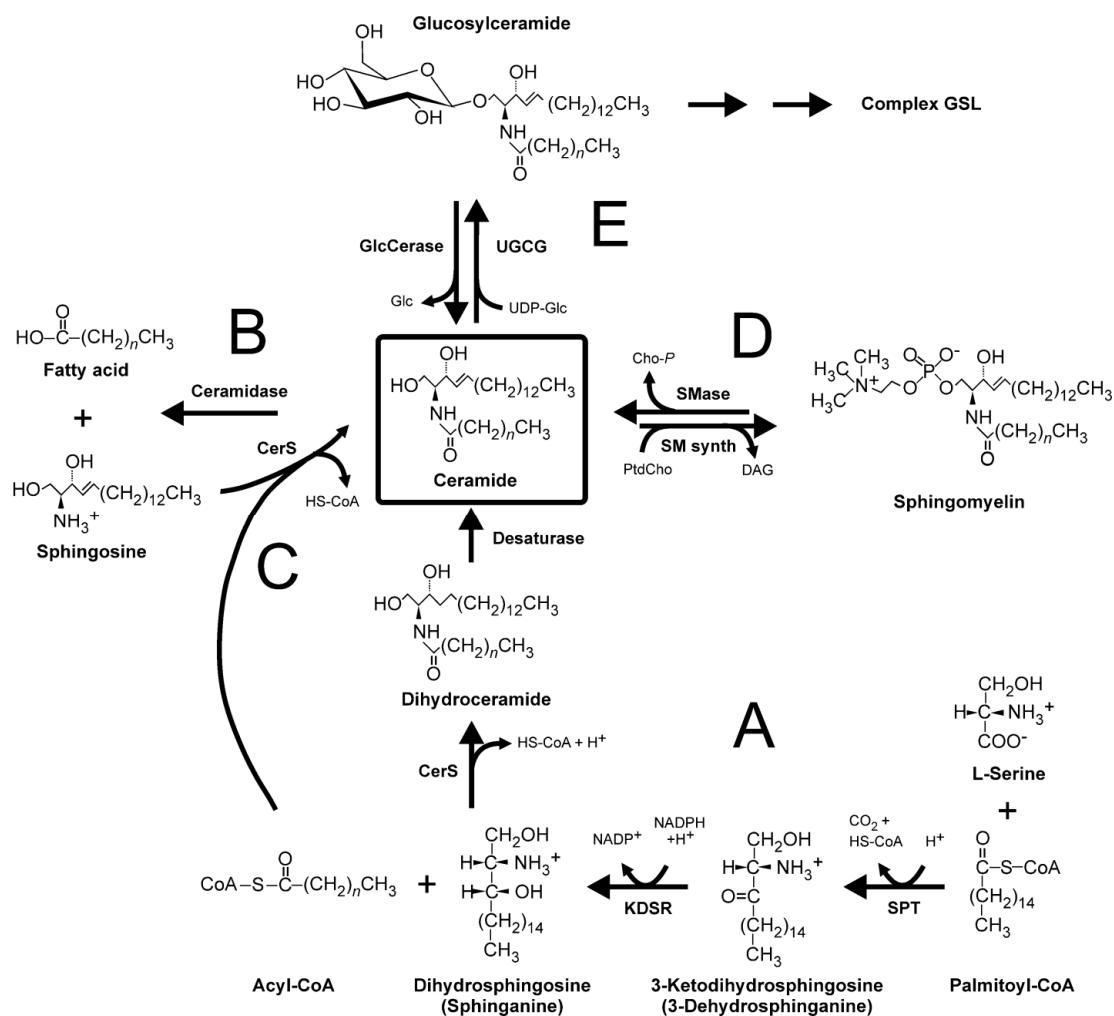


Figure 2 *De novo* ceramide synthesis, recycling and processing to higher SLs. (A) *De novo* ceramide synthesis begins with the condensation of L-serine and palmitoyl-CoA catalyzed by serine palmitoyltransferase (SPT). The product 3-keto-

dihydrosphingosine is reduced to dihydro sphingosine (sphinganine) via 3-ketodihydrosphingosine reductase (KDSR) and acylated by a ceramide synthase (CerS) to give dihydro ceramide and finally ceramide via a desaturase. Ceramide can be degraded by a ceramidase (B) to give sphingosine and a fatty acid. Sphingosine can be recycled (C) for ceramide formation in a CerS reaction. Ceramide serves as a precursor for more complex SLs such as sphingomyelin (D), glucosylceramide (E) or higher glycosphingolipids (GSLs). (from Amen, 2013)

Sphingosine recycled for Cer synthesis via the so called “salvage pathway” can be directly acylated, whereas Sphinganine can also undergo during the “*De Novo* pathway” direct acylation to form dihydroCer, which can then be further metabolized as shown in Figure 3.

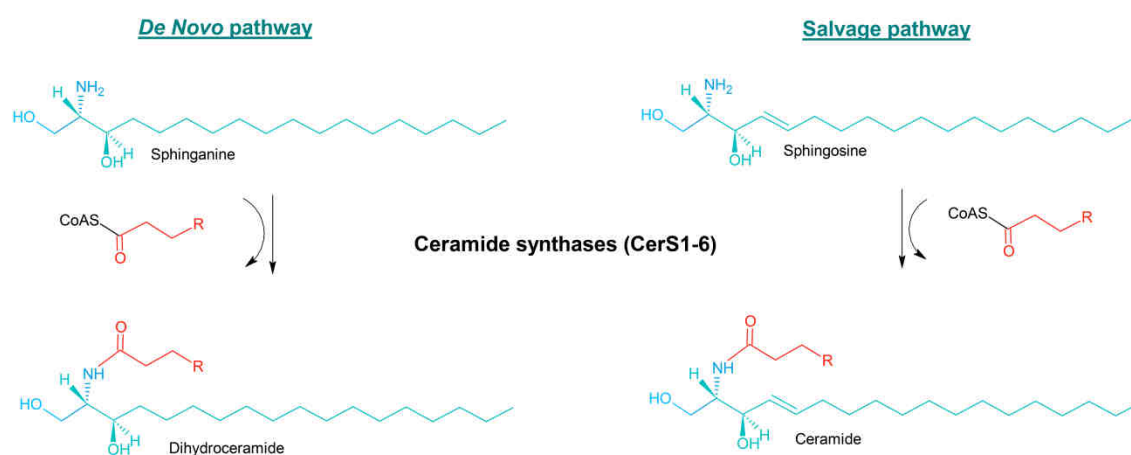


Figure 3 *De novo* and salvage (dihydro)ceramide synthesis catalyzed by the ceramide synthases. CerS facilitate the acylation of D-erythro-sphinganine derived from the *de novo* synthesis, as well as D-erythro-sphingosine from the salvage pathway to generate D-erythro-dihydro ceramide and D-erythro-ceramide, respectively.

SM synthesis takes place at the luminal side of the Golgi apparatus (Jeckel et al., 1992). This requires that Cer formed at the ER (with acyl chain-lengths of C16-C20) is moved by a ceramide transport protein to the Golgi apparatus (Hanada, 2006). Cer is converted into SM by the SM synthase within the so-called SM cycle and can also be recycled back to Cer by the action of a sphingomyelinase (Geilen et al., 1997), or in response to extracellular stimuli from plasma membrane (PM)-derived SM (e.g., TNF α , IL-1, endotoxin) (Levade et al., 1999).

For GSL synthesis, Cer is transported from the ER to the cytosolic side of the Golgi by vesicles (Jeckel et al., 1992). A key enzyme for GSL formation, the glucosylceramide synthase (UDP-glucose:ceramide glucosyltransferase (Ugcg); EC 2.4.1.80), transfers glucose from UDP-glucose to the Cer backbone (Figure 2) (Sprong et al., 1998). Addition of further monosaccharides, sulfatides or neuraminic acid molecules gives glucocerebrosides (e.g., Gb3,

Gb4), sulfatides (e.g., SM4) or gangliosides (e.g., GM1, GM3), respectively. Complex GSLs can be either transported to the PM, where they are incorporated, or they can be metabolized for other purposes (Bartke and Hannun, 2009). GSL serve for example as precursors for epidermal barrier formation, as most epidermal Cers are believed to derive from the corresponding GlcCer classes (Hamanaka et al., 2002; Uchida et al., 2000).

2. Hypothesis and aim

Keratinocytes of the epidermis synthesize and process unique SLs (glucosylceramides and ceramides with ω -hydroxylated saturated and monounsaturated ULC-FA moieties) in a not fully understood way to establish the WPB of the skin of land dwelling animals. Complex glycosphingolipids and ceramides containing ULC-PUFA moieties were first described in mature mouse testis (Sandhoff et al., 2005) and interestingly correlate with male fertility. The functional role of these non-classical testicular sphingolipids is unknown at the molecular level. However, understanding the requirements of ULC-sphingolipid biosynthesis and metabolism is a prerequisite in order to gain deeper insights into their role in cellular functions in both skin and testis. Preliminary work implicated strong expression of CerS3 in testis and skin, both being the only mammalian tissues containing ULC-sphingolipids (Sandhoff, 2010). Hence, we hypothesized that CerS3 might be essential in the synthesis of these ULC-ceramides and its derivatives and thus may contribute substantially to the pool of epidermal sphingosines. The latter had been discussed to have antimicrobial activity and could contribute to the epidermal immune barrier. Defective CerS3 thus may underlie skin barrier defects of human ichthyosis patients and limited fertility of males and may be a target for therapy.

The aims of this project were to understand the role of ceramides and ceramide metabolism during epidermal maturation and spermatogenesis in testis and to gain insights into the cellular topology of CerS3. Thus, my aim was to localize CerS3 in the skin and testis and to investigate pathways affected by the disturbed ceramide metabolism. For this purpose I focused on the examination of a mouse model with ceramide synthase deficiency (CerS3-deficient mice) and a mouse model with impaired ceramide degradation (Farber disease mouse model with reduced acid ceramidase activity), while focusing on sphingoid bases and the newly described 1-O-acylceramides. However, more related mouse models were integrated during the progress of this work. The *in vivo* data are fundamental for understanding the pathophysiology of certain cases of autosomal recessive congenital ichthyosis (ARCI) and of Farber disease.

3. Materials and Methods

3.1. Materials

Chemicals

Standard laboratory chemicals and reagents used for routine analyses in this study were purchased from Sigma-Aldrich (Deisenhofen), Merck (Darmstadt), Life Technologies (Darmstadt), Roche (Mannheim), Carl Roth (Karlsruhe), and Fluka (Neu-Ulm).

All other chemicals were obtained as indicated in the corresponding method section.

Buffers and solutions

All buffers and solutions were prepared with either *Aqua ad injectabilia* (Braun) or double distilled autoclaved water. Buffers and components are listed in the following Tables

Table 1 Buffers for genotyping and western blot

Buffers for genotyping	
TAE buffer (50x) 2 M Tris/AcOH, pH 8.0 0.1 M EDTA	Xylene cyanol loading buffer (10x) 20 mM Tris/HCl, pH 7.5 0.001% xylene cyanol (w/v) 50% glycerol (v/v)
Buffers for western blot	
Digitonin lysis buffer 1 (1x) 50 mM HEPES-NaOH buffer, pH 7.4 150mM NaCl 1x protease inhibitors mixtures ² 20µg/ ml digitonin ^{2,3}	Lämmli loading buffer¹ (4x) 250 mM Tris, pH 6.8 40% glycerol (v/v) 0.02% bromophenol blue (w/v) 8% SDS (w/v) 0.4 M DTT
Resolving gel buffer (8x) 3 M Tris-HCl, pH 8.8 0.1% SDS (w/v)	Stacking gel buffer (4x) 0.5 M Tris-HCl, pH 6.8 0.1% SDS (w/v)
Running buffer (10x) 250 mM Tris, pH 8.3 1.92 M glycine 1% SDS (w/v)	Transfer buffer (10x) 250 mM Tris, pH 8 1.92 M glycine 20% MeOH for dilution to 1x
PBS buffer (10x) 0.1 M Na ₂ HPO ₄ , pH 6.8 1.4 M NaCl 27 mM KCl	TBS-Tween® buffer (PBST) (1x) 2M Tris, pH 7.4 0.1% Tween® 20 (v/v) 80g NaCl
Ponceau red	Blocking buffer^{4,5}

0.5% Ponceau red (w/v) 1% AcOH (v/v)	1x TBST, pH 7.5 5% skimmed milk (w/v)
Naphthol blue black 0,1% Naphthol Blue black (w/v) 10% methanol (v/v) 2% acetic acid	Ripa buffer 150mM NaCl 5mM Tris 2μM EDTA 0,2% NP40 1x protease inhibitor mix 0,5 mM DTT 2,5 mM PMSF 1% SDS
Stripping buffer 2% SDS 50mM Tris-HCL pH 7 50mM DTT	

Table 2 Buffers for ICH and IF

Buffers and solutions for immunohistochemistry and immunofluorescence	
Citrate buffer (for antigen retrieval) 10 mM citric acid, 0.9 M sodium citrate, pH 6 0,05% Tween 20	TBS (for antigen retrieval) 0.01 M Tris base, pH 9.0. 15 M NaCl
PBS high salt(for washing) PBS 0,1% Tween 20	Blocking buffer PBS 5% BSA
Permeabilization buffer PBS 1x 0,1% Triton-X-100	3,5% PFA Fixative ⁵ 1x PBS, pH 7.4 3,5% paraformaldehyde

Table 3 Buffers for epidermis treatment

Buffers and solutions for epidermis treatment	
Thermolysin buffer ^{1,6} (500 µg/mL) 10 mM HEPES, pH 7.4 142 mM NaCl 6.7 mM KCl 0.43 mM NaOH 1 mM CaCl ₂	EDTA solution ⁶ 20mM EDTA in 1x PBS, pH7.4
Permeabilization buffer PBS 1x 0,5% triton-X-100	3% PFA Fixative ⁵ 1x PBS, pH 7.4 3% paraformaldehyde
Blocking buffer 5% goat serum 0,5% triton-X-100 PBS 1x	Collagen gels 4mg/ml Collagen type I in acetic acid 0,1% 10% HANKS buffered solution 10% DMEM 5M NaOH for pH adjustment

¹ Store at -20 °C.² Add freshly.³ A 10% stock solution was prepared by dissolving the powder in boiling water and keeping the solution at 95 °C for 10 min.⁵ Freshly prepared.⁶ Buffers used to separate epidermis from dermis.

DNA and Protein ladders

Type of Ladder	Range	Company
1 kb DNA ladder	506–12216 bp	Invitrogen
100 bp DNA ladder	100–2072 bp	Invitrogen
PageRuler™ plus prestained Protein ladder	10–250 kDa	Fermentas

Mouse lines

Table 4 List of mouse lines

Mouse strain	Tissue analyzed	Source
C57/BL6-N	skin, liver, kidney, blood	Charles River
CerS3-0 (d/d)	skin, esophagus, tongue	Generated by R. Jennemann
CerS3-Stra8	testis	Generated by R. Jennemann
CerS3 flox ik14	skin, esophagus, tongue	Generated by R. Jennemann
CerS2	skin	Kindly provided by K. Willecke
DGAT2	skin	Kindly provided by B. Farese
LCAT	skin	Kindly provided by M. Hoekstra
Elovl3	skin	Kindly provided by A. Jacobsson
CerS4	skin	Kindly provided by K. Willecke
Gb2a	skin	Kindly provided by D. Wachten
Scd1	skin	Jackson laboratories
PF2	skin	Jackson laboratories
Ugcg ik14	skin	Generated by R. Jennemann
Ugcg K14B	skin	Generated by R. Jennemann
LPLA2	skin	Kindly provided by J. Shayman
Asah1 ^{P361R/P361R}	brain, sciatic nerve, spleen, liver thymus, heart, kidney	Kindly provided by T. Levade

Primer

The following primer pairs were used for mouse genotyping

Table 5 List of primers

¹ Primers used for routine genotyping of CerS3^{-/-} mice and Cers3-Stra8 mice

Gene Primer	sequence	T (C°)	Product size (bp)
CerS3 – wt ¹	F 5' – ACA TAT CTC CCT TTG CCC TGA TG – 3' R 5' – ATA ATT GCA AGA GAC GGC AAT GA – 3'	58	315
CerS3 – ko ¹	F 5' – ACA TAT CTC CCT TTG CCC TGA TG – 3' R 5' – GAC AGC CCT GAA ATG TAT CAT GC – 3'	58	272
Stra8-wt	F 5' - CTA GGC CACA AGA ATT GAA AGA TCT – 3' R 5' - AGG GAC ACA GCA TTG GAG GGT GAA GGC GCA – 3'	60	324
Stra8-transgene	F 5' - GTG CAA GCT GAA CAA CAG GA – 3' F 5' - GGT GGA AAT TCT AGC ATC ATC C – 3'	60	179

Antibodies

Table 6 List of primary and secondary antibodies

Primary-Antibody Species reactivity	Gene name	Host ^a – clonality ^b	Application ^c (dilution)	Supplier	Order number
Autophagy LC3 mouse	<i>Apg8</i>	m - m	IHC – Paraffin (1:100)	Abgent ^j	AM1800a
β-Actin mouse	<i>Actb</i>	rb – p	WB (1:200)	Santa Cruz ^d	sc-1616-R
Calnexin	<i>Calr</i>				2433S
Calreticulin mouse	<i>Calr</i>	rb - p	IHC-Paraffin (1:100)	ProteinTech ^h	10292-1-AP
Cathepsin D human		Rb-		Dako	
CD45 mouse	<i>CD45- 30-F11</i>	r - m	IHC (1:25)	BD ^m	550539
CerS3 ^e mouse	<i>Lass3</i>	gp-p /rb-p	IHC (1:150), Paraffin (1:75), WB (1:100)	H. Heid ⁱ /Pick-Cell Laboratories	Custom made/C6603
CerS3 human	<i>Lass3</i>	m- p	IHC- Paraffin (1:100)	Acris ⁱ /custom made	H00204219- M02
Early endosome marker- EEA1- mouse	<i>EEA1</i>	rb - p	IHC – Paraffin (1:100)	Abcam ⁿ	ab2900
Glyceraldehyde-3- phosphatedehydroge nase- mouse	<i>Gapdh</i>	rb - p	WB (1:200)	Santa Cruz ^d	sc-25778
I-A/I-E- mouse	<i>MHCII 2G9</i>	r - m	IHC (1:25)	BD ^m	553621
lysosome marker lamp1- mouse	<i>Lamp1</i>	rb - p	IHC-Paraffin (1:100)	Abcam ⁿ	ab24170
Langerin mouse	<i>CD207</i>	rb - p	IHC (1:25)	Acris ⁱ	SP7357P
β3- tubulin mouse	<i>Tubb3</i>	m - m	IHC (1:50)	Santa Cruz ^d	Sc-80016
Samp32 mouse	<i>Samp32/Spaca1</i>	gp - p	IHC (1:100)	Acris ⁱ	BP5112
Secondary- Antibody	Species reactivity	Host ^a	Application ^c (dilution)	Supplier	Order number
IgG-HRP	Anti-guineapig	g	WB (1:2000)	Santa Cruz ^d	sc-2903
IgG-HRP	anti-rabbit	g	WB(1:2000)	Santa Cruz ^d	sc-2004
Cy5 TM	Anti-guineapig	d	IHC-Paraffin (1:300)	Dianova ^g	706-175-148
Cy2 TM	anti-rabbit	g	IHC-Paraffin (1:300)	Dianova ^g	711-225-152
Cy3 TM	Anti-guineapig	g	IHC-Paraffin (1:300)	Dianova ^g	106-165-003
Alexa488 [®]	Anti-mouse	d	IHC-Paraffin (1:300)	Molecular Pobes ^k	A21202
Alexa568 [®]	Anti-rat	g	IHC (1:750)	Molecular Pobes ^k	A11077
Alexa568 [®]	Anti-goat	d	ICC (1:300)	Molecular Pobes ^k	A11057

a g, goat; gp, guinea pig; m, mouse; rb, rabbit; r, rat, d, donkey ;b m, monoclonal; p, polyclonal.

c Cryo: cryosections; IHC: immunohistochemistry; Paraffin: paraffin sections; WB: western blot.

d Santa Cruz Biotechnology Inc., Heidelberg, Germany;

e against different peptides of CerS3 protein and in species reactivity for human and mouse

f H. Heid, Dept. of Cell Biology , DKFZ, Heidelberg, Germany

g Dianova, Hamburg, Germany; h Proteintech group, Chicago,USA;

i Acris Antibodies, Hiddenhausen, Germany; j ABGENT, San Diego, USA; k Molecular Probes, Life Technologies GmbH, Darmstadt, Germany; m BD Biosciences, Heidelberg, Germany

n Abcam plc, Cambridge, UK. ;

Cell lines and Plasmids

The following cell lines and Plasmids were used in this study:

- murine CerS3 Plasmid, with and without eGFP at the C-terminal end (pick cell Plasmid)
 Polyclonal CerS3 antibody against the mouse protein was generated by PickCell Laboratories.
 Thus, a synthetic peptide against our self-designed epitope (CGGKETEYLKNGGLGTRHLIANGQHGR) located at the C-terminus was used to immunize rabbits.

- HeLa: Human cervix carcinoma derived cell line with epithelial-like morphology.

- HeL_{am}CAT1-rtTA2-M2: Clone originated from HeLa cells stably transfected with mCAT1 (murine cationic aminoacid transporter 1), rtTA2-M2 (optimized reverse tetracycline controlled transactivator), and a truncated version of CD2 (cluster of differentiation 2). This clone was kindly provided by Prof. Dr. Walter Nickel.

- HeL_{am}CAT1-rtTA2-M2-hCerS3-eGFP: Clone originated from HeL_{am}CAT1-rtTA2-M2 stably transfected with hCerS3-eGFP.

- HeL_{am}CAT1-rtTA2-M2-mCerS3-eGFP: Clone originated from HeL_{am}CAT1-rtTA2-M2 stably transfected with mCerS3-eGFP.

- HeL_{am}CAT1-rtTA2-M2-eGFP: Clone originated from HeL_{am}CAT1-rtTA2-M2 stably transfected with eGFP.

Media for cell culture

Table 7 Media for cell culture

RPMI growth medium ^{1,2} 1x RPMI 1640 10% FCS ³ (v/v) 2 mM L-glutamine 10 mM HEPES	DMEM growth medium ⁴ 1x DMEM 100 U/ml penicillin 100 µg/ml streptomycin
Freezing medium 1x RPMI 1640 10% FCS 3 (v/v) 10% DMSO	Collagen gels ⁴ 80% 4mg/ml Collagen type I in HAc 0,1% 10% HANKS buffered solution 5M NaOH to titrate DMEM

¹ Stored at 4 °C. ² For culture of HeLa cells. ³ FCS was heat inactivated for 30 min at 56 °C prior to be used as a supplement. ⁴ for infection assay

Additional solutions used for cell culture were:

RPMI 1640 (1x) Roswell Park Memorial Institute medium (Sigma, R0883)

DMEM (1x) Dulbecco's modified Eagle's minimal essential medium (Lonza, BE12-604F)

D-PBS (1x) Dulbecco's phosphate buffered saline (Sigma, D8537)

Trypsin (10x) 0.25% trypsin (Gentaur) + 0.5 mM EDTA

Trypan blue (1x) 0.4% trypan blue + 0.81% NaCl + 0.06% KH₂PO₄

Kits and standards

Table 8 List of kits and standards

Compound	Supplier
ECL Western blotting analysis system	Amersham GE Healthcare
Sphingosine d18:1	Matreya LLC
Sphingosine d17:1	Matreya LLC
sphingosine d20:1	Matreya LLC
Sphinganine d18:0	Matreya LLC
Sphinganine d17:0	Matreya LLC
Sphinganine d20:0	Matreya LLC
1-deoxysphingosine m18:1	Matreya LLC
1-deoxymethylsphingosine m17:1	Matreya LLC
4-hydroxysphinganine d17:0	Matreya LLC
sphingosine-1P d18:1	Matreya LLC
Sphingosine-1P d17:1	Matreya LLC
Sphingosine-1P d20:1	Matreya LLC
Sphinganine-1P d18:0	Matreya LLC
Sphinganine-1P d17:0	Matreya LLC
Sphinganine-1P d20:0	Matreya LLC
C16 Ceramide-1P d18:1/16:0	Matreya LLC
C12 Ceramide-1P d18:1/12:0	Matreya LLC
C24 Ceramide-1P d18:1/24:0	Matreya LLC
Sphingosine (d14:1)	Matreya LLC
Cholesteryl nervonate	Santa Cruz
CE heptadecanoate C17:0	Matreya LLC
CE myristate C14:0	Matreya LLC
CE palmitate C16:0	Matreya LLC
CE lineolate C18:2	Matreya LLC
CE arachidonate C20:4	Matreya LLC
CE behenate C22:0	Matreya LLC
CE ecurate C22:1	Matreya LLC

Instrumentation

Table 9 List of instrumentations

Instrument	Company
Instruments used for genotyping (PCR analysis)	
Agarose gel electrophoresis chamber	Carl Roth, Karlsruhe, Germany
SM-30 Control rotary shaker	Neo Lab
GelDOCTM 2000 Gel Documentation System	Bio-Rad, München, Germany
GeneAmp® PCR System 2400, 2720 Thermal cycler – PCR	Life Technology (Applied Biosystems), Darmstadt, Germany
Instruments used for lipid extraction and analysis	
Alpha 1-2 Lyophilizer	Christ, Osterode, Germany
Evaporator	Liebisch, Bielefeld, Germany
Linomat IV	Camag, Muttenz, Switzerland
Sonorex Super RK 102H Sonicator	Bandelin, Berlin, Germany
Variofuge 3.0 R	Heraeus Sepatech, Osterode, Germany
Xevo® TQ-S Tandem MS Acquity UPLC® I-class	Waters, Eschborn, Germany
VG micromass model	Quattro II Waters
Instruments used for protein extraction and western blots	
Branson Sonifier® 250	G. Heinemann, Schwäbisch Gmünd, Germany
Classic autoradiography film developing machine	AGFA E.O.S., Bonn, Germany
Electrophoresis blotting apparatus	Bio-Rad, Munich, Germany
Mini-PROTEAN 3 Cell electrophoresis system	Bio-Rad, Munich, Germany
SM-30 Control rotary shaker	Neolab, Heidelberg, Germany
Ultrospec 2000 UV/visible spectrophotometer	Pharmacia Biotech, Uppsala, Schweden
Sonorex Super RK 102H	Sonicator Bandelin
Instruments used for histology and microscopy	
Autoanalyzer Hitachi 9-17-E	Hitachi, Frankfurt am Main, Germany
Biorevo BZ-9000 microscope	Keyence, Neu-Isenburg, Germany
Cryostat Leica CM 3050S	Leica Biosystems, Nussloch, Germany
Dako Autostainer	Dako, Hamburg, Germany
Microtome Microm HM355S	Thermo Scientific, USA
Ultramicrotom Leica Ultracut	Leica Microsystems GmbH, Wetzlar, Germany
Additional Equipment	
Dewar, liquid nitrogen container	KGW-Isotherm, Karlsruhe, Germany
Eppendorf refrigerated table top centrifuge 5417R, Eppendorf table top centrifuge 5415C	Eppendorf, Hamburg, Germany
Heating furnace (56°C)	Heraeus, Hanau, Germany
HP LaserJet 2410 PS	Hewlett-Packard, Böblingen, Germany
Laboratory scale	Ohaus, Pine Brook, USA
Laboratory micro scale	Sartorius, Göttingen, Germany
Minifuge RF (refrigerated centrifuge)	Heraeus, Hanau, Germany
pH Meter	Schott, Mainz, Germany
ScanMaker i800	Microtek, Taiwan
Thermomixer compfort (1.5mL)	Eppendorf, Hamburg, Germany
Vortexer	IKA Labortechnik, Staufen, Germany

3.2. Methods

Animal care

Animals were kept under specific pathogen-free conditions in barrier facilities, where a 12 h light / 12 h dark cycle was maintained. Mice were housed in groups up to five animals at a controlled temperature of 22 °C. They were fed regular laboratory chow diet and water, supplied *ad libitum*.

Generation of *CerS3d/d* mice

CerS3 d/d mice had been established previously (Jennemann et al., 2012). The *CerS3* gene (ceramide synthase 3, *Lass3*, NCBI gene ID: 545975) was used to generate offspring with the exon 7 flanked by loxP sites, which were further mated with cre-deleter mice to obtain a systemic deletion of exon 7. The cre-transgene was again removed by mating with C57Bl6 wild-type mice. Heterozygous mice were bred in order to generate homozygous offspring with complete exon 7 deletion in *Cers3* in both alleles resulting in *Cers3* d/d mice. All animal procedures were approved and performed in accordance with federal laws (Regierungspräsidium Karlsruhe, Germany, G-68/07, G-8/07 and A-62/06).

Generation of *Ugcg* mutant mice

As described before (Jennemann et al., 2007) the genes expressing keratins K5 and K14 are expressed in basal cells of epidermis. Because of its early expression in the basal layer, K14-promoted Cre-mice were bred with mice with a loxP flanked glucosylceramide synthase gene to obtain a blockade of the initial step of the GlcCer biosynthesis in epidermal keratinocytes. The resulting mouse model with loxP-flanked exons 6–8 of the *Ugcg* gene locus has been established previously (Jennemann et al., 2005). Generation of mutant animals and experiments were performed according to federal laws for animal experiments and were approved (Regierungspräsidium Karlsruhe, Germany).

Generation of *CerS3-Stra8* mice

Mice with a floxed ceramide synthase 3 gene (Jennemann et al., 2012) were crossbred with transgenic mice expressing Cre under the control of the stimulated by retinoic acid gene 8 (*Stra8*)-promoter (*Stra8* is expressed initially at postnatal day P3 in early-stage spermatogonia (Sadate-Ngatchou et al., 2008)).

Genotyping

In brief, genomic DNA was isolated from tail biopsies. Tails were digested overnight at 56 °C with 8 µL of proteinase K (10 mg/mL, Sigma) dissolved in ~800 µL of NID buffer depending on the tail size. Upon heat inactivation of the enzyme at 85 °C for 45 min, 1-2 µL of DNA solution was used for PCR analysis. Primers used for amplification of specific products corresponding to wild-type or mutant alleles are listed in the materials section

PCR conditions for amplification of the *L3* and *Stra8* transgenes:

<u>L3</u>				
PCR reaction L3(50 µL)	µL	PCR program	T [°C]	Time [s]
H2O	33.75	1. Denaturation	95	120
10x Buffer	5	2. Denaturation	95	45
MgCl ₂ (50 mM)	4	3. Annealing	58	30
dNTPs (10 mM)	1	4. Elongation	72	40
Forward primer (7.5 pmol/µL)	2	5. Elongation	72	320
Reverse primer (7.5 pmol/µL)	2	6. Cooling	4	∞
NID-DNA	2.00	Steps 2 to 4 are repeated for 35 cycles.		
Platinum Taq	0,25			
<u>Stra8</u>				
PCR reaction Stra8 (50 µL)	µL	PCR program	T [°C]	Time [s]
H2O	36.75	1. Denaturation	94	120
10x Buffer	5	2. Denaturation	94	30
MgCl ₂ (50 mM)	1	3. Annealing	60	30
dNTPs (10 mM)	1	4. Elongation	72	30
Forward primer (7.5 pmol/µL)	2	5. Elongation	72	320
Reverse primer (7.5 pmol/µL)	2	6. Cooling	4	∞
NID-DNA	2.00	Steps 2 to 4 are repeated for 35 cycles.		
Platinum Taq	0,25			

Cloning

mCerS3-EGFP had been generated before by inserting the corresponding cDNAs into the N-terminus of the pEGFP-N1 vector as described in (Rabionet, 2011). A map of the in this study used plasmid can be found in Figure 4 below.

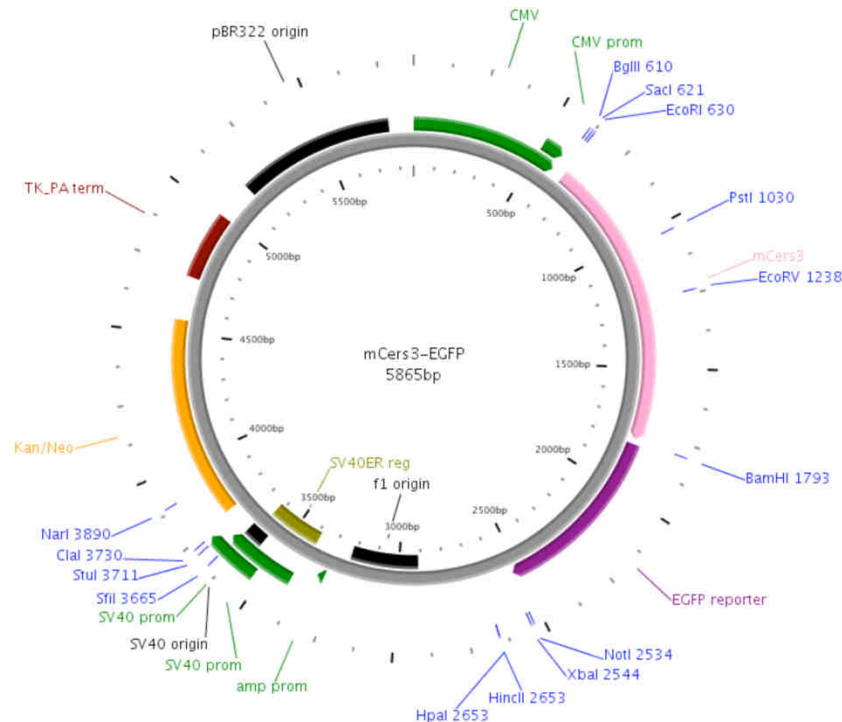


Figure 4 Plasmid map from mCers3-EGFP. Cers3 was inserted at the N-terminus of an enhanced GFP tag plasmid via the EcoRI-BamHI restriction sites.

Cell culture

Culture of eukaryotic cells

HeLa cells were grown in RPMI-1640 medium (Sigma, R0883) supplemented with 10% inactivated fetal calf serum, 2 mM L-glutamine, 10 mM HEPES. Cells were maintained in monolayer cultures in a humidified atmosphere of 5% CO₂ at 37 °C, and were sub cultured twice a week with trypsin-EDTA (0.25% in PBS).

Freezing and thawing of eukaryotic cells

To create stocks, cells in growth phase were trypsinized and harvested at 1000 x g for 5 min. Cells were then resuspended in freezing media consisting of 90% FCS and 10% DMSO, transferred into cryotubes (Nalgene) and kept for long time storage at – 80 °C.

For the revitalization of frozen cellular stocks, cryotubes were placed in a water bath at 37 °C until cells were thawed. Cells in freezing media were directly diluted 1:12 with prewarmed growth medium in a 75 cm² tissue culture flask. After cellular attachment, medium was exchanged to remove residual DMSO. Cells were passaged at least once before being used for experiments.

Transfection of eukaryotic cells

Transient transfection of plasmid DNA into HeLa cells was achieved by means of lipofection. HeLa cells were seeded in 6-well plates either 24 or 48 h prior to transfection. Highly confluent cells (90–95%) were then transfected with the optimal amount of plasmid DNA (previously tested for each plasmid) using Lipofectamine™ 2000 reagent (Invitrogen) according to manufacturer's recommendations. Thus, plasmid DNA (4 µg) was complexed with transfection reagent with a ratio optimized for each transfection in order to minimize cytotoxicity. DNA-cationic lipid complexes in serum-free RPMI medium were administered drop-wise to the cells, which were then incubated at 37 °C for 4 h. Subsequently, medium was exchanged by growth medium with FCS. Analyses were performed generally after 24 h of overexpression. Transfection efficiencies were determined by flow cytometric analysis according to the fluorescence signals generated from the overexpression of EGFP fusion proteins.

For subcellular localization studies, cell lines (2.5×10^5) were transfected with the desired vector 24 h after seeding using Lipofectamine™ at a 1:2.5 ratio (µg DNA/µl Lipofectamine™).

Immunohistochemistry

IHC of cultured cells

For subcellular localization of CerS3, cells were seeded and transfected on sterile 12 mm glass coverslips placed in 6-well plates. Following 24 h after transfection, cells were washed 3 times with chilled PBS. HeLa cells stably transfected with mouse and human CerS3, EGFPcontrol, as well as untreated cells (HeLa_{mCAT1-rTA2-M2}) were seeded onto 6-well plates with a density of 1×10^5 cells/well with or without induction with 2 µg/ml doxycycline. Cells were then fixed with 3.5% PFA for 5 min on ice, following 10 min at R.T. Afterwards, cells were washed with chilled PBS (3x for 5 min), following permeabilization with CH₃OH (-20°C) for 6 min. Subsequently, cells were washed once more with PBS (3x for 5 min), before blocking for 1 h with 3% BSA-PBS. Binding of primary antibodies was performed for 1.5 h at R.T. After three washing steps, incubation of secondary antibodies for 45 min followed. Primary and secondary antibodies were diluted in 1.5% BSA-PBS. Afterwards cells were washed once more and nuclear staining was performed with Dapi in PBS for 10 min. Finally,

cells were washed with PBS (4x for 5 min) and mounted with Fluoromount-G. Immunofluorescence images were acquired with Keyence Bioevo BZ-9000 microscope.

IHC of mouse epidermis and testis

Sections were prepared as follows.

Cryosections. Unfixed biopsies of newborn and adult animals were quickly placed onto an aluminum foil and frozen in pre-cooled isopentane with liquid nitrogen and embedded in tissue block. Cryosections of 3–5 μm thickness were obtained with a Leica CM 3050S and subsequently fixed with acetone for 10 min at R.T. Sections were permeabilized with 1% Triton X-100 in PBS (v/v) for 5 min and then blocked for 30 min with 10% FCS.

Paraffin. Fixed specimens were dehydrated in a graded ethanol series and embedded in Paraplast Plus. Paraffin sections of 3–5 μm thickness were obtained with a Microm HM 340E, then deparaffinized and subjected to antigen retrieval. They were subsequently washed three times for 5 min with PBS- 0.1% Tween and blocked for 1h with 5% PBS-BSA. For detection of antigens, sections were incubated with primary antibodies (dilution 1:50 for CerS4, or 1:100 for 1–16h at 4 °C or 1.5h at R.T. For CerS3 primary antibody was preincubated over night on ko sections before applying it on wt and freshly prepared ko samples. Sections were washed three times with PBS-Tween and incubated with secondary antibodies (1:300) for 45 min at R.T. Following another washing step, nuclear staining was performed with DAPI (20 ng/ml, Sigma). Sections were then mounted in Dako Cytomation fluorescent mounting medium.

Full skin sections (modified from (Chorro et al., 2009)). Newborn and embryonic mice were sacrificed and subsequently the skin was removed. To separate epidermis and dermis, skin was incubated in PBS containing 20mM EDTA for 2h at 37°C. Epidermis was peeled off and washed with PBS. Then epidermis was fixed in 3% PFA in PBS for 45 min on ice and then washed 3 times with PBS. Samples were blocked with dermal side up in 5% goat serum (GS) in PBS- 0,5% TritonX for 30 min. Incubation with primary antibody was performed over night at 4°C in 1% GS (1:25) whereby the slides were kept in a humid atmosphere. A washing step with 5% GS and two washing steps with PBS for 5 min were done before incubation with secondary antibody (1:750) for 45 min at R.T. Sections were washed three times with PBS

and nuclear staining was performed with DAPI (20 ng/ml, Sigma) before washing 4 times with PBS. Sections were then mounted in Dako Cytomation fluorescent mounting medium.

Specimen preparation and ultrastructural analyses were performed in cooperation with Prof. Dr. Karin Gorgas at the Department of Anatomy and Cell Biology of University of Heidelberg. PAS and HE staining of skin and testis biopsies was performed with the technical assistance of Gabriele Schmidt from DKFZ in Heidelberg.

Pathogenic growth experiments

Culture of mouse skin

Skin biopsies from the back of embryonic and newborn animals were maintained viable on collagen gels partially submerged in DMEM medium (Lonza, BE12-604F) supplemented with 50 U/ml penicillin and 50 µg/ml streptomycin (Gibco). Sphingosine (d18:1) was diluted to 0.16 µM in 50% Water/ Propyleneglycol (v/v) and added topically on the epidermal side of the skin biopsies and incubated in a humidified atmosphere of 5% CO₂ at 37 °C for 24h. Collagen gels were prepared as previously described (Stark et al., 2006). Thus, type I collagen was isolated from tail tendons of young rats and lyophilized. To a 4 mg/ml solution of collagen in 0.1% AcOH was added 10% of 10x Hank's balanced salt solution (Gibco) titrated with 5 M NaOH and 10% of DMEM medium. The mixture was allowed to jellify in PET-membrane filter inserts (Falcon) for 1 h at 37 °C, following the addition of 12 ml DMEM medium in each of the deep-wells (BD Biosciences, BD 355467).

Pathogenic infection

Pathogenic infection and growth studies were performed by Tatjana Eigenbrod and Prof. Dr. Alexander Dalpke at the department of Medical Microbiology and Hygiene of University of Heidelberg.

Candida albicans (ATCC 90028) was grown overnight in LB medium. Prior to infection, yeast concentration was determined by cell counting using a Neubauer chamber. Afterwards, cells were pelleted by centrifugation and resuspended in PBS to a concentration of 10⁹

cells/ml. *C. albicans* (1 μ l, 1×10^6 cells) was inoculated to the center of the skin biopsy and incubated at 30 °C for the specified time.

Determination of pathogenic growth

Infected skin biopsies were flushed with 10 ml PBS. An aliquot of these suspensions (100 μ l) were plated in two different dilutions on Sabouroud agar plates (BioMérieux). Multiple serial dilutions had been previously performed to determine optimal conditions. After 24 h incubation at 37°C, colonies were counted and concentrations were determined as CFU/ml. Technical triplicates from biopsies of mice were analyzed.

For pathogenic studies, infected skin biopsies from CerS3 deficient mice and controls were fixed together with collagen gels with 4% formalin for 24 h at R.T. and subsequently embedded in paraffin. Sections (Microm, HM 355S) of 1 μ m thickness were prepared and deparaffinized by short sequential immersions in xylene, ethanol solutions (100%, 96%, 80% and 70%) and water. Sections were then immersed in 0.75% HIO₄ for 10 min, carefully rinsed with water and incubated in Schiff solution for 5 min. Following rinsing and drying steps, biopsies were then counterstained with haemalaun solution. Sections were dehydrated by subsequent immersions in ethanol solutions of increasing concentrations (70–100%), followed by immersion in xylene. Sections were then mounted with Vitro-Cloud (Langenbrink) and analyzed using a Keyence BZ-9000.

Western blot

Preparation of total protein lysates

Skin biopsies were incubated at 37°C for 2h in PBS containing 20 mM EDTA in order to separate dermis from epidermis. Epidermis was obtained by peeling off the dermis. Epidermis or whole testis in digitonin lysis buffer was homogenized on ice by sonification (Branson sonifier 250) using 5 pulses every 30 s for 5 min. After 10 min incubation of samples on ice lysates containing epidermal proteins were cleared of cell debris by centrifugation at 500xg at 4°C for 10 min. Membrane fractions were isolated from cytosolic fraction by repeated centrifugation at 12.000xg for 10 min at 4°C. Pellets were dissolved in RIPA buffer stored at -20°C and concentration determined by Bradford assay.

Determination of protein concentration by BRADFORD assay

Protein concentration in total lysates was determined according to the Bradford method (Bradford, 1976). This method is based on the shift of absorption of Coomassie Brilliant Blue G-250 upon binding to proteins. Briefly, protein-dye solutions were prepared by mixing either 10 or 5 μ l of membrane fraction with Bradford reagent up to 1 ml. To determine the protein concentration, a dilution series of BSA standards ranging from 0 to 10 μ g/ μ l dissolved in Bradford reagent was prepared in parallel. The absorbance of protein-dye mixtures was measured at the absorption maximum (595 nm), and the protein content was calculated by interpolating the absorbance measured from the BSA standard curve.

SDS-polyacrylamide gel electrophoresis (SDS-PAGE)

Proteins were separated according to their molecular weight in 12% SDS polyacrylamide gels (Mini-PROTEAN TGX Gels, BioRad)

To protein samples 4x Lämmli buffer containing 8% SDS was added prior to electrophoresis and sequentially incubated at room temperature for 5 min. Equal amounts of protein (20 μ g) were electrophoresed at \sim 35 mA during the separation in the stacking gel and at \sim 45 mA in the resolving gel.

Immunoblotting

After electrophoresis, proteins were transferred onto nitrocellulose membranes. For transfer, 0.45 μ m membranes were placed on gels and covered with 3 pieces of Whatmann paper and a sponge on each side. These stacks were assembled in a bath of chilled transfer buffer (1x) containing methanol. Electrotransfer of proteins to the membranes were carried out at \sim 170 mA for 2.5 h on ice. Subsequently, membranes were stained with Ponceau red to assess the quality of the transfer, the equality of the loading of the SDS-PAGE and to indicate the position of the lanes in case that cutting the membranes was required. Following the transfer, membranes were blocked generally with 5% skimmed milk in TBS-Tween. Blocking was performed at room temperature for 1 h. Afterwards, membranes were incubated with primary antibodies in 3% skimmed milk-TBST. Binding of primary antibodies was carried out under constant rotation overnight at 4 °C. On the following day, unbound antibodies were washed from the membranes 3 times with TBST for 10 min. Coupling of HRP-conjugated secondary antibodies was performed at R.T. for 45–60 min. Then, membranes were washed 3 more times for 10 min each with TBST. The working dilutions of primary and secondary antibodies

used in this study are listed in the Table 6. Finally, proteins were detected by enhanced chemiluminescence using an ECL-detection kit (Amersham GEHealthcare) following the instructions of the manufacturer and additionally pulling the membrane through water quickly after incubating with ECL.

Lipid analysis

Sample preparation

Cells grown in tissue culture plates were trypsinized and harvested at 100 x· g for 5 min at 4 °C. Cell pellets were then washed with chilled PBS and dried with 1-propanol under nitrogen flow. For the extraction of epidermal lipids, skin biopsies from the back of CerS3 deficient mice and control littermates were rapidly dissected and snap-frozen in liquid nitrogen before being stored at – 80 °C. Skins were thawed and epidermis was isolated by treating the biopsies with 500 µg/ml thermolysin buffer or 20 mM EDTA for 2 h at 37 °C (Germain et al., 1993). Afterwards, epidermis was separated from dermis, cut into small pieces, and lyophilized and powdered. Other organs were collected, homogenized and directly lyophilized and further processed as described in the section lipid extraction.

Lipid extraction by modified BLIGH and DYER method

Sphingolipids were extracted according to Doering et al. with slight modifications (Doering et al., 1999a; Jennemann et al., 2007). In general, lipids were isolated using mixtures of CHCl₃/CH₃OH/H₂O. In particular, dried pellets from cultured cells were extracted with 2 ml 10/10/1 (v/v/v) solvent mixture at 37 °C for 15 min with occasional sonication. After centrifugation at ~ 2000x· g for 10 min, supernatants were collected and pellets were then reextracted once more with 10/10/1 solvent mixture, and finally with a 30/60/8 (v/v/v) solvent mixture. For the extraction of epidermal free lipids, ~ 3 mg of dried weight epidermis cut in small pieces was extracted once with CHCl₃/CH₃OH/H₂O 30/60/8, then with 10/10/1 and finally with CHCl₃/CH₃OH 2/1 (v/v/v) as described. Each extraction step was performed at 50 °C for 15 min under sonication. Supernatants were combined and dried under a nitrogen flow at 37°C. In parallel, pellets were dried and kept at 4 °C for further analysis.

Removal of phospholipids by mild alkaline methanolysis

Combined lipid extracts were subjected to methanolic mild alkaline hydrolysis (0.1 M KOH in CH₃OH) for the removal of phospholipids if needed. The saponification of cell culture

extracts was performed at 37 °C for 2 h, while epidermal and other tissue extracts required 4 h at 50 °C for complete hydrolysis. Sequentially, saponified lipid extracts were neutralized with glacial AcOH and solvent was removed under a mild nitrogen flow.

Desalinization by reverse-phase chromatography (RP-18)

Saponified lipid extracts were desalted by reverse phase chromatography prior to being analyzed either by TLC or ESI-MS/MS. Thus, columns packed with C18 material (Porasil silica 125Å 55–105 µm) were preconditioned consecutively with 3 times CH₃OH and 2 times with 0.1 M KCl. Salt-containing samples were dissolved in ddH₂O to a final concentration of 0.1–0.2 M KCl by brief sonication before being loaded into the columns. Following the loading of the samples, vials were washed twice with 0.1 M KCl, sonicated and loaded as well into the columns. Lipids bound to the column were then washed 3 times with ddH₂O. Finally, sphingolipids were eluted with CH₃OH and dried under a nitrogen flow. In case of desalinization of epidermal ceramides, an additional washing step with ddH₂O was performed prior to elute the lipids with CH₃OH into the original sample tubes, and subsequently dried under a nitrogen flow. Desalting of saponified lipids from cultured cells was performed using freshly prepared Pasteur pipettes. For tissue extracts, 100 mg of packing material was loaded into 5 ml polypropylene reusable columns. To assure complete removal of previous lipid extracts, polypropylene columns were carefully washed with 2 x 4 ml CHCl₃, 1 x 4 ml CHCl₃/CH₃OH 1:1, 1 x 4 ml CH₃OH, 1 x 4 ml CH₃OH /H₂O 1:1, and finally equilibrated with 2 ml 0.1 M KCl.

Quantification by electrospray ionization tandem mass spectrometry (ESI-MS/MS)

Sphingolipid quantification was performed by tandem mass spectrometry using a Xevo® TQ-S triple-quadrupole instrument (Waters) equipped with ultra-performance liquid chromatography hardware (Acquity UPLC® I-class, Waters) and a ESI source. Equivalent lipid samples regarding the dry or wet weight were dissolved in 95% methanol. Prior to being analyzed, internal standards were added to the aliquots. Sphingolipids, as well as Sphingoid bases were detected with precursor ion scans and neutral loss modulus, respectively. The samples (extract + standard) were injected (10 µL) and separated by UPLC using a reverse-phase column (Acquity UPLC® BEH C18, 130 Å 1.7 µm, 2.1 × 50 mm column) or for sphingoid bases using a reversed phase column with additional surface charges (CSH-column, 50 mm, 2.1 mm, 1.7µm, Waters).

MS/MS analysis was performed using the positive-ion ESI mode with multiple reaction monitoring (MRM) of daughter-ion fragments specific to each lipid class. For quantification,

chromatographic peak areas corresponding to each specific lipid species were normalized to the peak areas of the corresponding internal standards. Samples were injected and processed using MassLynx, whereas mass spectrometric peaks were quantified according to their peak area ratio with respect to the internal standard using TargetLynx (both v 4.1 SCN 843) both from Waters Corporation.

Ceramide Quantification

Lipid extract samples, equivalent to a dried weight of 12.5 μg , were dissolved in 95% methanol (1 mL) and mixed with non-endogenous lipid standards prior to analysis. Lipid standards included the ceramides (d18:1/14:0), (d18:1/19:0), (d18:1/25:0), (d18:1/31:0), 6.25 pmol each; the GlcCers (d18:1/14:0), (d18:1/19:0), (d18:1/25:0), (d18:1/31:0), 3.125 pmol each; and the SMs (d18:1/14:0), (d18:1/25:0), (d18:1/31:0), 3.125 pmol each.

The capillary voltage was set at 2.5 kV, whereas the cone and the source offset were fixed at 50 V. The source and desolvation temperatures were maintained at 90 and 300°C, respectively. The desolvation gas was delivered at 800 l/h, while the cone gas and the collision gas flow were fixed at 150 l/h and 0.15 ml/min, respectively. Classical Cers (d18:1; 14:0–36:0) were measured using increasing collision energies ranging from 25 to 30 eV according to their molecular mass.

The chromatographic eluent gradient at a constant flow rate of 0.45 mL/min is given in the following tables.

Table 10 UPLC-gradient elution of sphingolipids for detection by tandem mass spectrometry

Column temperature	40°C
Flow rate	0.45 mL/min
Mobile Phase A	95% methanol, 5% water, 0.05% formic acid, 1 mM ammonium formate.
Mobile Phase B	99% isopropanol, 1% methanol, 0.05% formic acid, 1 mM ammonium formate
Sample solvent	95% Methanol

Time [min]	Solvent A [%]	Solvent B [%]	Slope
0.0	100	0	Initial
0.1	100	0	linear
0.2	92	8	linear
5.0	10	90	concave
5.25	10	90	linear
5.50	100	0	linear
6.50	100	0	linear

1-O-acylceramide Quantification

As for classic ceramides, samples were dissolved in 95% methanol and 5% H₂O. Samples were treated in an ultrasound bath for 3 min at 40°C and then placed directly into the auto sampler, which was held at 20°C. The column was heated to 40°C and in 10µl aliquots were injected. Protonated 1-O-acylceramides were quantified in single reaction monitoring (SRM) mode using 7.65 pmol of 1-O-oleoyl Cer(d18:1;17:0) as internal standard per aliquot of epidermal lipids corresponding either to 0.1 mg mouse tissue dry weight. The capillary voltage was set at 2.5 kV, whereas the cone and the source offset were fixed at 50 V. The source and desolvation temperatures were maintained at 90 and 300°C, respectively. The desolvation gas was delivered at 800 l/h, while the cone gas and the collision gas flow were fixed at 150 l/h and 0.15 ml/min, respectively. 1-O-acylceramides were detected using a fixed collision energy of 20 eV, while maintaining the dwell time at 8 ms. Significant in-source decay of 1-O-acylceramides leading to water loss appeared. Therefore, each compound was detected by two transitions, which were added up for quantification (a list of MRMs can be found in Table 11). The gradient is the same as for classical ceramides.

Table 11 Multiple SRM transitions (MRM) used for detection and quantification of 1-O-acylceramides. For description of fragment c see Figure 22. From (Rabionet et al., 2013).

1-O-Acylceramide			Transitions		1-O-Acylceramide			Transitions			
1-O-Acyl	So	N-Acyl	$[M+H]^+$ & $[(M-H_2O)+H]^+$	Fragment c	1-O-Acyl	So	N-Acyl	$[M+H]^+$ & $[(M-H_2O)+H]^+$	Fragment c		
HO-groups, C-atoms : double bonds					[m/z]	HO-groups, C-atoms : double bonds					[m/z]
14:0			734.7 & 716.7	488.5	14:0			764.7 & 746.7	518.5		
16:0			762.7 & 744.7		16:0			804.8 & 786.8			
18:0	d17:1	16:0	790.8 & 772.8		18:0			832.8 & 814.8			
20:0			818.8 & 800.8		20:0	d18:1	h16:0	860.8 & 842.8			
22:0			846.8 & 828.8		22:0			888.9 & 870.9			
24:0			874.9 & 856.8		23:0			902.9 & 884.9			
26:0			902.9 & 884.9		24:0			916.9 & 898.9			
14:0			750.7 & 732.7	504.5	25:0			930.9 & 912.9	530.5		
16:0			790.8 & 772.8		26:0			944.9 & 926.9			
18:0	d17:1	h16:0	818.8 & 800.8		14:0			776.7 & 758.7			
20:0			846.8 & 828.8		15:0			790.8 & 772.8			
22:0			874.9 & 856.8		16:0			804.8 & 786.8			
24:0			902.9 & 884.9		18:0	d18:1	18:0	832.8 & 814.8			
26:0			930.9 & 912.9		20:0			860.8 & 842.8			
14:0			762.7 & 744.7	516.5	22:0			888.9 & 870.9	558.6		
16:0			790.8 & 772.8		23:0			902.9 & 884.9			
18:0	d17:1	18:0	818.8 & 800.8		24:0			916.9 & 898.9			
20:0			846.8 & 828.8		26:0			944.9 & 926.9			
22:0			874.9 & 856.8		14:0			804.8 & 786.8			
24:0			902.9 & 884.9		15:0			818.8 & 800.8			
26:0			930.9 & 912.9		16:0			832.8 & 814.8			
14:0			790.8 & 772.8	544.5	18:0	d18:1	20:0	860.8 & 842.8	586.6		
16:0			818.8 & 800.8		20:0			888.9 & 870.9			
18:0	d17:1	20:0	846.8 & 828.8		22:0			916.9 & 898.9			
20:0			874.9 & 856.8		23:0			930.9 & 912.9			
22:0			902.9 & 884.9		24:0			944.9 & 926.9			
24:0			930.9 & 912.9		26:0			973.0 & 955.0			
26:0			959.0 & 940.9		14:0			832.8 & 814.8			
14:0			818.8 & 800.8	572.6	16:0			860.8 & 842.8	614.6		
16:0			846.8 & 828.8		18:0			888.9 & 870.9			
18:0	d17:1	22:0	874.9 & 856.8		20:0	d18:1	22:0	916.9 & 898.9			
20:0			902.9 & 884.9		22:0			944.9 & 926.9			
22:0			930.9 & 912.9		24:0			973.0 & 955.0			
24:0			959.0 & 940.9		25:0			987.0 & 969.0			
26:0			987.0 & 969.0		26:0			1001.0 & 983.0			
14:0			846.8 & 828.8	600.6	14:0			860.8 & 842.8	502.5		
16:0			874.9 & 856.8		15:0			874.9 & 856.8			
18:0	d17:1	24:0	902.9 & 884.9		16:0			888.9 & 870.9			
20:0			930.9 & 912.9		17:0			902.9 & 884.9			
22:0			959.0 & 940.9		18:0	d18:1	24:0	916.9 & 898.9			
24:0			987.0 & 969.0		20:0			944.9 & 926.9			
26:0			1015.0 & 997.0		22:0			973.0 & 955.0			
14:0			748.7 & 730.7	502.5	23:0			987.0 & 969.0	614.6		
16:0			776.7 & 758.7		24:0			1001.0 & 983.0			
18:0			804.8 & 786.8		25:0			1015.0 & 997.0			
20:0	d18:1	16:0	832.8 & 814.8		26:0			1029.0 & 1011			
22:0			860.8 & 842.8								
23:0			874.9 & 856.8								
24:0			888.9 & 870.9								
25:0			902.9 & 884.9								
26:0			916.9 & 898.9								

Sphingoid base quantification

Epidermal extracts were achieved like described above and 0.1 mg DW aliquoted for each sample. Plasma samples (25 μ L) were extracted with 100 μ L of chloroform/methanol (2:1); this solution was then allowed to stand for 5 min at room temperature, followed by vortexing for 30 s. After centrifuging (12000x g, for 5 min at 4°C) the lower organic phase was collected in a new vial and evaporated to dryness under vacuum. Immediately prior to analysis the lipid extract was diluted with isopropanol/acetonitrile/water (2:1:1, 250 μ L).

Quantification of Sphingoid bases was performed by using tandem MS (QqQ, Xevo TQ-S) in MRM mode coupled to a UPLC (Aquity I class). A CSH-C18 (50 mm, 2.1 mm, 1.7 μ m) column and solvent system was used according to Isaac, G. (2011; Waters Corporation, Application Note), but with citrate as additive. CSH particles incorporate a low level surface charge, to improve sample loadability and peak asymmetry. Citrate additionally helps to avoid unspecific column - metal ion – analyte interactions (Seidler et al., 2011).

The capillary voltage was set at 2.0 kV, whereas the cone and the source offset were fixed at 30 V. The source and desolvation temperatures were maintained at 120 and 550°C, respectively. The desolvation gas was delivered at 900 l/h.

The chromatographic eluent gradient at a constant flow rate of 0.4 mL/min is given in the following tables.

Table 12 LC Parameters for sphingoid base quantification

Column temperature	55°C
Flow rate	0.40 mL/min
Mobile Phase A	ACN:H ₂ O 60/40, 10mM NH ₄ FA, 0,1% Formic acid
Mobile Phase B	Iprop:ACN 90:10, 10mM NH ₄ FA, 0,1% Formic acid
Sample solvent	Iprop:ACN:H ₂ O 2:1:1, 50mM, Citrate

Table 13 Gradient for sphingoid base quantification

Time [min]	Solvent A [%]	Solvent B [%]	Slope
initial	40	60	Initial
2.0	57	43	linear
2.1	50	50	concave
12.0	46	54	linear
12.1	30	70	concave
18.0	1	99	linear
18.1	60	40	linear
20	60	40	concave

A list of MRM can be seen in results part.

Statistics

If not else described, all experiments included a minimum of 3 animals. The results obtained are shown as mean \pm SD. All statistical tests were performed using GraphPad Prism® 5 software. Measurements in control (heterozygous, wildtype) and mutant mice were compared by the Student's t-test or by the ANOVA test. Differences between group means were considered significant for $p < 0.05$ (*), $p < 0.01$ (**) and $p < 0.001$ (***). If not significant on a 5% level significances were also tested on a 10% level, and if used indicated as such.

Thesis structure

Detailed knowledge of ceramide metabolism is fundamental for the understanding of skin pathophysiology and hence is prerequisite for targeted therapy of skin disorders. In this work, pathways connected to ceramide synthesis were investigated, to gain further insight into consequences out of a disturbed ceramide metabolism. Therefore this thesis was split into three parts:

In the first part altered levels of ceramide downstream products, the sphingoid bases and free fatty acids and their impact on altered tissue homeostasis and function in epidermis were analyzed.

The second part covers investigations about the class of 1-O-acylceramides, as their epidermal steady state levels increased upon CerS3-deficiency. The pathway leading to 1-O-AcylCer in mammals is unknown and first attempts in uncovering the responsible enzymes were shown.

The third and last part deals with the location of CerS3 within skin and testis and its intracellular location in order to understand the topology of ULC-ceramide production.

Part I

I. Sphingosine in antimicrobial defense of the skin

I.1 Introduction

I.1.1 Skin topology and Epidermis

The skin is formed by an outer squamous epithelium (epidermis and hair follicles) and the inner dermis (Figure 5). The dermis is mainly composed out of extracellular matrix, which includes fibroblasts and fibroblast-derived proteins (collagen, elastin, glycosaminoglycans) to give the skin tensile strength and elasticity. The primary function of the epidermis, which is a self-renewing and cornifying epithelium, is to protect the body from environmental influences by maintaining the skin barrier. For this purpose the epidermis synthesizes a unique composition of long chain (LC) and ultra long chain (ULC) FA-containing SLs which, together with junction proteins, allow for the formation of a barrier in the outermost epidermal layers.

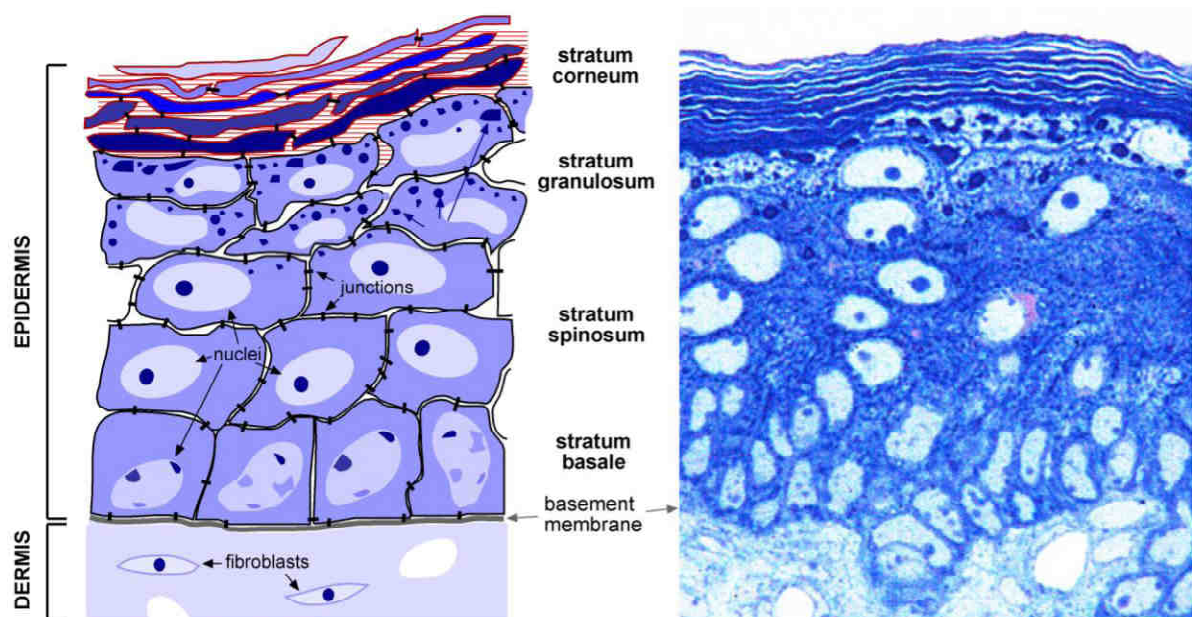


Figure 5 The epidermal structure. The epidermis is a self-renewing tissue, where keratinocytes at the stratum basale progressively differentiate and migrate through the stratum spinosum and the stratum granulosum to terminally differentiate in the stratum corneum, where they finally shed during desquamation. Right: PAS-methylene blue-Azur II staining of neonatal mouse skin. KG: keratohyalin granules. Scheme modified from (Sandhoff, 2009).

Keratinocytes, the main type of all epidermal cells, derive from stem cells in the lower basal layer and differentiate on their way to the skin surface (Watt, 2002). The lowest layer is the stratum basale (SB), followed by the stratum spinosum (SS), the stratum granulosum (SG) and on top the stratum corneum (SC) (Figure 5). During terminal differentiation the cells in

the SC form dead, flattened corneocytes and finally shed off by desquamation (Candi et al., 2005). SC formation is a repetitive process which can take up to 6 or 7 weeks in humans (Halprin, 1972) and 8 to 10 days in the mouse (Ghazizadeh and Taichman, 2001; Potten et al., 1987).

SG keratinocytes extrude their cellular contents and become anucleate corneocytes of the SC. During this process, the cornification, the corneocyte PM is gradually replaced by a scaffold of cross-linked structural proteins. Such proteins are for example lipid-bound involucrin and loricrin. The result is an insoluble, rigid cornified envelope (CE), which is a prerequisite for epidermal barrier function (Candi et al., 2005). In parallel, lipid synthesis increases in SG keratinocytes and small secretory organelles, the so-called lamellar bodies (LBs). LBs deliver lipids, catalytic enzymes and antimicrobial peptides to the apical PM and exocytose their content in the upper SG and at the SG/SC interface (Jennemann et al., 2012). Then, the extracellular lipids are enzymatically processed and form lipid lamellae or are covalently bound to proteins of the CE, forming the cornified lipid envelope (CLE) as the first barrier against epidermal water loss (Nemes et al., 1999; Sandhoff, 2010).

The integrity of the epidermis is maintained by cell-cell junctions, i.e. tight junctions, adherens junctions and desmosomes. Tight junctions (TJs, zonula occludens) are expressed in the more differentiated layers (SS, SG) of the epidermis and have been shown to protect from epidermal water loss (Furuse et al., 2002). Adherens junctions (AJs) are created by multifunctional adhesive proteins, which interconnect the cytoskeleton of neighboring cells. The most characteristic epidermal junctions are desmosomes which are structurally similar to adherens junctions. Desmosomes, sitting in the viable epidermal layers, function as “mechanical junctions” connecting the keratin cytoskeleton via catenins to neighboring cells or to the ECM (in the form of hemidesmosomes). In the SC, desmosomes specialize further to corneodesmosomes. In the lower SC layers the latter are regularly expressed on corneocytes as compounds of the CE. Degradation of corneodesmosomes by LB-derived proteases (e.g., kallikreins of the KLK family) is a key factor for normal desquamation (Ishida-Yamamoto et al., 2011). Changes in protease (inhibitor) activities, calcium concentration, or SC pH and hydration can impair the regular desquamatory process and result in hyperkeratosis (ichthyosis) and other skin pathologies.

1.1.1.1 Long chain-, very long chain- and ultra long chain fatty acids

Whereas the mammalian PM of cells primarily contains saturated long chain (LC) (C16-C20) and very long chain (VLC) (C22-C26) FAs, the epidermis expresses also a unique diversity of Cers with ultra long chain (C28-C36) acyl moieties (Figure 6). LC and VLC-Cers are mainly localized in the nucleus, in mitochondria, in the Golgi or in the PM of cells of the lower layers of epidermis (Uchida and Hamanaka, 2006).

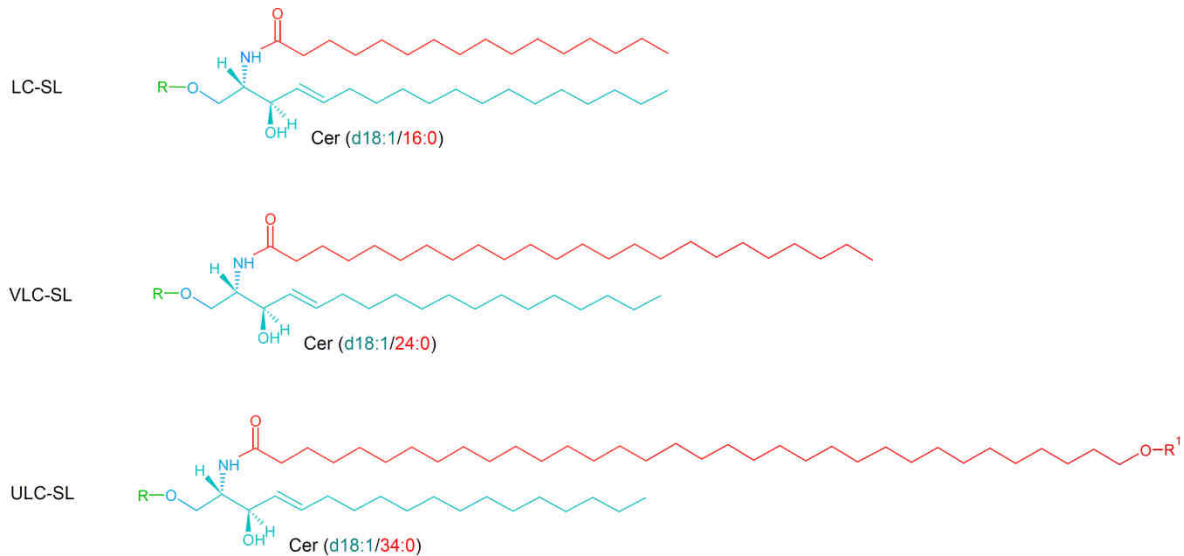


Figure 6 Acyl FA chain length in sphingolipids. Plasma membrane sphingolipids (SLs) typically contain FAs with chain lengths of C16 (palmitic) to C24 (nervonic) (red) amide-linked to the sphingoid base (blue) and are designated here as long chain (LC-) and very long chain (VLC-) SLs. The sphingolipid class is determined by the head group R1. However, in the epidermis differentiated keratinocytes produce SLs with ultra long chain (ULC-) FAs with 32 to 36 carbons, which may be hydroxylated in the terminal ω position. The ω -hydroxyl group may be esterified to an additional FA, typically linoleic acid (C18:2, ω -6), designated here as R2. The ULC-SL depicted here contains C34:0 geddic acid, which is the most abundant ULC-FA in epidermal ω -hydroxylated Cers. Scheme modified from (Rabionet 2011).

The lipid modification in the higher epidermal layers is important for barrier formation in skin. ULC-FAs and to some extent also LC and VLC-FA, are esterified in differentiating keratinocytes to form Cers and used in compartments such as the trans-Golgi network, LBs, CE, or within corneocyte interstices (Vielhaber et al., 2001). ULC-FA may be saturated or mono-unsaturated and are to a great extent hydroxylated either at the α or the ω position (Jennemann et al., 2012). This ω -hydroxy group of a ULC-SL can either be esterified with an additional FA, predominantly linoleic acid (C18:2, ω -6) or to a protein side chain on corneocytes to establish the cornified lipid envelope, a prerequisite for epidermal barrier formation (Uchida and Hamanaka, 2006).

Cholesterol, free FAs and (ULC) Cers are the major lipid classes in epidermis. Thereby Cers comprise almost half of the total SC lipid mass by weight (Hamanaka et al., 2002; Weerheim and Ponc, 2001). Additionally to differences in the FA moiety variations in the sphingoid backbone give rise to more than 340 different Cer species that have been described in the SC (Masukawa et al., 2008). As shown in Figure 7, a commonly used scheme distinguishes between nonhydroxylated FAs (NS), α -hydroxy FAs (AS), and ω -hydroxy FAs (OS), which in turn, might be esterified to a protein amino acid side chain (POS) or to an FA (EOS). Recently, our group has identified a complete new class of epidermal ceramides, which differ from the “classical” and above described species by esterification in 1-O-position. This novel class of 1-O-acylceramides (1-O-AcylCers) contains saturated LC- to VLC acyl residues in both N- and O-position. They could be described in murine as well as in human epidermis (Figure 7) (Rabionet et al., 2013, 2014).

Approximately 62% of SC Cers are hydroxylated (subclasses AS, OS, EOS, POS) (Hamanaka et al., 2002), whereas AS- and minor NS-Cers do not contain ULC-FAs and are typically linked to saturated FAs with 16 to 26 carbon atoms (Coderch et al., 2003). Hydroxylated Cers with acyl chain lengths longer than C26 are primarily ω -hydroxylated and can be esterified to FAs (EOS) or to proteins on corneocytes (POS), thereby establishing the already mentioned CLE. In Gaucher’s disease and related mouse models, loss of OS-type Cers, particularly POS, coincide with severe epidermal barrier defects (Doering et al., 1999), indicating the significance of these Cers and the CLE for barrier function (Jennemann et al., 2012). EOS-Cers are the most abundant Cer class in the epidermis. In human epidermis for example ~95% of the EOS are ω -linked to linoleic acid, but in mouse epidermis only 45% (Uchida and Hamanaka, 2006).

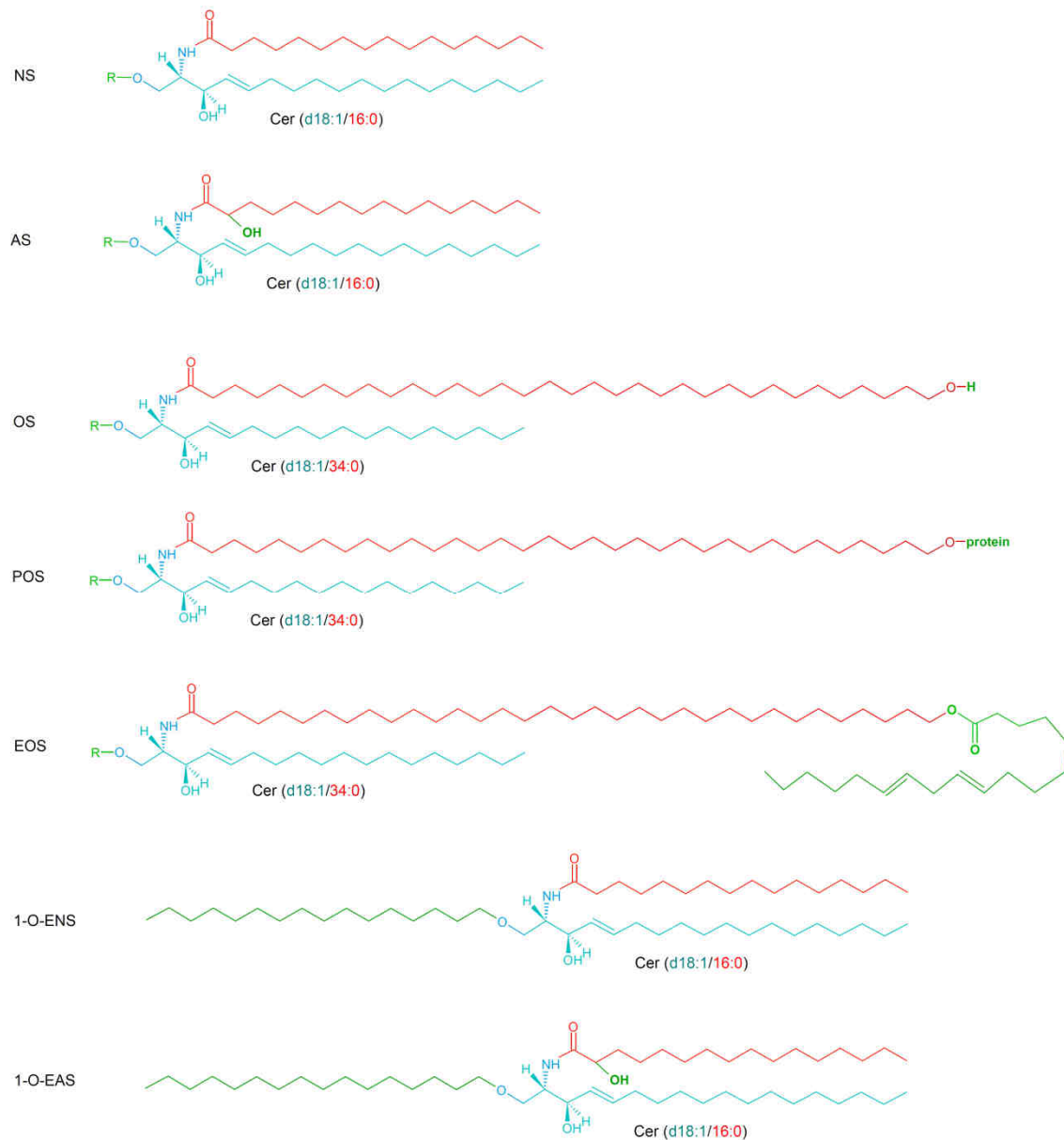


Figure 7 Major epidermal ceramide subclasses distinguished by acyl FA chain length and hydroxylation. In keratinocyte-produced ceramides the amide-linked FA residues with chain lengths of C16 (palmitic) to C26 (cerotic) are typically nonhydroxylated (NS) or α -hydroxylated (AS). The ceramides with FA chain lengths of C32 (lacceroic) to C36 (hexatriacontylic) generally carry a ω -hydroxy group (OS), which may be esterified to a protein sidechain (POS) or the unsaturated FA linoleic acid (EOS).

I.1.1.1.1 Elovl

The elongation of FAs beyond 16 carbon atoms length is catalyzed by members of the elongation of very long chain fatty acids (*elovl*) gene family. In the ER the elongation of palmitate to LC-, VLC- and ULC-FAs is achieved during a four step reaction cycle that

involves the Elovl enzymes as the first regulatory condensing enzyme (Figure 8). Malonyl-CoA is used as an acyl donor for the addition of two-carbon units to a FA acyl-CoA and thereby generates 3-ketoacyl-CoA by means of decarboxylation. The 3-ketoacyl-CoA reductase catalyzes the reduction of the carbonyl group yielding in 3-hydroxyacyl-CoA. Finally dehydration results in the synthesis of *trans*-2-enoyl-CoA, which is reduced to generate the elongated acyl-CoA.

In mammals, the Elovl family consists of seven members (Elovl1-7), which are described as localized within the ER membrane (Guillou et al., 2010). Elovls exhibit a preference for the acyl-CoA substrates depending on their chain length and degree of unsaturation (see Table 14). Regarding the latter, Elovls can be classified according to their specificity for utilizing saturated and monounsaturated FAs as substrates, namely Elovl6 (C16 and C16:1), Elovl1 (C18–C24), Elovl3 (C18–C24, both saturated and monounsaturated) and Elovl7 (C18–C22). Polyunsaturated LC-FAs are preferably processed by Elovl5 (C18–C20) and Elovl2 for VLC-FAs (C20–C24). The biosynthesis of epidermal FAs longer than 24 carbon atoms exclusively depends on Elovl4 (Agbaga et al., 2008; Guillou et al., 2010; Jakobsson et al., 2006). In 2008, *in vitro* studies using Elovl4 overexpressing cells could show that it is required for the synthesis of saturated and polyunsaturated ULC-CoAs (Agbaga et al., 2008).

Table 14 Tissue distribution and substrate specificity of the Elovl proteins. Tissue expression and substrate preferences of the Elovl proteins described in this table were obtained from (Guillou et al., 2009; Leonard et al., 2004). Lipid profile changes due to depletion of Elovl3 is associated with triacylglycerides (Westerberg et al., 2004). Cig30: cold- inducible glycoprotein of 30 kDa; Helo1: homolog of yeast long chain polyunsaturated fatty acid elongation enzyme *1: S: saturated; M: monounsaturated; P: polyunsaturated. *2: BAT: brown adipose tissue; WAT: white adipose tissue; Seb. glands: sebaceous glands.

Enzyme name	Synonyms	Tissue mRNA expression	Fatty acyl-CoA substrate	
			Carbon Nr.	Saturation level*1
Elovl1	Ssc1	Brain, ubiquitous	18-24	S,M
Elovl2	Ssc2	Testis, liver	20-24	P
Elovl3	Cig30	² BAT, WAT, seb. Glands, liver	18-24	S,M
Elovl4		Retina, brain, skin	28-30	S,P
Elovl5	Helo1	Liver, testis, ubiquitous	18-20	P
Elovl6		Liver, WAT, ubiquitous	16	S,M
Elovl7		Kidney, pancreas, ubiquitous	18-24	S,M

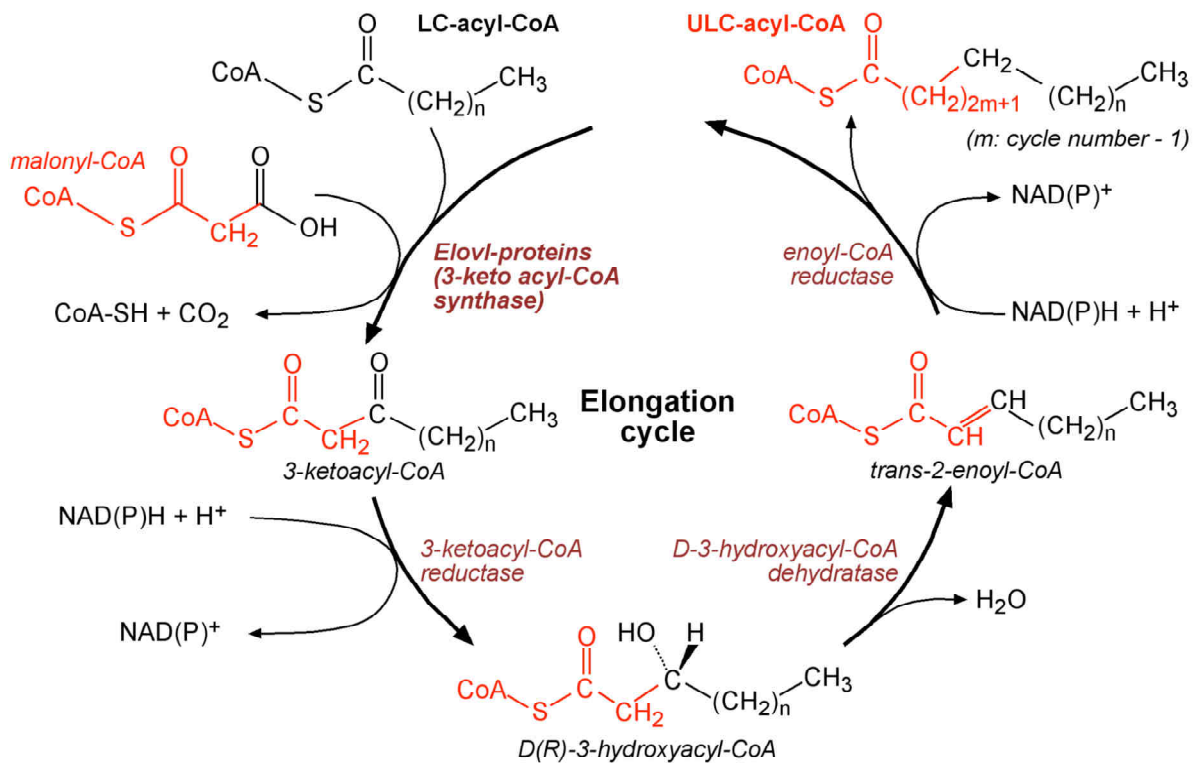


Figure 8 Synthesis of LC-, VLC- and ULC-CoAs by elongation cycle of FAs. Elovl proteins residing in the ER catalyze the rate-limiting step of the fatty acid synthesis consisting of the condensation of a precursor fatty acid with malonyl-CoA. The formed 3-ketoacyl-CoA derivative is reduced, dehydrated and further reduced resulting in the formation of a fatty acyl-CoA with an additional two-carbon unit in its chain. From (Sandhoff, 2010).

To date, mouse models for each of the Elovl proteins have been investigated with the exception of Elovl7. *In vivo* only the disruption of Elovl4 and Elovl1 caused a lethal skin phenotype. Elovl4 mutant mice were identified to suffer a form of Stargardt disease, as well as Elovl4-deficient mice were phenotypically described with a scaly, wrinkled skin combined with dramatic impairment of the water permeability barrier. Lipid profiles revealed Elovl4 mutant mice to be devoid of epidermis-essential ULC-ceramides (Cameron et al., 2007; Li et al., 2007; McMahon et al., 2007; Vasireddy et al., 2007). On the other hand within Elovl1-deficiency reduction of ω h-ceramides was not as severe. Nevertheless, Elovl1-knockout mice died shortly after birth due to epidermal barrier defects including degraded SC lipid lamellae. Interestingly, only VLC-sphingomyelins were lost while VLC-ceramides even increased (Sassa et al., 2013). Disruption of Elovl3 in mice resulted in an increased transepidermal water loss, accompanied by a sparse hair coat, a hyperplastic pilosebaceous system and disturbed hair lipid content. FA metabolism was affected concerning neutral lipids rather than ceramides, which in combination with the confined Elovl3 expression in sebaceous glands and epithelial cells of the hair follicles, suggested the requirement of Elovl3 for the elongation of FAs in hair lipids (Westerberg et al., 2004a).

I.1.1.1.2 CerS

In mammals, six homologue genes are known to be part of the ceramide synthase family (CerS1–6). Whereas a single enzyme appears to encode for a ceramide synthase in *D. melanogaster* (Bauer et al., 2009), three homologues are required in *C. elegans* (Menuz et al., 2009) and *S. cerevisiae* (Schorling et al., 2001; Vallée and Riezman, 2005). The mammalian CerS are characterized by their distinct preferences towards length and saturation grade of acyl-CoA substrates similar to the Elovl proteins. In addition, they exhibit a tissue-specific distribution pattern, which has been described in several reviews (Mizutani et al., 2009; Mullen et al., 2012; Tidhar and Futerman, 2013). Table 145 gives an overview about the properties of the CerS family.

CerS5 and CerS6 for example exhibit their highest affinity for C16-CoA (Mizutani et al., 2005; Riebeling et al., 2003), whereas CerS1 prefers C18-CoA (Venkataraman et al., 2002). CerS4 uses mainly C18 to C22 acyl-CoAs for esterification, but *in vitro* activity studies demonstrate that it is also capable of the synthesis of C24- and C26-ceramides. Similarly, CerS2 exhibits a broad affinity towards VLC- acyl residues ranging from C20 to C26 carbon atoms (Laviad et al., 2008). Among the CerS family, ceramide synthase 3 (CerS3) has been identified to specifically synthesize VLC/ULC-Cers in testis and epidermis (Jennemann et al., 2012; Laviad et al., 2008). Deficiency of CerS3 in mice revealed the lack of 90% of epidermal ceramides including all ω -esterified ceramides. It was demonstrated that the absence of ω -Cers triggers an epidermal maturation arrest at an embryonic pre-barrier stage. Alterations in CerS3 mutant mouse skin include discontinuity of ELL, impairment of the CLE, hyperkeratosis, persistence of the periderm, non-peripheral corneodesmosomes (CDs) and defective profilaggrin processing. Consequently, epidermal and antimicrobial barrier is disrupted leading to pathogen invasion (*Candida albicans*) and death shortly after birth (Jennemann et al., 2012). CerS3 function cannot be replaced by one of the other five CerS, as shown in cell culture experiments (Jennemann et al., 2012). Similarly to the affinity of CerS3, Elovl4 is preferentially elongating FA to the length of ULC-acyl residues (Agbaga et al., 2008). Ceramide synthesis depends on both, the Elovls and the CerS, which makes an enzyme complex likely. Overexpression of Elovl1 with CerS2 in HEK 293 cells leads to ceramides with C22- and C24-acyl chains, whereas the combination of CerS3 with Elovl1 shifts acyl chain length in ceramides to C24- and to C26-acyl chains (Sassa et al., 2013). Elovl1 knockout mice exhibit neonatal lethality due to water loss caused by impaired epidermal barrier formation, additionally total amount of Cer was decreased to $\geq 45\%$. Also, levels of ULC-FA-containing Cers (C26 to C36) were significantly decreased in the knock- out mice.

This suggests the possibility of isozyme switching from CerS2 to CerS3 during keratinocyte differentiation which drives Elovl1 to synthesize C26-CoAs, further elongated by Elovl4 to generate Cers with \geq C26 ULCFAs and ω -O-acyl Cers (Sassa et al., 2013).

Table 15 Tissue distribution and substrate specificity of the CerS proteins. Tissue expression was summarized from (Laviad et al., 2008). Lass: longevity assurance homolog; Uog1: upstream of GDF1; Trh: translocating chain-associating membrane protein homolog; T3L: Trh3-like protein.

Enzyme name	Synonyms	Tissue mRNA expression	Acyl-CoA substrate Nr. of C-atoms	References for substrate affinity
CerS1	Lass1, Uog1	Brain, skeletal muscle	18	(Venkataraman et al., 2002)
CerS2	Lass2, Trh3	Kidney, liver	22-24	(Laviad et al., 2008)
CerS3	Lass3, T3L	Testis, skin	26-36	(Sandhoff, 2010)
CerS4	Lass4, Trh1	Liver, heart, skin	18-22	(Riebeling et al., 2003)
CerS5	Lass5, Trh4	ubiquitously	16-18	(Riebeling et al., 2003)
CerS6	Lass6, Trh1-like	Intestine, kidney, ubiquitously	14-16	(Mizutani et al., 2005)

I.1.2 Skin barrier defects

The epidermal barrier is stabilized by TJs (Furuse et al., 2002; Kirschner et al., 2010) but also by the lipids and the lipid-embedded corneocytes in the SC (Elias, 2005). The lipid matrix around the corneocytes is composed of Cers, cholesterol and free FAs (50%, 25% and 15% respectively). Minor components of this barrier are cholesterol-sulfates (2-5%), which regulate protease activity during desquamation (Elias et al., 1984; Sato et al., 1998) and free sphingoid bases, important lipids for microbial defense (Nagpal, Patel, and Gibson 2008; Nenoff and Haustein 2002; Candia D. Payne, Ray, and Downing 1996; Veerman et al. 2010; P W Wertz 1992; Bibel, Aly, and Shinefield 1992).

Lipid barrier formation begins with Cer formation at the ER in keratinocytes by CerS and Elovl proteins. This key step is followed by various processes, such as precursor lipid processing and lamellar arrangement of OS/EOS-GlcCers within LBs and finally exocytosis of the LB content into the extracellular space. There GlcCers and SMs are converted back into their corresponding Cers by the action of GlcCerases and acid SMases. Furthermore, FAs, glycerol and cholesterol are released (from phospholipids and cholesterol esters, respectively) by the secretory phospholipase A2 (sPLA2) and cholesterol sulfatase. These components,

together with Cers (OS, EOS), establish the extremely hydrophobic extracellular lipid lamellae (ELL) of the skin barrier (Candi et al., 2005).

Mutations or loss of function of the involved enzymes, result in severe skin barrier defects. In Gaucher's disease for example depletion of GlcCerase or its activator protein prosaposin leads to inhibition of GlcCer processing and of Cer formation and consequently to impaired lipid lamellar membranes and WPB loss (Doering et al., 1999). Loss-of-function mutations in the gene encoding for the keratinocyte transporter ABCA12, which supports lamellar arrangement of EOS-GlcCers, have been described for lamellar ichthyosis type II (LI2) as well as harlequin ichthyosis (HI). Both are severe autosomal recessive congenital ichthyoses (ARCI), characterized by hyperkeratosis and permeability barrier loss. Ichthyotic lesions revealed an accumulation of EOS-GlcCers, whereas EOS-Cers were significantly reduced (Zuo et al., 2008).

The important role of Cers, in skin barrier function has been determined by *in vivo* and *in vitro* studies of cutaneous disorders such as ichthyosis, lysosomal storage diseases, psoriasis and AD. These diseases may result from environmental factors such as allergens and irritants (UV radiation, detergents, carcinogenic agents, and stress) but are also the result of genetic defects affecting proteins of the lipid metabolic pathways. Ichthyosis comprises a heterogeneous family of dry hyperkeratotic skin disorders but may also be a symptom of more systemic diseases such as lysosomal storage diseases (e.g., Gaucher's disease or Niemann-Pick disease) (Doering, Thomas; Proia, Richard L.; Sandhoff, 1999, McGovern & Schuchman, 2009). In Gaucher's disease a defect in the GlcCerase enzyme disturbs the GlcCers degradation pathway, resulting in loss of Cers and POS-Cers and followed by permeability barrier breakdown. Congenital ichthyosis (CI) are diseases with deficits in Cer and FA processing, leading to epidermal WPB loss, like for example by mutations in genes encoding for the ABCA12 transporter (Akiyama et al., 2005; Jobard, 2002). Psoriasis is a complex inflammatory skin disease of unknown etiology, which may derive from genetic (e.g., *flg* gene mutation), infectious or environmental (e.g., stress) factors. Psoriatic lesions are characterized by a thickened dry scaling skin and basal inflammation. The overall reduction of Cers in some psoriatic patients has been related to a decrease in SPT activity and reduced *de novo* Cer synthesis (Hong et al., 2007). Moreover, atopic dermatitis (AD) is a chronic relapsing inflammatory skin disorder, also of unknown etiology. For long time, AD was regarded as an immune-mediated disease until *flg* gene mutations leading to disturbed barrier function were shown to be associated with atopy in some populations (Palmer et al., 2006).

Patients suffering from AD display dry, itchy skin with inflammatory rashes, and have a high risk for bacterial or viral infections, about 4-fold higher than in psoriasis (Elias, 2005). In both diseases, depletion of POS-Cers and an impaired lamellar organization were considered to be responsible for the subsequent WPB breakdown (Macheleidt et al., 2002).

I.1.3 Antimicrobial barrier

In the protection from microbial organisms the innate immune system plays a number of crucial roles (Holmskov, 2000; Medzhitov and Janeway, 2000a) and can for example also limit the infection prior to the induction of adaptive immune responses. It also designates the appropriate response type and effectors of the adaptive immune system appropriate for the infecting pathogen (Bendelac and Fearon, 1997; Medzhitov and Janeway, 2000b, 1998). The ability of the innate immune system to detect infectious microorganisms and to induce a set of endogenous signals like the secretion of cytokines by macrophages and natural killer cells is important for proper immune function (Fearon, 1997; Unanue, 1997). Innate host defense components range from simple inorganic molecules (e.g., hydrochloric acid, peroxidases, and nitric oxide)(Song et al., 2000) up to defensins (defensin HBD1 (Mathews et al., 1999; Weinberg et al., 1998)). Under normal resting conditions, antimicrobial peptides are thought to be produced by keratinocytes near potential points of microbial entry, such as around hair follicles (Ali et al., 2001; Dorschner et al., 2001). But after physical damage to the skin barrier a quick elevation in antimicrobial peptide synthesis (Imokawa, 2001) is observed. In addition to direct antibacterial action, these peptides are also chemotactic and can attract leukocytes to sites of infection (Dale, 2002; Gallo et al., 2002). It has been suggested that the function of the innate immune system and its components may not to eliminate infective bacteria, but to limit their growth while signaling and activating the adaptive immune system (Drake et al., 2008). The migration of leukocytes to a site of infection, subsequent phagocytosis by macrophages and neutrophils and thereby activating the adaptive immune system would complete the response.

Specific (LC-) SLs are key players in antimicrobial defense mechanisms of the skin. They derive either from mature keratinocytes in the epidermis, or from sebaceous glands (Drake et al., 2008; Gallo et al., 2002; Wertz and Downing, 1990). Burtenshaw showed in the 1940s that lipid extracts from the skin surface have the ability to kill *Staphylococcus aureus in vitro*, and it was thought that free fatty acids were the active agent (Burtenshaw, 1942). In addition

to a potential role for antimicrobial FAs, studies have demonstrated high amounts of free sphingoid bases (So, dihydrosphingosines, 6-hydroxysphingosines) in the stratum corneum (Stewart and Downing, 1995; Wertz and Downing, 1990). Several studies have demonstrated that these LC-bases are potent antimicrobials also against *candida albicans* (Bibel et al., 1989, 1995; Payne et al., 1996). Antimicrobial epidermal lipids are also a part of the innate immune system of the skin. Lauric acid, sapienic acid, and the sphingoid bases are all present at the skin surface, and all have documented antibacterial activity against various potential skin pathogens (Drake et al., 2008). In addition to the free ceramides in the intercellular spaces of the SC the covalently bound ceramides of the cornified envelope may also be a source of these LC-bases.

Patients with atopic dermatitis are colonized with *S. aureus*, similarly to psoriatic patients, but suffer a much higher incidence of skin infection (30% vs. 7%)(Christophers and Henseler 1987; Ong et al. 2002). An inverse correlation has been demonstrated between the free sphingosine level and the quantitative carriage of *S. aureus* in AD (Strum et al., 1997). Also in AD, the level of ceramides in the stratum corneum is reduced, owing to a defect in sphingomyelin and glucosylceramide metabolism resulting in lower levels of free sphingosine (Imokawa, 2001).

In contrast So (and Cer), S1P has been implicated in mediating cell proliferation and antagonizing Cer-mediated apoptosis (Spiegel and Kolesnick, 2002). A model has been proposed in which the balance between the intracellular levels of Cer and S1P, i.e. the 'Cer/S1P rheostat', could determine whether a cell survives or dies (Spiegel and Kolesnick, 2002). S1P is also known to regulate cell migration through binding to its cell surface receptors (S1P₁₋₅) (Hla, 2003; Spiegel and Kolesnick, 2002). S1P is abundant in plasma and is physiologically important, especially in the vascular and immune systems (Hla, 2003; Hwang et al., 2005). S1P signaling is also involved in the immune system (Japtok and Kleuser, 2009; Spiegel and Milstien, 2011), which was shown by the discovery of the potent immunosuppressive drug FTY720, which is phosphorylated in vivo and binds to S1P receptors (Brinkmann et al., 2002). Studies with mice whose haematopoietic cells lack the receptor S1P1, demonstrated that it is essential for lymphocyte recirculation from the thymus and lymph nodes and that phosphorylated FTY720 can induce the down-regulation of S1P1 on lymphocytes and inhibits their recirculation (Allende et al., 2004; Matloubian et al., 2004). Thus, it is well investigated that the egress of T- and B-cells from lymphoid organs and their localization in these organs are mediated by S1P signaling (Allende et al., 2004; Brinkmann et

al., 2002; Kabashima et al., 2006; Matloubian et al., 2004). On top, S1P is involved in the modulation of several functions of natural killer cells, neutrophils, mast cells, macrophages and DCs (Allende et al., 2011; Martino, 2007; Olivera and Rivera, 2011; Walzer et al., 2007; Weigert et al., 2009). Most recently, it has been shown that S1P influences Langerhans cell (LCs) homeostasis (Christensen and Haase, 2012; Röse et al., 2012). It has been suggested that S1P inhibits LC migration in contact hypersensitivity mice (Gollmann et al., 2008).

1.1.3.1 Langerhans cells

A number of specialized antigen presenting cells (APCs) is located in the skin, which belong to the family of classical dendritic cells (DCs). In the skin, one such group of DCs is the Langerhans cell population. They can recognize and capture foreign haptens and are therefore important cells for a first immune answer (Christensen and Haase, 2012; Japtok et al., 2012; Kaplan, 2010; Steinman, 2007). After recognition of foreign molecules, LCs migrate to skin-associated lymph nodes and cross-communicate with T-lymphocytes. As LCs are able to initiate immune answers they have been discussed as central causes in the development of allergic contact dermatitis ACD (Christensen and Haase, 2012; Kaplan et al., 2012). In a contact hypersensitivity (CHS) model to examine causes of ACD, it was described that topically applied S1P inhibited the inflammatory reaction of CHS (Reines et al. 2009; Christensen and Haase 2012; Röse et al. 2012). It was suggested that S1P inhibits LC migration after antigen capture to the draining lymph node via the S1P1 receptor subtype (Gollmann et al., 2008; Reines et al., 2009). Topical administration of S1P in high concentrations could induce a S1P1 receptor internalization leading to reduced LC migration suggesting a treatment possibility of ACD with S1P (Japtok et al., 2012). Recently it was also shown that S1P inhibits the ability of LCs to capture antigen with participation of the S1P2 receptor subtype (Japtok et al., 2012). S1P is produced from So by sphingosine kinases (SphK) from which two types are known (SphK1 and SphK2) (Kihara et al., 2006; Liu et al., 2002). A multiply of signaling pathways branching from S1P are known and this complexity can be explained by the fact that it functions not only intracellularly but also acts as a ligand of G-protein coupled receptors (GPCRs), when it is secreted into the extracellular environment.

I.2 Results

Certain SC lipids have been suggested to have antimicrobial activity also against *candida albicans* (Arikawa et al., 2002; Bibel et al., 1989, 1992; Drake et al., 2008; Fischer et al., 2013). Among them, decreased sphingosine levels have been suggested to play a significant role in the vulnerability of microbial infections in patients suffering atopic dermatitis or psoriasis which are phenotypically colonized with pathogens (Ong et al., 2002). This reduction in sphingosine concentration in diseased SC could be a consequence of diminished ceramide turnover.

I.2.1 Method development for quantification of sphingoid bases

Analyzing endogenous levels of sphingoid bases from complex biological samples requires highly sensitive and compound-specific methods. Liquid chromatography/tandem mass spectrometry (LC/MS/MS) using electrospray ionization (ESI) is suitable for the reliable simultaneous analysis of multiple compounds because of its high specificity and sensitivity.

The first report of LC/MS/MS for the quantitative analysis of sphingolipids was by Mano et al. in 1997. They simultaneously analyzed SMs, Cers, So, and other compounds in cultured cells. However, the chromatographic peak for phosphorylated sphingosine was broad in selected reaction monitoring (SRM) mode, and several other publications have also reported this problem (Bielawski et al., 2009; Yoo et al., 2006). The peak broadness can be caused by binding of the phosphorylated group to residual metal ions in the silica gel by a coordinate bond as well as by zwitter-ionic properties of the compounds. The use of a certain pH and an organic synthetic polymer as stationary phase can inhibit this peak-tailing effect in LC with silica gel (Saigusa et al., 2012). However, methods using polymer-based columns often have issues with reproducibility (Saigusa et al., 2012).

A method for the simultaneous detection of all endogenous sphingoid bases is required, because S1P and So are thought to work in an agonistic manner (Rosen et al., 2009). Using a hydrophilic interaction chromatography (HILIC) column, is a possibility which is often used for the analysis of small hydrophobic compounds. However, HILIC columns perform poorly in the separation of hydrophilic compounds such as phospholipids, and often induce ion suppression (Cutignano et al., 2010; Saigusa et al., 2012). C18-based columns separate phospholipids well, and a simultaneous detection method for sphingoids in several types of

tissue should be developed using this type of column. Other methods for the determination of So use gas liquid/MS, HPLC, and LC/MS/MS (Crossman and Hirschberg, 1977; Iwamori et al., 1979; Scherer et al., 2010). However, these methods were not applied to other sphingoids and their phosphates and required sample derivatization.

Saigusa et al. (Saigusa et al., 2012) were the first to describe a method in which they addressed the peak-tailing problem of S1P, and established a simple and effective method for the simultaneous quantification of seven sphingoids using a simple methanol deproteinization and LC/MS/MS. They used a Capcell Pak C18 ACR column (1.5 mm i.d. × 250 mm, 3 μm, Shiseido) to obtain good peak shapes. Nevertheless we were not able to reproduce these data by applying this method on our instrument (Acquity UPLC® I-class, Waters) and by using a C18-BEH column (2.1 mm i.d. × 50 mm, 1.7 μm, Waters).

In 2011 an application note of waters was published (Isaac et al., 2011) in which they described the use of a Ultra Performance Liquid Chromatography (UPLC®) with Charged Surface Hybrid (CSH™) C18 Technology. This column shows superior performance over traditional reversed-phase techniques and gives fast, sensitive separation of lipids based upon their acyl chain length, and the number, position, and geometry of double bonds providing an attractive solution for analyzing complex lipid mixtures in biological samples and comparative lipidomic analysis.

Additionally of performing on a CSH column to increase quality of peak shape we decided to use citrate in the sample solvent as metal ion-mobilizing additive (Seidler et al., 2011). With this method we were able to increase peak quality for all measured sphingoid bases as shown in Figure 9 and Figure 10.

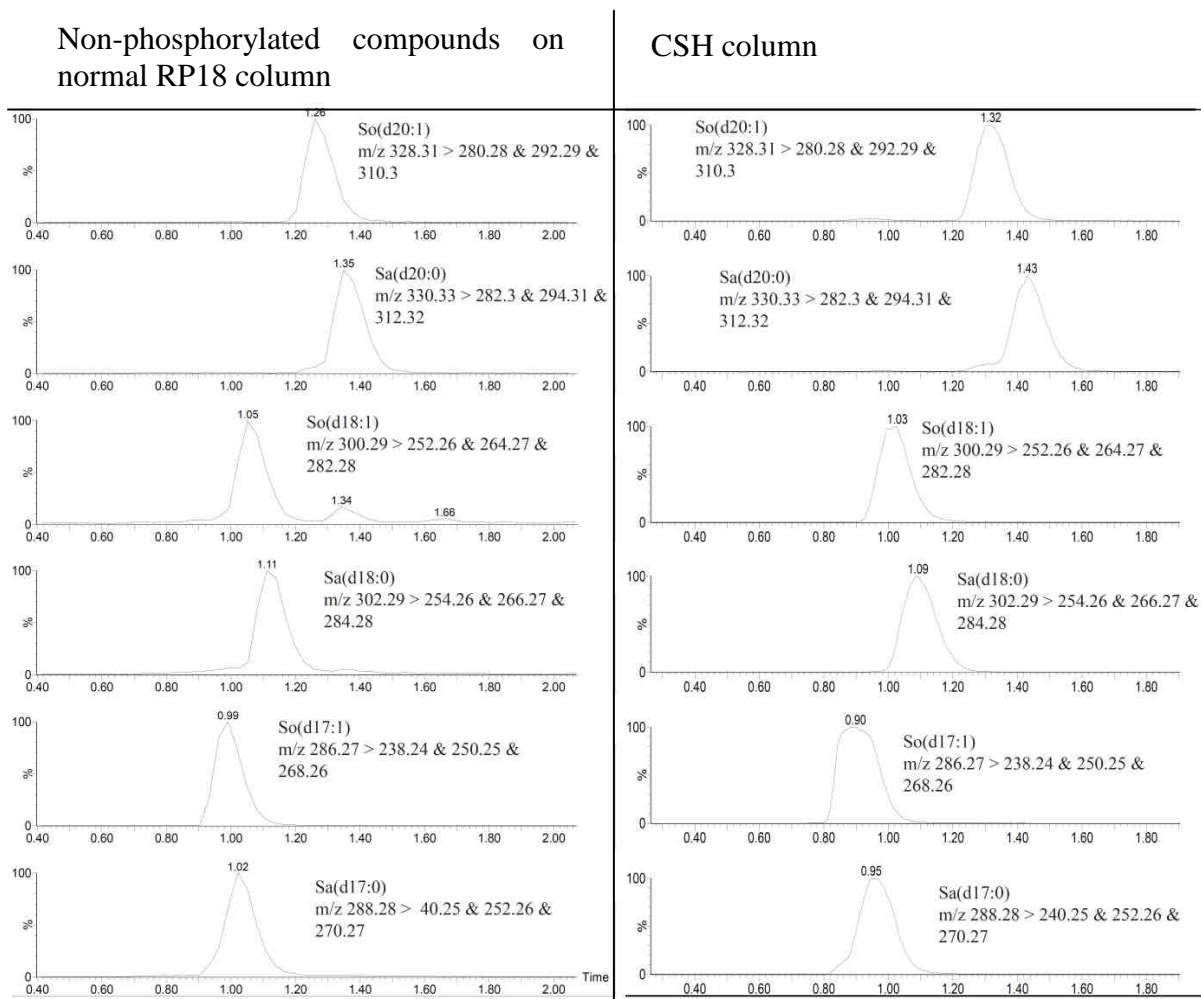


Figure 9 Chromatogram of non-phosphorylated sphingoid bases without and with CSH column. Using of CSH columns improves the peak shape

In the chromatograms of both, the non-phosphorylated and phosphorylated sphingoid bases, you can see the comparison of measurements of defined amounts of standard substances on a normal RP-18 column in opposite to the measurements on a CSH- column. For non-phosphorylated sphingoid bases like Sphingosine (d17:1; d18:1; d20:1) and Sphinganine (d17:0; d18:0; d20:0) with peak widths of 0.3 min, there is hardly any improvement to be seen, but that the peak shape is improved. For the corresponding 1-phosphates peak tailing can be strongly reduced and peak width shortened.

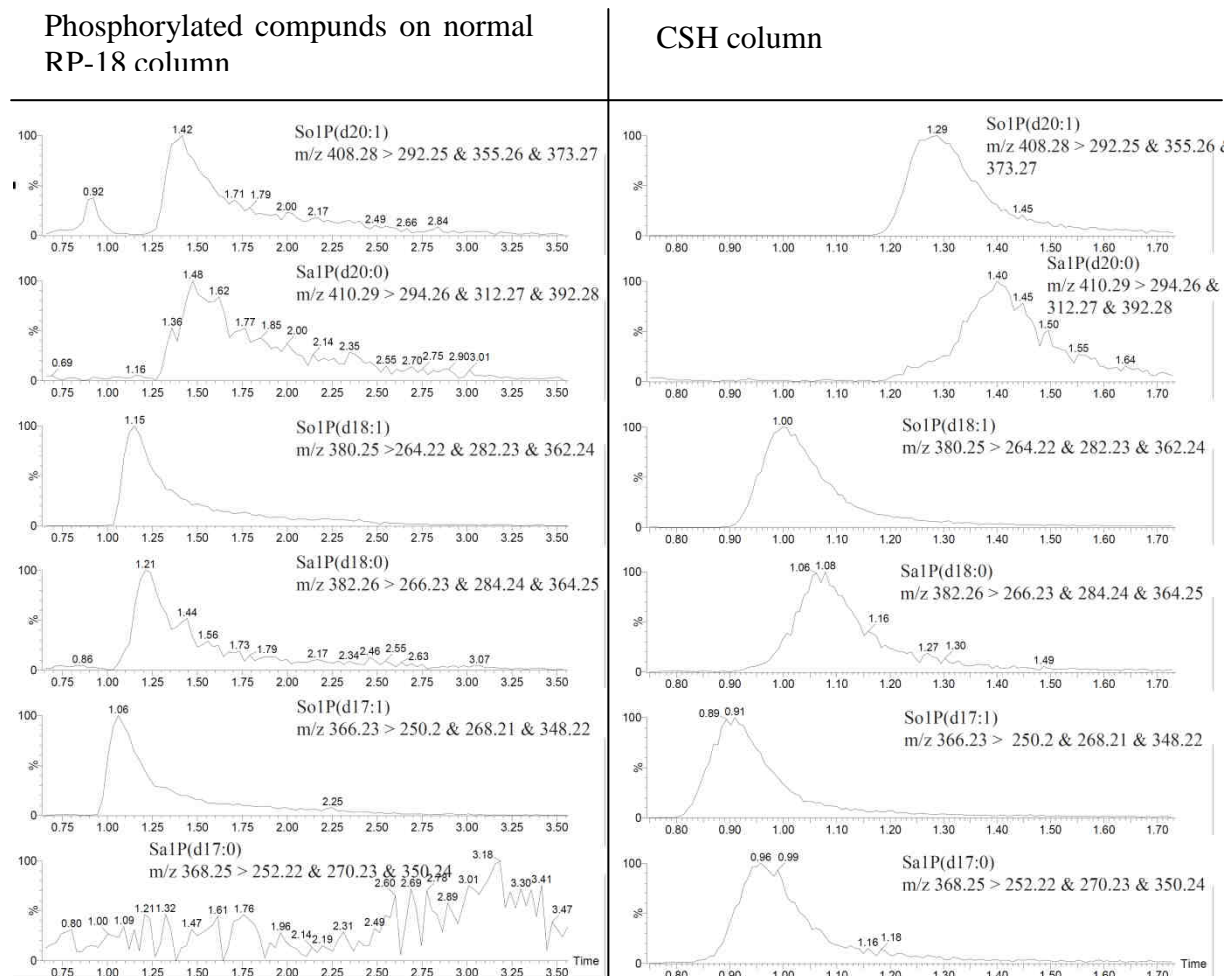


Figure 10 Chromatogram of phosphorylated sphingoid bases without and with CSH column. Using of CSH column improves both peak shape, by suppressing peak tailing, and resolution.

By using the CSH- column peak widths for the phosphorylated compound could be improved. Peak widths of 1.25 up to 1.75 min can be shortened to 0.3 min, hence by factor 4 for all compounds. For SaIP (d17:0) a signal can be detected with the CSH column, where was none by using a RP18 column. Nevertheless, peak tailing can't be completely inhibited but greatly improved. Furthermore it could be assured that the saturated and unsaturated forms of each compound are eluting at different time points so that no peak overlapping occurs. For both the phosphorylated and non- phosphorylated, the saturated compounds elute approximately 0.5-0.1 min later.

LC and MS condition details can be found in Table 16 and in materials and methods.

Table 16 LC and MS conditions for measurement of sphingoid bases

LC system: ACQUITY UPLC Column: ACQUITY UPLC CSH C18, 2.1 x 100 mm, 1.7 μ m Column temp: 55 °C Flow rate: 400 μ L/min Mobile phase A: Acetonitrile/water (60:40) with 10 mM ammonium formate and 0.1% formic acid Mobile phase B: Isopropanol/acetonitrile (90:10) with 10 mM ammonium formate and 0.1% formic acid Sample solvent: isopropanol/acetonitrile/ water (2:1:1); 50mM citrate	Gradient			
	Time [min]	Solvent A [%]	Solvent B [%]	Slope
	Initial	40	60	Initial
	2.0	57	43	linear
	2.1	50	50	concave
	12.0	46	54	linear
	12.1	30	70	concave
	18.0	1	99	linear
	18.1	60	40	linear
	20	60	40	concave

1.2.1.1 Method validation

LC/MS/MS was conducted on a Xevo TQ-S (Waters) triple quadrupole mass spectrometer equipped with an ESI source coupled to an Acquity I class UPLC. Out of product ion scans the transitions of each compound were determined. Main transitions of the $[MH]^+$ ions to their product ions are described in Figure 11 and were summed up for quantification procedure. For sphingoid bases and corresponding 1-phosphates three major transitions were observed and for Cer1P four major transitions, which are due to loss of water, formaldehyde, phosphoric acid and/ or the acyl chain. The operating conditions were then optimized for each compound by continuously infusing standard solutions dissolved in methanolic 5mM ammonium acetate (10.0 μ M) at a rate of 5 μ L/ min, while recording the respective transition with increasing collision energies. The optimized collision energies for the chosen transitions can be found in Table 17. ESI was performed in the positive ion mode for all compounds. Samples were analyzed in the SRM mode, using the transitions of the $[M+H]^+$ precursor ions to their product ions.

For sphingoid bases and ceramides the following fragmentation patterns, shown at the example of compounds with So(d18:1) as core structure, in MS are most prominent:

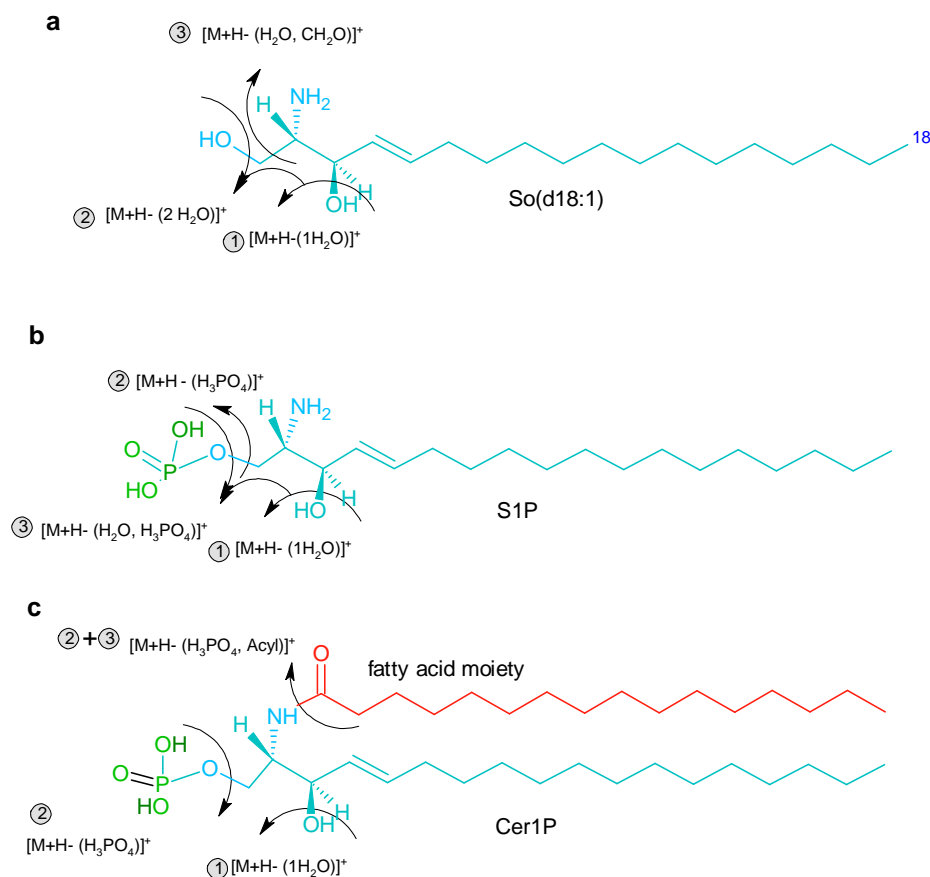


Figure 11 fragmentation patterns of standard substances. Shown are sphingosine(d18:1), S1P(d18:1) and a classical ceramide(d18:1;16:0). For So(d18:1) and S1P and corresponding compound three major transitions are observed and for Cer1P four major transitions, which are due to loss of water, formaldehyde, phosphoric acid and/ or the acyl chain.

a): for pure sphingoid bases without any esterification one or two water molecules can be cleaved off (1 and 2), or one water together with a formaldehyde molecule (3).

b): for sphingoid bases with phosphorylation at carbon atom 1, one water molecule (1), phosphoric acid (2) and water and phosphoric acid (3) can be cleaved off.

c): for ceramide-1-phosphates four different fragmentations are possible- one water molecule and phosphoric acid (1 and 2), both together (1+2), as well as phosphoric acid and the attached acyl-chain (1+3).

Table 17 Optimized collision energies and of major transitions of phosphorylated and free sphingoid bases.

	m/z of [M+H] ⁺	Transition to [M+H-1 H ₂ O] ⁺ / collision energy	Transition to [M+H -2 H ₂ O] ⁺ / collision energy	Transition to [M+H-(1 H ₂ O + CH ₂ O)] ⁺ / collision energy	
Sphingosine(d18:1)	300.282	282.26/4 eV	264.27/ 10 eV	252.28/8 eV	
Sphingosine(d17:1)	286.267	268.24/ 3eV	250.25/ 11eV	238.26/9eV	
sphingosine(d20:1)	328.314	31028/2eV	292.29/16eV	280.3/9eV	
Sphinganine(d18:0)	302.298	284.25/4eV	266.26/4eV	254.27/12eV	
Sphinganine(d17:0)	288.282	270.27/6eV	252.28/5eV	240.29/14eV	
Sphinganine(d20:0)	330.329	312.32/5eV	294.31/8eV	282.3/16eV	
		Transition to [M+H-1H ₂ O] ⁺ / collision energy			
1-deoxysphingosine(m18:1)	284.288	266.28/4eV			
1-deoxymethylsphingosine (m17:1)	270.272	252.27/5eV			
4-hydroxysphinganine(t17:0)	304.277	286.27/6eV			
		Transition to [M+H-1H ₂ O] ⁺ / collision energy	Transition to [M+H -H ₃ PO ₄] ⁺ / collision energy	Transition to [M+H - (H ₃ PO ₄ + H ₂ O)] ⁺ / collision energy	
sphingosine-1P(d18:1)	380.249	362.24/2eV	282.23/2eV	264.22/8eV	
Sphingosine-1P(d17:1)	366.233	348.23/2eV	268.22/2eV	250.21/9eV	
Sphingosine-1P(d20:1)	408.28	390.28/6eV	310.27/11eV	292.26/4eV	
Sphinganine-1P(d18:0)	382.264	364.26/2eV	284.25/2eV	266.24/8eV	
Sphinganine-1P(d17:0)	368.249	350.25/2eV	270.24/3eV	252.23/9eV	
Sphinganine-1P(d20:0)	410.296	392.29/2eV	312.28/0eV	294.27/10eV	
		Transition to [M+H-1H ₂ O] ⁺ / collision energy	Transition to [M+H -H ₃ PO ₄] ⁺ / collision energy	Transition to [M+H - (H ₃ PO ₄ + H ₂ O)] ⁺ / collision energy	Transition to [M+H - (H ₃ PO ₄ +R-COOH)] ⁺ / collision energy
Ceramide-1P(d18:1/16:0)	618.505	600.5/14eV	520.5/3eV	502.5/6eV	264.5/20eV
Ceramide-1P(d18:1/12:0)	562.442	544.4/16eV	464.4/2eV	446.4/4eV	264.4/22eV
Ceramide-1P(d18:1/24:0)	730.630	712.6/2eV	632.6/9eV	614.6/9eV -	264.6/28eV

Despite high precision, systematic errors can lead to variances between measured values and true values. Further method validation was achieved by considering and determination of the following typical validation characteristics: detection and quantification limit, linearity and range and reliability.

The linear dynamic range of each analyte was determined by calibration curves prepared with each standard alone, as well as in presence of mouse epidermal matrix. Standard rows were prepared in triplicate and also injected in triplicate. Linear regression on the calibration curves was performed. Sphingosine(d14:1), sphingosine-1-P(d17:1) and ceramide-1-P(d18:1;12:0) were chosen as internal standards as these compounds are low abundant in most tissues. The relative response factors (rRF) were calculated to correct for the real analyte concentration in samples as well as in standard curves. It is a measure of the relative mass spectral response of an analyte compared to its internal standard.

$$rRF = [Area(sample) \times theor.Conc.(IS)] / [theor.Conc.(sample) \times Area(IS)]$$

Each relative response factor (rRF) represents the slope of the line between the response for a given standard and the response of the concentration zero, the origin (Barra et al., 2014). The average calibration factor or relative response factor of the standards for each analyte is then used to calculate the concentration of the sample. For rRF values lying in a range between approximately 0.8 and 1.2 no correction of response is necessary (Chakravarthy et al., 2011). As most of the calculated values are out of this range, all calculated rRFs were used. The like this calculated rRF are listed below.

Table 18 List of calculated relative response factors (rRFs)

	mean rRF	% SD
So(d18:1)	2,04	10
So(d17:1)	2,74	8
So(d20:1)	1,49	10
Sa(d18:0)	1,98	17
Sa(d17:0)	1,41	11
Sa(d20:0)	0,69	8
1-deoxy-So(m18:1)	2,25	16
1-deoxymethyl-So(m17:1)	0,73	15
4-HydroxySa/PHS (t17:0)	0,22	49
So1P(d18:1)	3,02	20
So1P(d17:1)	1,33	6
So1P(d20:1)	0,42	5
Sa1P(d18:0)	0,18	29
Sa1P(d17:0)	0,46	30
Sa1P(d20:0)	0,14	14
Cer1P(d18:1,16:0)	0,81	7
Cer1P(d18:1,12:0)	1,17	9
Cer1P(d18:1,24:0)	0,77	10

These rRF values were then used to correct for the concentrations of the measured standard curves. Results can be seen for the sphingoid bases in Figure 12 and their 1-phosphates in Figure 14.

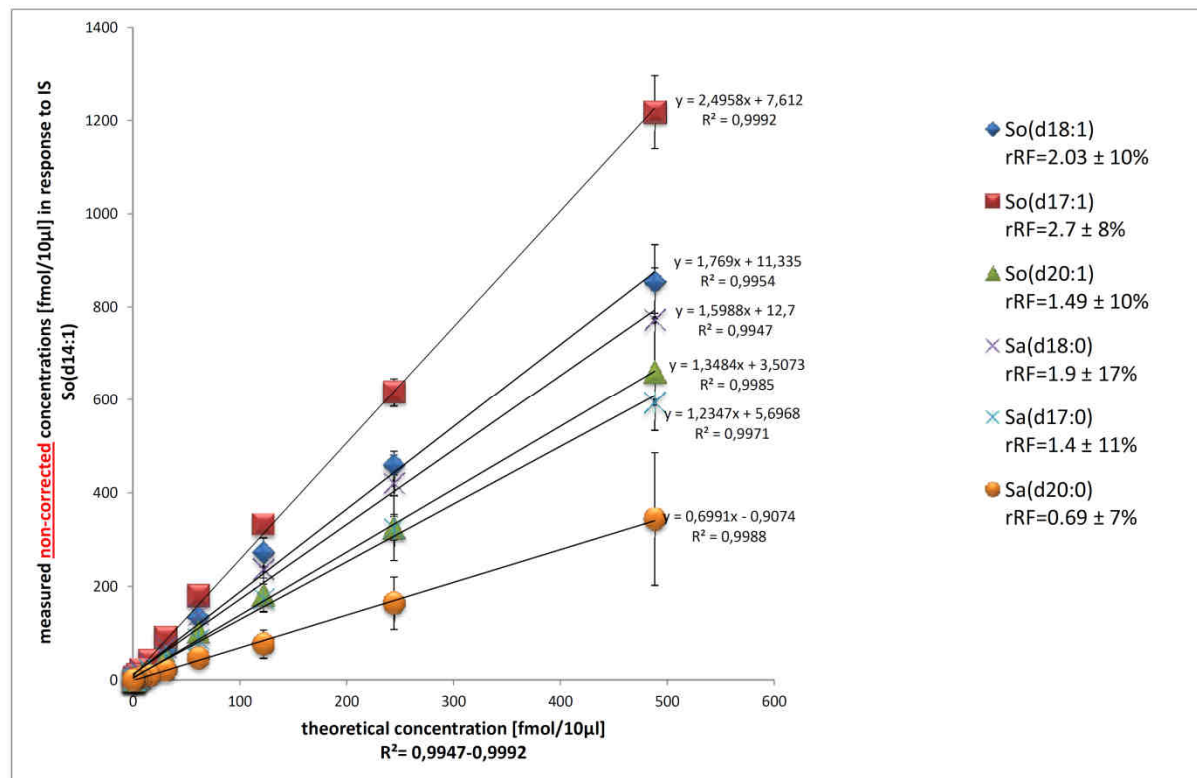


Figure 12 Calibration curves of available unphosphorylated standard substances. All curves have R² between 0,9947 and 0,9992. The relative response factor (rRF) was calculated out of these curves and used for correction of analyte concentration in samples. The volume of 10µl corresponds to the injection volume. n= 3 samples.

Calibration curves with a slope of 1 are optimal. With this method for non-phosphorylated sphingoid bases slopes between 0.7 and 2.5 are reached, whereas the coefficients of determination (R²) range from 0.995 to 0.999. Best response is found for So(d18:1) and weakest response is found for Sa(d20:0). It has to be considered that in these plots the uncorrected curves are shown, which directly reflects the quality of the response for each compound. Later on the rRF values were calculated out of these curves and they were applied for their correction. This results in corrected standard curves with a slope of 1

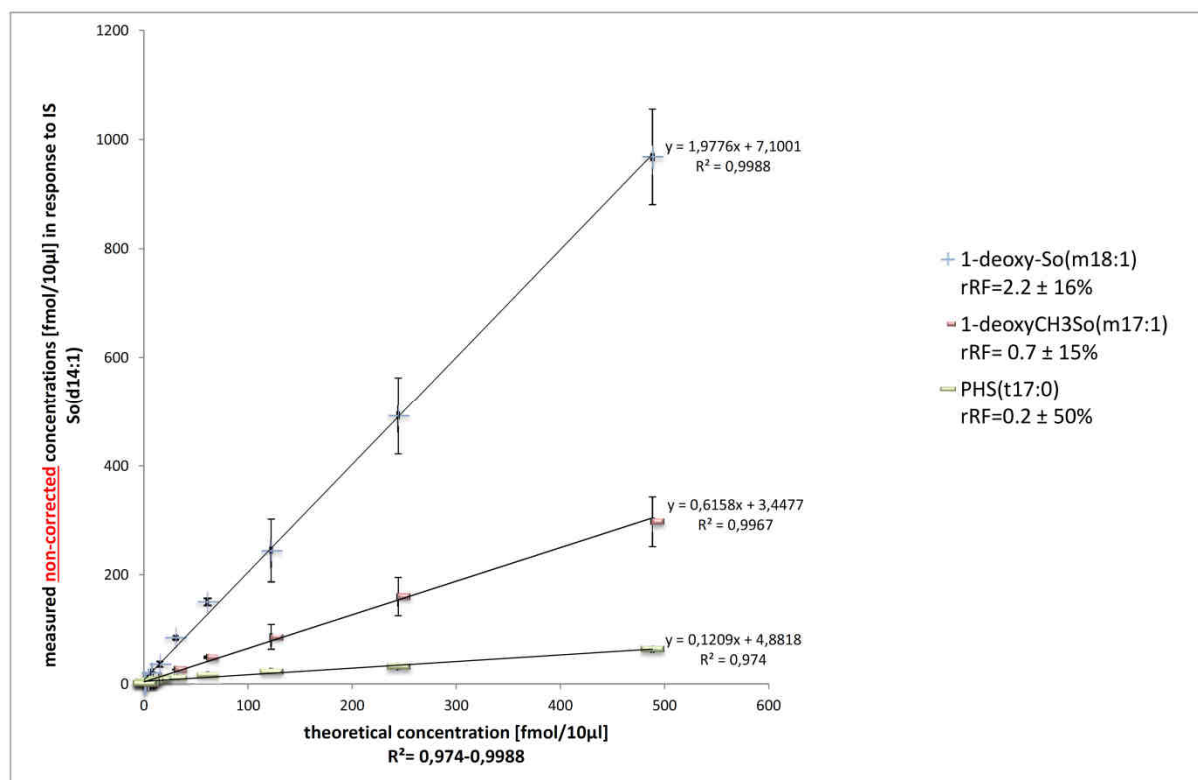


Figure 13 Calibration curves of available standard substances. All curves have R^2 between 0,974 and 0,9988. The relative response factor (rRF) was calculated out of these curves and used for correction of analyte concentration in samples. The volume of 10 μ l corresponds to the injection volume. $n=3$ samples.

The curve of 4-hydroxysphinganine(t17:0) (PHS) is the flattest and is therefore not to be quantified with this method. For 1-desoxy-So(m18:1) a slope of 1.9 and for 1-deoxymethylsphingosine(m17:1) a slope of 0.6 are achieved.

For 1-phosphorylated sphingoid bases slopes between 0.05 and 0.48 are accomplished, whereas the coefficients of determination (R^2) range from 0.996 to 0.9997. The detector shows the weakest response for So1P(20:0), Sa1P(17:0), Sa1P(20:0) and Sa1P(18:0). In general the responses for the saturated sphinganine seem lower than for the corresponding unsaturated sphingosines.

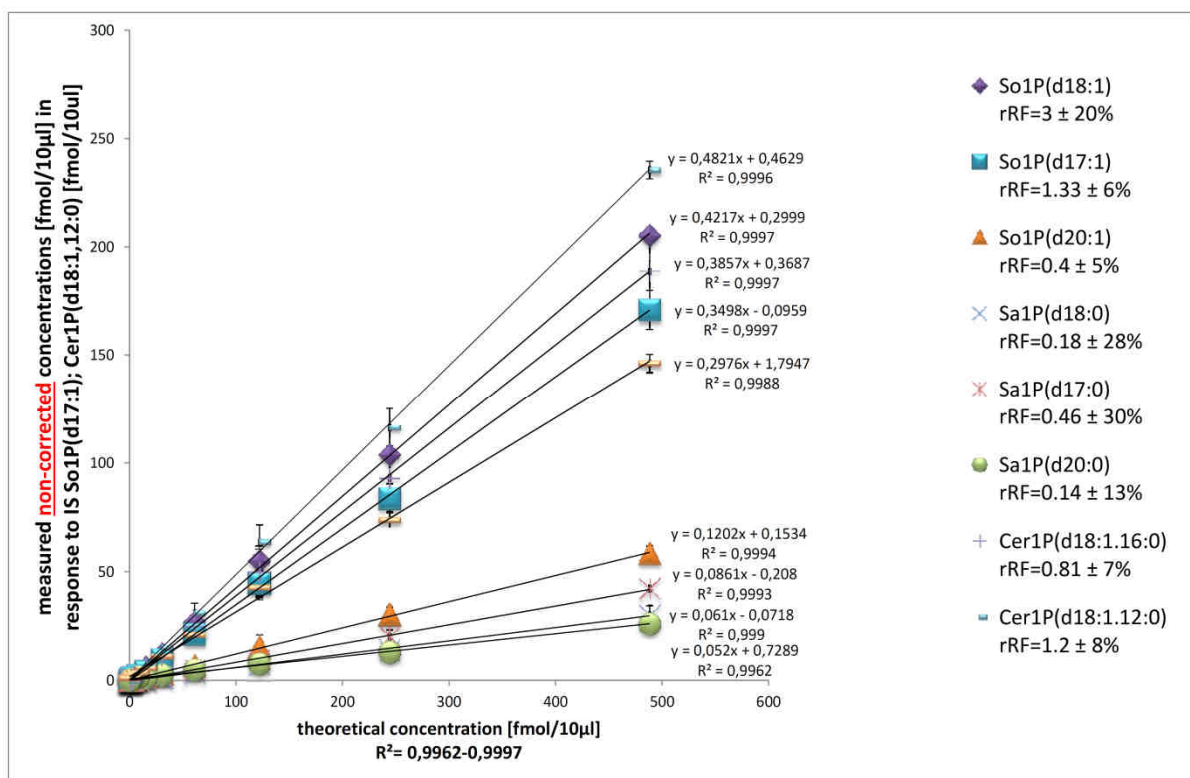


Figure 14 Calibration curves of available phosphorylated standard substances. All curves have R^2 between 0,987 and 0,999. The relative response factor (rRF) was calculated out of these curves and used for correction of analyte concentration in samples. The volume of 10µl corresponds to the injection volume. $n = 3$ samples.

For further determination of method quality LODs and LOQs were determined by the signal to noise ratio (S/N). The limit of detection (LOD) is determined by a signal to noise ratio (S/N) of 3 and higher as well as the limit of quantification by a signal to noise ratio of 10 and higher. Therefore S/N was determined for each compound out of the before established calibration curves. For the measured analytes the mean background was subtracted from the peak height and divided by the standard deviation of the background height, as described in the equation below:

$$S/N = ((\text{mean analyte signal} - \text{mean background}) / \text{standard deviation of background})$$

In Table 19 the like this assigned LOD and LOQ as well as the exact S/N for the corresponding concentration are shown. For the most abundant sphingoid base, So (d18:1), the detection limit is found at ~0.25 fmol, and the quantification limit at approximately 1 fmol of the injected compound. For the 1-phosphorylated sphingoid bases the LODs and LOQs are in general higher and LOQs are estimated between ~4 and 30 fmol. PHS as described already for the calibration curves has a LOQ of 480 and is therefore not to be quantified with this method.

Table 19 LOD and LOQ for quantification of sphingoid bases

	Detection limit (fmol); S/N ≥ 3	S/N	Quantification limit (fmol); S/N ≥	
			10	S/N
So(d18:1)	0.25	5.83	1	10.03
So(d17:1)	0.25	4.98	2	10.70
So(d20:1)	0.5	3.38	4	12.03
Sa(d18:0)	0.25	3.49	2	14.61
Sa(d17:0)	0.5	3.81	4	14.79
Sa(d20:0)	2	3.88	7.5	12.76
1-deoxy-So(m18:1)	0.5	3.59	2	16.97
1-deoxymethyl-So(m17:1)	2	3.30	7.5	11.04
PHS(t17:0)	4	3.04	480	13.74
So1P(d18:1)	0.25	3.37	4	10.03
So1P(d17:1)	1	4.09	7.5	12.26
So1P(d20:1)	15	3.75	60	10
Sa1P(d18:0)	4	4.3	30	10.47
Sa1P(d17:0)	4	3.27	30	14.2
Sa1P(d20:0)	0.25	40.39	0.5	42.63
Cer1P(d18:1,16:0)	1	3.62	8	13.46
Cer1P(d18:1,12:0)	2	6.10	8	15.79
Cer1P(d18:1,24:0)	0.25	8.06	1	10.96

The Z-factor is a measure for the power or the quality of a large assay (Birmingham et al., 2010; Zhang, 1999). It is widely used in high-throughput screening assays to judge whether one particular sample is significantly different in comparison to a positive or negative control. The Z-factor is calculated with the following equation:

$$Z = 1 - ((3SD \text{ of sample} + 3SD \text{ of control}) / (\text{mean of sample} - \text{mean of control}))$$

Ideal Z-values equal 1, which can't be reached in practice. In excellent assays the Z-factors are between 0.5 and 1, whereas for a marginal assay factors range between 0 and 0.5. Assays with Z factors lower than 0 are practically not useful. In practice, assays with values >0.2 are often defined as poor, but not impossible. This is why we decided to group our data into possible assays with values ranging from 0.2-1 and impossible assays with factors from 0-0.2.

In Table 20 and Table 21 the calculated Z-factors for each standard are displayed. In green values are labeled, in which the factor indicates a possible assay. In general for injected amounts of about 15 fmol assay quality is acceptable.

Table 20 Z- Factor of unphosphorylated sphingoid bases. In green values are marked which the Z-factor determines as possible assay. The red line indicates the average detection limit.

Z'-Faktor										
So(d18:1) rRF=2.03 ± 10%	So(d17:1) rRF=2.7 ± 8%	So(d20:1) rRF=1.49 ± 10%	Sa(d18:0) rRF=1.9 ± 17%	Sa(d17:0) rRF=1.4 ± 11%	Sa(d20:0) rRF=0.69 ± 7%	1-deoxy- So(m18:1) rRF=2.2 ± 16%	1- deoxyCH ₃ So(m1 7:1) rRF= 0.7 ± 15%	PHS(t17:0) rRF=0.2 ± 50%	fmol	
0.72	0.83	0.50	0.60	0.75	0.92	0.64	0.57	0.54	488.25	
0.55	0.81	0.35	0.41	0.77	0.98	0.48	0.27	0.54	244.13	
0.69	0.86	0.53	0.70	0.85	0.87	0.46	0.31	0.05	122.06	
0.54	0.77	0.87	0.89	0.70	0.88	0.87	0.63	-0.03	61.03	
0.49	0.82	0.71	0.79	0.73	0.34	0.91	0.87	-1.25	30.52	
0.06	0.85	0.10	0.76	0.82	0.54	0.70	0.64	-0.92	15.26	
-1.04	0.61	0.37	0.79	0.23	0.32	0.61	0.51	-1.59	7.63	
-1.84	0.21	0.79	0.14	0.68	-1.44	0.59	-1.51	-2.05	3.81	
-4.55	-0.12	-0.94	-1.18	-0.53	-0.75	0.49	-2.50	-4.72	1.91	

For the non-phosphorylated sphingoid bases, So(d20:1) shows the best result. Here with an injected amount of ~4fmol, we achieve already Z-Factors above 0.2. For 1-desoxy-So(m18:1) the result is even better, as the Z-factor is above 0.2 already at amounts lower than ~2 fmol. The poorest results shows 4-hydroxysphinganine (PHS) with acceptable Z-factors at an injected amount of 244 fmol, which confirms the results of the previous tests, that PHS should not be quantified with this method.

Table 21 Z-factor of phosphorylated sphingoid bases and ceramides. In green values are marked which the Z-factor determines as possible assay. The red line indicates the average detection limit.

So1P(d18:1) rRF=0.43 ± 5%	So1P(d17:1) rRF=0.35 ± 5%	So1P(d20:1) rRF=0.12 ± 6%	Sa1P(d18:0) rRF=0.06 ± 11%	Sa1P(d17:0) rRF=0.1 ± 4.4%	Sa1P(d20:0) rRF=0.07 ± 24%	Cer1P(d18:1.16 :0) rRF=0.4 ± 3%	Cer1P(d18:1.12 :0) rRF=0.5 ± 3.7%	Cer1P(d18:1.24 :0) rRF=0.3 ± 8.7%	fmol	
0.95	0.87	0.77	0.67	0.94	0.81	0.85	0.92	0.79	488.25	
0.92	0.82	0.65	0.68	0.54	0.84	0.67	0.80	0.83	244.13	
0.68	0.61	0.20	0.88	0.63	0.60	0.43	0.70	0.72	122.06	
0.66	0.45	0.35	0.22	0.59	0.62	0.77	0.52	0.71	61.03	
0.83	0.10	0.55	-0.10	0.25	0.56	0.85	0.77	0.78	30.52	
0.27	-0.14	0.00	0.09	0.29	0.70	0.62	0.76	0.48	15.26	
-0.17	-0.33	-0.82	-0.61	-2.30	0.48	0.55	0.31	0.40	7.63	
-1.22	-1.31	-3.22	-1.06	-2.23	-0.09	-0.57	0.39	0.32	3.81	
-2.97	-4.26	-19.11	-1.80	437.74	0.68	-0.25	0.34	-0.15	1.91	

For the 1-phosphorylated sphingoid bases, the Cer1P(d18:1;12/16/24:0) show the best result. For injected amounts of ~2-8 fmol, we achieve already Z-Factors above 0.2. The poorest results show So1P(d17:1) and So1P(d18:0) with acceptable Z-factors at an injected amount of ~60 fmol.

At last proof of reliability, experiments were performed by measuring sphingoid base amounts in positive controls. Samples were chosen where literature already described the presence of So (d18:1) and So1P (d18:1) (Mouse liver, kidney (Saigusa et al., 2012); HeLa (Shaner et al., 2009); Plasma So1P (He et al., 2009); Plasma So (Saigusa et al., 2012)). Results show that all literature values are close to measured values and that the method is reliable (a more detailed description of So composition in HeLa cells can be found in the upper right corner of Figure 16. Because the S1P content in cells is usually low we measured it in plasma samples, as S1P is stored in platelets in higher amounts. We could detect in S1P in plasma samples in amounts of 3 pmol/ μ l.

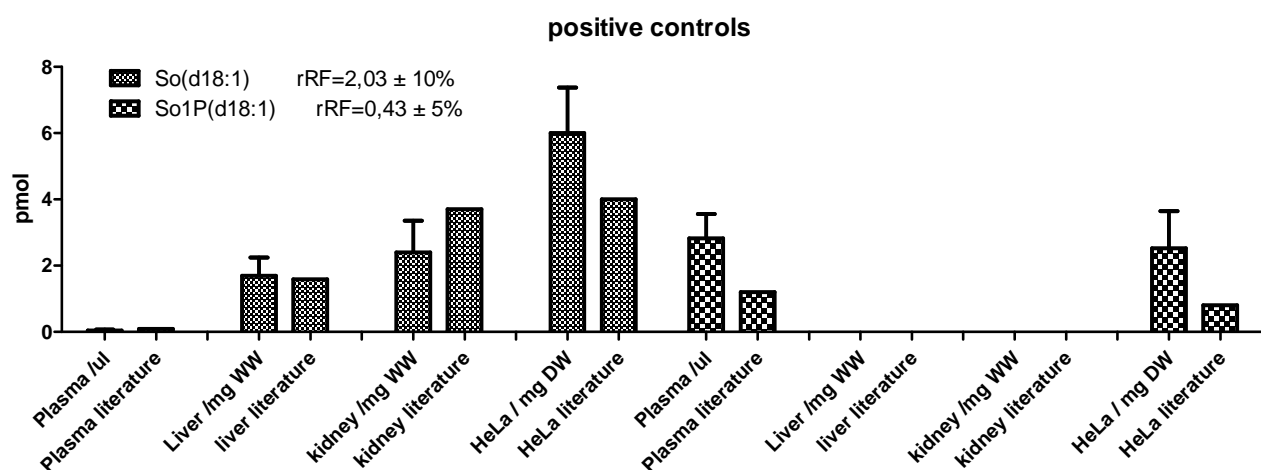


Figure 15 Comparisons of data derived by own LC-MS/MS method in mg wet weight or per μ l with that published in literature in the same units (sources are cited in the text).n= 3 biological samples per group.

I.2.2 Quantification of sphingoid bases in epithelial tissue

In stratum corneum of skin, ceramides are cleaved by the secreted acid ceramidase during terminal cornification and acidification to yield in the corresponding FA and free sphingosine. Therefore it is likely that a reduction of ULC-ceramides, observed in CerS3 mutant mice (Jennemann et al., 2012), would lead to a reduction of free sphingosine.

For this purpose epidermal (skin) samples were taken from mutant CerS3 and Ugcg mice.

1.2.2.1 Sphingoid bases in *CerS3* deficient epidermis

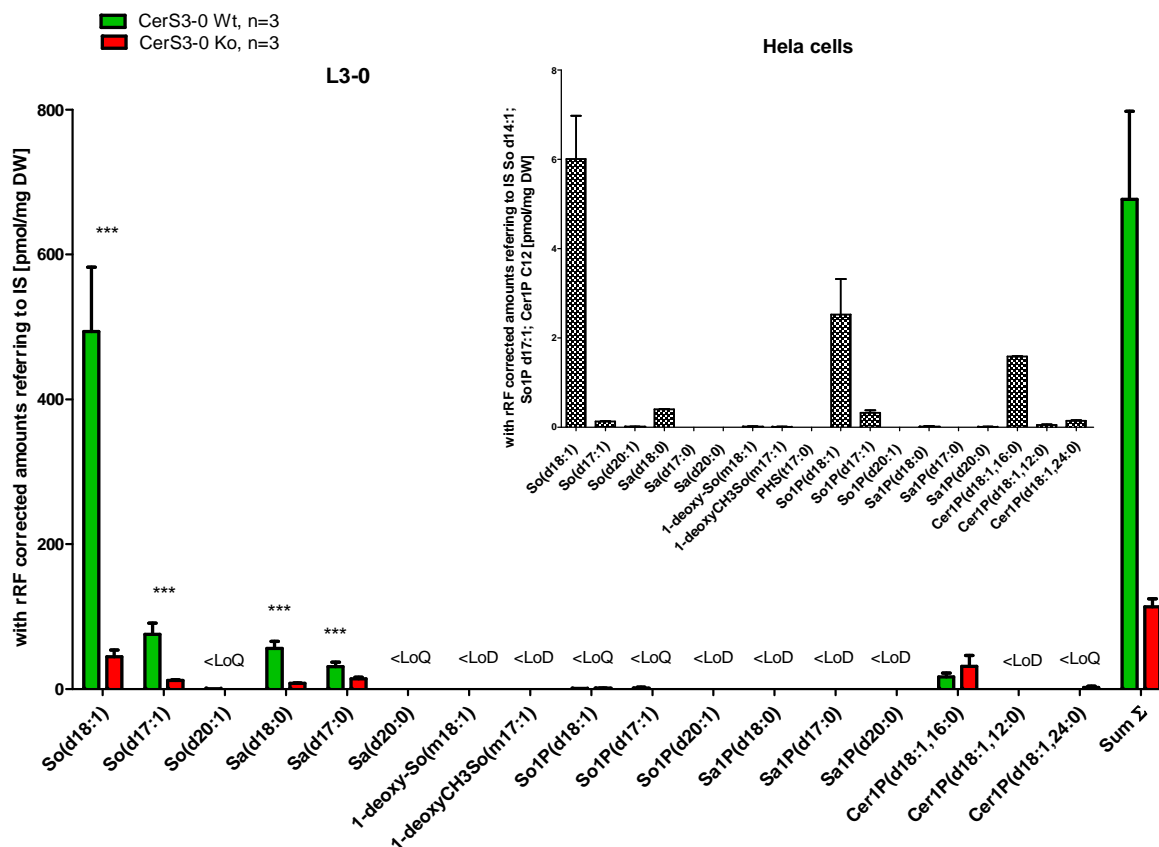


Figure 16 Quantification of free and phosphorylated sphingoid bases as well as ceramide-1-phosphates in skin of *CerS3* mutant mice. As internal standards (IS) So (d14:1), So1P (d17:1) and Cer1P (d18:1; 12:0) were used and values were corrected with the rRF. In mutant mice the sum of free and phosphorylated sphingoid bases and ceramide-1-P values are significantly reduced to ~16%. n=3 biological samples per group. Ttest was applied on 5% level.

In epidermal extracts of mutant and control mice, sphingosine(d18:1) is found to be most abundant. Also present but low abundant, is sphingosine(d17:1) and the matching dehydro-compounds of sphingosine: sphinganine(d18:0) and sphinganine(d17:0). Another known sphingoid base, sphingosine(d20:1) was not quantifiable in mouse epidermis. Most of the phosphorylated analogs of the residing sphingoid bases and ceramides, besides Cer1P(d18:1/16:0), are not detectable or below the LoQ.

In the ko levels for sphingosine(d18:1) are decreased to 10 % compared to the wt. For sphingosine(d17:1) values are reduced to 14% of the wt level. Similarly, significant reductions can be found for sphinganine(d18:0) and(d17:0). In the upper right corner of Figure 16 a comparison of the sphingoid composition and amount found in HeLa cells is

shown The composition is similar to that found in epidermis, with So(d18:1) being most abundant followed by So(d17:1). Strikingly different is that in 1 mg of dry weight of HeLa cells, 100 times less So(d18:1) is present versus nearly 600 pmol of So(d18:1) per mg DW in epidermis of CerS3 control mice (wt).

1.2.2.2 Sphingoid bases in *Ugcg* deficient epidermis

In an earlier study mice with constitutive *Ugcg* gene deletion in the epidermis were investigated (Jennemann et al., 2007). Newborn mice died at postnatal day P5 due to dehydration upon WPB loss, thus demonstrating the importance of Cer-glucosylation in epidermal barrier development. Complete loss of GlcCers and accumulation of the free ω -hydroxy Cers was observed together with distorted LBs. Although the total amount of epidermal protein-bound ceramides remained unchanged, free ω -hydroxy Cers increased 4-fold and ω -hydroxy SM increased in amounts comparable to those of amounts of lost GlcCer (Jennemann et al., 2007).

To investigate if loss of GlcCers has, similar to CerS3-deficiency, an influence on the free sphingosine levels, the latter were quantified by LC-MS/MS (Figure 17).

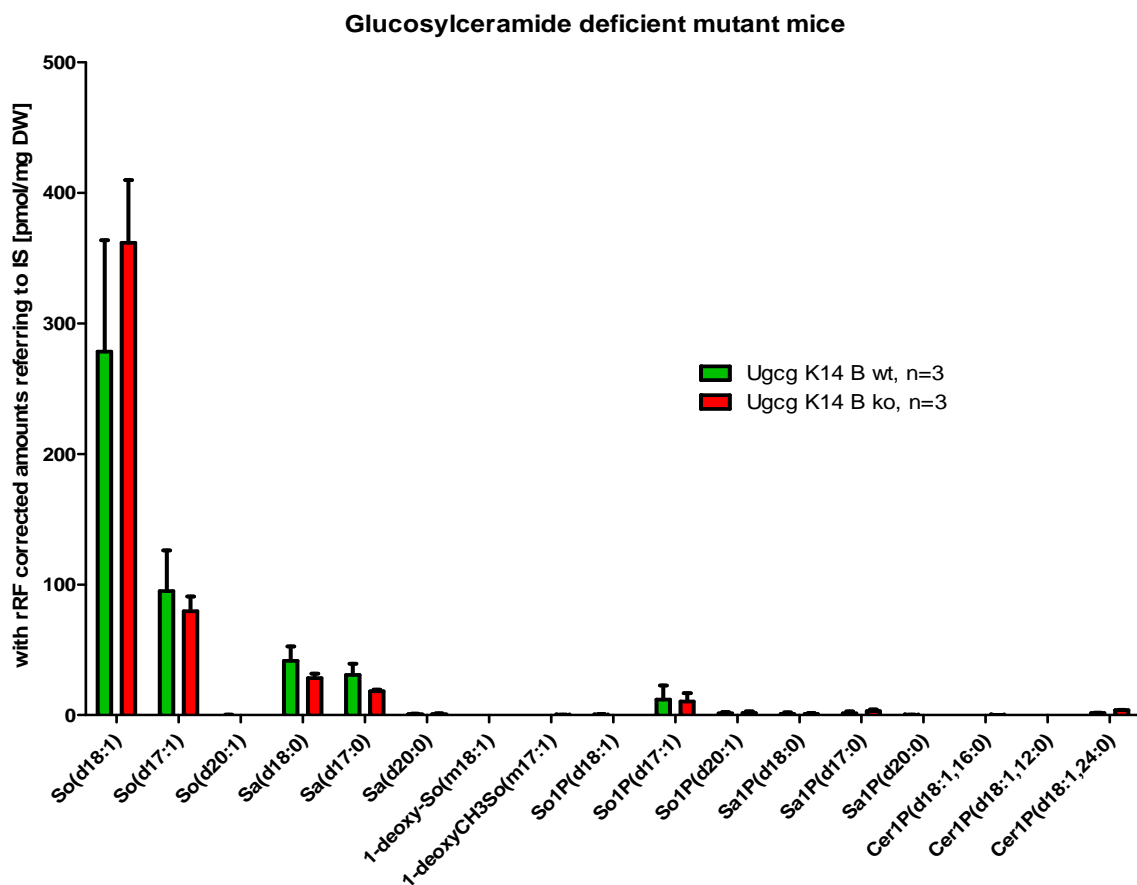


Figure 17 Quantification of sphingoid bases in constitutive keratinocyte specific Ugcg mutant mice. As internal standards (IS) So (d14:1), So1P (d17:1) and Cer1P (d18:1; 12:0) were used. Levels show no significant differences. n= 3 biological samples per group.

The main compound is sphingosine(d18:1), with So(d17:1) being the next highest value. So (d18:1) levels are by trend elevated in the ko. In opposite to this trend all other sphingoid bases show no significant differences. Increasing the sample number would probably lead to significant differences, but due to a lack of suitable samples this experiment was not performed.

1.2.2.3 Sphingoid bases in other epithelial tissue

The Epidermis is not the only epithelial tissue in mammals it also lines the inside cavities and lumen. In all tissues epithelial cells provide a protective barrier against harmful extracellular factors and infectious microorganisms. The surface ectoderm also forms the epithelium of the

oral cavity and tongue, where the defensive barrier is established by appendages such as teeth, filiform papillae, taste papillae, and salivary glands (Jonker et al., 2004).

Dorsal epithelium of tongue of CerS3 d/d and control mice was taken and lipids extracted like described in the methods section. Even though the properties of epidermis in skin and tongue are similar, the results in Figure 18 show no similar trend of reduction of sphingoid bases like seen in CerS3 deficient mouse epidermis. The distribution pattern is also unlike the one seen in epidermis of skin, besides that So(d18:1) is the most abundant compound, as well as the data of ko animals is very inhomogeneous. A reason for that could be that only n=2 animals for wt and ko respectively could be sampled and analyzed.

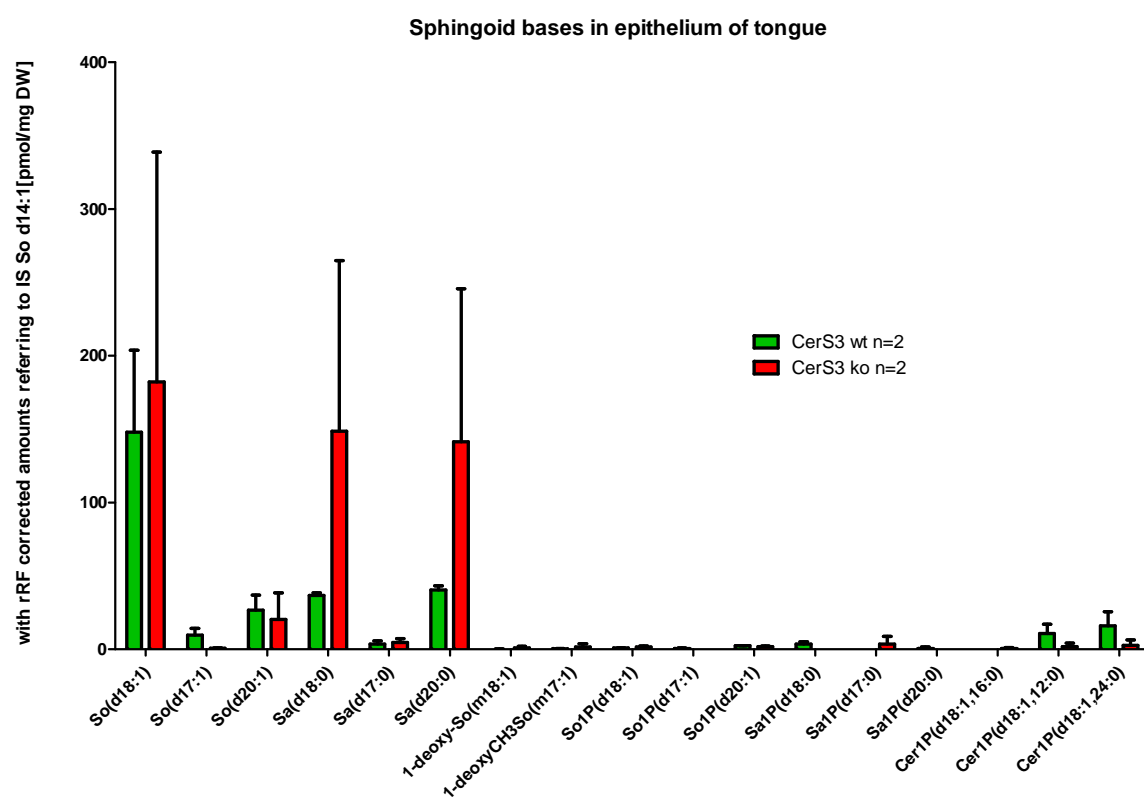


Figure 18 Quantification of free and phosphorylated sphingoid bases in epithelium of tongue. As internal standards (IS) So (d14:1), So1P (d17:1) and Cer1P (d18:1; 12:0) were used. Levels of sphingoid bases are not significantly altered in control and mutant samples. n=2 biological samples per group.

I.2.3 Dendritic cells and immune barrier

The most important dendritic cell family located in the skin is the Langerhans cells, which capture foreign antigens. (Christensen and Haase, 2012; Kaplan, 2010; Steinman, 2007). S1P is known to be able to attract DCs (Maeda et al., 2007; Matloubian et al., 2004; Olivera and Rivera, 2011; Yasuhiro et al., 2007) and could be responsible for the migration of LCs and DCs into epidermis. Via MS we could detect a decreased level of sphingosine (d18:1) suggesting an altered level of its product S1P.

To further investigate the high infection risk in our CerS3 mouse model, demonstrated by *candida albicans* infection, dendritic cell populations in the epidermis were studied.

Like described in the methods section a modified method to immunolabel mice full epidermal sheets was established (Chorro et al., 2009). Langerhans cells express the lectin langerin (CD207) on their surface, which can be used as a marker for LCs in mice and humans. As LCs are also positive for the common DC marker CD45, a staining procedure was established and full skin sheets of CerS3 mutant mice and controls investigated. In CerS3 deficient newborn (P0) mice increased amounts of CD45 positive dendritic cells are found to infiltrate the epidermis compared to the wt and is suggesting an abnormal reacting immune system (Figure 19 A and B; CD45 in red). To identify these dendritic cells as the unique subset of LCs, double staining of CD45 and langerin was performed (Figure 19 C and D). Unfortunately we determined that mouse langerin is starting to be expressed with the age of P5 and not yet with the age of P0. Due to the lethal phenotype of newborn CerS3 deficient mice, LC identification at P0 was unsuccessful. Nevertheless at P5 all the CD45 positive cells found in control (wt) epidermis are positive for langerin, identifying them as LCs. Only one single langerin⁺ cell could be found in the ko at P0. Furthermore numbers of CD45 positive cells in epidermis of newborn (P0) mice were calculated per area of a 20x magnification field, revealing a significant increase of 400% in the ko compared to the control (Figure 19 E). On the other hand we find a decrease of CD45 positive cells in epidermis of embryonic mice (E19), which is shortly after the epidermal barrier is established. This indicates that non-sterile circumstances influence the health of the animals at P0.

To verify these results, ko and wt full skin of mice at the age of E19 and P0 respectively, were incubated under sterile conditions over a time period of 3 days on a humidified collagen matrix to keep tissue alive (Figure 19 F). Then Epidermis was taken and stained for CD45 positive cells with the same procedure described for the previous experiment. This enabled us to track the migrational behavior of DCs through the dermis towards epidermis and to avoid secondary immunological effects caused by unsterility. For the wt both at P0 and E19 DCs move constantly from dermis to epidermis over time, doubling their amounts in epidermis, even though at E19 amounts of DCs are ~3 times lower than at P0 (Figure 19 F). In opposite results are not clear for the ko. At P0 DCs seem to disappear over time, even though a migration back into the dermis is very unlikely. At E19 there seems to be a tendency that DCs infiltrate more slowly or to a lesser extent the epidermis than compared to the wt, but in comparison to P0 DC amounts is steady.

I.2.4 Sphingosine and antimicrobial barrier

Studies have demonstrated significant levels of free sphingosines in the epidermis (Stewart and Downing, 1995; Wertz and Downing, 1990) and they were demonstrated to be potent antimicrobials also against *candida albicans* (Bibel et al., 1989, 1995; Payne et al., 1996). Also an inverse correlation has been demonstrated between the free sphingosine level and the amounts of *S. aureus* in atopic patients (Strum et al., 1997), which connects free sphingosine with an impact on a proper antimicrobial barrier.

To further investigate if the observed high infection risk, especially for *candida albicans*, of our CerS3 mouse model (Jennemann et al., 2012) correlates with a function of So, infections assays in the presence or without addition of So were performed. Therefore on skin of newborn CerS3 deficient and control mice sphingosine was topically administered. To enhance transdermal delivery So was dissolved in a water/ propylene glycol mixture (Ramesh Panchagnula et al. 2001). Then skin was incubated for 60h with *candida albicans*.

Figure 20 shows the results after infection. Wt and ko CerS3 mice which were treated either with a solution of So in PG and water, with PG and water alone or without any additives. On wt skin the growth of *candida albicans* on the surface seems generally lower than on the ko. Furthermore, in comparison to samples without So, the growth can be visibly reduced on the ko and wt surface by addition of So (Figure 20 A). On the negative controls growth is by trend lower on the wt than on the ko. However the comparison of the ko without any additives (neg. control) shows that on samples treated with and without So, *candida* cells are growing less. By looking not only at the growth on the surface, but at the infiltration depth it seems that infiltration depth is smaller in the So treated ko samples than in So- untreated samples. The wt is not invaded by the fungus at all. In the ko negative control many more infiltration sites compared to treated and non-treated samples are present.

Statistically Figure 20 B shows that bacterial growth of *candida* can be inhibited by sphingosine. The colony forming units (CFU) were calculated for the samples with or without the treatment of So. For both sample types the CFU is lower for the wt than for the ko. For the untreated sample pair the CFU is even significantly different, which supports the histological results in Figure 20 A. Furthermore the CFU is significantly smaller in the with So treated ko sample than in the untreated ko sample. In the negative controls the CFU of the wt is smaller than that of the ko. To be able to also measure the differences in infiltration sites, the numbers of active infiltration sites per section in the ko of treated and non-treated samples were

counted. Per section the amount of infiltration sites is by trend smaller in the samples treated with sphingosine, than compared to the ones without sphingosine. In CerS3 deficient skin treated with So approximately 0.5 candida invading sites per section could be detected, while the skin without So treatment is not significantly different with 0.7 sites per section. As only very few infiltration sites could be detected the ratio between with So treated ko samples and untreated ko samples was calculated (Figure 20 C). A ratio smaller than one implies less infiltration sites in the whole sample of treated compared to untreated ko skin, which is true for all four ko samples. No significant differences were observed.

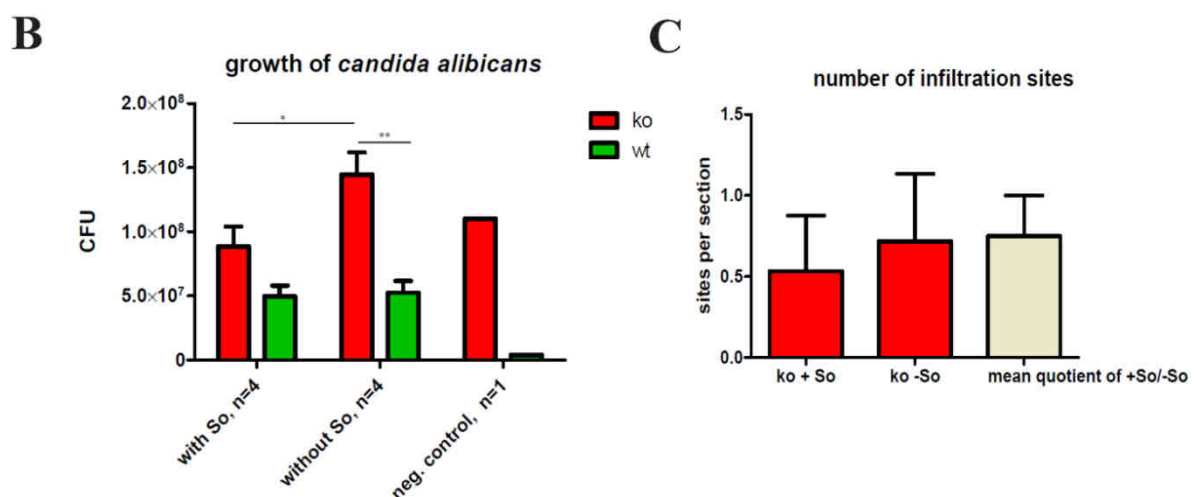
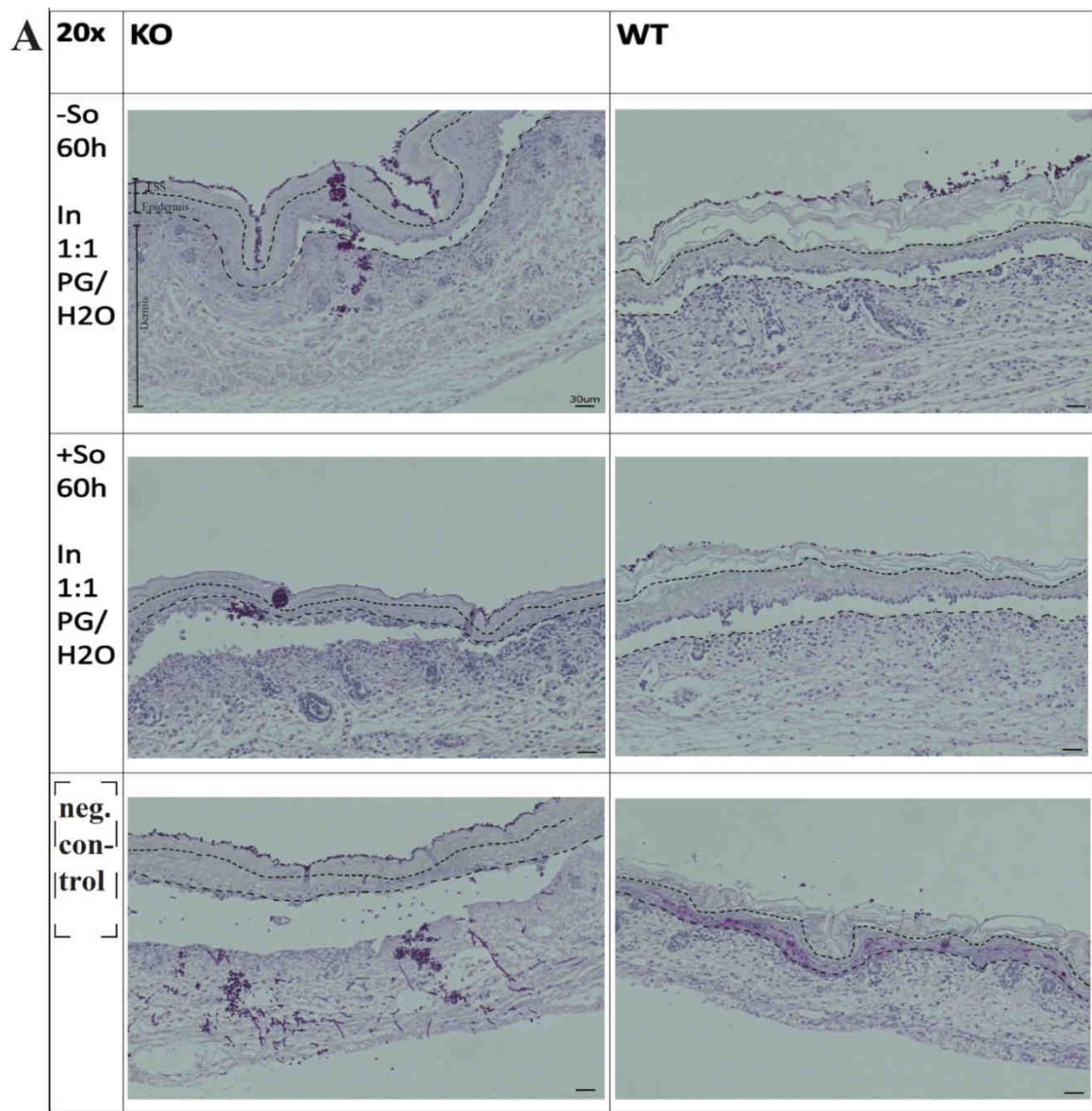


Figure 20 Infection assay. A: whole skin of CerS3 mutant mice was treated with sphingosine to restore the antimicrobial barrier; n=4 biological samples per group (wt and ko). B: statistical analysis of growth of *candida albicans*. With So treated ko skin samples have significantly less growth on the surface. C: the numbers of infiltration sites in CerS3 deficient skin of *candida* were calculated. With So treated samples show by trend less sites. So reduces infiltration sites by trend, which is why the Quotient of treated to untreated samples concerning the infiltration sites of *candida* is smaller than one. Ttest was applied on a 5% level.

I.3 Discussion

For establishment of a method to quantify multiple sphingoid bases and sphingoid-1-phosphates, including ceramide-1-phosphates, several parameters had to be optimized. First of all the usage of a CSH-column improved the resolution and the peak shapes of the phosphorylated compounds. By the surface charges on the column material, interaction between the analytes and stationary phase could be improved and peak tailing strongly reduced. Additionally citrate added to the sample solvent, captures contaminants of the solvent system, such as metal ions, by complexing them and removes them out of the system (Winter et al., 2008). The like this blocked positions on the column material by contaminants are given free and interaction between analyte and stationary phase increased. A common problem of sphingolipid phosphate analysis by LC-MS/MS is its carryover caused by zwitterionic properties of the analytes (Berdyshev et al., 2005). While in classical HPLC postcolumn derivatization and the use of phosphate-buffered eluents can prevent S1P carryover, for LC-MS/MS analysis residue-free solvents are required. Any solid residues will accumulate in the ion source and interfere with the measurements. In this case residue free additives for the mobile phase like formic acid and ammonium formate can be used. Carry over was avoided by injecting blanks between every 5-10 samples, which prevents false-positive signals. Furthermore, while determining the optimal collision energies for each transition, we observed that for the classical sphingoid bases and also for the sphingoid base-1-phosphates water loss appeared already at low eV values by in source decay. Therefore each compound was detected by 3-4 transitions from their $[M+H]^+$ mother ion, which were added up for quantification yielding in a higher specificity. So far, most methods for quantification of sphingoid bases used only one transition for each compound (Saigusa et al., 2012; Schmidt et al., 2006). However sphingoid base-1-phosphates showed a lower response and higher limits of detection and quantification than the corresponding classical sphingoid bases. With this method sensitivity for these compounds could not be further improved. Nevertheless, the method was reliable as shown with the measurement of positive controls. Levels of S1P were generally low in cells, but we could verify that measured amounts in plasma samples and in HeLa cells are in the same range than in published literature.

Quantifying the endogenous sphingoid bases revealed that in CerS3 mutant epidermis the levels for sphingosine(d18:1) were decreased to 10 % compared to the wt, which equals the reduction of ceramide. Sphingosine(d17:1) values were reduced to 14% to that of the wt level. These reductions were most likely caused by a decreased ceramide processing in the SC in the

CerS3 mutants. As sphingosines are derived from ceramide-degradation, it seems that reduced substrate concentrations are directly converted into reduced steady state levels of sphingosine in epidermis. The reduction of sphinganine that can be principally synthesized in CerS3-0 epidermis could be explained by the fact that most of the epidermal sphingoid bases are produced after secretion of the lamellar bodies content into the extracellular space. Hence free sphingoid bases are probably not directly secreted, but in form of ceramide and glucosylceramide precursors. In CerS3 mutant mice also the formation of dihydroceramides with ULC-FA moieties is probably affected, leading to decreased amounts of dihydroceramide in the epidermis and hence to decreased amounts of sphinganine. Investigation of glucosylceramide synthase mutant mice showed that sphingoid base levels are not affected upon the deletion in keratinocytes. Even though the total amount of epidermal protein-bound ceramides remained unchanged, free ω -hydroxy Cers increased 4-fold and ω -hydroxy SM increased (Jennemann et al., 2007). Both free ω -hydroxy Cers and ω -hydroxy SM are potential precursors of sphingoid bases and their elevation could also lead to elevation of sphingoid bases. Here we couldn't observe such, but an increment of the sample number could probably lead to significant differences. The distribution pattern in epithelium of tongue was unlike the ones seen in epidermis of skin, as well as the data of ko animals were very inhomogeneous. A reason for that could be that only n=2 animals per sample group could be analyzed. Nevertheless, it is largely unknown how tongue-specific epithelial differentiation pathways are genetically controlled or which proteins are involved. For example it was suggested that genes are differentially expressed in the cornified envelope of the skin and tongue (Marshall et al., 2001; Wang et al., 2001). It is unclear if barrier formation in wet environment requires similar conditions than in dry environment and if sphingosine is also important for microbial defense. The fact that in epidermis of control mice sphingosine(d18:1) values were approx. double as high as in epithelium of tongue, suggested that sphingosine has a bigger role in skin than in tongue (and the oral surroundings). And even though *candida albicans* are one of the components of normal oral microflora, oral candidiasis for example is a disease which is one of the most common fungal infection (Singh et al., 2014). The in comparison to epidermis low levels of sphingosine in tongue, suggested that there So has different functions, or that oral mucosa is not as well protected towards *candida* infections than the skin.

Also proving the importance and potential function of sphingoid bases and especially So(d18:1) in skin was the comparison of levels with those found in HeLa cell extracts. 100 times more So(d18:1) was detected in epidermal samples than in similar amounts of HeLa cell

extracts. Without the antimicrobial defense of sphingosine skin could be more likely infected. Hence, the missing activity of sphingosine could participate in the formation of *candida albicans* infection in CerS3 deficient mice.

In newborn CerS3 deficient mice more dendritic cells were recruited into the epidermis as compared to control mice. On the other hand in embryonic mutant epidermis 70% decreased amounts of DCs were detected. These DCs could not be clearly identified as the unique subset of LCs in both embryonic and newborn mice. It has been indicated that S1P plays a pivotal function in a variety of cells including immune cells (Czeloth et al., 2005; Japtok and Kleuser, 2009; Maeda et al., 2007; Spiegel and Milstien, 2011). Thus, it is well established that the egress of dendritic cells and lymphocytes (T- and B-cells) are mediated by S1P signaling (Allende et al., 2004; Brinkmann et al., 2002; Kabashima et al., 2006; Maeda et al., 2007; Matloubian et al., 2004). Even though S1P could not be detected in epidermis via MS, out of reduced levels of free sphingosine, reduced levels of S1P could consequently follow. For embryonic mutant mice it could be hypothesized that activation of DCs failed, highlighting the need of free sphingoid bases and ceramides to recruit immune cells and to keep forwarding immune answers. However it is more likely that skin of CerS3 deficient mice is more sensible to infections due to secondary DC infiltration and not due to altered S1P trafficking of DCs. General infertility at birth of mice and irritations by unsoft bedding in cages could cause an overreacting immune response. In this case the observed DC subsets are not necessarily Langerhans cells, but could be also dermal DCs, T-cells or macrophages, which are also CD45 positive. Proteinkinase C for example, is crucial in activating T-cell signaling pathways and so helps recognizing and responding to foreign antigens. If sphingosine, naturally immunosuppressive and able to inhibit the proteinkinase C (Baier and Wagner, 2009; Merrill and Stevens, 1989), is diminished, T-cell signaling could be overresponsive and could account for the DC-phenotype in newborn (P0) mice. Furthermore tracking the migrational behavior of DCs under sterile conditions through the dermis towards epidermis showed that DCs migrated by trend more intensively to the skin surface in the wt than in the ko , but differences were not significant (in both P0 and E19). In the newborn (P0) ko samples, DCs seemed to disappear over time, possibly retrieving back into the dermis. This effect was maybe caused by tissue degradation of the very sensible mutant skin. This tendency was not significant and is only hinting towards the finding that under sterile conditions DCs in CerS3 d/d mice seem to wander less into epidermis, corresponding to a missing or altered activation signal and so provoking more infections.

In summary the DC phenotype in *Cers3* deficient newborn mice was contrary to the observed phenotype in embryonic mice. In newborn *CerS3* deficient mice more DC, and in E19 mice less DC than controls were present. Both can't be explained by migration of DCs towards S1P. Furthermore primary findings at P0 and E19 can't be compared to findings in cell culture after 1 and 3 days, as circumstances like blood flow were different at the time DCs were counted. Hence, we concluded that at P0 the DC phenotype could be caused due to secondary infections and not due to S1P signaling and at E19 due to reduced migration of DCs towards S1P.

At last, the direct effect of sphingosine(d18:1) on *candida albicans* infection was tested. Sphingosine, topically applied on the skin, was shown to help to restore the antimicrobial barrier by not only reducing pathogen growth on the skin surface, but also by hindering the pathogens to pass the stratum corneum and infiltrate the skin barrier. Therefore So could prevent infections in diseases like atopic dermatitis, psoriasis and ichthyosis. Patients with this kind of diseases are often not satisfied with current treatment methods (Linden and Weinstein, 1999; Nijsten et al., 2005). Emollient creams and lotions may relieve part of the symptoms, but often only temporarily. For most antiinflammatory creams, continued use may reduce the effectiveness and they are also not always adapted to restore a disturbed barrier function. Hence, sphingosine could help by treating inflammatory diseases.

Part II

II. 1-O-acylceramides

II.1 Introduction

Cers are involved in a great variety of key cellular functions, including the control of cellular fate in programmed cell death (Hannun and Obeid, 2008; Mullen et al., 2012). In SL biosynthesis Cers reflect a branching point. Their degradation leads either to free sphingoid bases and further to S1Ps, which function as signaling molecules (Zhang et al., 1991), or they may be used as building blocks for membrane lipids such as SMs and GlcCers. Further glycosylation of GlcCers leads to the formation of hundreds of more complex GSLs (Kolter, T., Sandhoff 1999). Finally, Cers may also be phosphorylated directly and the resulting ceramide-1-phosphate can stimulate group IVA cytosolic phospholipase A2 to release arachidonic acid from phosphatidylcholines leading to the class of signaling eicosanoids (Gómez-Muñoz, 2006; Lamour and Chalfant, 2005; Subramanian et al., 2005). In this study also the newly discovered class of 1-O-acylceramides will be investigated to unveil details of ceramides up- and downstream pathways.

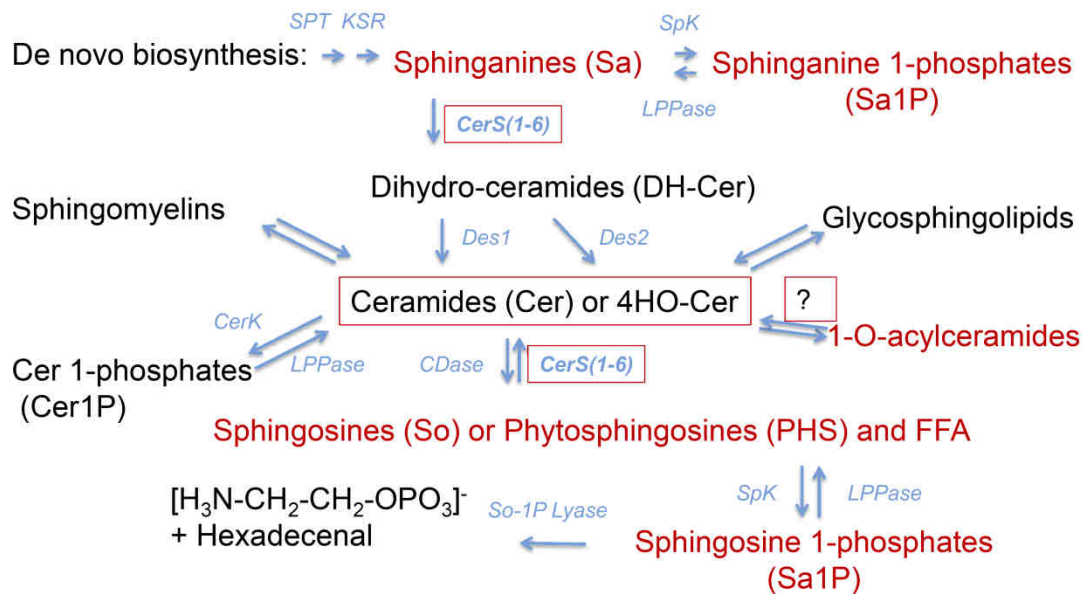


Figure 21 Ceramides are branching points of SL pathways. Ceramides can be either cleaved to give sphingosine or sphingosine-1-phosphate, or it can be modified to yield in glycosphingolipids, 1-O-acylceramids, sphingomyelin or Cer1P. In red compounds and reactions are shown, which are being investigated in this study.

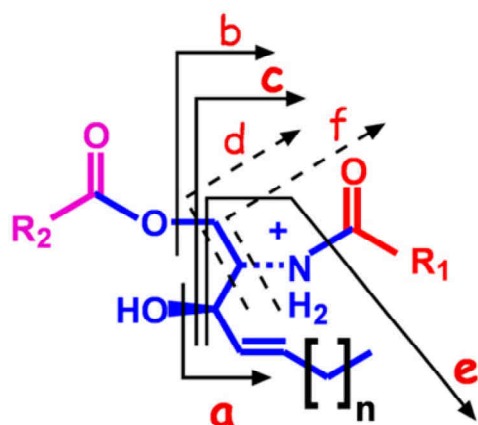
II.1.1 1-O-acylceramides

First knowledge about alternative metabolic pathways for Cers was gained in the late seventies, when it was discovered that in some tissues or cells Cers with esterification in 1-O-position of the sphingoid base occurred. Injection of 3 H- and 14 C-labeled Cers (d18:1;16:0 and d18:1;24:0) led amongst others to 1-O-acylceramides (Okabe and Kishimoto, 1977). Furthermore the group XV lysosomal phospholipase A 2 (LPLA 2) was identified in MDCK cells, mouse brain, spleen, liver, and kidneys to be able to transacylate *in vitro* radioactive short chain Cers in 1-O-position (Abe et al., 1996; Shayman et al., 2011). LPLA2 is ubiquitously present but is most highly expressed in alveolar macrophages (Hiraoka et al., 2006).

In 2012 a pathway in yeast was described that also led to the formation of 1-O-acylceramides. Here two enzymes were described to be involved: the phosphatidylcholine:diacylglycerol acyltransferase (Lro1p) and the diacylglycerol O-acyltransferase (Dga1p). These enzymes were able to also use VLC-Cers (C26-Cer) for esterification in 1-O-position (Voynova et al., 2012). The mammalian lecithin:cholesterol acyltransferase (LCAT) and LPLA2 are homologous of the yeast Lro1p. In opposite to Lro1p which is expressed in the lumen of the ER, LCAT and LPLA2 are localized either outside of the cell or within lysosomes (Choudhary et al., 2011; Voynova et al., 2012). The mammalian diacylglycerol O-acyltransferase 2 (DGAT2) is a homolog to Dga1p. The DGAT family is composed of many different enzymes and they have been identified in several species. DGAT1 and DGAT2 for example are two of the enzymes that are responsible for the main part of triacylglycerol synthesis in most organisms. Both enzymes belong to a large family of membrane-bound O-acyltransferases (MBOAT) (Turchetto-Zolet et al., 2011). DGAT2 is localized in the ER, but it is spatially closely related to lipid droplets (Jacquier et al., 2011; Sorger and Daum, 2002). Mice being deficient for DGAT2 develop not only lipopenia, but also skin barrier abnormalities (Stone et al., 2004).

Based on these recently gained facts our group could discover a group of almost 100 similar natural 1-O-acylceramide species in mouse and human epidermis (Rabionet et al., 2013). These epidermal Cers contain long to very long acyl chains attached at both of the N- and 1-O-position. To our knowledge, endogenously expressed 1-O-acylceramides in mammals were not described before. The structures of the 1-O-acylceramides first caught our attention by screening total epidermal lipid extracts for Cers containing a C18-sphingosine base (d18:1) by

MS/MS. Signals in a C18-sphingosine containing SL-specific precursor ion scan for the transition to $m/z+264$ occurred, which did not fit to any epidermal Cers and GlcCers masses or ULC-Cers. As these signals were present in samples of CerS3-deficient mice and in samples of GlcCer-synthase deficient mice, we concluded that they neither belonged to GlcCers nor to Cers with ULC-FA moieties. Furthermore alkaline treatment led to loss of the undefined signals while LC- and VLC-Cers increased in wild-type but especially in GSL-free



epidermis. Product ion spectra from the main peaks showed that all fragmentation spectra contained three dominant product ions due to: *i*) loss of a water molecule, *ii*) loss of a water molecule and lignoceric acid, and *iii*) a residual dehydrated d18:1-sphingosine base (Figure 22).

Figure 22 Structure of 1-O-acylceramides. The structure of 1-O-acylceramides and the product ions (derived by collision-induced dissociation) annotated with small red letters. From (Rabionet et al., 2013).

With the knowledge of the principle structure of So(d18:1) containing 1-O-AcylCers and the CID induced fragmentation behavior a group of almost 100 species was identified in mice (Rabionet et al., 2013). Combinatorial calculations suggest the existence of more than 200 subspecies in mouse epidermis. So far no detailed descriptions of 1-O-AcylCers containing So(d17:1) exist and it is not known if they are similarly metabolized like the corresponding 1-O-AcylCers with So(d18:1) anchor (Rabionet et al., 2013). Furthermore the enzymes responsible for 1-O-AcylCer synthesis were up to now not identified and therefore investigations about 1-O-AcylCer metabolism in epidermis and other tissues will be part of this study.

II.1.2 Farber disease and the lysosomal acid ceramidase

The phospholipase A2 releases the FAs of phospholipids in *sn*-2 position (Burke and Dennis, 2009). Typically, the *sn*-1 position of phospholipids is occupied by saturated fatty acids, whereas the *sn*-2 position is occupied by polyunsaturated fatty acids such as arachidonic or docosahexaenoic acids (Darios et al., 2007), which are not found to be attached to 1-O-AcylCers. However, even though LPLA2 was shown not to be involved in 1-O-AcylCer production under normal circumstances (Rabionet et al., 2013), if the Cer levels in lysosomes are unnaturally increased there still might be a lysosomal pathway by LPLA2 to form 1-O-AcylCer. LPLA2 normally only hydrolyses phospholipids in the presence of water, but in competition with high concentrations of short chain ceramides, it used ceramides as substrate for Acyl-attachment instead of water (Abe et al., 1996; Shayman et al., 2004). Hence, we decided to study the lysosomal metabolism in more detail by investigations of a newly established mouse line with reduced activity of the acid ceramidase, also called Farber disease (*asah1*).

Farber disease (FD) (Lipogranulomatosis) is a rare multisystemic autosomal recessive disease. The inherited metabolic disorder was firstly described by Sidney Farber in 1957 (Farber et al.). Farber disease is caused by mutations in the lysosomal acid ceramidase gene. Therefore, the Farber disease is classified as a lysosomal storage disorders (LSDs) amongst many other known types. Acid ceramidase (ACDase) is a lysosomal enzyme being responsible for the cleavage of ceramide to FAs and sphingoid bases. While low levels ($\leq 10\%$ normal) of ACDase activity result in the progressive accumulation of ceramide in most tissues, no correlation between ACDase levels and disease severity is known. The childhood disorder is already manifested early after birth with minor symptoms (Levade et al., 1995) but neurological and visceral involvement are also observed (Antonarakis et al., 1984), that lead to psychomotor retardation and enlargement of liver and spleen, respectively. Most FD patients suffer an early death with live spans not longer than 2 years and show growth and developmental impairment (Haraoka et al., 1997). So far no cure of FD was found and the severity of the disease made research *in vivo* difficult. Complete ‘knock-out’ models in mice of FD resulted in early embryonic lethality (Li et al., 2002) and a tissue specific reduction of ACDase activity in the ovaries resulted in oocyte apoptosis (Eliyahu et al., 2012).

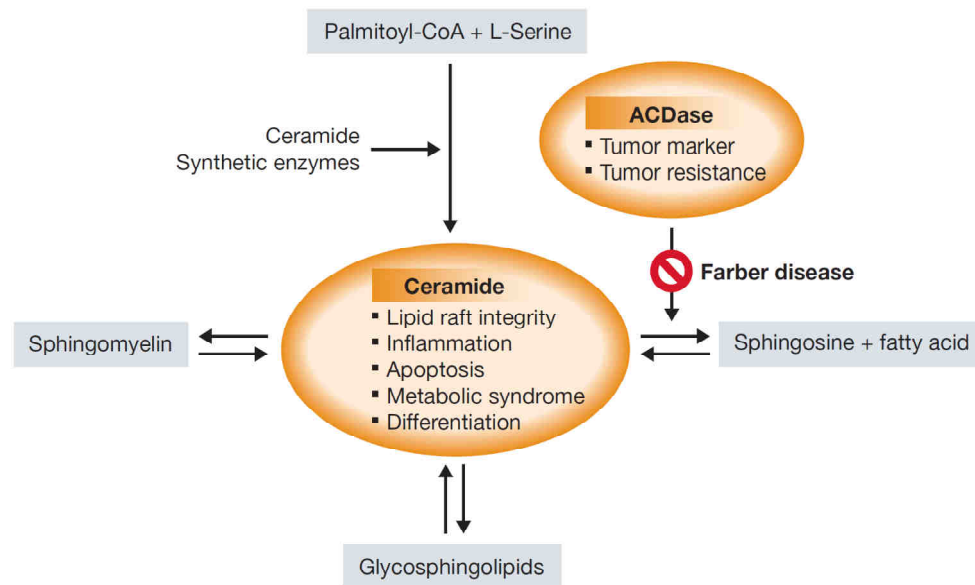


Figure 23 Affected pathways by FD (Sands 2013). Ceramide is a key metabolite to the further synthesis of several membrane lipids such as sphingomyelin and the glycosphingolipids, galactosylceramide and glucosylceramide. Ceramide has also been shown to be directly involved in a number of biological processes, including inflammation, apoptosis and differentiation. Acid ceramidase (ACDase) is a soluble lysosomal enzyme responsible for the degradation of ceramide to sphingosine and fatty acid. A deficiency in ACDase activity leads to the accumulation of ceramide in many tissues, a characteristic of Farber disease.

Recently, Alayoubi et al (2013) described the development of a nonlethal 'knock-in' mouse model of FD. They used a homoallelic missense mutation (P362R) discovered in a patient with a 'classical' Farber disease and inserted this into the *asah1* gene. This mutation is located within the most highly conserved amino acid region of the mouse and human *asah1* genes and results in normal levels of protein but reduced (<10%) ACDase activity *in vitro* (Li et al., 1999). They described that the mouse model has low levels of ACDase activity, ceramide accumulation in many tissues, histiocytic infiltrations, reduced body weight, shortened life span (median ~65 days), impaired ovary development, altered myeloid parameters, shortened epiphyseal plates and elevated MCP-1 levels in liver, spleen, brain and thymus (Sands, 2013).

II.2 Results

II.2.1 Epidermal 1-O-acylceramide production

II.2.1.1 Identification of 1-O-acylceramides

To further investigate the 1-O-acylCer identity the developed MS/MS method (Rabionet et al., 2013) was extended also for the quantification of 1-O-acylceramides with sphingosine(d17:1) as core structure.

Therefore product ion spectra were recorded. In Figure 24 A two product ion spectra can be seen. The upper lane shows the fragmentation pattern of 1-O-stearoyl-Cer(d18:1;h16:0), eluting at 3.75 min and with a m/z ratio of the protonated form of 820.5. Cleavage of water leads to a fragment of the m/z 802.3 and loss of the fatty acid moiety in 1-O position and another water molecule to the fragment m/z 518.2. The fragment with the mass of 264.1 derives from the sphingoid base So(d18:1). In the lower lane the fragmentation pattern of 1-O-stearoyl-Cer(d17:1;h16:0) can be seen, but with interference of 1-O-17:0-Cer(d18.1;h16:0) as both species are structurally isomeric and elute at the same time (in this case at 3.63 min). The loss of one water molecule leads to a fragment with m/z 788.3 which can be further fragmented either into the protonated Cer(d18:1; h16:0) or into the protonated Cer(d17:1;h16:0) by the loss of 2 water molecules and the corresponding fatty acid moiety. Finally, the smallest fragment is either So(d17:1) (m/z 250) or So(d18:1) (m/z 264).

While scanning for other compounds, it occurred that signals for Cers with a So(d17:1) sphingoid base are less intense than the corresponding Cer with So(d18:1), as well as signals strongly overlap with fragmentation patterns which probably derive from ammonium adducts of triglyceride species (Figure 24 B). While for 1-O-24:0-Cer(d18:1;24:0) no prominent interference with other species occurs, for the corresponding 1-O-acylCer with d17:1 base (and structural isomers) many more fragments are detected. From the ion with the m/z of 968.4, not only the fatty acid moieties derived from Cers can be cleaved off. Its further fragmentation also leads to molecules with masses fitting to fragments derived from triglycerides (loss of neutrals corresponding to FA 18:1; 18:2; 20:1; 22:1; 24:0; 24:1).

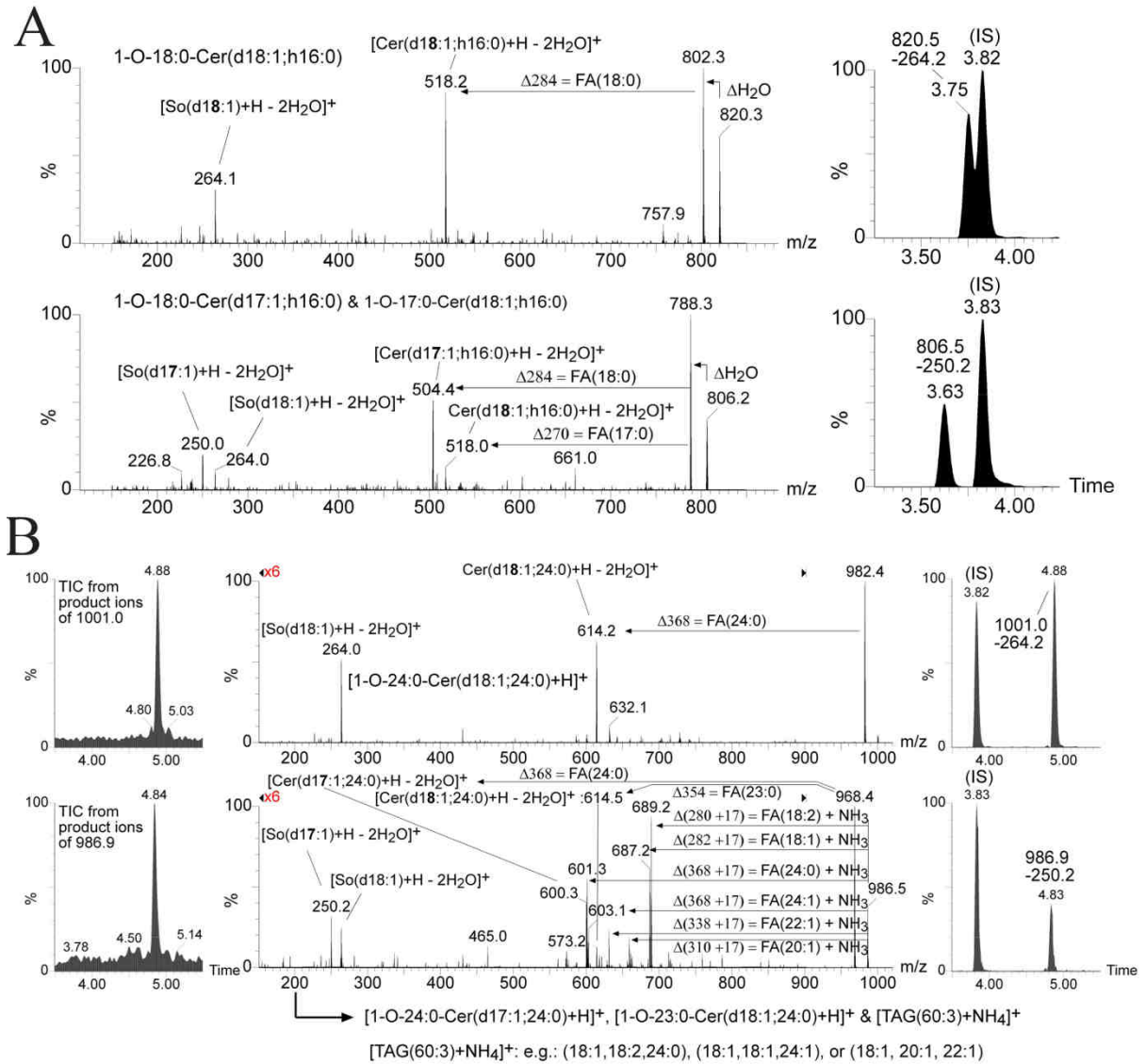


Figure 24 Product ion spectra of protonated 1-O-acylceramides ($[\text{M}+\text{H}]^+$) from epidermal lipid extract of CerS3-deficient mice. Average product ion spectra were recorded for the time span of the transitions i) m/z 820 to m/z 264 and ii) m/z 806 to m/z 250 as seen in the corresponding chromatograms on the right side of the picture. A: fragmentation patterns of 1-O-18:0-Cer(d17:1/d18:1;h16:0). B: fragmentation pattern of 1-O-24:0-Cer(d18:1/d17:1;24:0). On the left are plotted the TICs of the corresponding product ion spectra and on the right the peaks of the corresponding transitions of i) m/z1000 to m/z264 and ii) m/z986 to m/z250 (nominal masses) in relation to the transition recorded for the internal standards (m/z816 to m/z264).

Similar to what is published for 1-O-AcylCers with sphingosine(d18:1), characteristic elution times were obtained out of the information of the product ion spectra for the series of 1-O-AcylCers(d17:1;X:0) that depend on the length of the acyl chain in ester linkage and on the ceramide backbone (Figure 25A). These patterns were achieved by using the transitions of the molecular ions to their c-type fragment, which is specific for the parent Cer backbone (for descriptions of c-type fragment see also II.1.1). By keeping the 1-O-acyl chain constant the retention times increased with increasing length of the FA (ceramide) anchor (Figure 25B vertical lines). With these curves predictions of further unknown compounds and peaks with regard to the O-acyl chain length of 1-Oacylceramides can be made. Structurally isomeric 1-O-acylceramides eluted simultaneously and could only be differentiated by the SRMs used. For example a ceramide (d17:1;24:0) with behenic acid in 1-O position (Figure 25A, series m/z 600, peak G) and 1-O-lignoceroyl Cer(d17:1;22:0) (Figure 25A, series m/z 572, peak I) eluted at the same time but differed in their SRM. Hence, a series of lipids appropriate to the esterification of the corresponding Cer backbone with long to very long chain saturated fatty acids was identified also for 1-O-AcylCers containing So(d17:1).

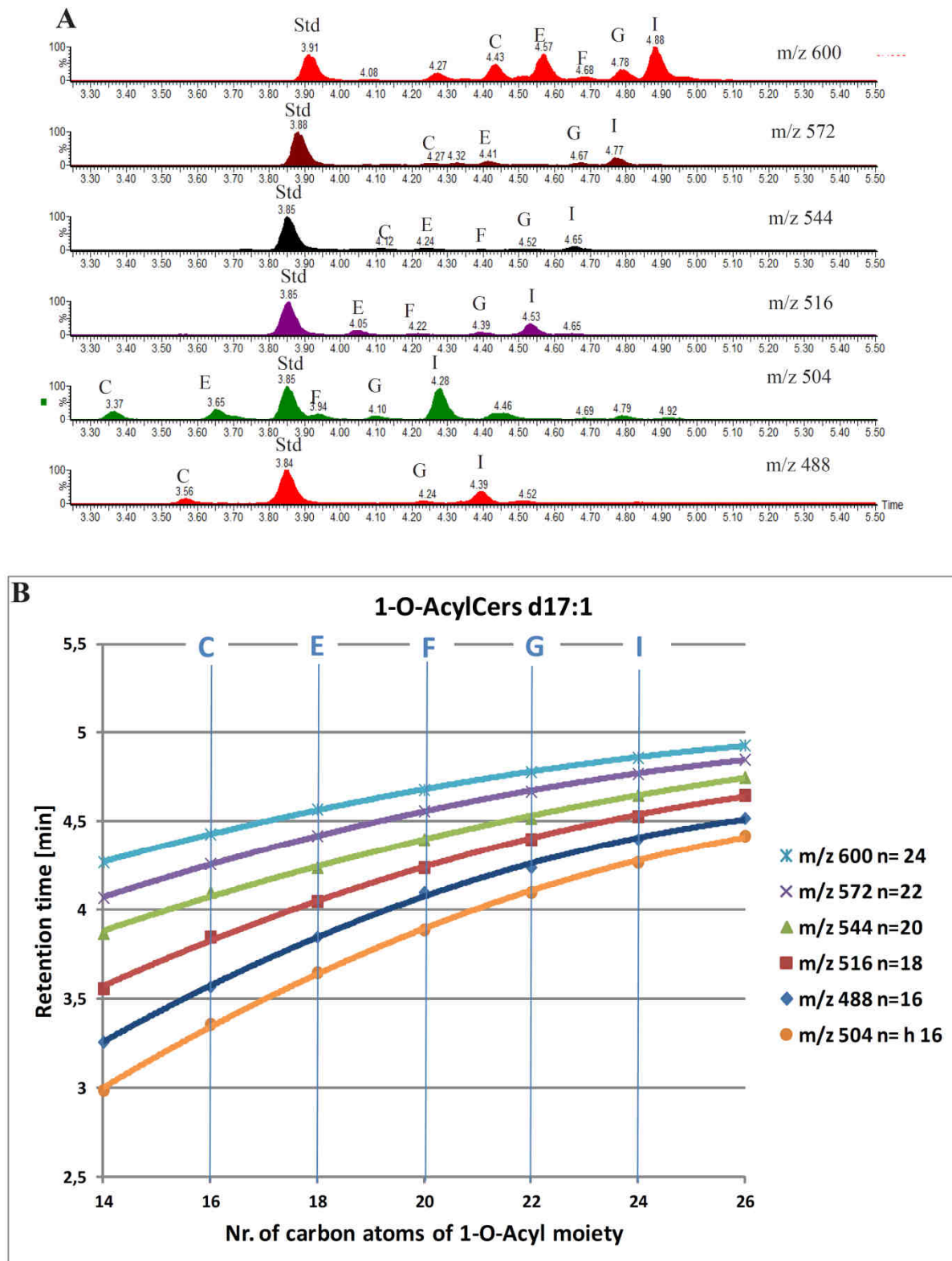


Figure 25 RP chromatography of 1-O-acylceramides with a C17-So backbone. 1-O-acylceramide (with a C17-sphingosine, d17:1) were recorded in subseries according to the parent Cers they derived from [h16, Cer(d18:1;h16:0); 16, Cer(d18:1;16:0); 18, Cer(d18:1;18:0); 20, Cer(d18:20:0); 22, Cer(d18:22:0); and 24, Cer(d18:24:0)]. A: Total ion chromatogram of the subseries of 1-O-acylceramides. Lipids were separated using a RP-18 column. Letters depict peaks of acylceramides with defined 1-O-acyl chain: C, C16:0; E, C18:0; F, C20:0; G, C22:0; I, C24:0. Other species recorded either appear in between these peaks and are not annotated or their concentration is too low to be observed in total ion chromatograms. Std. denotes the internal standard 1-O-oleoyl Cer(d18:1;17:0). B: Retention times of 1-O-acylceramides on RP-18 column are plotted in dependence of the saturated acyl chain in ester linkage for the different parent Cer backbones. Curves were obtained by nonlinear regression (second order polynomial).

II.2.1.2 Quantification in epidermal samples

II.2.1.2.1 Analysis of 1-O-AcylCer levels during the development of the water permeability barrier

If 1-OAcylCer also function as barrier lipids they should emerge during the establishment of this barrier. Such increase in wildtype animals would further verify the biosynthetic origin of these compounds, excluding methodological artifacts during sample preparation. Therefore skin of BL6 mice from prenatal day 16 (E16) up to postnatal day 1 (P1) was examined for 1-O-acylceramide composition (Figure 26).

As it was not possible to separate epidermis from dermis at E16, due to a not fully developed epidermis, full skin of E16 and E17 mice was collected and compared. At E16 1-O-AcylCers are hardly synthesized, while at E17 they increase directly to maximum amounts. After stage E17 levels of 1-O-acylceramides stay steady at around 200 pmol/mg of dry weight, which is in accordance with all our shown control values.

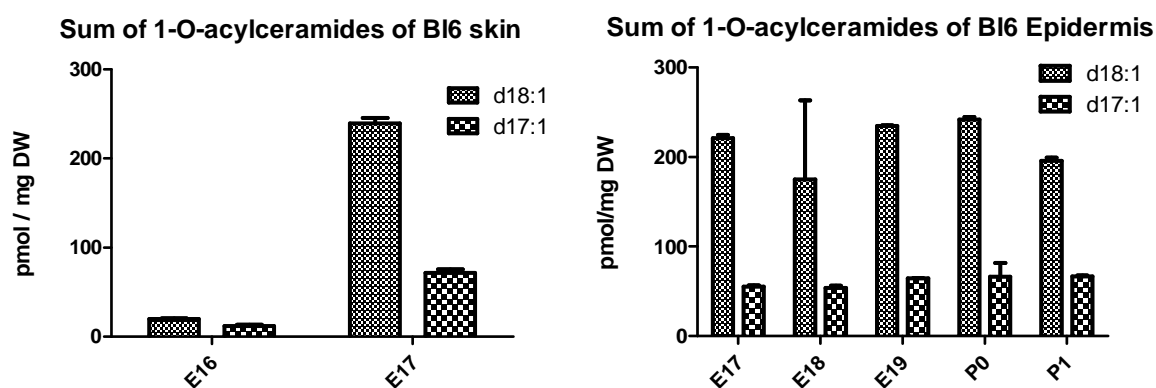


Figure 26 Correlation of occurrence of 1-O-acylceramides with establishment of water permeability barrier. 1-O-AcylCers occur together with establishment of WPB. n= 3 biological samples per group.

II.2.1.2.2 Analysis of competing pathways

Cers can be either modified into GSLs and alternatively into SM, or they can be acylated to form 1-O-acylceramides. All three pathways theoretically compete with each other. To investigate whether GlcCer production and 1-O-acylCer formation exclude each other, we analyzed the epidermis of mice deficient in GlcCer synthesis (Figure 27). Epidermal lipid extracts from wild-type mice with keratinocyte specific deficiency of GlcCer-S (Ugcg) cells at postnatal day 4 (P4) (Figure 27) revealed that 248 ± 53 pmol of 1-O-acylceramides contained a C18-sphingosine base and 155 ± 31 pmol a C17-sphingosine base. A comparison with the published (Jennemann et al., 2007) total amount of ω -esterified C18-sphingosine base-containing Cers, showed that 1-Oacylceramides (d18:1;X:0) make up 4.6% of all esterified Cers (sum of EOS-, POS-, and 1-O-acylceramides with a C18-sphingosine base) or 4.3% of all esterified SLs (including esterified GlcCers and SMs with a C18-sphingosine base). The amounts of 1-O-AcylCers(d18:1;X.:0) in epidermis of mice deficient in GlcCer synthesis on the other hand, increased to about 900% , and to about 450% for 1-O-AcylCers(d17:1;X.0) in 4 day old mice. While 1-O-AcylCers with a VLC moiety, e.g., 1-O-lignoceroyl Cers, increased only 3- to 4-fold, 1-O-palmitoyl and 1-O-stearoyl Cers (LC) increased 60- and 80-fold, respectively (Rabionet et al., 2013).

As LPLA2 is o homologue of Lro1, the involvement of LPLA2 in epidermal 1-O-acylceramide synthesis was also investigated. By measuring the 1-Oacylceramide levels from extracts of controls and LPLA2 mutants it was revealed that at the 5% level, no differences were observed. These results were conformed in samples of both, newborn or 4 days old mice, excluding a major role of LPLA2 in epidermal 1-O-acylceramide synthesis (Figure 27).

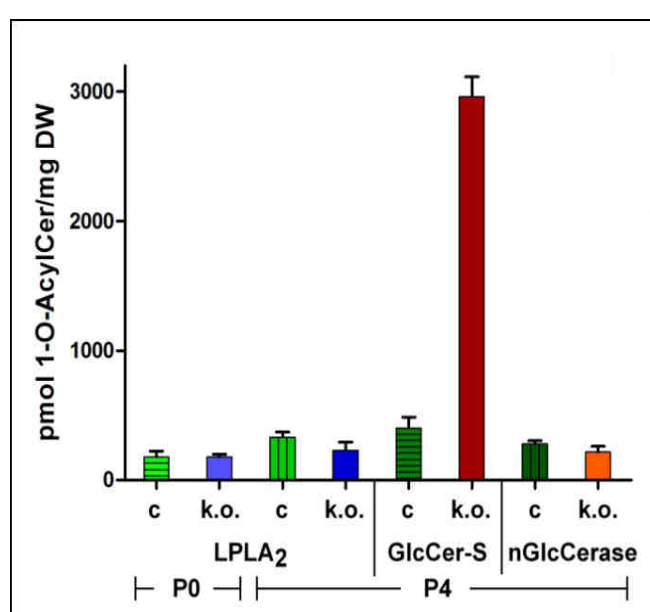


Figure 27 Quantification of 1-O-acylceramide levels in the epidermis of LPLA2 -deficient, keratinocyte-specific GlcCer-S-deficient, nGlcCerase-deficient, and corresponding control mice. A: 1-O-acylceramides containing saturated 1-O-acyl chains from C14 to C26 and parent Cer backbones with either a C17-sphingosine (d17:1) or a C18-sphingosine (d18:1) combined with the N-linked acyl chains hC16:0, C16:0, C18:0, C20:0, C22:0, or C24:0 were quantified by UPLC-MS/MS. 1-O-acylceramide levels were compared between control (c) and the different knockout (ko.) mice at birth [post natal day (P)0] and 4 days postnatal (P4). The full list of compounds is listed in supplementary Table II. nGlcCerase, neutral glucosylceramidase/Gb2a; n = 3 for LPLA 2 (P0 and P4), and GlcCer-S control and mutant (ko.) groups, n = 6 for nGlcCerase controls and n = 4 for nGlcCerase-deficient samples (ko.). From (Rabionet et al., 2013).

In the following the data of the quantifications of 1-O-acylceramides were grouped into lengths of the N-linked anchor moiety (d18:1/d17:1; X:0) and lengths of the 1-O-acyl moiety for better visibility of 1-O-acylCer compositions.

Figure 28 shows data of mice with deficiency of the cytosotically located neutral glucosylceramidase (nGlcCerase), which is tightly attached to membranes of the Golgi and the ER (Körschen et al., 2013) or the plasma membrane (Aureli et al., 2012). Deletion of nGlcCerase was accompanied by a significant decrease of 1-O-acylceramides with anchor lengths of 16 carbon atoms (also for hydroxyl 16:0). The corresponding precursor Cers (Figure 28 left panel) are also significantly reduced. Moreover the ceramides with stearic (16:0) and arachidonic (18:0) acid moieties are significantly reduced, while Cer(d18:1;24:0) levels are elevated. The overall glucosylated ceramides are, in opposite to Cers, significantly increased. The GlcCers (d18:1;h16:0) and (d18:1;24:0) show an elevation only by trend.

On the other hand, several FAs in 1-O position are by trend decreased in nGlcCerase deficient mice. 1-O-acylceramides with stearic acid (C18:0), lignoceric acid (C24:0), pentacosanoic acid (C25:0) and cerotic acid (C26:0) in 1-O position are significantly different on a 5% level (Figure 28 right panel).

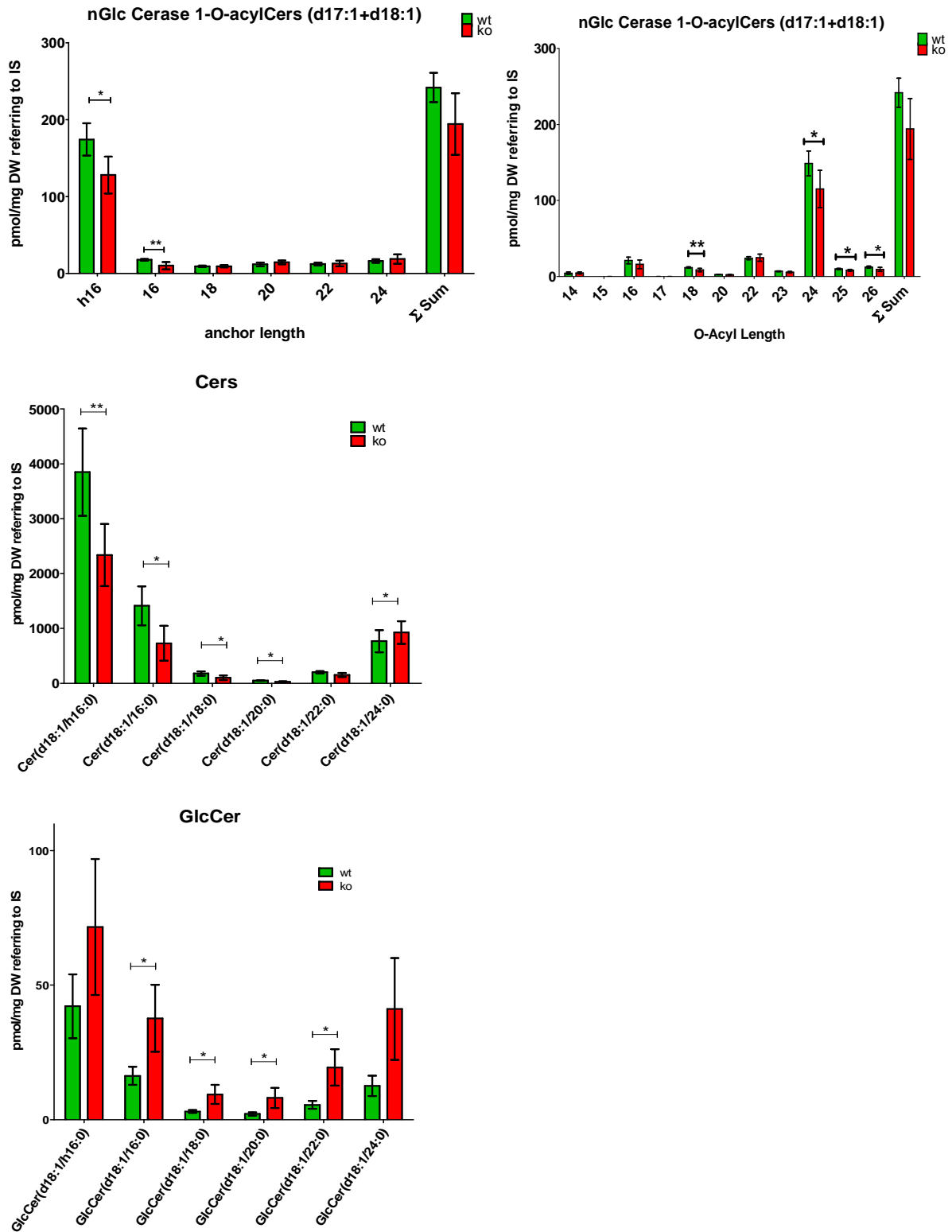


Figure 28 Detailed analysis of epidermal 1-O-acylceramides from neutral glucosylceramidase-deficient mice. C18 and 17-sphingosines containing 1-O-acylceramides were grouped according to their parent Cer [1-O-acyl Cer(d18:1;X:0)] and according to their 1-O-acyl moiety. Note a significant decrease of those 1-O-AcylCers containing an N-linked hydroxy-palmitoyl chain (h16; 73% of controls) or an N-linked palmitoyl chain (16; 56% of controls), which nicely corresponds to a simultaneous decrease of these free Cers [Cer(d18:1;h16:0) and Cer(d18:1;16:0)] in neutral glucosylceramidase-deficient mice; $p < 0.05$. GlcCers are generally elevated. $n = 4-6$ animals per sample group. Significance was calculated with the students Ttest.

II.2.1.2.3 Search for potential enzymes catalyzing the acylation of ceramides *in vivo*

To further explore which enzymes could be responsible for epidermal 1-O-acylceramide production epidermal skin extracts of DGAT2 and LCAT mutant mice (provided by B. Farese and M. Hoekstra) were investigated. Mice were 4 days old and wildtype as well as heterozygous mice were used as controls compared to knockout mice. DGAT2 and LCAT are both homologous of the diacylglycerol acyltransferases Dga1p and Lro1p and possibly 1-O-acylate VLC-Cers. Hence a deficiency of these enzymes could cause a decrease of 1-O-acylceramide levels.

In Figure 29 quantification of 1-O-acylceramides including those with sphingoid bases with 17 and 18 carbon atoms, is shown for DGAT2 mutant and control mice. Distribution of FAs in 1-O-position of ceramides is similar to other mouse models, for example comparable to CerS3 mutant mice (Rabionet et al., 2013), with lignoceric acid moieties (C24:0) being the most abundant species in both ko and control mice. The most abundant FA anchor incorporated into Cers by N-linkage is hydroxy-palmitic acid (h16:0). Overall, 1-O-acylceramides are by trend increased in DGAT2 mutant mice for all lengths of moieties in 1-O-position with both, So(d18:1) and So(d17:1) as Cer bases. In mutant DGAT2 samples 1-O-palmitoyl, 1-O-stearoyl and 1-O-arachitoyl Cer levels are significantly increased from control mice. Interestingly, FAs with lengths from 16 C-atoms on which are incorporated as anchors into Cers seem elevated in the mutants, while the h16:0 anchor seems to be less often used for 1-O-AcylCersynthesis (second row in Figure 29). To be able to judge, if 1-O-AcylCers production with h16 moieties is reduced, the ratio of 1-O-AcylCers to the sum out of the corresponding precursor Cers and the 1-O-AcylCers was calculated (Figure 29, second row and the right side). Here, levels of 1-O-AcylCers(d18:1;h16) in mutant samples are also significantly reduced in comparison to control samples. Furthermore the classic Cer and GlcCer levels were determined (Figure 29, bottom; left side). Overall Cer levels in DGAT2 deficient mice are by trend elevated (significant for Cer(d18:1, 18:0/20:0/22:0/24:0), corresponding to GlcCers of which the types GlcCer(d18:1;h16.0/20:0/22:0) are significantly increased. Also interesting is, that Cer levels of the species shown, are quite low and in the same range of 1-O-AcylCers, in comparison to Cer levels of other mouse models

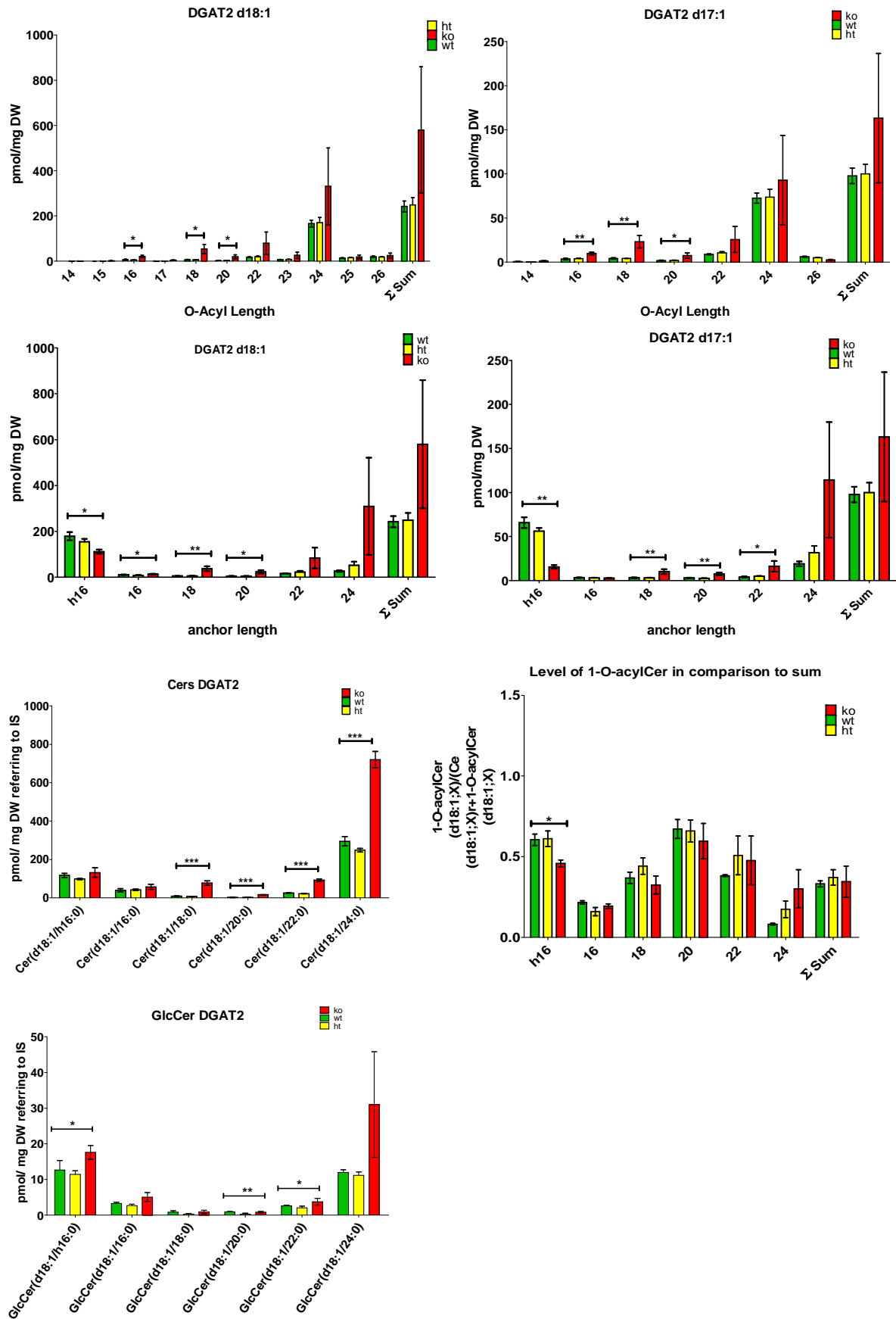


Figure 29 Detailed analysis of epidermal 1-O-acylceramides from DGAT2-deficient mice. C18 and 17-sphingosines containing 1-O-acylceramides were grouped according to their parent Cer [1-O-AcylCer(d18:1;X:0)] and according to their 1-OAcyl moiety. Besides 1-O-AcylCers(d18:1/17:1;h16:0) , 1-O-AcylCers, classic free Cers and GlcCers are by trend elevated. n=3animals per sample group. Significance was calculated with the one sided ANOVA test.

LCAT on the other hand is essentially a specialized phospholipase A that utilizes cholesterol as an acyl acceptor in place of water. LCAT reaction is responsible for the synthesis of most of the cholesteryl esters present in human plasma and is a critical component of the reverse cholesterol transport pathway (Subbaiah et al., 2006). Here wildtype, homozygous (hom) (LCAT activity is 1% of wildtype) and heterozygous (LCAT activity is 70% of wildtype) mice were used for investigations (Ng et al., 1997).

Figure 30 shows the quantifications for 1-O-acylceramides containing both sphingoid bases with 17 and 18 carbon atoms. Lignoceric acid moieties (C24:0) are most abundantly incorporated in 1-O position in both hom and control mice. The most abundant FA anchor in Cers is hydroxy-palmitic acid (h16:0). Overall, 1-O-acylceramides are by trend increased for some lengths of moieties in 1-O- position (16:0/20:0/22:0/24:0) with So(d18:1) as Cer base. 1-O-AcylCers Y(d17:1;X) are not elevated. Also FAs with lengths from 16 C-atoms on which are incorporated as anchors into Cers seem elevated in the mutants (second row in Figure 30). Furthermore the classic Cer and GlcCer levels were determined (Figure 30, bottom; left side). Besides hydroxyl-palmitoyl overall Cer levels in LCAT deficient mice are by trend elevated (significant for Cer(d18:1, 16:0/18:0/24:0), corresponding to GlcCers of which the types GlcCer(d18:1;18:0.0/20:0/22:0;24:0) are significantly increased.

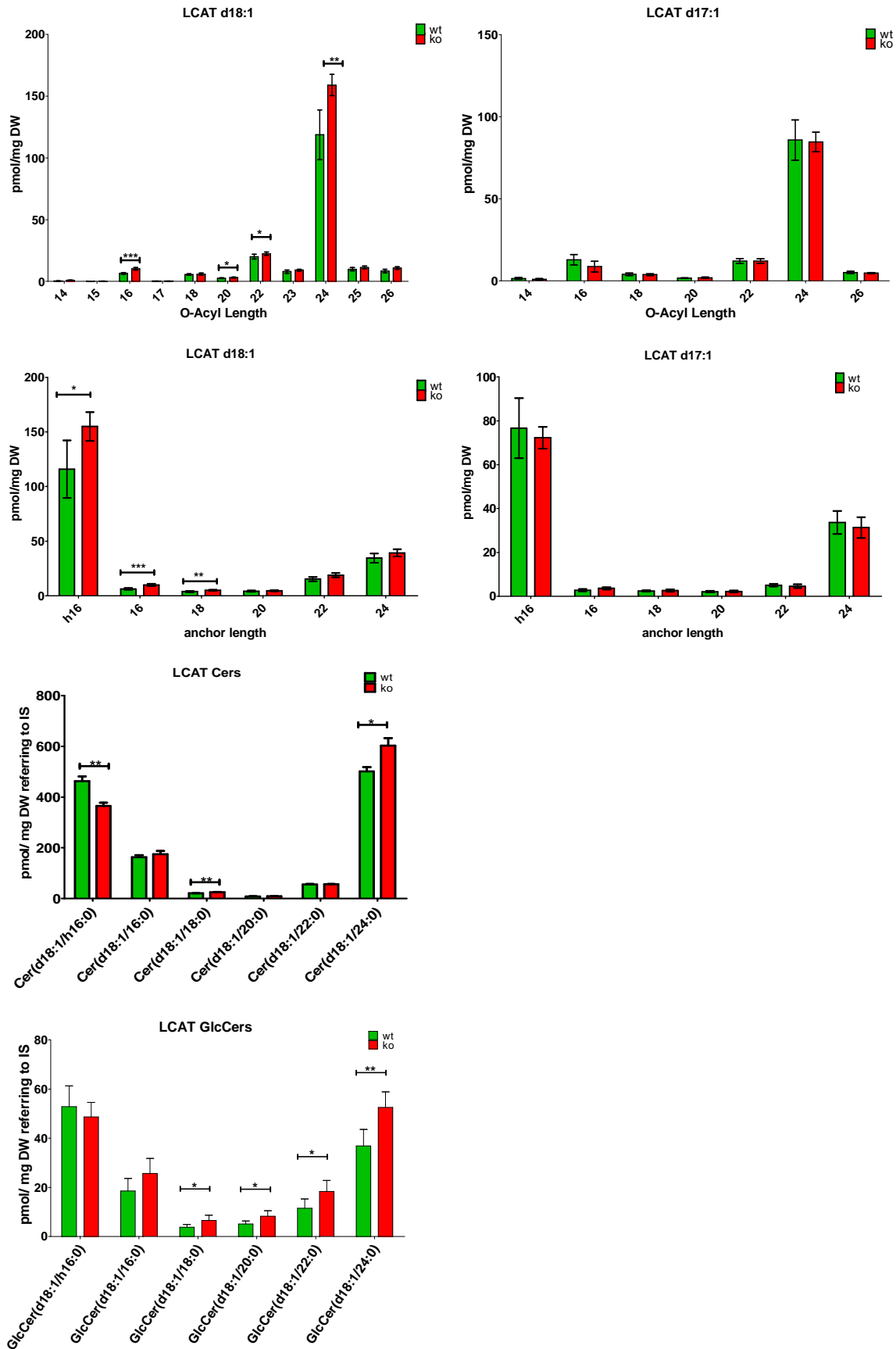


Figure 30 Quantification of 1-O-Acylceramides in LCAT mutant mice. So(d18.1) containing 1-O-acylCer levels are tendentially elevated between wt and mutant samples, whereas So(d17:1) containing 1-O-AcylCers levels are not altered. Classic free Cers and GlcCers are by trend elevated. n=3animals per sample group. Significance was calculated with the students Ttest.

II.2.1.2.4 Which ceramide synthases and fatty acid elongases are essential for the production of the VLC-ceramide backbone of 1-O-AcylCers?

It was suggested as CerS3 deficient mice show accumulation of 1-O-AcylCers, that only VLC-FAs are used for 1-O-acylCer production, (Rabionet et al., 2013). One prominent Ceramid-backbone of 1-O-AcylCer contained N-linked lingoceric acid. This backbone should depend on either of the three ceramide synthases CerS2, CerS3, or CerS4 and could also involve Elovl3 or Elovl1 to elongate long chain fatty acids to 24 carbon atoms. With CerS2, CerS3, CerS4 and Elovl3 mutant mice in hands, the question was addressed if any of those enzymes is quintessential for 1-O-AcylCer(dX:1,24:0) production. 1-O-AcylCer were quantified in these mutant and control mice and data are plotted together with those of LCAT and DGAT2 mutant mice for better comparison in Figure 31.

Total amounts of 1-O-acylceramides are significantly elevated in CerS3, LCAT and by trend in DGAT2 mutant samples. Only in Gb2a mutant epidermis a significant reduction can be noted. In all other samples (CerS2, CerS4) no significant alteration is observed (Figure 31). Neither in CerS2, CerS3, and CerS4 nor in Elovl3 mutant mice single species of 1-O-AcylCers containing VLC moieties are reduced. As 1-O-AcylCers are downstream products of Cers, total free ceramide levels were determined. Besides Gb2a, which levels are reduced, and DGAT2 which levels are increased, all values are unchanged in the mutant samples, whereas values are significantly different only for Cers in Gb2a and DGAT2 mice. GlcCers are all by trend elevated in the mutants but significantly different only in Gb2a mice. The ratio of 1-O-AcylCers to the sum of 1-O-AcylCers and corresponding Cers shows no significant differences for either of the mouse models.

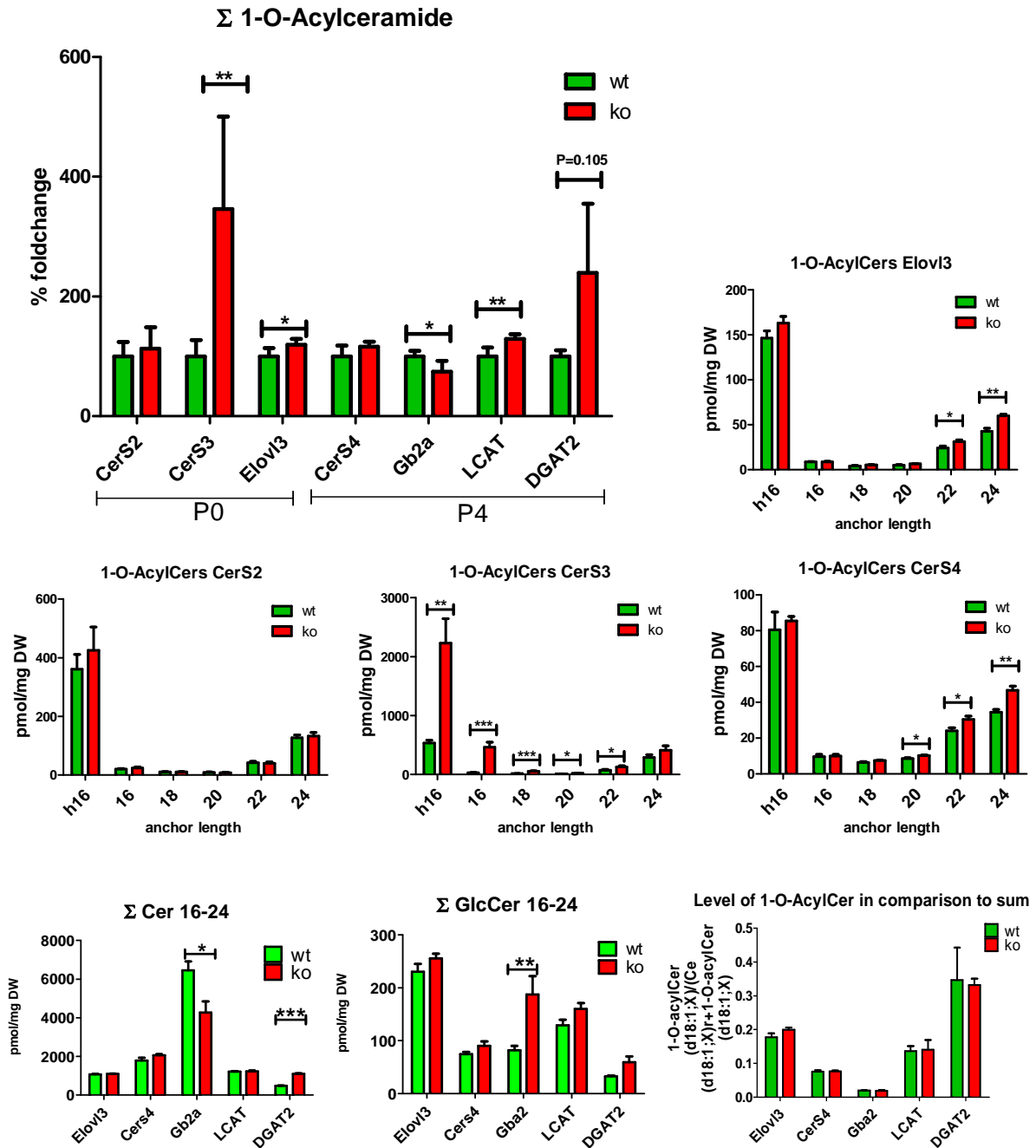


Figure 31 Sums of 1-O-acylceramides in mutant mice models. Total amounts of 1-O-acylceramides are elevated in CerS3, LCAT and by trend in DGAT2 mutant samples. In Elov13 and Gb2a mutant epidermis a reduction can be noted. In all other samples there is no significant alteration observed. Also total ceramide and glycosylceramide amounts for each mouse model were determined. Besides Gb2a all levels are by trend elevated or unchanged in the mutant samples, whereas values are significantly different for Cers in Gb2a and DGAT2 mice, as well as for GlcCers in Gb2a mice. The ratio of 1-O-AcylCers to the sum of 1-O-AcylCers and corresponding Cers shows no significant differences for either of the mouse models. n=3-6 biological samples per group. Significance was calculated with the student's T test.

II.2.1.3 Sphingoid base quantification

In parallel to 1-O-AcylCer analysis CerS3, Ugcg, CerS4, Elovl3, Gb2a, LCAT and DGAT2 were also investigated upon their levels of free sphingoid bases with the method developed in Part I. As shown in Figure 32 levels nicely reflect results out of Cer and 1-O-AcylCer measurements. Free So is always proportional to free Cer levels. Only in epidermis of CerS3 deficient mice sphingoid base levels are reduced. GlcCer synthase, CerS4, Elovl3, nGlcCerase and LCAT deficient mice show no alteration in sphingoid base levels. The mean increase observed in Dgat2 mutants was not significant for the number of samples analyzed.

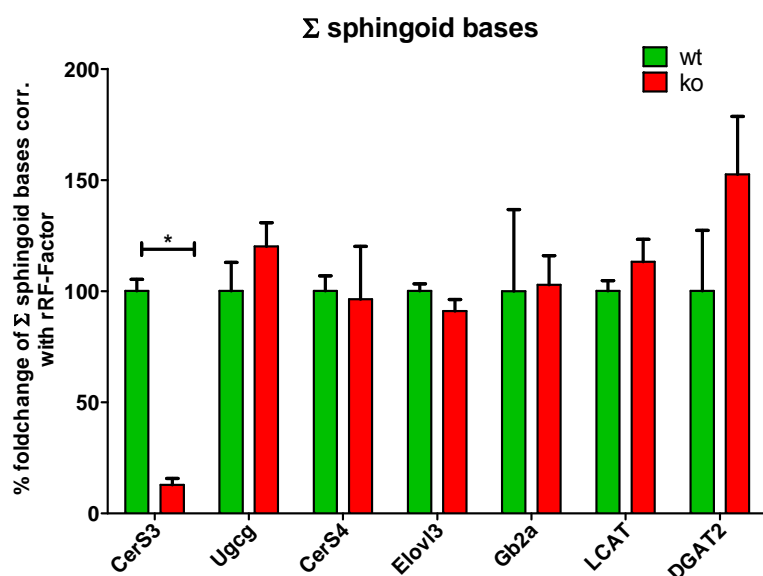


Figure 32 Total amount of sphingoid bases in mutant mouse models. Significance was calculated with the students Ttest.

II.2.2 Farber disease and the lysosomal acid ceramidase

As both, water and short-chain ceramides were published to compete for the acylacceptor role when LPLA2 hydrolysis phospholipids (Abe et al., 1996; Shayman et al., 2004), we decided to analyze mice with endogenously higher lysosomal ceramide levels. Mice with a mutation of *asah1* resembling the human Farber disease, were obtained from T.Levade. Furthermore, we were interested to see, if by increased ceramide levels, 1-Oacylceramides could be detected in significant amounts also in other tissue than epidermis.

In cooperation we analyzed organs of these mice (spleen, thymus, heart and kidney) and analyzed them for 1-O-AcylCer composition to find out more about origins of 1-O-acylceramides.

Alayoubi et al (2013) suggested that upon deficiency of ACDase activity macrophages fail to degrade the sphingolipids and the ceramide they store, which results in more ceramide accumulation (especially livers, brains, spleens, and thymuses) and their subsequent foamy appearance that is characteristic of FD.

Figure 33 and Figure 35 illustrate, that elevated 1-O-AcylCer levels in mutant organs of Farber diseased mice are present. In spleen levels are particular high, namely a 100 fold increased compared to controls. In thymus we can also find a 10 fold increase whereas in other organs (Kidney, heart and brain) an increase of 2-4 fold compared to controls can be observed. In all organ types, FAs of 16 and 18 C-atoms length, are most frequently bound to the O-position of the ceramide backbone. Concerning the unsaturated species, we can also observe elevated values, but levels are in general 10 times smaller than the saturated ones.

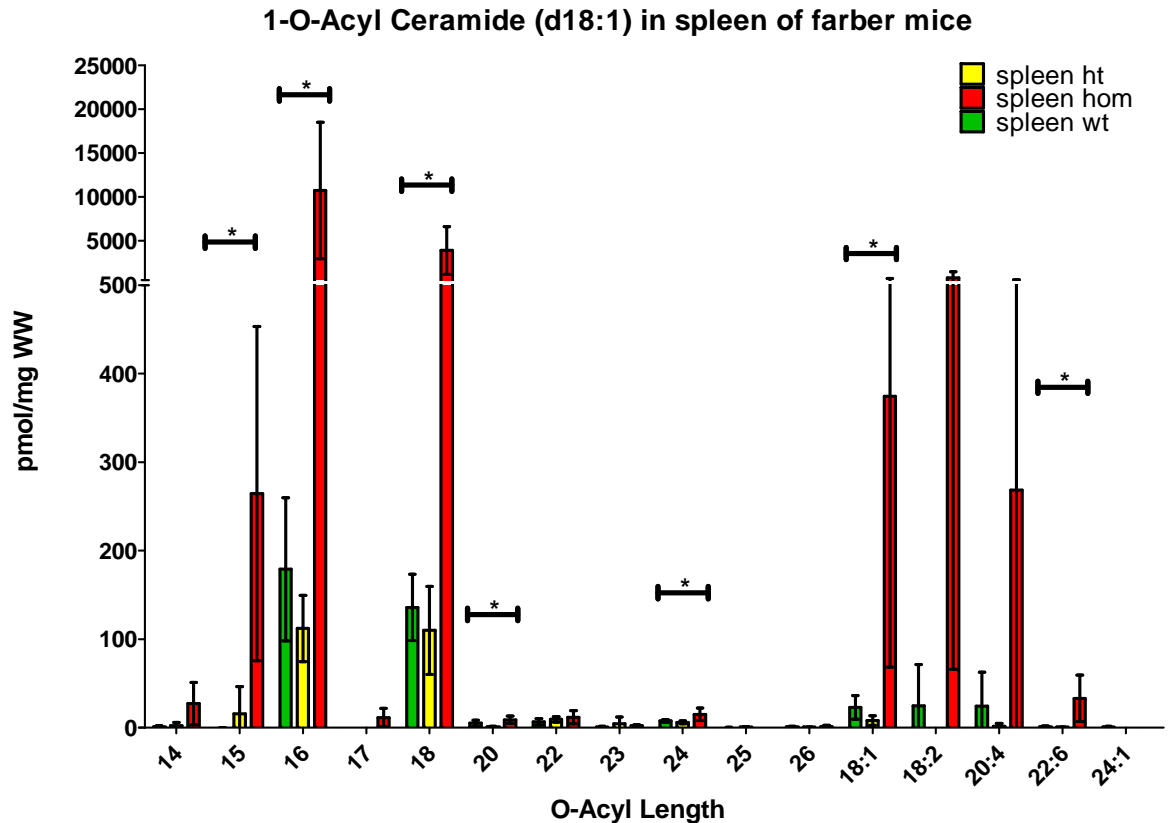


Figure 33 1-Oacylceramide levels of Farber mutant spleen (hom) and controls (wt and het) sorted after 1-O-acyl moiety length. Levels for hom samples are 100 fold higher than for control samples. One way ANOVA significant on a 5% level. n=4 biological samples per group.

In homozygous spleen 1-O-acylceramides (d18:1) with the saturated FAs pentadecylic acid, palmitic acid, stearic acid, arachidonic acid, lignoceric acid and the unsaturated FAs oleic acid and docosahexaenoic acid in 1-O position are significantly elevated. 1-O-AcylCers with unsaturated moieties make up ~15% in wt and 10% in hom samples. Also The FAs N-linked to the sphingosine(d18:1) are elevated in samples with reduced Asah1 activity, whereas palmitoyl-Cers are the most abundant species. Similar to O-linked FAs, differences between homozygous and control samples concerning FAs incorporated at the N-position are significant (Figure 34). In homozygous spleen values are 100 fold increased, in thymus 20 fold and in kidney and heart 4-5 fold (Data not shown).

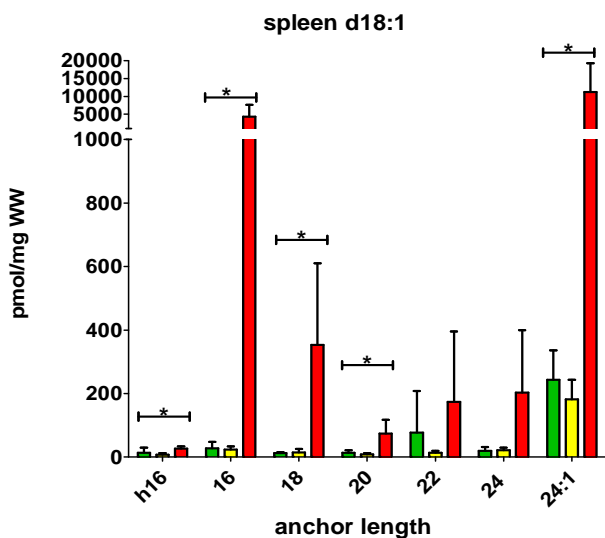


Figure 34 1-Oacylceramide (sorted according the anchor lengths) levels of Farber mutant spleen (hom) and controls (wt and het). Levels for hom samples are elevated in comparison to control samples. One way ANOVA significant on a 5% level. n=4 biological samples per group.

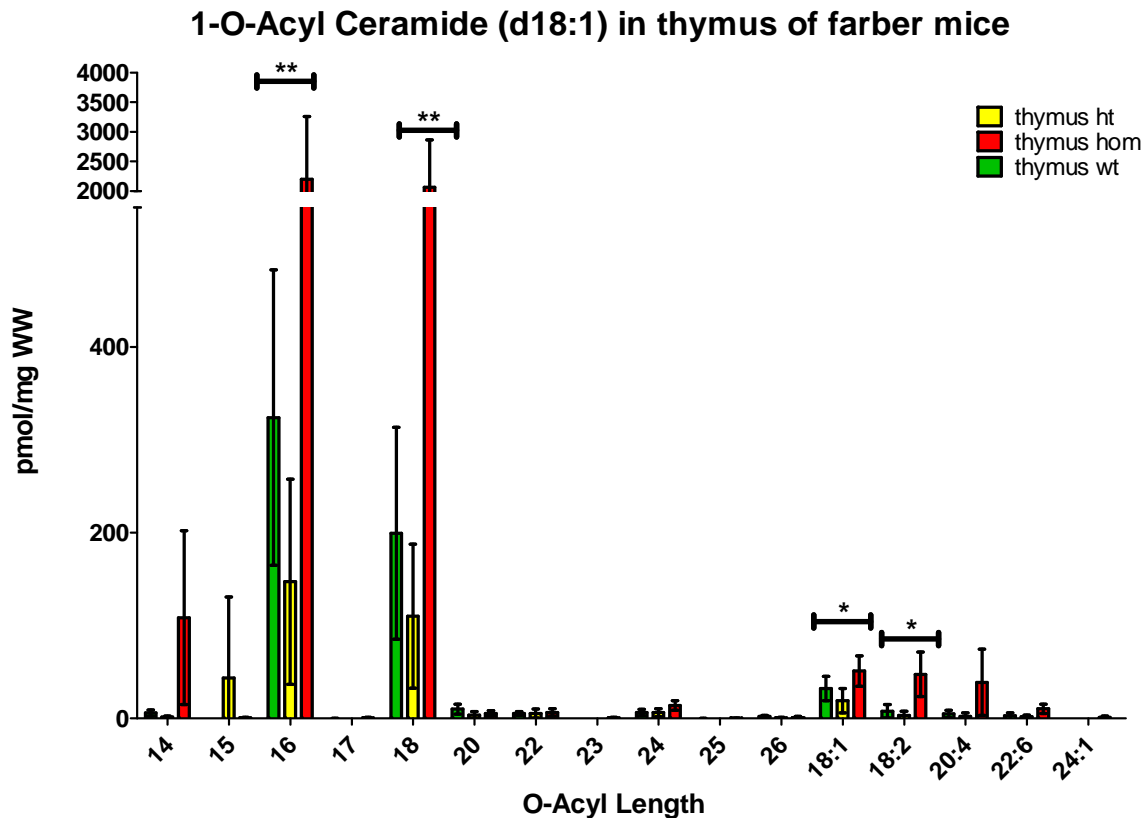


Figure 35 1-O-acylceramide levels of Farber mutant thymus (hom) and controls (wt and het). Levels for hom samples are 10 fold higher than for control samples. Significance calculated by one way ANOVA test. n=4 biological samples per group.

Also in heart and kidney values of homozygous samples are 5 times higher than in control samples. In heart of homozygous mice 1-O-palmitoyl- and 1-O-stearoyl-Cer levels are significant different from control samples, whereas in kidney only 1-O-stearoyl-Cer shows significant differences on the 5% level and 1-O-palmitoyl-Cer differ only on the 10% level (Figure 36).

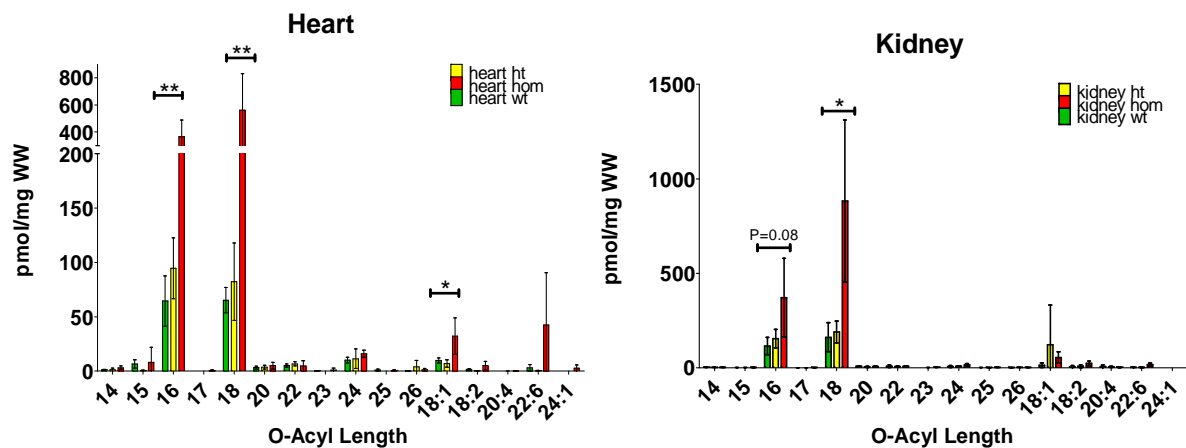


Figure 36 1-O-acylceramide levels of Farber mutant heart and kidney (hom) and controls (wt and het). Levels for hom samples are 5 times higher than for control samples. Significance was calculated with the one sided ANOVA test. n=4 biological samples per group.

Classic free ceramide levels in homozygous heart and kidney are approximately 10 fold increased compared to controls. Due to technical difficulties free Cer levels could not be measured in thymus and spleen.

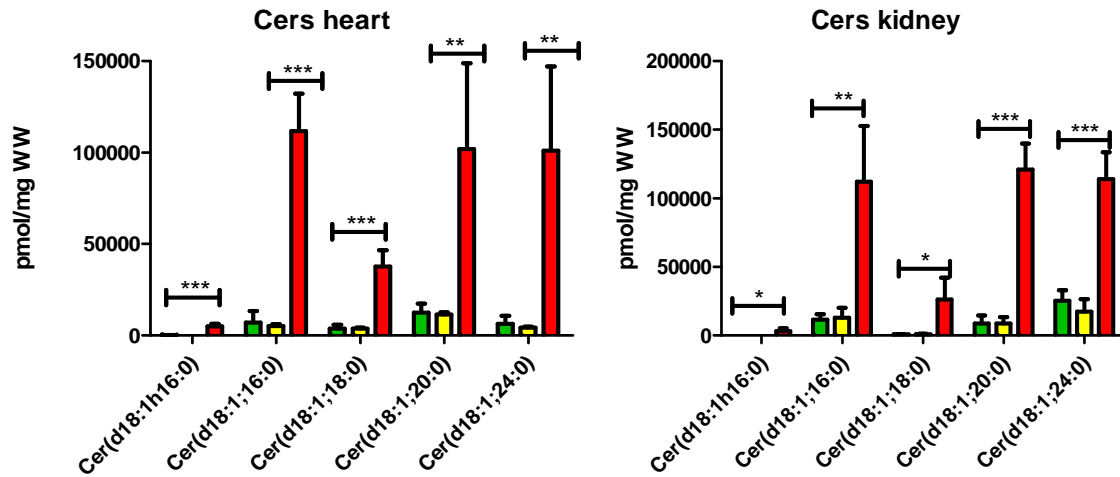


Figure 37 Free Ceramide levels in organs of Farber mutant and control mice. Ceramide levels are significantly elevated in heart and kidney of mutant mice. Significance was calculated with the one sided ANOVA test. n=4 biological samples per group.

The pathway how and by which enzymes, 1-O-acylceramides are formed and degraded is still unclear. In skin, unsaturated FAs make up approximately 25% (determined by 1-O-(18:1)Cer) of saturated FAs in 1-O-position of Cers (Figure 38). Furthermore in skin FAs with a length of 22:0 and 24:0 carbon atoms are the FAs, which are most frequently added to the ceramide backbone in 1-O position, while in other organs (kidney, heart, spleen and thymus) FAs with a length of 16 and 18 carbon atoms are most abundant. However in the here investigated tissues, proportions of saturated to unsaturated species is ~4:1 in skin samples and also in spleen, thymus, heart and kidney. 1-O-Acyl (24:1)Cer was not taken into account for these calculations as it is not present in both, skin and other organs (kidney, heart spleen, and thymus).

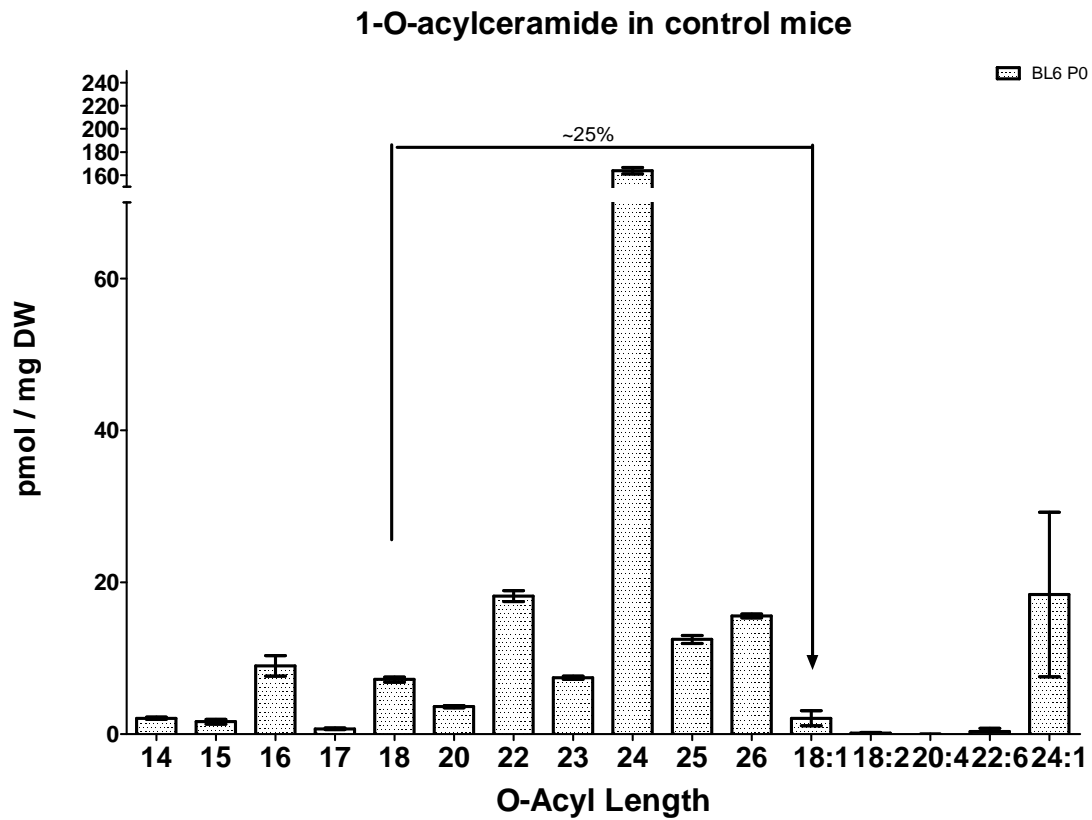


Figure 38 1-O-acylceramide levels in BL6 control epidermis samples. Mice were newborn and of age postnatal day 0.1-O-AcylCers with unsaturated FAs in 1-O position make up 25% of the corresponding 1-O-AcylCers with saturated FAs in 1-O position. n=4 biological samples per group.

II.3 Discussion

The biosynthetic pathways of Cer 1-O-acylation were described for yeast, but only recently also the composition and structure of endogenous 1-O-AcylCers containing So(d18:1) and their natural concentrations were characterized (Rabionet et al., 2013). In this work the method for quantification of 1-O-acylceramides was adapted to also identify 1-O-AcylCers containing So(d17:1). While for So(d18:1) containing 1-O-AcylCers the fragmentation patterns were limited to loss of 1-2 water molecules, followed by loss of the O-linked acyl moiety and ending with the sphingosine(d18:1) as smallest fragment, total product ion scans of 1-O-AcylCers containing So(17:1) in skin were more complex. Product ion scans showed that 1-O-AcylCers seem to coelute with structurally isomeric triglyceride ammonium adducts. By recording product ion scans only the most abundant (50-100) ions are detected and fragmented within a certain time frame, called untargeted LC-MS/MS analysis. This may lead to negligence of the less abundant 1-O-AcylCer(d17:1;X:0). Thus in the targeted analysis of 1-O-AcylCers by multiple reaction monitoring, So(d17:1) containing Cers can be more reliably identified.

As the enzyme(s) responsible for epidermal 1-O-AcylCer-production in mammalian are unknown, it was hypothesized that homologues of the yeast enzymes may be involved in this pathway in mammals. LCAT and LPLA2 are both human homologous of the yeast Lro1p. Furthermore LPLA2, which was shown to contain transacylation activity towards using short chain Cers (Cer(d18:1;2.:0)) (Shayman et al., 2011), was excluded to play a major role in epidermal 1-O-acylceramide synthesis (Rabionet et al., 2013). Even though 1-O-acylceramides could be produced by lysosomal phospholipases which are secreted during keratinocyte degradation and could transfer FAs from phospholipids to Cers, it is unlikely that the FAs found in 1-O-AcylCers derive from phosphoglycerolipids (Rabionet et al., 2013). Phosphoglycerolipids do not contain VLC chain FAs (especially C24:0; lingoceric acid) which was found to be frequently attached to the 1-O position of Cers. In epidermis, 1-O-acylceramide synthesis rather seems to compete with GlcCer synthesis, as a loss of GlcCer synthase leads to a strong increase of 1-O-acylceramide amounts. GlcCer derived Cers at the Golgi might be transported back to the ER or to lipid droplets where they could be 1-O-acylated by DGAT2, the homolog of the yeast Dga1p.

Interestingly, deficiency of the neutral glucosylceramidase, which is tightly attached to membranes of the Golgi and the ER (Körschen et al., 2013) or the plasma membrane (Aureli

et al., 2012), was accompanied by a decrease of those 1-O-acylceramides (hydroxyl 16:0 and 16:0 FAs) for which we also observed a decrease of the corresponding precursor Cers. Also the sums of all measured 1-O-AcylCers were by trend decreased which suggests that the neutral glucosylceramidase activity is topologically related and upstream of 1-O-acylceramide production. Glucosylceramides were in opposite increased in epidermis of mutants proving that GlcCers degradation is disturbed. If neutral glucosylceramidase is located closely to sites of 1-O-acylCer production, it could enhance local concentrations of Cers used for 1-O-acylation. Correspondingly, loss of this enzyme then would lead to decreased substrate availability and to lower 1-O-acylceramide levels. Furthermore 1-O-AcylCer synthesis seemed not to depend on LPLA2, as in LPLA2 deficient mice no reduction in either of the 1-O-AcylCer species could be observed.

DGAT2 was speculated to be responsible for 1-O-AcylCer production in mammals (Jacquier et al., 2011; Sorger and Daum, 2002). Interestingly, only the 1-O-AcylCers with hydroxy-palmitoyl moieties in N-position were significantly reduced in the homozygous samples, whereas all other species with FAs esterified to the O-position were by trend increased. In DGAT2 deficient mice the corresponding free ceramide species were not reduced, but corresponding glycosylceramides were significantly increased. This could be interpreted in a way, that DGAT2 is only responsible for the utilization of Cers with h16 anchor to form 1-O-AcylCers, even though it was described for preferring endogenously synthesized monounsaturated FAs (Yen et al., 2008). Consequently Cers containing N linked hydroxy-palmitic acid could then instead be used for GlcCer production. On the other hand, could also be uniquely synthesized in cell types, in which loss of DGAT2 activity towards 1-O-AcylCers(X;h16:0) cannot be fully compensated by other enzymes. DGAT2, as part of the DGAT enzyme family, is usually responsible for triacylglycerol (TGs) synthesis (Yen et al., 2008). In addition to DGAT2, its family includes acyl-CoA:monoacylglycerol acyltransferase-1 (MGAT1) (Yen et al., 2002), MGAT2 (Cao et al., 2003; Yen and Farese, 2003), MGAT3 (Cheng et al., 2003), and wax monoester synthases (AWATs 1-2 and hDC3) (Cheng and Russell, 2004; Turkish and Sturley, 2007; Turkish et al., 2005; Yen et al., 2005). DGAT1 on the other hand, is part of a large family of membrane-bound O-acyltransferases (MBOAT, National Center for Biotechnology Information (NCBI) Conserved Domains Database accession number: pfam03062) (Hofmann, 2000). MBOAT family members transfer fatty acyl moieties onto the hydroxyl or thiol groups of lipids and proteins (Chamoun et al., 2001; Kadowaki et al., 1996; Yang et al., 2008; Zhai et al., 2004). Even though DGAT1 and DGAT2 probably interact with different cellular proteins and participate in different

pathways of TG synthesis (Stone et al., 2004; Yen et al., 2008) loss of DGAT2 could be compensated by another family member. If DGAT1 or DGAT2 family members like AWAT, MGAT or hDC3, have O-transacylation abilities towards VLC-Cers is not known. Even though DGAT1 is topologically not closely localized to lipid droplets and has a different specificity towards FAs it cannot be excluded that DGAT1 could compensate for the activity towards Cers of DGAT2 or if other enzymes DGAT2 is working in a complex with, can counterbalance for its loss. For example it was demonstrated that DGAT1 from *arabidopsis thaliana* can restore TAG synthesis to the yeast *dga1:lro1:are1:are2* quadruple mutant (Turchetto-Zolet et al., 2011). Also a human multifunctional O-acyltransferase (MFAT) that belongs to the acyl-CoA:diacylglycerol acyltransferase 2/acyl-CoA:monoacylglycerol acyltransferase (MGAT) gene family and is highly expressed in the skin was recently characterized (Yen et al., 2005) and it is not known if MFAT possibly 1-O-acylates also Cers. As all other Cers and GlcCers without h16:0 anchor seemed to accumulate in DGAT2 deficient mice, it is possible that acyl-CoAs which can't be used for TG production are instead used for Cer and GlcCer synthesis and therefore led to enhanced 1-O-AcylCer levels.

LCAT is known to synthesize high density lipoprotein-cholesterylesters by transferring acyl-CoAs to cholesterol (Hoekstra et al., 2013; Saeedi et al., 2014). The sum of 1-O-AcylCers for LCAT deficient mice is only slightly, but significantly increased. The sum of VLC- FA containing Cers and GlcCers remained unchanged compared to control mice, whereas some Cer and 1-O-AcylCerspecies containing So(d18:1) were increased. A defect in LCAT activity could lead to excess acyl-CoA amounts and hence to increased substrate availability for LCAT. Hence, LCAT is most likely not involved in 1-O-AcylCer formation.

In CerS3 deficient mice the Cers containing C24 FAs were significantly reduced to 50% of control levels after alkaline hydrolysis, but no significant changes were detected in corresponding 1-O-AcylCer levels. Cers containing LC- and VLC-FAs on the other hand, remained unchanged in CerS3 mutants. Hence it was concluded that only VLC- FAs are probably used for 1-O-AcylCer synthesis and VLC-Cers produced by CerS3 are no substrates for 1-O-AcylCers. That's why the impact of further enzyme deficiencies on VLC-FA synthesis and subsequently 1-O-acylCer production was investigated. CerS2 and CerS4 both favor the synthesis of Cers with FAs ranging from C22-26, by definition VLC-Cers. Deficiency of both enzymes led to no significant changes in 1-O-acylCer levels. Ceramide and GlcCer levels were also not changed for CerS4 mutant mice. Obviously the synthesis of 1-O-AcylCer with N-linked VLC-FAs is redundant and does not rely on a single CerS. Also

loss of Elov13, which elongates FAs up to a length of 18-24 carbon atoms, has only a minor influence on 1-O-AcylCer production. While 1-O-AcylCer levels were significantly reduced in Elov13 mutant mice, ceramide and GlcCer levels remained unchanged. Elov13 expression is restricted to certain cells of hair follicles and to sebaceous glands (Westerberg et al., 2004b). Hence, 1-O-AcylCers are not produced in sebaceous glands or other enzymes of the Elov1 family (Elov11; (Sassa et al., 2013)) compensate for the loss of Elov13 and elongate saturated FAs to VLC chain lengths. Also the ratios out of 1-O-AcylCers and the sum of the corresponding Cers and 1-O-AcylCers reflect the minor impact of CerS4, Elov13, nGlcCerase, LCAT and DGAT2 on 1-O-AcylCer production, as none of the ratios showed significant reductions of the level in mutants towards the controls. Levels of sphingoid bases were proportional to Cers. An increase of ceramides in DGAT2 led to an increase of free sphingoid bases. As already discussed in Part I, free sphingoid bases are probably not secreted, but are a product of ceramide degradation in the extracellular space. Results of Ugcg and Cers3 were discussed in Part I. In summary none of the enzymes investigated seemed to be directly or uniquely involved in 1-O-acylCer synthesis. Nevertheless, as in samples of E16-embryonic skin no 1-O-AcylCer could be detected, artificial production of these compounds during sample preparation can be excluded. Furthermore, their occurrence correlated with the establishment of the water permeability barrier between embryonic stage E17.5 and E18.5 (Hardman et al., 1998), suggesting their participation during barrier development.

Similar to the findings in yeast, 1-O-AcylCers are more likely synthesized in ER or ER-related organelles, than in lysosomes. However, an additional lysosomal pathway could not be fully excluded and increased lysosomal Cer levels could then lead to form 1-O-AcylCers by the lysosomal LPA2. In lysosomal storage disorders, like the Farber disease, it was hypothesized that an accumulation of ceramide in most tissues leads to recruitment of monocytes to help dispose of the excess ceramide (Alayoubi et al., 2013). The recruited macrophages fail to degrade the ceramides, which results in more ceramide storage and the subsequent foamy appearance of these macrophages, a characteristic of Farber disease. Also 1-O-acylceramides were elevated in the here investigated tissues of mice with reduced ceramidase activity (~10%). An accumulation of 1-O-acylceramides occurred especially in thymuses (100xfold increase) and spleen (10xfold increase), which are important parts of immunity. Also in kidney and heart a 4-5xfold increase was observed. These differences were significant on the 5% level, but homozygous samples showed strong varieties of Cer and 1-O-AcylCer levels. We could also show that the free ceramide levels of animals with diminished ceramidase activity were, as expected, increased in heart and kidney. In thymus and spleen,

free Cer levels could not be measured due to technical difficulties. Therefore, the results obtained here have to be verified with a new set of samples before further speculations arise.

Based on our results we suggest that in excess ceramides could lead to excess 1-O-AcylCers. In thymus and spleen on the other hand, maybe tissue specific cells, (or a higher activity/number of enzymes) are uniquely able to convert Cers into 1-O-AcylCers and like this eliminate excess Cer. As macrophages strongly infiltrate the enlarged spleen and thymus in Farber diseased animals, they could be the cells to produce the excess 1-O-AcylCers. Tissue staining also showed that most organs of the Farber mice are infiltrated by macrophages, but that spleen and thymus are massively invaded and almost completely covered by macrophages by 9 weeks (Alayoubi et al., 2013). Alayoubi et al (2013) suggested that the accumulation of ceramide prompts the release of a 'call signal' (MCP-1) that recruits circulating monocytes to help dispose of the excess ceramide from tissues (especially livers, brains, spleens, and thymuses). Being deficient of acidic ceramidase activity themselves, recruited macrophages fail to degrade the sphingolipids and ceramide they store, which results in more ceramide accumulation. Maybe 1-O-acylceramides are synthesized in macrophages in enhanced amounts due to scavenging of other lipids and ceramides from cells. The pathways how and by which enzymes 1-O-acylceramides are formed and degraded are still unclear, but the distribution pattern of saturated and unsaturated FAs incorporated into 1-O-AcylCers suggested that the pathway leading to 1-O-AcylCers is not tissue specific and is similar to the one in skin. In skin, the proportions of saturated to unsaturated FA in O-position of Cers, is approx. 4:1. The abundances of FAs used for 1-O-AcylCer production are similar in skin and other organs proposing similar metabolisms in all organs. The results of accumulation of 1-O-acylceramides in Farber diseased organs is not just a unique phenomenon, it is possible that the same enzymes than in all other organs are involved. However, the enzymatic responsibilities for 1-O-acylceramide synthesis still have to be discovered.

The functions of 1-O-acylceramides are not known. 1-O-acylceramides are more polar than triglycerides, wax esters, or cholesterol esters as they contain a free hydroxyl group, which allows them to undergo oriented hydrogen bonding interactions. Due to their predicted physicochemical properties, 1-O-acylceramides might constitute building blocks of extracellular lipid lamellae and may contribute to their stability and correct organization. Lamella phase organization was demonstrated to be disturbed in patients with atopic eczema (Janssens et al., 2011). In spite of their relatively low abundance (5% of all esterified Cers, or 2.3% of all Cers (Rabionet et al., 2013). In epidermis 1-O-acylceramides could contribute to a

functional water permeability barrier as they are among the most hydrophobic epidermal Cers and as 4 times more 1-O-AcylCers are found in skin than in the other organs investigated. Besides the thymus of wt animals, in which similar amounts of 1-O-AcylCers as in skin were found (both in average 100pmol/mg DW), in spleen, kidney and heart ~10-25 pmol/mg DW were present. The high amounts in thymus could suggest, that there 1-O-AcylCers have a tissue specific role, like for example as storage molecule or in signaling (Youm et al., 2012). It will be topic of further research if this pathway represents a detoxification mechanism to protect cells from toxic amounts of ceramides or fatty acids (like speculated for Farber disease), or whether it also serves as a storage molecules (similar to TAGs), which are mobilized for membrane biosynthesis. In membranes themselves, 1-O-AcylCers may not necessarily support a highly ordered membrane domain formation and properties range between bilayer forming lipids and those of storage lipids. Due their predicted inverted cone shape and size which probably spans through both layers of the membrane bilayer, they may stabilize the extracellular lipid lamellae of the stratum corneum, but could be as well deposited in lipid droplets (Rabionet et al., 2013; Voynova et al., 2012).

Part III

III. CerS3 localization

III.1 Introduction

III.1.1 Testis

CerS3 is not only expressed in skin but also in testis, where it was up-regulated more than 700-fold during postnatal testicular maturation (Rabionet et al., 2008). The testis is composed of loops of seminiferous tubules which are required for sperm cell formation, and which are embedded in interstitial tissue. In each spermatogenic cycle spermatozoa are continuously produced from differentiated germ cells in seminiferous tubules (Figure 39). Sertoli cells deliver nutrients to germ cells during spermatogenesis (Mruk and Cheng, 2004). They are also needed for the maintenance of the integrity of the seminiferous epithelium, regulation of differentiating germ cells and for the phagocytosis of residual bodies left by spermatids upon transformation into spermatozoa (Rabionet, 2011). Additionally, Sertoli cells are crucial for the establishment of the blood-testis barrier (BTB). The BTB is a junctional complex that generates a physical barrier separating the seminiferous tubules into an adluminal and a basal compartment (Mok et al., 2013). Leydig cells are located in the interstitium between tubules and are the endocrine cells responsible for the androgen production, mainly testosterone. Additionally, myeloid cells are localized in the interstitium enclosed within the lymphatic endothelium.

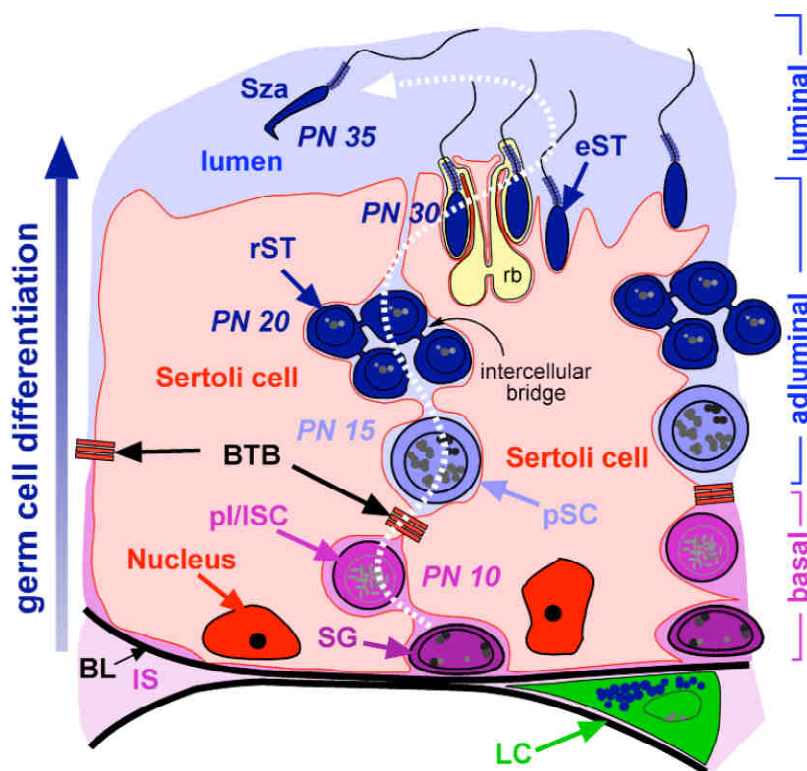


Figure 39 Testis structure and spermatogenesis. In the seminiferous tubules of the testis, spermatogonial stem cells (SGs) adhered at the basal lamina (BL) proliferate generating spermatogonia type B that differentiate into preleptotene and

leptotene spermatocyte (pl/ISC), which are the most differentiated germ cells present at post natal day (PN) 10. These primary SCs must traverse the blood-testis barrier (BTB) and further differentiate into pachytene spermatocytes (pSC), which are present at PN 15 of the first spermatogenic cycle. At PN 20, the first round spermatids (rST) are formed and 10 days later the tubules contain significant amount of elongated spermatids (eST). These must further differentiate to generate spermatozoa (Sza), which are released into the lumen of the tubules from PN 35 onwards, and transported into the epididymis where they acquire full maturation. In the interstitium (IS) between adjacent tubules, androgen producing Leydig cells (LC) are located. Scheme modified from (Sandhoff, 2009).

III.1.1.1 The spermatogenic cycle

Spermatogenesis is the process in which diploid spermatogonia differentiate into mature haploid spermatozoa (Mok et al., 2013). The location of the spermatogenic cycle is inside seminiferous tubules and each cycle has to run through three stages known as spermatocytogenesis, spermatidogenesis and spermiogenesis. During spermatogenesis, the seminiferous epithelium can be classified into 12 stages (stage I–XII) in mice, 14 stages in rats (stage I–XIV) and six stages (I–VI) in humans according to the developmental stages of germ cells (Mruk et al., 2008). In mammals the spermatogonial stem cells located at the basal lamina undergo several mitotic divisions within a highly proliferative phase. These rapid successive divisions generate firstly different type A spermatogonia, which can be distinguished by the amount of chromatin in the nuclear envelope and secondly further differentiation steps lead to type B spermatogonia. This is followed by the formation of primary spermatocytes, i.e. preleptotene and leptotene spermatocytes (plSC and ISC). These primary SCs induce the prophase of the first meiotic division and thereby initiate the spermatidogenesis. During spermatidogenesis, primary SCs overcome the active BTB and migrate to the adluminal compartment which leads to the formation of secondary SCs. There, in the pachytene, SCs (pSC) enter the second meiotic division which yields in the formation of haploid spermatids. Spermiogenesis continues with the transformation of round spermatids (rST) into elongated spermatids (eST) and ends with fully differentiated spermatozoa. The therefore required morphological changes of the spermatids include the development of the flagellum for motility of spermatozoa, the formation of an acrosome membrane containing digestive enzymes necessary for fertilization and nuclear transformation and the elimination of excess cytoplasm by the excretion of a residual body (rb) (Rabionet, 2011). Spermatozoa which were generated with each spermatogenic cycle must be released into the lumen of the seminiferous tubules during a process known as spermiation (O'Donnell et al., 2011). Subsequently, spermatozoa are transported into the epididymis where their maturation is completed and spermatozoa are stored. The complete spermatogenic cycle requires repeated mitotic and meiotic divisions. A single type A spermatogonium undergoes 10 consecutive

rounds of mitosis leading to 1024 primary spermatocytes, which then enter meiosis to produce in theory 4096 spermatids (Cheng and Mruk, 2012). Only the first mitotic division generates two separated daughter cells. All following divisions generate sister cells that remain connected by intercellular bridges due to an incomplete cytokinesis, and thereby share one unique cytosol and plasma membrane (Haglund et al., 2011). However, efficiency of spermatogenesis is only approximately 25% and the majority of germ cells undergo apoptosis, a process regulated by Leydig, Sertoli and germ cells (Tegelenbosch and de Rooij, 1993).

III.1.1.2 Testicular polyenoic ultra long chain sphingolipids

Mice require testicular glycosphingolipids (GSLs) for proper spermatogenesis. Mutant mice strains deficient in specific genes encoding biosynthetic enzymes of the GSL pathway including *Galgt1* (encoding GM2 synthase) and *Siat9* (encoding GM3 synthase) lack various subsets of GSLs (Sandhoff et al., 2005). Although male *Galgt1* deficient mice are infertile, male *Siat9* deficient mice are fertile. GSLs which were thought to be essential for male spermatogenesis were absent in these mice strains. The comparison of these GSL patterns led to the discovery of a novel class of complex GSLs present only in the fertile mouse model (Sandhoff et al., 2005). Structural analysis of these 8 novel molecules revealed that a fucose residue is attached to their oligosaccharide chains. Interestingly, the novelty depended on the fatty acid residue incorporated in these complex GSLs, being almost exclusively polyunsaturated (4 to 6 double bonds) and with a chain length of 28 to 32 carbon atoms (Figure 40). Previously, sphingolipids containing ULC-PUFA residues have only been described as minor components incorporated into sphingomyelin molecules of various mammals (Robinson et al., 1992). GSLs of this class are expressed differentially in testicular germ cells. Infertile mice lack this neutral subset due to a genetic disruption of the *GM2S/Galgt1*^{-/-} and developed multinuclear giant cells at the stage of spermatid formation. The intercellular bridges connecting the sister spermatids were lost, leading to an arrest of spermatogenesis in these mutant mice. Hence, polyunsaturated, fucosylated GSLs are essential for spermatogenesis and male mouse fertility (Sandhoff et al., 2005).

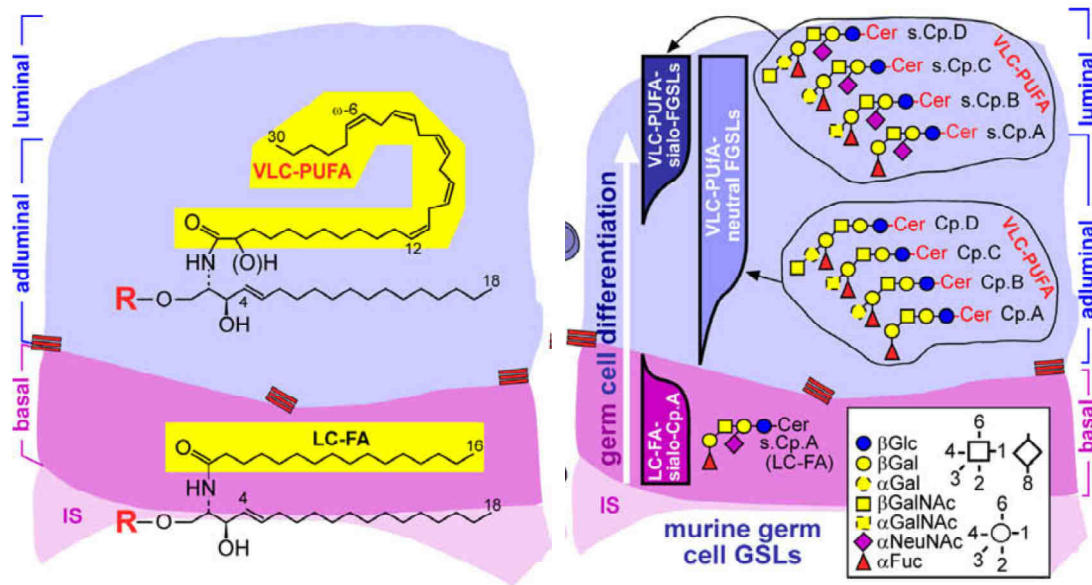


Figure 40 GSL structures expressed in mouse testis. Ceramide moieties of testicular sphingolipids consist of a d18:1-sphingosine base to which a fatty acid is linked through an amide bond. In case of interstitial cells, Sertoli cells and germ cells of the basal compartment, these fatty acid moieties are of long chain and saturated (mainly palmitic acid), whereas in the case of adluminal germ cells and spermatozoa, they are of very long chain (C28–32) and polyunsaturated (5–6 double bonds). The sphingolipid head group (R) may be ceramide (H), phosphorylcholine (sphingomyelin), Glc, Lac, Gb3–5, or a complex ganglioside oligosaccharide in case of somatic cells (e.g. Sertoli, Leydig cells, myofibroblasts) and ceramide, phosphorylcholine, Glc, Lac, and acidic or neutral fucosylated complex ganglio series oligosaccharides (see C) in case of germ cells. (modified from(Sandhoff, 2010). Spermatozoa and basal germ cells express sialo-compound A (s.Cp.A, FucGM1, IV2-a-Fuc,II3-a-NeuNAc-Gg4Cer) with LC-FAs, pachytene spermatocytes, round and elongating spermatids synthesize four complex asialo-glycosphingolipids compounds A–D, with VLC-PUFAs. Compounds B–D are derivatives of Cp.A (Cp.A, FucGA1, IV2-a-Fuc-Gg4Cer; Cp.B: IV3-a-Gal-FucGA1; Cp.C: IV3-a-GalNAc- FucGA1; and IV3-a-GalNAcb3Gal-FucGA1). Elongating spermatids additionally sialylate these compounds giving rise to four complex gangliosides with VLC-PUFAs: sialo- Cp.A-D (s.Cp.A-D; s.Cp.A: II3-a-NeuNAc-Cp.A, FucGM1; s.Cp. B: IV3-a-Gal-FucGM1; Cp.C: IV3-a-GalNAc-FucGM1; and IV3-a-GalNAcb3Gal-FucGM1). Scheme modified from (Sandhoff, 2010).

III.1.2 Epithelial tissue

The epidermis is a derivative of the surface ectoderm, which also forms the epithelium of the oral cavity and tongue (Jonker et al., 2004). A slightly different barrier is developed by appendages such as teeth, filiform papillae, taste papillae and salivary glands that are all functionally involved in food ingestion (Jonker et al., 2004). How this region-specific differentiation is genetically controlled is largely unknown.

The upside of the tongue consists of a connective tissue covered with a stratified squamous epithelium (Iwasaki, 2002). In the mouse tongue, the barrier formation starts at around embryonic day 16.5 (E16.5) and is fully established within 48 hours (Marshall et al., 2000). Barrier formation in the tongue follows the expression pattern of *Sprr1A*, a member of a family of ‘small proline-rich region proteins’ which encode for key components of the CE (Steinert et al., 1998). *Sprr1A* is not expressed in the skin and the analysis of recently

identified *Sprr*-like genes in mice and humans (called *late envelope proteins* (LEP) genes in humans) within the epidermal differentiation complex suggests that these genes are differentially expressed in CEs of the skin and tongue (Marshall et al., 2001; Wang et al., 2001). These differences may show the need to develop specific barriers in a different (wet or dry) environment. Also, specific patterns of keratin genes are expressed in the epithelium of skin, oral cavity, and tongue and they are required to form an organ specific architecture. Deletion of *keratin 6 α* and *keratin 6 β* genes in mice result in severe lesions of the tongue epithelium, whereas the skin is not affected in these mutants (Wong et al., 2000). The surface ectoderm, also a derivative of the epidermis, forms the epithelium of the oral cavity and tongue. Barrier formation is, like in epidermis of skin, achieved by a highly coordinated differentiation program of the keratinocytes (Marshall et al., 2000).

The stratum corneum of esophagus serves mainly as mechanical barrier for the defense against luminal contents (Chen et al., 2013). The combination of apical junction complexes and apical cell membranes within the SC is largely what makes the esophageal epithelium 'electrically tight' (Amir et al., 2014). Its lumen is lined by an epithelium, followed by a vascular connective tissue, the lamina propria, and on top of the lamina propria is in turn is a narrow band of smooth muscle (*muscularis mucosae*). Together these three tissues form the mucosa of the alimentary canal. In the esophagus the epithelial mucosa is formed by stratified squamous epithelial cells. Since this epithelium is normally not exposed to dryness or to abrasion, it is non-keratinized. Esophageal epithelium may be transformed to a simple columnar form in the condition called Barrett's esophagus. Barrett's esophagus can be associated with esophageal obstruction from scarring and/or carcinoma.

III.2 Results

III.2.1 Localization of CerS3

To elucidate epidermal topology of CerS3 in mice, CerS3 was localized at the cellular and subcellular level using fluorescence microscopy. No specific antibodies for immunohistochemistry and immunoprecipitation of murine CerS3 exist so far. To this end, peptides containing soluble domains, specific to CerS3, were designed and ordered as KLH-conjugates at Peptide Specialty Laboratories GmbH. Guinea pigs were then immunized by Hans Heid (DKFZ) to generate polyclonal antibodies.

Antibodies were raised in guinea pigs against the following peptides:

A1/2: against N-terminal end of CerS3 (mouse); amino acid sequence KPSHTDIYGLAKKC

B1/2: against N-terminal end of CerS3 (mouse); amino acid sequence CNLTERQVERWLR

C1/2: against C-terminal end of CerS3 (mouse); amino acid sequence CTKGKETEYLKNGLG

D1/2: against C-terminal end of CerS3 (mouse); amino acid sequence CTNRHLIANGQHG

H1/2: against C-terminal end of CerS3 (human); amino acid sequence CLKNGLR AERH

III.2.2 Antibody establishment in cell culture

At first antibodies A-H were tested on functionality and specificity in cell culture. Therefore stably transfected cells lines were provided by Mariona Rabionet. Cells were either transfected with mouse or human CerS3 with +/- GFP attached at the C-terminal end (for plasmid structure see Figure 4) and expression of CerS3-protein was induced by doxycyclin treatment (see methods section for details).

In Figure 41 results of IHC with transfected cells lines are shown. Negative controls are either uninduced cells (-Dox) or non-transfected cells. Cells stably transfected with the mCerS3+GFP fusion protein, did not reveal a specific signal for CerS3 using any of the antibodies (shown in red, secondary AB Cy3). No colocalization with GFP was observed. As published before (Jennemann et al., 2012) a different antibody against mCerS3-EGFP showed

colocalization of CerS3 with the ER marker (Pdi), but not with those for Golgi (Golga1) or lysosomes (Lamp1).

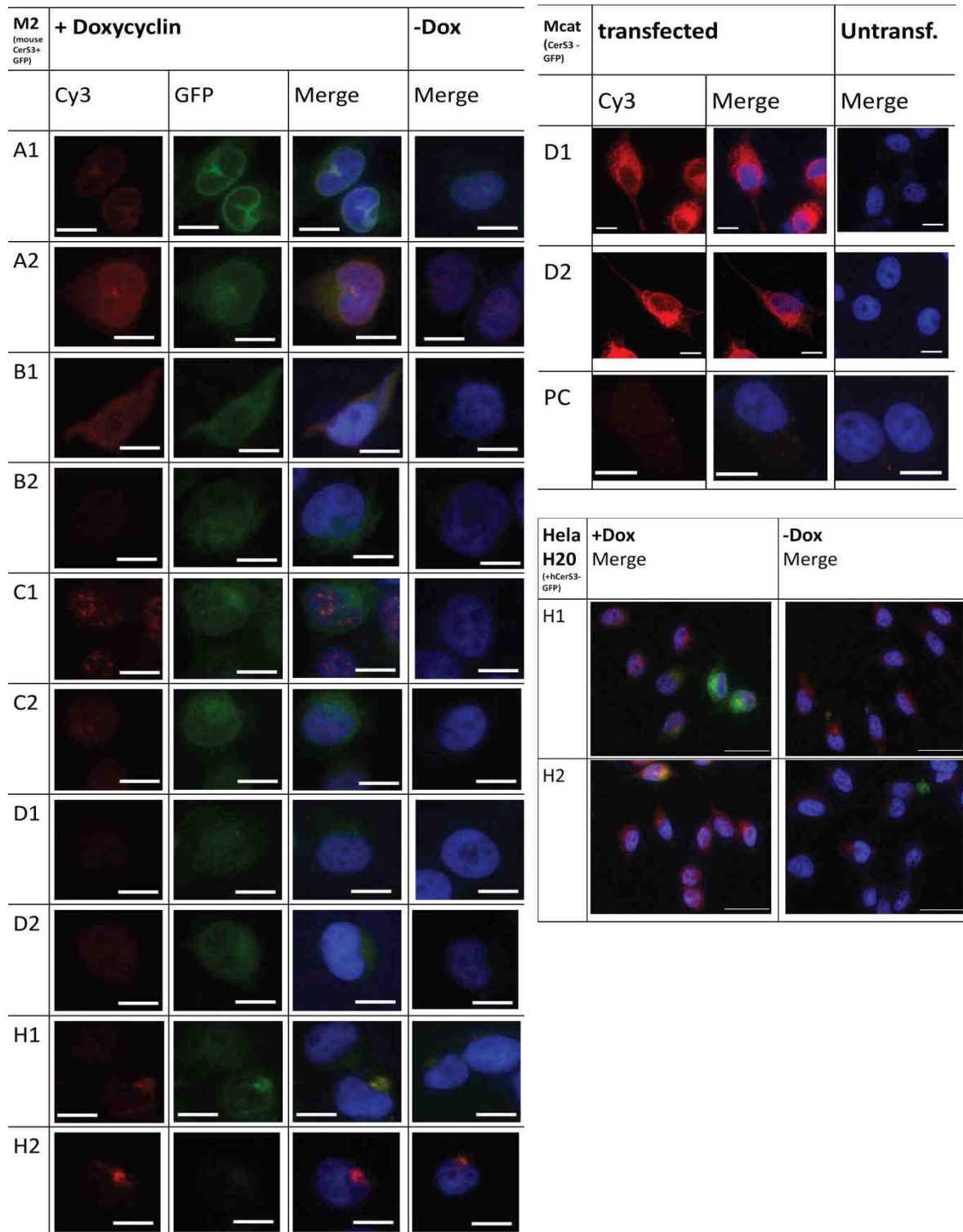


Figure 41 Cell lines transfected with CerS3: MCAT is a control HeLa cell line, transfected with CerS3; M2= HeLa cells stably transfected with the fusion protein mouse CerS3+GFP; H20 = HeLa cells stably transfected with the fusion protein of the human CerS3+GFP. Scales are 5 μ m, or for H20 10 μ m. CerS3 in red, nuclei in blue (Dapi)

As no intense signals were observed for either of the antibodies using the mouse CerS3+GFP fusion protein, cells expressing CerS3 without a tag were analyzed for antibodies D1 and D2, which were raised against the C-terminal peptide.

Therefore we tested the antibody D, on cells expressing only CerS3 without a GFP tag (Mcat). Indeed for both aliquots D1 and D2 a strongly specific signal for CerS3, in a typical ER-like pattern was observed.

The antibody against the human CerS3 was tested in H20 cells which after induction with doxycyclin expressed the fusion protein of hCerS3+GFP. Colocalization with GFP should prove signal specificity. Only the antibody H2 shows colocalization, but the signal is weak and seems not to be positive. Also negative controls show a slight red signal, probably due to unspecificity.

Hence, for further analysis of CerS3 topology antibody D2 was used as it seemed more specific in the staining of the M2 and Mcat cell lines. In the following D2 will be just entitled with CerS3 AB.

The antibody previously used for CerS3 detection in HeLa cells and mouse skin (a synthetic peptide located at the C-terminus of mouse CerS3 protein was generated to immunize rabbits (PickCell Laboratories), (Jennemann et al., 2012)) wasn't successful for detection of the protein in testis. Therefore we decided to use the now established CerS3 AB (D2) and stained in repetition for CerS3 in murine epithelial tissues and testis.

III.2.3 Localization of CerS3 in skin

CerS3 deficiency in mice led to WPB disruption and neonatal death. Phenotypically, CerS3^{d/d} mice were easily distinguished from CerS3^{+/d} and CerS3^{+/+} mice, as their skin appeared unwrinkled, erythematous and sticky. Working with an antibody, produced by Pick cell laboratories, revealed that CerS3 clustered in scattered dots within keratinocytes of upper stratum spinosum and stratum granulosum. In contrast, CerS3 expression was not detected in mutants (Fig. 35A and A'), thereby indicating that deletion of exon 7 renders synthesis or stability of mutated CerS3 dysfunctional. Mutant SC was almost twice as thick with ~40% more corneocyte layers constituting only a stratum compactum, but lacking a stratum disjunctum. (all results published in (Jennemann et al., 2012)).

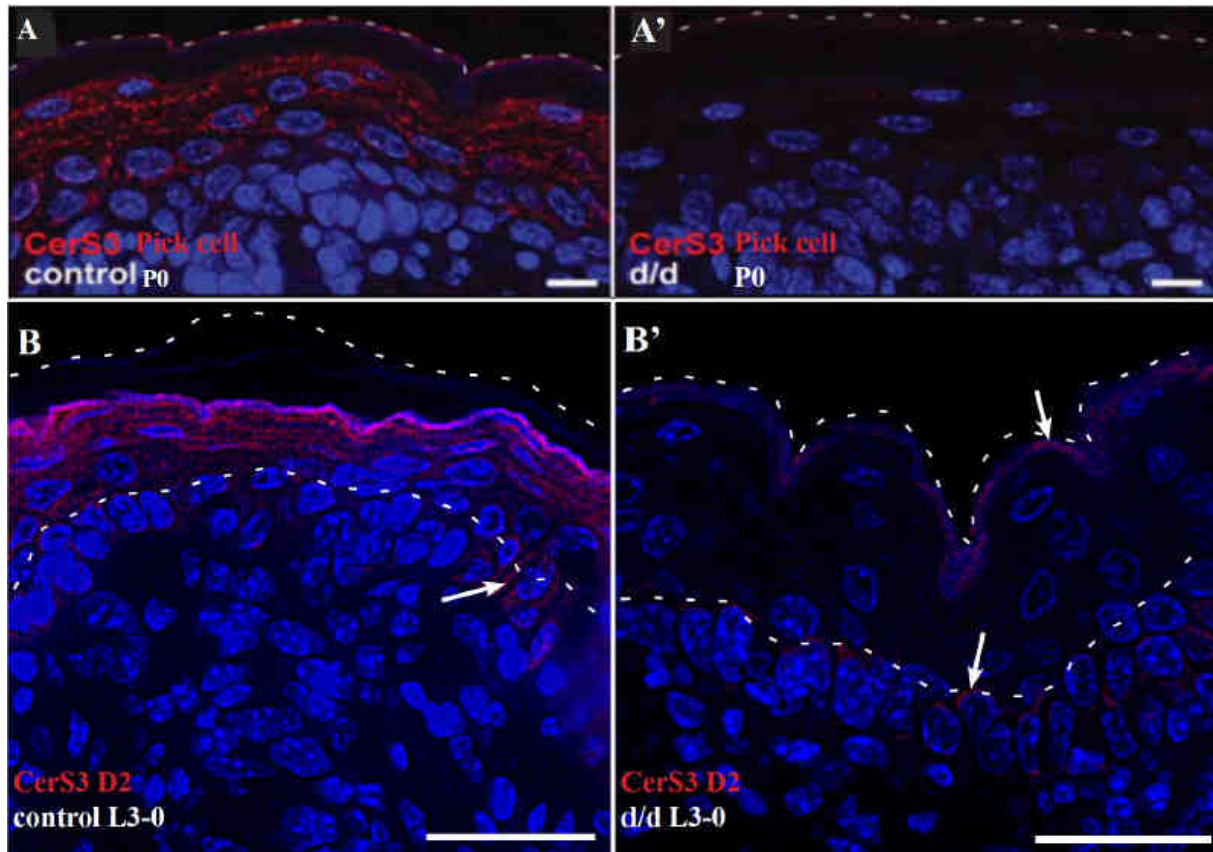


Figure 42 *Cers3* (D2) staining in skin. *Cers3* in red, Dapi in blue. A and A': wt and ko skin of L3-0 mice stained with custom made PC antibody (modified from Rabionet et. al.); B and B': D2 on embryonic (E19) wt and ko skin of L3-0 mice. Scales are 10 μ m and 30 μ m respectively.

Antibody D2 for detection of CerS3 was applied on embryonic skin and on adult skin of the L3-0 mouse model as shown in Figure 42 B. In agreement to our previous findings (A) CerS3 is mainly expressed in stratum granulosum and stratum spinosum. In embryonic skin signal is not as intense as in P0. Staining with D2 in skin of ko mice reveals that CerS3 is also detected to some extent in stratum basale and also on the most upper layer of stratum corneum (indicated by arrows). In control samples a very faint signal in stratum basale is also seen, suggesting that the D2 antibody shows some unspecificity towards skin proteins. Nevertheless the specific signal in SG and SS (comparable as seen in A) is absent in ko mice.

III.2.3.1 Epithelium of oral cavities and tongue

CerS3 is important for establishing the CE in epidermal skin and it could be that it is also involved in barrier formation in epithelial tongue. Therefore its expression in tongue epithelium, as well as in oral cavities of CerS3 mutant mice was investigated. Figure 43

shows that similar expression pattern in control samples as compared to skin epithelium can be seen. CerS3 is expressed in SS and SG of tongue epithelium, whereas in deficient mice no signal for CerS3 in can be detected. Also SC is thickened in tongue epithelium (Figure 43 B). Oral mucosa shows a positive signal for CerS3 in mutants as well as in control mice. However this part of the mouth should be non- keratinized and a function of ceramides produced by CerS3 is not known (Figure 43 A).

Epithelial tissue of esophagus was also investigated but no signal could be detected. Nevertheless, esophagus consists of nonkeratinized epithelium, and no signal was expected.

To verify results out of epidermal CerS3 staining, western blots (WB) of epidermal proteins like described in the methods section were performed and are shown in (Figure 43C). One band appearing at ~40kDa (marked) suits to the molecular weight of the native CerS3 (Mizutani et al., 2013; Radner et al., 2013) and is thereby proving antibody recognition of the protein in skin. As already explained above, staining for CerS3 was not only restricted to SS and SG but a signal is seen also in SB and SC. Multiple bands in the WB also show that the antibody D2 is obviously crossreactive also for other proteins in skin. No corresponding signal at the height of ~40 kDa is seen in the ko samples.

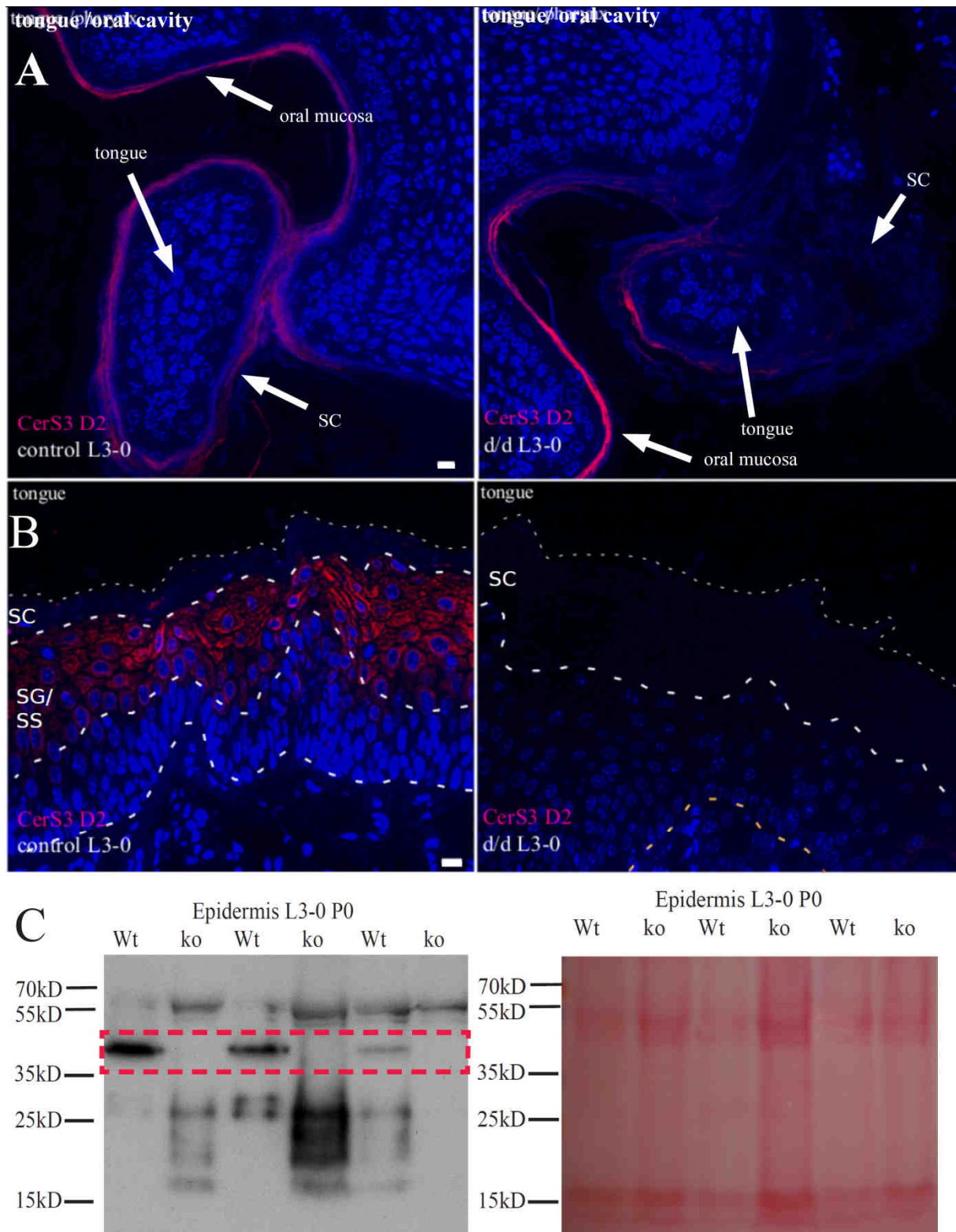


Figure 43 CerS3 expression in oral cavities and tongue. D2 (red), Dapi (blue). A and B: staining in epithelium of tongue and oral cavities. On the left control tissue and on the right mutant tissue is shown. C: WB of membrane fraction of *Cers3*^{wt} and *ko* epidermis on the left (n=3, wt and ko samples each) and loading control with Ponceau red on the right.

III.2.4 Localization of CerS3 in testis

The fact that adluminal germ cells express unique polyunsaturated, fucosylated GSLs gave rise for speculations about their role in germ cell differentiation as well as their appearance correlated with testicular CerS3 expression (Rabionet et al., 2008; Sandhoff et al., 2005). To analyze the role of these unique sperm-sphingolipids CerS3 was deleted exclusively in germ cells (Cers-Stra8) which demonstrated the requirement of germ cell GSLs and adluminal germ cell ULC-PUFA sphingolipids for correct spermatogenesis (Rabionet, Bayerle et al., unpublished results).

III.2.4.1 Mouse

To determine the expression pattern of CerS3-dependent ceramide synthesis in testis cellular localization of CerS3 in wt and testis with a dysfunctional mutation of CerS3 in spermatogonia (Cers3(Germ)-ko) as negative controls were performed. Immunocytochemical data reveal staining within wild type seminiferous tubules (Figure 44). The distribution pattern of the CerS3 signal appears heterogeneous and tubular stage-specific, indicating a germ cell differentiation specific expression during the spermatogenic wave. In Cers3(Germ)-ko testis, CerS3 protein expression in a similar pattern is not detectable in either cell type at any tubular stage. However, tubular stages in ko- testis are not easy to determine, and in some rare cases a signal in spermatocytes can be seen. Histological in ko testis in very few tubules (<1%), normal spermatogenesis can be observed (data not shown here). Immunoblots show a single band at ~42kDa for wt, but also a very decent band at 40kDa for germ cell-CerS3 deficient mice. Heights for wt samples fit the expected size of the native CerS3 (Mizutani et al., 2013) and its dysfunctional form in the ko, without exon 7, with slightly lower size. At higher magnification distribution patterns of CerS3 is better observed, showing low levels of CerS3 throughout the cytoplasm of prophase pachytene spermatocytes (tubular stage II to XI), which have crossed the BTB and locate within the adluminal compartment (B). The staining intensity gradually increased in early pachytene (tubular stage II, B' and tubular stage III/IV, C) and peaked in mid-pachytene (tubular stages VII-VIII, Fig. B'' and C'), whereas in late pachytene to diplotene spermatocytes (tubular stage IX-XI, Fig. B''' , C'' and C''') CerS3 protein levels faded away. In spermatocytes during meiotic divisions I and II (tubular stage XII, B''' inset) still a faint CerS3 staining was observed whereas round haploid spermatids (Fig. B-B'', C-C', and D) no longer appeared to express CerS3. However, in elongated

spermatids of stage 10 to 15 (for spermatid staging see F) a distinct positive punctuate structure appeared suggesting lysosomal CerS3 accumulation within cytoplasmic lobes (B-B', C, C'''). Hence, also compartmental localization of CerS3 was investigated. To gain insight into the nature and localization of intensely stained puncta and to clarify specificity of those, colocalization studies were performed. Even though it was shown in cell culture, that CerS3 localized within the ER (Jennemann et al., 2012), staining with common ER markers like Calreticulin and Calnexin did not work on paraffin fixed sections and direct proof for ER localization could not be provided. As in elongating spermatids, dispensable cell organelles and cytosol are collected in residual bodies for degradation, colocalization studies with markers of lamp1 (lysosomal-associated membrane protein-1) as a lysosomal marker, and Lc3 (also Map1lc3a or Apg8, microtubule-associated protein 1 light chain 3 alpha) to identify autophagosomes and Piwil1 (or MIWI, RNA-binding protein) were performed. The double immunofluorescent stainings with Lamp1 and Lc3 clearly demonstrate the CerS3-positive puncta not to colocalize neither with lysosomes (Figure 44 D), nor with autophagosomes (Figure 45 B).

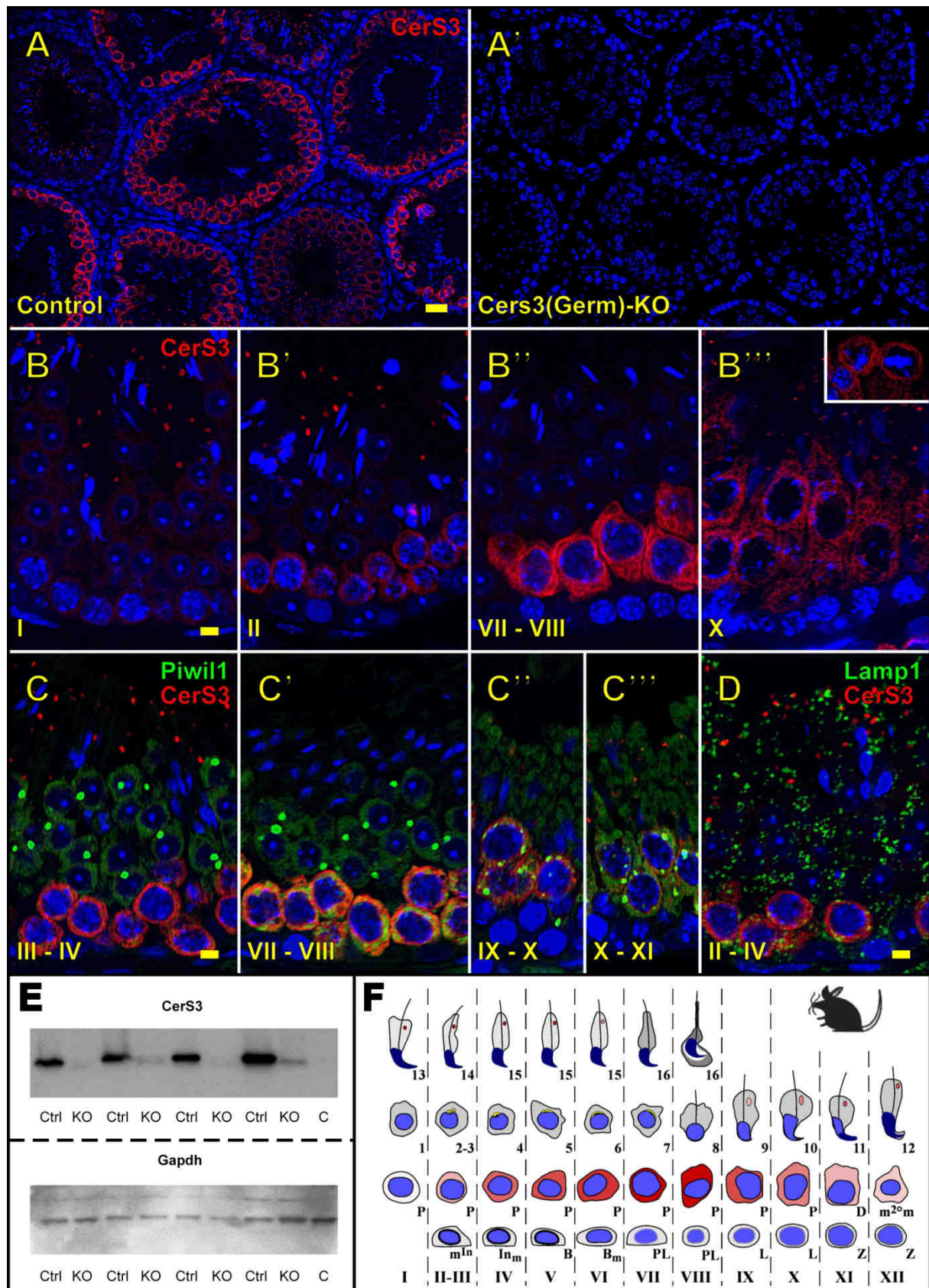


Figure 44 *CerS3* expression in control and mutant *CerS3*-depleted testis. Whereas *CerS3* labeling displays the full spectrum of signal intensity in control testis (A), testicular cells of *Cers3*(Germ)-KO (A') were absent of *CerS3* labeling. *CerS3*(Germ)-control testis exhibited weak *CerS3* signals within the cytoplasm of early pachytene spermatocytes, as well as in a specialized structure within the tail of elongated spermatids in stage I (B). Through stage II-spermatocytes and elongated spermatid-puncta, *CerS3* signal progressively increases reaching its maximum intensity in mid pachytene (B') while

disappearing from the specialized structures of elongated spermatids (B''). In late pachytene/diplotene spermatocytes CerS3 immunolabeling gradually decreases (B''', stage X) likewise in spermatocytes undergoing the I and II meiotic divisions (B''', inset). CerS3 does not colocalized within the Piwil1 positive-chromatoid body (green) of round spermatids in none of the stages investigated (C, stage III-IV; C', stage VII-VIII; C'', stage IX-X; C''', stage X-XI), neither with the lysosomal marker Lamp1 (green, D). Western blot of four controls and four Cer3(Germ)-KOs demonstrating the lack/extreme reduction of CerS3 protein in the membrane fraction of CerS3-depleted testis (E). CerS3 band in control animals appear at the height of about 42 kDa, whereas in the KO appeared reduced at about 40 kDa and Gapdh was used as loading control. Scheme representing the morphological changes of germ cells during murine spermatogenesis including the stages described first by Russel et al. C: cytosolic fraction of control. Scale bars: 30 μ m (A) and 5 μ m (B-D).(from Rabionet, Bayerle et al. 2014,unpublished)

A structure named chromatoid body (CB) functions as a subcellular coordinator of different RNA-processing pathways (Kotaja and Sassone-Corsi, 2007). The mRNAs molecules are transported to the cytoplasm and shuttled through nuclear pores to the CB, where the male-germ-cell-specific RNA-binding proteins, MIWI and MVH are localized. As MIWI is probably a germ cell specific protein, we searched not only for colocalization with CerS3 but also investigated the effects on MIWI during spermatogenesis (Figure 45 and 44). CerS3 does not colocalize within the MIWI (Piwil1) positive-chromatoid body (green) of round spermatids in none of the stages investigated (C, stage III-IV; C', stage VII-VIII; C'', stage IX-X; C''', stage X-XI). The CB/MIWI appears for the first time in the cytoplasm of meiotic pachytene spermatocytes as fibrous–granular structures in the interstices of mitochondria clusters. After meiosis, the CB condenses into one single granule in round spermatids and remains in the cytoplasm of post-meiotic spermatids until they elongate and form the spermatozoa (Figure 44 C-C''') concordant with a previous study (Kotaja and Sassone-Corsi, 2007).

As targeted deletion of *Cers3* in mouse germ cells led to infertility, the phenotypic alterations of arrested spermatogenesis during the first wave of the spermatogenic cycle were investigated. Absence of elongated spermatids in the germ cell-specific knockout was accompanied by a remarkable atrophy of the seminiferous tubules and the formation of multinuclear giant cells. MIWI staining of CerS3(Germ)-Ko tissue revealed that in an earlier tubular stage MIWI is normally expressed in spermatocytes, whereas by the formation of round spermatids multinuclear giant cells develop with one single CB often centered in the middle of the grouped nuclei (Figure 45 A- A'').

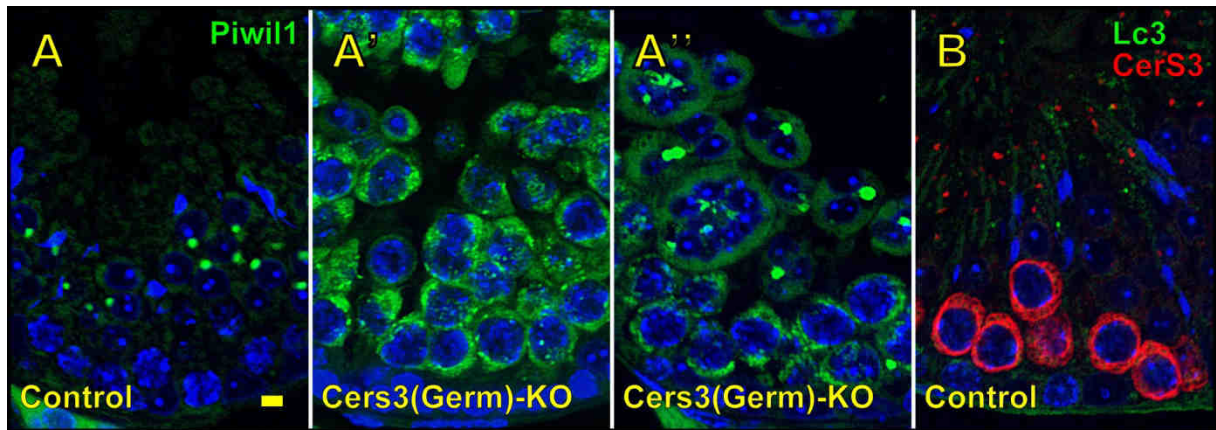


Figure 45 Aberrant expression of Piwil1-associated chromatoid body (green) in CerS3 deficient testis (A' earlier stage and A'' and later stage) as compared to endogenous expression in control (A). Lack of colocalization of CerS3 (red) in autophagosomes as shown with Lc3 (green) immunostaining (B). Scale bar: 30 μm . (from Rabionet, Bayerle et al. 2014,unpublished)

III.3 Discussion

In search for an antibody that i) recognizes CerS3 tissue unspecifically, ii) enables the colocalization with commercial antibodies from mouse and rabbit and iii) in search for an antibody that may be used for immunoelectron microscopy, customized peptides were designed to raise anti-mouse and anti-human CerS3 antibodies in guinea pigs. Therefore CerS3 was localized at the cellular and subcellular level by use of antibodies against the C- and N-terminal end of the mouse CerS3. The antibody D2(C-terminal end) was shown to be specifically towards Cers3 without a tag. In cells expressing the fusion protein of mCerS3+GFP no specific signal for D2 was visible as the antibody probably binds in a region where the GFP tag was inserted into the CerS3 sequence masking the epitope. In cell culture the CerS3 D2 antibody yielded in a typical ER-like signal as similarly already published before (Jennemann et al., 2012).

In mouse skin CerS3 was found to be mainly expressed in stratum granulosum and stratum spinosum. In contrast, CerS3 expression in SS and SG was not detected in mutants, thereby indicating that deletion of exon 7 renders synthesis or stability of mutated CerS3 dysfunctional. These expression pattern of CerS3 and the observed thickened SC were in agreement with previous findings (Jennemann et al., 2012; Rabionet et al., 2014). Some unspecific signal in the most upper layer of the stratum corneum and in the basal cell layer was detected, which was also present in the mutant samples. As also in western blot additional bands were detected, these signals are considered to be unspecific and due to cross reactivity. It was recently discovered that homozygous mutations in the human *CerS3* gene cause a new type of autosomal recessive congenital ichthyosis (Eckl et al., 2013; Radner et al., 2013). There epidermal antibody studies demonstrated that the CerS3 localized at the interface between the stratum granulosum and the stratum corneum, which is similar to our findings and confirms the functionality of our antibody. The by Elovl proteins newly synthesized activated VLC or ULC-FAs are usually transferred to CerS3 which is also known to reside in the SS/SG (Rabionet et al., 2014). Then in the SG, the by CerS3 synthesized ULC-ceramides are quickly transported to the Golgi apparatus for GlcCer and SM formation. Finally at the SG–SC interface, LBs are transported apically toward the plasma membrane where they fuse and secrete their contents into the extracellular space. Hence, the CerS3 localization correlates with the cells where the Cers production pathway is initiated.

Depending on the region of the mouth, the epithelium may be nonkeratinized or keratinized. Nonkeratinized squamous epithelium covers for example the soft palate, inner lips and cheeks, the mouth bottom, and ventral sides of the tongue. Keratinized squamous epithelium is present in the attached gingiva and hard palate as well as areas of the dorsal surface of the tongue. In keratinized tongue epithelium *Cers3* expression was also detected in stratum granulosum and spinosum in the wt, whereas the signal was absent in the ko. Furthermore stratum corneum of mutant tongue epithelium was thickened, similar to findings in *CerS3* deficient epidermis (Jennemann et al., 2012; Rabionet et al., 2014), suggesting that *CerS3* also participates in barrier establishment in the tongue. In Part I sphingoid base levels of tongue epithelium were determined. Even though in mutant animals dysfunctionality of *CerS3* was suggested by immunohistochemistry, levels of sphingoid bases in tongue were not altered. So far no *CerS3* expression was immunohistochemical detected and the consequences of *CerS3* loss on barrier establishment of the tongue epithelium are not known. Both skin and oral barrier is established by the keratinocyte cornified envelope (Marshall et al., 2000). The CE is crosslinked to aggregated keratin (Candi et al., 1998) and to lipids (Marekov and Steinert, 1998). As some genes are differentially expressed in CEs of the skin and tongue (Marshall et al., 2001; Wang et al., 2001) it is likely that barriers in a wet or dry environment are differently established. Dysfunctionality of *CerS3* should lead to reduction of ULC-Cers and hence to reduced sphingosine levels. Although antimicrobial lipids at the surfaces of the oral mucosa are known to be part of innate immunity (Dawson et al., 2013), in tongue of *Cers3* deficient mice no altered So levels were found, maybe caused due to an inhomogeneous sample group. Unfortunately not much information is available about ceramides in tongue, but that FAs of Cers are 20–28 carbons long (Dawson et al., 2013). Nevertheless it could be that only Cers with shorter chain length are needed in epithelium of tongue and used for establishment of the CE and that their synthesis is done by other CerS (*CerS2*). Oral mucosa on the other hand showed a positive signal for *CerS3* in mutants as well as in control mice. However this part of the mouth should be non-keratinized and a function of ULC-Cers produced by *CerS3* is not known. A generally higher water permeability of oral regions may reflect the presence of low amounts of unsaturated ceramides, but free phospholipids and free glucosylceramides (Dawson et al., 2013; Wertz et al., 1986). Epithelial tissue of esophagus was also investigated by immunohistochemistry and via mass spectrometry, but no signal for *CerS3* or sphingoid bases could be detected. Most of what is known about the esophageal barrier properties has been determined in the context of gastroesophageal reflux disease (Katz et al., 2013) and from whole-organ permeability studies in vitro (Diaz-Del Consuelo et al.,

2005) which showed that barrier comprises of a layer of mucus and unstirred water, surface bicarbonate (HCO_3^-), junction proteins and lipids (Diaz-Del Consuelo et al., 2005). Nevertheless esophagus consists of nonkeratinized epithelium, and therefore there is no need for CerS3 to provide ULC-Cers for the formation of a CE and ELL.

In testis it was demonstrated that murine *Cers3* mRNA was activated at postnatal day 15 coinciding with the formation of pachytene spermatocytes in the adluminal compartment (Rabionet et al., 2008). In mice which lack the CerS3 exclusively in germ cells, ULC-FGSLs were lost in those cells. To closely define the testicular CerS3 activity in these CerS3(Germ)-ko mice, antibodies were raised in guinea pigs and testicular immunohistological studies performed. The distribution pattern of the CerS3 signal appeared heterogeneous and tubular stage-specific, indicating a germ cell differentiation specific expression during the spermatogenic wave. CerS3 was neither localized in lysosomes, autophagosomes or the CB and its expression started with pachytene spermatocytes. During this first phase of CerS3 expression, immunolabeling was detected in a structured pattern in the cytoplasm, possibly indicating ER localization as demonstrated previously by colocalization studies in cultured HeLa cells (Jennemann et al., 2012). CerS3 was active from tubular stage II to XI, fading with diplotene spermatocytes and being turned off in round spermatids, suggesting that there is no production of ULC-PU-sphingolipids. However ULC-PU-gangliosides, which were observed in elongating spermatids by immunohistochemistry (Sandhoff et al., 2005), still have to be produced in elongating spermatids, which coincide with the reactivation of CerS3 expression of elongated spermatids of stage 9 to 15. Yet, the expression pattern during re-activation differed appearing in distinct positions of the posterior part of elongated spermatids which did colocalize with neither lysosomes, autophagosomes nor Piwil1-associated complexes. This novel location may reflect a condensed ER-structure. Such a structure was indeed previously described as radial body recognized in mouse (stage 14/15) and rat (stage 15) spermatids (Herme et al., 2010; Nakamoto and Sakai, 1989). During the early elongation phase of spermiogenesis peculiar radial arrangements of endoplasmic reticulum (ER) cisternae were observed in the cytoplasm of the spermatids (Soley, 1994). These structures were similar in appearance to the radial bodies described in rat spermatids (Soley, 1994). As spermiogenesis progresses, the spread-out endoplasmic reticulum gradually aggregates to form the radial body, a condensed, glomerulus-like structure consisting of a very thin endoplasmic reticulum connected to the surrounding ER (Nakamoto and Sakai, 1989). Thus, the ER may aggregate, condense, be transformed into a radial body, and is then probably removed from the cytoplasm. Hence, with the potential expression of CerS3 in these structures and with the

knowledge that CerS3 still has to be active, the condensing ER of late spermatids thus may not only reflect a degrading organelle but may still harbor enzymatic activity. The deletion of *Cers3* in germ cells resulted in a loss of these ULC-PUFA sphingolipids (Rabionet et. al., unpublished). *Cers3*-deficiency was accomplished by an arrest of spermatogenesis and the formation of multinuclear giant cells at the round spermatid stage, as also seen by MIWI stainings in Figure 45. Deficiency of the ULC-PUFA sphingolipids resulted in enhanced apoptosis especially of meiotic spermatocytes and consequently smaller multinuclear giant cells and early arrested acrosomal cap formation (Rabionet et. al. unpublished). This is in line with the stage specific expression of *Cers3* in pachytene spermatocytes, where it seems to produce lipid products which are subsequently needed for membrane growth at the end of meiosis and for germ cell survival and correct establishment of intercellular bridges. Hence, *Cers3*, which is also highly expressed in human testis (Rabionet et. al. unpublished) appears to be quintessential for proper completion of meiosis and ongoing spermiogenesis.

IV. Conclusions

A detailed knowledge of ceramide metabolism is fundamental for the understanding of skin pathophysiology and hence is a prerequisite for targeted therapy of skin disorders. When the two main barrier functions against transepidermal water loss and pathogen invasion become deficient, such as in ichthyosis, atopic dermatitis and psoriasis, specific barrier components of the cornified epidermal layer, particularly the CE and the extracellular lipid lamellae are severely altered (Hong et al., 2007; Kaplan et al., 2012; Moon et al., 2013; Palmer et al., 2006; Radner et al., 2013).

The prominent coexpression of CerS3 and of ULC- sphingolipids in skin and testis suggested CerS3 to be involved in water permeability barrier formation and ongoing spermiogenesis (Jennemann et al., 2012; Rabionet et al., 2008). CerS3 was located in differentiating cells, e.g. in keratinocytes of SS and SG as well as in adluminal spermatocytes and elongating spermatids and hence, could be classified as a differentiation marker. Furthermore the punctuated staining of CerS3 in elongating spermatids may hint to its expression in condensing ER structures, possibly the radial body. Colocalization studies with pathway related ER enzymes such as the fatty acid 2-hydroxylase (FA2H) could bring further insight into the identity of this structure. In both skin and testis, deletion of CerS3 led to an arrest of epidermal maturation and of spermatogenesis highlighting its importance for proper barrier establishment. CerS3-deficient mice lacked all epidermal SLs with ULC-FAs resulting in WPB disruption and pathogen invasion (*candida albicans*). Sphingosine, which is a degradation product of Cer, was identified as antimicrobial agent. Levels of sphingoid bases in CerS3 mutant skin were decreased to 10% compared to control mice. Phenotypically, in newborn CerS3 deficient mice dendritic cells intensively migrated into epidermis, which could either, be induced by a higher sensitivity to infection and a malfunction of protection mechanisms or by a missing inhibition of proteinkinase C by sphingosine and a consequently overreactive activation of T-and or B-cells. Also sphingosine(d18:1) was shown to be able to inhibit growth of *candida albicans* thereby indicated its potential role in therapy of skin disorders.

The discovery of epidermal 1-O-acylceramides opens a new pathway for mammalian ceramides. These very hydrophobic compounds may contribute to stability of extracellular lipid lamellae and correct lamella phase organization. Neutral glucosylceramidase activity seemed to be topologically related and upstream of 1-O-acylceramide production. Furthermore, 1-O-acylceramide synthesis seemed to compete with GlcCer synthesis, as a loss of GlcCer synthase led to a strong increase of 1-O-acylceramide amounts. GlcCer derived

ceramides at the Golgi might be transported back to the ER or to lipid droplets where they could be 1-O-acylated by enzymes of the MBOAT or DGAT family. These enzymes are all O-acyltransferases, but none of them was shown so far to actively use VLC-FAs and produce 1-O-AcylCers in mammals. Besides a reduction of 1-O-AcylCers(d18:1;h16:0) no alteration in DGAT2 deficient mice was detected. Hence, DGAT2 could be exclusively responsible for the utilization of Cers with h16:0 anchor to form 1-O-AcylCers. Loss of DGAT2 could be also compensated by another O-acyltransferase, such as DGAT1, AWAT, MGAT or hDC. If one of these enzymes has O-transacylation abilities towards VLC-FAs is not known and could be topic of further research. The human homologous of the yeast Lro1p, LCAT and LPLA2 were shown not be uniquely responsible for 1-O-AcylCer production. Hence, 1-O-AcylCers could be synthesized in ER or ER-related organelles, but by majority not in lysosomes. However, if the Cer levels in lysosomes are unnaturally increased there still might be a lysosomal pathway to form 1-O-AcylCer. A summary of what is known about the 1-O-AcylCer metabolism is shown in Figure 46.

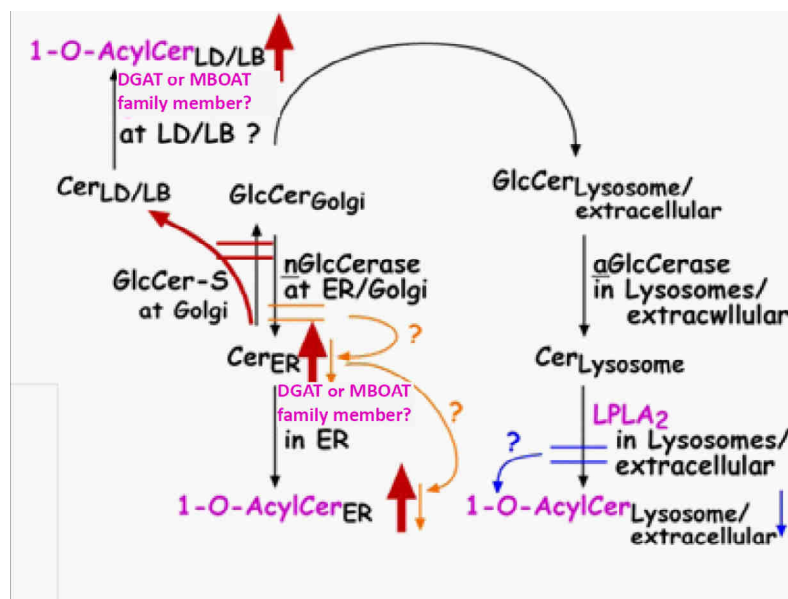


Figure 46 possible pathways leading to 1-O-AcylCer formation.

It was hypothesized that in lysosomal storage disorders, like Farber disease, an accumulation of ceramide in most tissues leads to recruitment of monocytes to help dispose of the excess ceramide (Alayoubi et al., 2013). Here, accumulations of 1-O-acylceramides in ACDase deficient tissues (activity <10%) especially in thymuses (100 fold increase) and spleen (10xfold increase) were detected. Also in kidney and heart a 4-5 fold increase was observed.

Based on our results we suggested that in non-immune tissues, like heart and kidney, excess ceramide amounts could lead to excess 1-O-AcylCers. In thymus and spleen on the other

hand, a higher ceramide turnover is caused maybe due to tissue specific cells. As macrophages, deficient in ACDase, strongly infiltrate the enlarged spleen and thymus in Farber diseased animals they could try to eliminate excess Cer by transformation into 1-O-AcylCers. However the enzymes being responsible for 1-O-acylceramide synthesis still have to be discovered and investigations of Farber diseased mice indicated that macrophages could be one production site of 1- O-acylceramides.

The complex molecular events presumably altered upon ceramide metabolism might as well contribute to the pathogenesis of many different skin diseases. Ichthyosis, atopic dermatitis and psoriasis are just some few skin diseases where ceramides are involved, but also other parts of the body will be affected. Farber disease is one example of lysosomal storage disorders where ceramide accumulation has lethal consequences. Recently it was discovered that depressive patients have an increased activity of acid sphingomyelinase (Beckmann et al., 2014; Gulbins et al., 2013). Mutated mice overexpressing this sphingomyelinase developed elevated ceramide levels in the brain developed depressive like symptoms (Gulbins et al., 2013). Hence, lowered ceramide abundances may be a central goal for the future development of antidepressants.

Defects at a branching point of such complex pathways can lead to a broad diversity of changes on a product level. These changes cannot be predicted only due to a genetic disorder or due to epigenetic diversifications. Analysis on a product level is needed to help to unravel the progression on a molecular scale and shows how important it is to investigate metabolic processes *in vivo*.

V. References

- Abe, A., Shayman, J.A., and Radin, N.S. (1996). A novel enzyme that catalyzes the esterification of N-acetylsphingosine. Metabolism of C2-ceramides. *J. Biol. Chem.* *271*, 14383–14389.
- Agbaga, M.-P., Brush, R.S., Mandal, M.N.A., Henry, K., Elliott, M.H., and Anderson, R.E. (2008). Role of Stargardt-3 macular dystrophy protein (ELOVL4) in the biosynthesis of very long chain fatty acids. *Proc. Natl. Acad. Sci. U. S. A.* *105*, 12843–12848.
- Akiyama, M., Sugiyama-Nakagiri, Y., Sakai, K., McMillan, J.R., Goto, M., Arita, K., Tsuji-Abe, Y., Tabata, N., Matsuoka, K., Sasaki, R., et al. (2005). Mutations in lipid transporter ABCA12 in harlequin ichthyosis and functional recovery by corrective gene transfer. *J. Clin. Invest.* *115*, 1777–1784.
- Alayoubi, A.M., Wang, J.C.M., Au, B.C.Y., Carpentier, S., Garcia, V., Dworski, S., El-Ghamrasni, S., Kirouac, K.N., Exertier, M.J., Xiong, Z.J., et al. (2013). Systemic ceramide accumulation leads to severe and varied pathological consequences. *EMBO Mol. Med.* *5*, 827–842.
- Ali, R.S., Falconer, A., Ikram, M., Bissett, C.E., Cerio, R., and Quinn, A.G. (2001). Expression of the peptide antibiotics human beta defensin-1 and human beta defensin-2 in normal human skin. *J. Invest. Dermatol.* *117*, 106–111.
- Allende, M.L., Dreier, J.L., Mandala, S., and Proia, R.L. (2004). Expression of the sphingosine 1-phosphate receptor, S1P1, on T-cells controls thymic emigration. *J. Biol. Chem.* *279*, 15396–15401.
- Allende, M.L., Bektas, M., Lee, B.G., Bonifacino, E., Kang, J., Tuymetova, G., Chen, W., Saba, J.D., and Proia, R.L. (2011). Sphingosine-1-phosphate lyase deficiency produces a pro-inflammatory response while impairing neutrophil trafficking. *J. Biol. Chem.* *286*, 7348–7358.
- Amen, N. (2013). The role of Glucosylceramides in Keratinocyte Differentiation and Epidermal Barrier Function.
- Amir, I., Konikoff, F.M., Oppenheim, M., Gophna, U., and Half, E.E. (2014). Gastric microbiota is altered in oesophagitis and Barrett's oesophagus and further modified by proton pump inhibitors. *Environ. Microbiol.* *16*, 2905–2914.
- Antonarakis, S.E., Valle, D., Moser, H.W., Moser, A., Qualman, S.J., and Zinkham, W.H. (1984). Phenotypic variability in siblings with Farber disease. *J. Pediatr.* *104*, 406–409.
- Arikawa, J., Ishibashi, M., Kawashima, M., Takagi, Y., Ichikawa, Y., and Imokawa, G. (2002). Decreased levels of sphingosine, a natural antimicrobial agent, may be associated with vulnerability of the stratum corneum from patients with atopic dermatitis to colonization by *Staphylococcus aureus*. *J. Invest. Dermatol.* *119*, 433–439.

- Aureli, M., Bassi, R., Loberto, N., Regis, S., Prinetti, A., Chigorno, V., Aerts, J.M., Boot, R.G., Filocamo, M., and Sonnino, S. (2012). Cell surface associated glycohydrolases in normal and Gaucher disease fibroblasts. *J. Inherit. Metab. Dis.* *35*, 1081–1091.
- Baier, G., and Wagner, J. (2009). PKC inhibitors: potential in T cell-dependent immune diseases. *Curr. Opin. Cell Biol.* *21*, 262–267.
- Barra, P.M.C., Oliviera, P.L., Aragao, D.M.O., Sabaranese, C.M., Aarestrup, B.J. V, Costa, A.C.O., Micke, G.A., and Oliveira, M.A.L. (2014). Study of fatty acids profile in biological sample by capillary zone electrophoresis associate to chemometric approach. *J. Bras. Chem. Soc.* *25*, 675–685.
- Bartke, N., and Hannun, Y.A. (2009). Bioactive sphingolipids: metabolism and function. *J. Lipid Res.* *50 Suppl*, S91–S96.
- Bauer, R., Voelzmann, A., Breiden, B., Schepers, U., Farwanah, H., Hahn, I., Eckardt, F., Sandhoff, K., and Hoch, M. (2009). Schlank, a member of the ceramide synthase family controls growth and body fat in *Drosophila*. *EMBO J.* *28*, 3706–3716.
- Beckmann, N., Sharma, D., Gulbins, E., Becker, K.A., and Edelman, B. (2014). Inhibition of acid sphingomyelinase by tricyclic antidepressants and analogons. *Front. Physiol.* *5*, 331.
- Bendelac, A., and Fearon, D.T. (1997). Innate pathways that control acquired immunity. *Curr. Opin. Immunol.* *9*, 1–3.
- Berdyshev, B. V, Gorshkova, I., Garcia, J.G.N., Natarajan, V., and Hubbard, W.C. (2005). Quantitative analysis of sphingoid base-1-phosphates as bisacetylated derivatives by liquid chromatography-tandem mass spectrometry. *Anal. Biochem.* *339*, 129–136.
- Bibel, D.J., Miller, S.J., Brown, B.E., Pandey, B.B., Elias, P.M., Shinefield, H.R., and Aly, R. (1989). Antimicrobial activity of stratum corneum lipids from normal and essential fatty acid-deficient mice. *J. Invest. Dermatol.* *92*, 632–638.
- Bibel, D.J., Aly, R., and Shinefield, H.R. (1992). Antimicrobial activity of sphingosines. *J. Invest. Dermatol.* *98*, 269–273.
- Bibel, D.J., Aly, R., and Shinefield, H.R. (1995). Topical sphingolipids in antisepsis and antifungal therapy. *Clin. Exp. Dermatol.* *20*, 395–400.
- Bielawski, J., Pierce, J.S., Snider, J., Rembiesa, B., Szulc, Z.M., and Bielawska, A. (2009). Comprehensive quantitative analysis of bioactive sphingolipids by high-performance liquid chromatography-tandem mass spectrometry. *Methods Mol. Biol.* *579*, 443–467.
- Birmingham, A., Selfors, L.M., Forster, T., Wrobel, D., Kennedy, J., Shanks, E., Santoyo-lopez, J., Dunican, D.J., Kelleher, D., Smith, Q., et al. (2010). Statistical Methods for Analysis of High-Throughput RNA Interference Screens. *Nat. Methods* *6*, 569–575.
- Bourbon, N.A., Yun, J., and Kester, M. (2000). Ceramide directly activates protein kinase C zeta to regulate a stress-activated protein kinase signaling complex. *J. Biol. Chem.* *275*, 35617–35623.

- Breiden, B., and Sandhoff, K. (2014). The role of sphingolipid metabolism in cutaneous permeability barrier formation. *Biochim. Biophys. Acta* 1841, 441–452.
- Brinkmann, V., Davis, M.D., Heise, C.E., Albert, R., Cottens, S., Hof, R., Bruns, C., Prieschl, E., Baumruker, T., Hiestand, P., et al. (2002). The immune modulator FTY720 targets sphingosine 1-phosphate receptors. *J. Biol. Chem.* 277, 21453–21457.
- Burke, J.E., and Dennis, E.A. (2009). Phospholipase A2 structure/function, mechanism, and signaling. *J. Lipid Res.* 50 Suppl, S237–S242.
- Burtenshaw, J.M. (1942). The mechanism of self-disinfection of the human skin and its appendages. *J. Hyg. (Lond.)* 42, 184–210.
- Cameron, D.J., Tong, Z., Yang, Z., Kaminoh, J., Kamiyah, S., Chen, H., Zeng, J., Chen, Y., Luo, L., and Zhang, K. (2007). Essential role of Elovl4 in very long chain fatty acid synthesis, skin permeability barrier function, and neonatal survival. *Int. J. Biol. Sci.* 3, 111–119.
- Candi, E., Tarcsa, E., Digiovanna, J.J., Compton, J.G., Elias, P.M., Marekov, L.N., and Steinert, P.M. (1998). A highly conserved lysine residue on the head domain of type II keratins is essential for the attachment of keratin intermediate filaments to the cornified cell envelope through isopeptide crosslinking by transglutaminases. *Proc. Natl. Acad. Sci. U. S. A.* 95, 2067–2072.
- Candi, E., Schmidt, R., and Melino, G. (2005). The cornified envelope: a model of cell death in the skin. *Nat. Rev. Mol. Cell Biol.* 6, 328–340.
- Cao, J., Lockwood, J., Burn, P., and Shi, Y. (2003). Cloning and functional characterization of a mouse intestinal acyl-CoA:monoacylglycerol acyltransferase, MGAT2. *J. Biol. Chem.* 278, 13860–13866.
- Chakravarthy, V.K., Babu, G.K., Dasu, R.L., Prathyusha, P., and Kiran, G.A. (2011). The role of relative response factor in related substances method development by high performance liquid chromatography (HPLC). *RJC* 4, 919–943.
- Chamoun, Z., Mann, R.K., Nellen, D., von Kessler, D.P., Bellotto, M., Beachy, P.A., and Basler, K. (2001). Skinny hedgehog, an acyltransferase required for palmitoylation and activity of the hedgehog signal. *Science* (80-). 293, 2080–2084.
- Chen, H., Fang, Y., Li, W., Orlando, R.C., Shaheen, N., and Chen, X.L. (2013). NFκB and Nrf2 in esophageal epithelial barrier function. *Tissue Barriers* 1, e27463.
- Cheng, C.Y., and Mruk, D.D. (2012). The blood-testis barrier and its implications for male contraception. *Pharmacol. Rev.* 64, 16–64.
- Cheng, J.B., and Russell, D.W. (2004). Mammalian wax biosynthesis. II. Expression cloning of wax synthase cDNAs encoding a member of the acyltransferase enzyme family. *J. Biol. Chem.* 279, 37798–37807.
- Cheng, D., Nelson, T.C., Chen, J., Walker, S.G., Wardwell-Swanson, J., Meegalla, R., Taub, R., Billheimer, J.T., Ramaker, M., and Feder, J.N. (2003). Identification of acyl coenzyme

- A:monoacylglycerol acyltransferase 3, an intestinal specific enzyme implicated in dietary fat absorption. *J. Biol. Chem.* 278, 13611–13614.
- Chorro, L., Sarde, A., Li, M., Woollard, K.J., Chambon, P., Malissen, B., Kissenpfennig, A., Barbaroux, J.B., Groves, R., and Geissmann, F. (2009). Langerhans cell (LC) proliferation mediates neonatal development, homeostasis, and inflammation-associated expansion of the epidermal LC network. *J. Exp. Med.* 206, 3089–3100.
- Choudhary, V., Jacquier, N., and Schneider, R. (2011). The topology of the triacylglycerol synthesizing enzyme Lro1 indicates that neutral lipids can be produced within the luminal compartment of the endoplasmatic reticulum. *Commun. Integr. Biol.* 4, 781–784.
- Christensen, A.D., and Haase, C. (2012). Immunological mechanisms of contact hypersensitivity in mice. *APMIS* 120, 1–27.
- Christophers, E., and Henseler, T. (1987). Contrasting disease patterns in psoriasis and atopic dermatitis. *Arch. Dermatol. Res.* 279 Suppl, S48–S51.
- Coderch, L., López, O., de la Maza, A., and Parra, J.L. (2003). Ceramides and skin function. *Am. J. Clin. Dermatol* 4, 107–129.
- Cork, M.J., Danby, S.G., Vasilopoulos, Y., Hadgraft, J., Lane, M.E., Moustafa, M., Guy, R.H., Macgowan, A.L., Tazi-Ahnini, R., and Ward, S.J. (2009). Epidermal barrier dysfunction in atopic dermatitis. *J. Invest. Dermatol.* 129, 1892–1908.
- Crossman, M.W., and Hirschberg, C.B. (1977). Biosynthesis of phytosphingosine by the rat. *J. Biol. Chem.* 252, 5815–5819.
- Cutignano, A., Chiuminatto, U., Petruzzello, F., Vella, F.M., and Fontana, A. (2010). UPLC-MS/MS method for analysis of sphingosine 1-phosphate in biological samples. *Prostaglandins Other Lipid Mediat.* 93, 25–29.
- Czeloth, N., Bernhardt, G., Hofmann, F., Genth, H., and Förster, R. (2005). Sphingosine-1-phosphate mediates migration of mature dendritic cells. *J. Immunol.* 175, 2960–2967.
- Dale, B.A. (2002). Periodontal epithelium: a newly recognized role in health and disease. *Periodontol.* 2000 30, 70–78.
- Darios, F., Connell, E., and Davletov, B. (2007). Phospholipases and fatty acid signalling in exocytosis. *J. Physiol.* 585, 699–704.
- Dawson, D. V, Drake, D.R., Hill, J.R., Brogden, K.A., Fischer, C.L., and Wertz, P.W. (2013). Organization, barrier function and antimicrobial lipids of the oral mucosa. *Int. J. Cosmet. Sci.* 35, 220–223.
- Diaz-Del Consuelo, I., Jacques, Y., Pizzolato, G.-P., Guy, R.H., and Falson, F. (2005). Comparison of the lipid composition of porcine buccal and esophageal permeability barriers. *Arch. Oral Biol.* 50, 981–987.

- Doering, T., Proia, R.L., and Sandhoff, K. (1999). Accumulation of protein-bound epidermal glucosylceramides in β -glucocerebrosidase deficient type 2 gaucher mice. *FEBS Lett.* *447*, 167–170.
- Dorschner, R.A., Pestonjamas, V.K., Tamakuwala, S., Ohtake, T., Rudisill, J., Nizet, V., Agerberth, B., Gudmundsson, G.H., and Gallo, R.L. (2001). Cutaneous injury induces the release of cathelicidin anti-microbial peptides active against group A *Streptococcus*. *J. Invest. Dermatol.* *117*, 91–97.
- Drake, D.R., Brogden, K.A., Dawson, D. V, and Wertz, P.W. (2008). Thematic review series: skin lipids. Antimicrobial lipids at the skin surface. *J. Lipid Res.* *49*, 4–11.
- Eckl, K.-M., Tidhar, R., Thiele, H., Oji, V., Hausser, I., Brodesser, S., Preil, M.-L., Onal-Akan, A., Stock, F., Müller, D., et al. (2013). Impaired epidermal ceramide synthesis causes autosomal recessive congenital ichthyosis and reveals the importance of ceramide acyl chain length. *J. Invest. Dermatol.* *133*, 2202–2211.
- Elias, P.M. (2005). Stratum corneum defensive functions: an integrated view. *J. Invest. Dermatol.* *125*, 183–200.
- Elias, P.M., Williams, M.L., Maloney, M.E., Bonifas, J.A., Brown, B.E., Grayson, S., and Epstein, E.H. (1984). Stratum corneum lipids in disorders of cornification. Steroid sulfatase and cholesterol sulfate in normal desquamation and the pathogenesis of recessive X-linked ichthyosis. *J. Clin. Invest.* *74*, 1414–1421.
- Eliyahu, E., Shtraizent, N., Shalgi, R., and Schuchman, E.H. (2012). Construction of conditional acid ceramidase knockout mice and in vivo effects on oocyte development and fertility. *Cell. Physiol. Biochem. Int. J. Exp. Cell. Physiol. Biochem. Pharmacol.* *30*, 735–748.
- Farber, S., Cohen, J., and Uzman, L.L. Lipogranulomatosis; a new lipo-glycoprotein storage disease. *J. Mt. Sinai Hosp. N. Y.* *24*, 816–837.
- Fearon, D.T. (1997). Seeking wisdom in innate immunity. *Nature* *388*, 323–324.
- Fischer, C.L., Walters, K.S., Drake, D.R., Blanchette, D.R., Dawson, D. V, Brogden, K.A., and Wertz, P.W. (2013). Sphingoid bases are taken up by *Escherichia coli* and *Staphylococcus aureus* and induce ultrastructural damage. *Skin Pharmacol. Physiol.* *26*, 36–44.
- Furuse, M., Hata, M., Furuse, K., Yoshida, Y., Haratake, A., Sugitani, Y., Noda, T., Kubo, A., and Tsukita, S. (2002). Claudin-based tight junctions are crucial for the mammalian epidermal barrier: a lesson from claudin-1-deficient mice. *J. Cell Biol.* *156*, 1099–1111.
- Gallo, R.L., Murakami, M., Ohtake, T., and Zaiou, M. (2002). Biology and clinical relevance of naturally occurring antimicrobial peptides. *J. Allergy Clin. Immunol.* *110*, 823–831.
- Geilen, C.C., Wieder, T., and Orfanos, C.E. (1997). Ceramide signalling: regulatory role in cell proliferation, differentiation and apoptosis in human epidermis. *Arch. Dermatol. Res.* *289*, 559–566.

- Ghazizadeh, S., and Taichman, L.B. (2001). Multiple classes of stem cells in cutaneous epithelium: a lineage analysis of adult mouse skin. *EMBO J.* *20*, 1215–1222.
- Gollmann, G., Neuwirt, H., Tripp, C.H., Mueller, H., Konwalinka, G., Heufler, C., Romani, N., and Tiefenthaler, M. (2008). Sphingosine-1-phosphate receptor type-1 agonism impairs blood dendritic cell chemotaxis and skin dendritic cell migration to lymph nodes under inflammatory conditions. *Int. Immunol.* *20*, 911–923.
- Gómez-Muñoz, A. (2006). Ceramide 1-phosphate/ceramide, a switch between life and death. *Biochim. Biophys. Acta* *1758*, 2049–2056.
- Grimm, M.O.W., Grimm, H.S., Pätzold, A.J., Zinser, E.G., Halonen, R., Duering, M., Tschäpe, J.A., De Strooper, B., Müller, U., Shen, J., et al. (2005). Regulation of cholesterol and sphingomyelin metabolism by amyloid-beta and presenilin. *Nat. Cell Biol.* *7*, 1118–1123.
- Guillou, H., Zdravec, D., Martin, P.G., and Jacobsson, A. (2010). The key roles of elongases and desaturases in mammalian fatty acid metabolism: Insights from transgenic mice. *Prog. Lipid Res.* *49*, 186–199.
- Gulbins, E., Palmada, M., Reichel, M., Lüth, A., Böhmer, C., Amato, D., Müller, C.P., Tischbirek, C.H., Groemer, T.W., Tabatabai, G., et al. (2013). Acid sphingomyelinase-ceramide system mediates effects of antidepressant drugs. *Nat. Med.* *19*, 934–938.
- Haglund, K., Nezis, I.P., and Stenmark, H. (2011). Structure and functions of stable intercellular bridges formed by incomplete cytokinesis during development. *Commun. Integr. Biol.* *4*, 1–9.
- Hakomori, S. (1981). Glycosphingolipids in cellular interaction, differentiation, and oncogenesis. *Annu. Rev. Biochem.* *50*, 733–764.
- Halprin, K.M. (1972). Epidermal “turnover time”—A re-examination. *Br. J. Dermatol.* *86*, 14–19.
- Hamanaka, S., Hara, M., Nishio, H., Otsuka, F., Suzuki, A., and Uchida, Y. (2002). Human epidermal glucosylceramides are major precursors of stratum corneum ceramides. *J. Invest. Dermatol.* *119*, 416–423.
- Hanada, K. (2003). Serine palmitoyltransferase, a key enzyme of sphingolipid metabolism. *Biochim. Biophys. Acta* *1632*, 16–30.
- Hanada, K. (2006). Discovery of the molecular machinery CERT for endoplasmic reticulum-to-Golgi trafficking of ceramide. *Mol. Cell. Biochem.* *286*, 23–31.
- Hannun, Y.A., and Obeid, L.M. (2008). Principles of bioactive lipid signalling: lessons from sphingolipids. *Nat. Rev. Mol. Cell Biol.* *9*, 139–150.
- Haraoka, G., Muraoka, M., Yoshioka, N., Wakami, S., and Hayashi, I. (1997). First case of surgical treatment of Farber’s disease. *Ann. Plastic Surg.* *39*, 405–410.
- Hardman, M.J., Sisi, P., Banbury, D.N., and Byrne, C. (1998). Patterned acquisition of skin barrier function during development. *Development* *125*, 1541–1552.

- He, X., Huang, C.-L., and Schuchman, E.H. (2009). Quantitative analysis of sphingosine-1-phosphate by HPLC after naphthalene-2,3-dicarboxaldehyde (NDA) derivatization. *J. Chromatogr. B. Analyt. Technol. Biomed. Life Sci.* 877, 983–990.
- Hermo, L., Pelletier, R.-M., Cyr, D.G., and Smith, C.E. (2010). Surfing the wave, cycle, life history, and genes/proteins expressed by testicular germ cells. Part 2: changes in spermatid organelles associated with development of spermatozoa. *Microsc. Res. Tech.* 73, 279–319.
- Hiraoka, M., Abe, A., Lu, Y., Yang, K., Han, X., Gross, R., and Shayman, J. (2006). Lysosomal phospholipase A2 and phospholipidosis. *Mol. Cell. Biol.* 26, 6139–6148.
- Hla, T. (2003). Signaling and biological actions of sphingosine 1-phosphate. *Pharmacol. Res.* 47, 401–407.
- Hoekstra, M., Korporaal, S.J., van der Sluis, R.J., Hirsch-Reinshagen, V., Bochem, A.E., Wellington, C.L., Van Berkel, T.J., Kuivenhoven, J.A., and Van Eck, M. (2013). LCAT deficiency in mice is associated with a diminished adrenal glucocorticoid function. *J. Lipid Res.* 54, 358–364.
- Hofmann, K. (2000). A superfamily of membrane-bound O-acyltransferases with implications for wnt signaling. *Trends Biochem. Sci.* 25, 111–112.
- Holleran, W.M., Takagi, Y., and Uchida, Y. (2006). Epidermal sphingolipids: metabolism, function, and roles in skin disorders. *FEBS Lett.* 580, 5456–5466.
- Holmskov, U.L. (2000). Collectins and collectin receptors in innate immunity. *APMIS. Suppl.* 100, 1–59.
- Hong, K.-K., Cho, H.-R., Ju, W.-C., Cho, Y., and Kim, N.-I. (2007). A study on altered expression of serine palmitoyltransferase and ceramidase in psoriatic skin lesion. *J. Korean Med. Sci.* 22, 862–867.
- Huwiler, A., Johansen, B., Skarstad, A., and Pfeilschifter, J. (2001). Ceramide binds to the CaLB domain of cytosolic phospholipase A2 and facilitates its membrane docking and arachidonic acid release. *FASEB J.* 15, 7–9.
- Hwang, Y.-H., Tani, M., Nakagawa, T., Okino, N., and Ito, M. (2005). Subcellular localization of human neutral ceramidase expressed in HEK293 cells. *Biochem. Biophys. Res. Commun.* 331, 37–42.
- Imokawa, G. (2001). Lipid abnormalities in atopic dermatitis. *J. Am. Acad. Dermatol.* 45, S29–S32.
- Isaac, G., McDonald, S., and Astarita, G. (2011). Lipid Separation using UPLC with Charged Surface Hybrid Technology. Waters Corp. Milford, MA, USA 1–8.
- Ishida-Yamamoto, A., Igawa, S., and Kishibe, M. (2011). Order and disorder in corneocyte adhesion. *J. Dermatol.* 38, 645–654.

- Iwamori, M., Costello, C., and Moser, H.W. (1979). Analysis and quantitation of free ceramide containing nonhydroxy and 2-hydroxy fatty acids, and phytosphingosine by high-performance liquid chromatography. *J. Lipid Res.* *20*, 86–96.
- Iwasaki, S.-I. (2002). Evolution of the structure and function of the vertebrate tongue. *J. Anat.* *201*, 1–13.
- Jacquier, N., Choudhary, V., Mari, M., Toulmay, A., Reggiori, F., and Schneider, R. (2011). Lipid droplets are functionally connected to the endoplasmic reticulum in *Saccharomyces cerevisiae*. *J. Cell Sci.* *124*, 2424–2437.
- Jakobsson, A., Westerberg, R., and Jacobsson, A. (2006). Fatty acid elongases in mammals: their regulation and roles in metabolism. *Prog. Lipid Res.* *45*, 237–249.
- Janssens, M., van Smeden, J., Gooris, G.S., Bras, W., Portale, G., Caspers, P.J., Vreeken, R.J., Kezic, S., Lavrijsen, A.P.M., and Bouwstra, J.A. (2011). Lamellar lipid organization and ceramide composition in the stratum corneum of patients with atopic eczema. *J. Invest. Dermatol.* *131*, 2136–2138.
- Japtok, L., and Kleuser, B. (2009). The role of sphingosine-1-phosphate receptor modulators in the prevention of transplant rejection and autoimmune diseases. *Curr. Opin. Investig. Drugs* *10*, 1183–1194.
- Japtok, L., Schaper, K., Baumer, W., Radeke, H.H., Jeong, S.K., and Kleuser, B. (2012). Sphingosine 1-phosphate modulates antigen capture by murine Langerhans cells via the S1P2 receptor subtype. *PLoS One* *7*, e49427.
- Jeckel, D., Karrenbauer, A., Burger, K.N., van Meer, G., and Wieland, F. (1992). Glucosylceramide is synthesized at the cytosolic surface of various Golgi subfractions. *J. Cell Biol.* *117*, 259–267.
- Jennemann, R., Sandhoff, R., Wang, S., Kiss, E., Gretz, N., Zuliani, C., Martin-Villalba, A., Jager, R., Schorle, H., Kenzelmann, M., et al. (2005). Cell-specific deletion of glucosylceramide synthase in brain leads to severe neural defects after birth. *Proc. Natl. Acad. Sci. U. S. A.* *102*, 12459–12464.
- Jennemann, R., Sandhoff, R., Langbein, L., Kaden, S., Rothermel, U., Gallala, H., Sandhoff, K., Wiegandt, H., and Grone, H.J. (2007). Integrity and barrier function of the epidermis critically depend on glucosylceramide synthesis. *J. Biol. Chem.* *282*, 3083–3094.
- Jennemann, R., Rabionet, M., Gorgas, K., Epstein, S., Dalpke, A., Rothermel, U., Bayerle, A., van der Hoeven, F., Imgrund, S., Kirsch, J., et al. (2012). Loss of ceramide synthase 3 causes lethal skin barrier disruption. *Hum. Mol. Genet.* *21*, 586–608.
- Jobard, F. (2002). Lipoyxygenase-3 (ALOXE3) and 12(R)-lipoyxygenase (ALOX12B) are mutated in non-bullous congenital ichthyosiform erythroderma (NCIE) linked to chromosome 17p13.1. *Hum. Mol. Genet.* *11*, 107–113.
- Jonker, L., Kist, R., Aw, A., Wappler, I., and Peters, H. (2004). Pax9 is required for filiform papilla development and suppresses skin-specific differentiation of the mammalian tongue epithelium. *Mech. Dev.* *121*, 1313–1322.

- Kabashima, K., Haynes, N.M., Xu, Y., Nutt, S.L., Allende, M.L., Proia, R.L., and Cyster, J.G. (2006). Plasma cell S1P1 expression determines secondary lymphoid organ retention versus bone marrow tropism. *J. Exp. Med.* *203*, 2683–2690.
- Kadowaki, T., Wilder, E., Klingensmith, J., Zachary, K., and Perrimon, N. (1996). The segment polarity gene porcupine encodes a putative multitransmembrane protein involved in Wingless processing. *Genes Dev.* *10*, 3116–3128.
- Kannagi, R., Izawa, M., Koike, T., Miyazaki, K., and Kimura, N. (2004). Carbohydrate-mediated cell adhesion in cancer metastasis and angiogenesis. *Cancer Sci.* *95*, 377–384.
- Kaplan, D.H. (2010). In vivo function of Langerhans cells and dermal dendritic cells. *Trends Immunol.* *31*, 446–451.
- Kaplan, D.H., Igyártó, B.Z., and Gaspari, A.A. (2012). Early immune events in the induction of allergic contact dermatitis. *Nat. Rev. Immunol.* *12*, 114–124.
- Katz, P.O., Gerson, L.B., and Vela, M.F. (2013). Guidelines for the diagnosis and management of gastroesophageal reflux disease. *Am. J. Gastroenterol.* *108*, 308–328; quiz 329.
- Kendall, A.C., and Nicolaou, A. (2013). Bioactive lipid mediators in skin inflammation and immunity. *Prog. Lipid Res.* *52*, 141–164.
- Kihara, A., Anada, Y., and Igarashi, Y. (2006). Mouse sphingosine kinase isoforms SPHK1a and SPHK1b differ in enzymatic traits including stability, localization, modification, and oligomerization. *J. Biol. Chem.* *281*, 4532–4539.
- Kirschner, N., Houdek, P., Fromm, M., Moll, I., and Brandner, J.M. (2010). Tight junctions form a barrier in human epidermis. *Eur. J. Cell Biol.* *89*, 839–842.
- Kolter, T., and Sandhoff, K. (1999). Sphingolipids - Their Metabolic Pathways and the Pathobiochemistry of Neurodegenerative Diseases. In *Angewandte Chemie Int. Ed. Eng.* pp. 1532–1568.
- Kolter, T., Proia, R.L., and Sandhoff, K. (2002). Combinatorial ganglioside biosynthesis. *J. Biol. Chem.* *277*, 25859–25862.
- Körschen, H.G., Yildiz, Y., Raju, D.N., Schonauer, S., Bönigk, W., Jansen, V., Kremmer, E., Kaupp, U.B., and Wachten, D. (2013). The non-lysosomal β -glucosidase GBA2 is a non-integral membrane-associated protein at the endoplasmic reticulum (ER) and Golgi. *J. Biol. Chem.* *288*, 3381–3393.
- Kotaja, N., and Sassone-Corsi, P. (2007). The chromatoid body: a germ-cell-specific RNA-processing centre. *Nat. Rev. Mol. Cell Biol.* *8*, 85–90.
- Lahiri, S., and Futerman, A.H. (2007). The metabolism and function of sphingolipids and glycosphingolipids. *Cell. Mol. Life Sci.* *64*, 2270–2284.
- Lamour, N.F., and Chalfant, C.E. (2005). Ceramide-1-phosphate: the “missing” link in eicosanoid biosynthesis and inflammation. *Mol. Interv.* *5*, 358–367.

- Laviad, E.L., Albee, L., Pankova-Kholmyansky, I., Epstein, S., Park, H., Merrill, A.H., and Futerman, A.H. (2008). Characterization of ceramide synthase 2: tissue distribution, substrate specificity, and inhibition by sphingosine 1-phosphate. *J. Biol. Chem.* *283*, 5677–5684.
- Levade, T., Moser, H.W., Fensom, A.H., Harzer, K., Moser, A.B., and Salvayre, R. (1995). Neurodegenerative course in ceramidase deficiency (Farber disease) correlates with the residual lysosomal ceramide turnover in cultured living patient cells. *J. Neurol. Sci.* *134*, 108–114.
- Levade, T., Andrieu-Abadie, N., Ségui, B., Augé, N., Chatelut, M., Jaffrézou, J.P., and Salvayre, R. (1999). Sphingomyelin-degrading pathways in human cells role in cell signalling. *Chem. Phys. Lipids* *102*, 167–178.
- Li, C.-M., Park, J.H., He, X., Levy, B., Chen, F., Arai, K., Adler, D.A., Disteché, C.M., Koch, J., Sandhoff, K., et al. (1999). The human acid ceramidase gene (ASAH): structure, chromosomal location, mutation analysis, and expression. *Genomics* *62*, 223–231.
- Li, C.-M., Park, J.-H., Simonaro, C.M., He, X., Gordon, R.E., Friedman, A.-H., Ehleiter, D., Paris, F., Manova, K., Hepbaldikler, S., et al. (2002). Insertional mutagenesis of the mouse acid ceramidase gene leads to early embryonic lethality in homozygotes and progressive lipid storage disease in heterozygotes. *Genomics* *79*, 218–224.
- Li, W., Sandhoff, R., Kono, M., Zerfas, P., Hoffmann, V., Ding, B.C.-H., Proia, R.L., and Deng, C.-X. (2007). Depletion of ceramides with very long chain fatty acids causes defective skin permeability barrier function, and neonatal lethality in ELOVL4 deficient mice. *Int. J. Biol. Sci.* *3*, 120–128.
- Linden, K.G., and Weinstein, G.D. (1999). Psoriasis: current perspectives with an emphasis on treatment. *Am. J. Med.* *107*, 595–605.
- Liu, H., Chakravarty, D., Maceyka, M., Milstien, S., and Spiegel, S. (2002). Sphingosine kinases: a novel family of lipid kinases. *Prog. Nucleic Acid Res. Mol. Biol.* *71*, 493–511.
- Macheleidt, O., Kaiser, H.W., and Sandhoff, K. (2002). Deficiency of epidermal protein-bound omega-hydroxyceramides in atopic dermatitis. *J. Invest. Dermatol.* *119*, 166–173.
- Maeda, Y., Matsuyuki, H., Shimano, K., Kataoka, H., Sugahara, K., and Chiba, K. (2007). Migration of CD4 T cells and dendritic cells toward sphingosine 1-phosphate (S1P) is mediated by different receptor subtypes: S1P regulates the functions of murine mature dendritic cells via S1P receptor type 3. *J. Immunol.* *178*, 3437–3446.
- Majoul, I., Schmidt, T., Pomasanova, M., Boutkevich, E., Kozlov, Y., and Söling, H.-D. (2002). Differential expression of receptors for Shiga and Cholera toxin is regulated by the cell cycle. *J. Cell Sci.* *115*, 817–826.
- Malecheidt, O., Kaiser, H.W., and Sandhoff, K. (2002). Deficiency of epidermal protein-bound w-hydroxycermaides in atopic dermatitis. *Soc. Investig. Dermatology* *119*.
- Marekov, L.N., and Steinert, P.M. (1998). Ceramides are bound to structural proteins of the human foreskin epidermal cornified cell envelope. *J. Biol. Chem.* *273*, 17763–17770.

- Marshall, D., Hardman, M.J., and Byrne, C. (2000). SPRR1 gene induction and barrier formation occur as coordinated moving fronts in terminally differentiating epithelia. *J. Invest. Dermatol.* *114*, 967–975.
- Marshall, D., Hardman, M.J., Nield, K.M., and Byrne, C. (2001). Differentially expressed late constituents of the epidermal cornified envelope. *Proc. Natl. Acad. Sci. U. S. A.* *98*, 13031–13036.
- Martino, A. (2007). Sphingosine 1-phosphate as a novel immune regulator of dendritic cells. *J. Biosci.* *32*, 1207–1212.
- Masukawa, Y., Narita, H., Shimizu, E., Kondo, N., Sugai, Y., Oba, T., Homma, R., Ishikawa, J., Takagi, Y., Kitahara, T., et al. (2008). Characterization of overall ceramide species in human stratum corneum. *J. Lipid Res.* *49*, 1466–1476.
- Mathews, M., Jia, H.P., Guthmiller, J.M., Losh, G., Graham, S., Johnson, G.K., Tack, B.F., and McCray, P.B. (1999). Production of beta-defensin antimicrobial peptides by the oral mucosa and salivary glands. *Infect. Immun.* *67*, 2740–2745.
- Matloubian, M., Lo, C.G., Cinamon, G., Lesneski, M.J., Xu, Y., Brinkmann, V., Allende, M.L., Proia, R.L., and Cyster, J.G. (2004). Lymphocyte egress from thymus and peripheral lymphoid organs is dependent on S1P receptor 1. *Nature* *427*, 355–360.
- McGovern, M.M., and Schuchman, E.H. (2009). Acid Sphingomyelinase Deficiency.
- McMahon, A., Butovich, I.A., Mata, N.L., Klein, M., Ritter, R., Richardson, J., Birch, D.G., Edwards, A.O., and Kedziarski, W. (2007). Retinal pathology and skin barrier defect in mice carrying a Stargardt disease-3 mutation in elongase of very long chain fatty acids-4. *Mol. Vis.* *13*, 258–272.
- Medzhitov, R., and Janeway, C. (2000a). Innate immune recognition: mechanisms and pathways. *Immunol. Rev.* *173*, 89–97.
- Medzhitov, R., and Janeway, C. (2000b). The Toll receptor family and microbial recognition. *Trends Microbiol.* *8*, 452–456.
- Medzhitov, R., and Janeway, C.A. (1998). An ancient system of host defense. *Curr. Opin. Immunol.* *10*, 12–15.
- Menuz, V., Howell, K.S., Gentina, S., Epstein, S., Riezman, I., Fornallaz-Mulhauser, M., Hengartner, M.O., Gomez, M., Riezman, H., and Martinou, J.-C. (2009). Protection of *C. elegans* from anoxia by HYL-2 ceramide synthase. *Science* (80-.). *324*, 381–384.
- Merrill, A.H., and Stevens, V.L. (1989). Modulation of protein kinase C and diverse cell functions by sphingosine - a pharmacologically interesting compound linking sphingolipids and signal transduction. *Biochim. Biophys. Acta* *1010*, 131–139.
- Mizukoshi, K., Matsumoto, K., Hirose, R., Fujita, T., Ishida-Yamamoto, A., and Iizuka, H. (2011). Effects of serine palmitoyltransferase inhibitor ISP-I on the stratum corneum of intact mouse skin. *Biol. Pharm. Bull.* *34*, 1383–1389.

- Mizutani, Y., Kihara, A., and Igarashi, Y. (2005). Mammalian Lass6 and its related family members regulate synthesis of specific ceramides. *Biochem. J.* *390*, 263–271.
- Mizutani, Y., Mitsutake, S., Tsuji, K., Kihara, A., and Igarashi, Y. (2009). Ceramide biosynthesis in keratinocyte and its role in skin function. *Biochimie* *91*, 784–790.
- Mizutani, Y., Sun, H., Ohno, Y., Sassa, T., Wakashima, T., Obara, M., Yuyama, K., Kihara, A., and Igarashi, Y. (2013). Cooperative Synthesis of Ultra Long-Chain Fatty Acid and Ceramide during Keratinocyte Differentiation. *PLoS One* *8*, e67317.
- Mok, K., Mruk, D.D., and Cheng, C.Y. (2013). Regulation of blood-testis barrier (BTB) dynamics during spermatogenesis via the “Yin” and “Yang” effects of mammalian target of rapamycin complex 1 (mTORC1) and mTORC2. *Int. Rev. Cell Mol. Biol.* *301*, 291–358.
- Moon, S.H., Kim, J.Y., Song, E.H., Shin, M.K., Cho, Y.H., and Kim, N.I. (2013). Altered levels of sphingosine and sphinganine in psoriatic epidermis. *Ann. Dermatol.* *25*, 321–326.
- Mruk, D.D., and Cheng, C.Y. (2004). Sertoli-Sertoli and Sertoli-germ cell interactions and their significance in germ cell movement in the seminiferous epithelium during spermatogenesis. *Endocr. Rev.* *25*, 747–806.
- Mruk, D.D., Silvestrini, B., and Cheng, C.Y. (2008). Anchoring junctions as drug targets: role in contraceptive development. *Pharmacol. Rev.* *60*, 146–180.
- Mullen, T.D., Hannun, Y.A., and Obeid, L.M. (2012). Ceramide synthases at the centre of sphingolipid metabolism and biology. *Biochem. J.* *441*, 789–802.
- Muramatsu, T. (2000). Essential roles of carbohydrate signals in development, immune response and tissue functions, as revealed by gene targeting. *J. Biochem.* *127*, 171–176.
- Nagpal, R., Patel, A., and Gibson, M.C. (2008). Epithelial topology. *Bioessays* *30*, 260–266.
- Nakamoto, T., and Sakai, Y. (1989). Changes in endoplasmic reticulum during spermiogenesis in the mouse. *Cell Tissue Res.* *257*, 279–284.
- Nemes, Z., Marekov, L.N., Fésüs, L., and Steinert, P.M. (1999). A novel function for transglutaminase 1: attachment of long-chain omega-hydroxyceramides to involucrin by ester bond formation. *Proc. Natl. Acad. Sci. U. S. A.* *96*, 8402–8407.
- Nenoff, P., and Haustein, U.-F. (2002). In vitro activity of phytosphingosines against *Malassezia furfur* and *Candida albicans*. *Acta Derm. Venereol.* *82*, 170–173.
- Ng, D.S., Francone, O.L., Forte, T.M., Zhang, J., Haghpassand, M., and Rubin, E.M. (1997). Disruption of the Murine Lecithin:Cholesterol Acyltransferase Gene Causes Impairment of Adrenal Lipid Delivery and Up-regulation of Scavenger Receptor Class B Type I. *J. Biol. Chem.* *272*, 15777–15781.
- Nijsten, T., Margolis, D.J., Feldman, S.R., Rolstad, T., and Stern, R.S. (2005). Traditional systemic treatments have not fully met the needs of psoriasis patients: results from a national survey. *J. Am. Acad. Dermatol.* *52*, 434–444.

- O'Donnell, L., Nicholls, P.K., O'Bryan, M.K., McLachlan, R.I., and Stanton, P.G. (2011). Spermiation: The process of sperm release. *Spermatogenesis 1*, 14–35.
- Okabe, H., and Kishimoto, Y. (1977). In vivo metabolism of ceramides in rat brain. Fatty acid replacement and esterification of ceramide. *J. Biol. Chem.* 252, 7068–7073.
- Olivera, A., and Rivera, J. (2011). An emerging role for the lipid mediator sphingosine-1-phosphate in mast cell effector function and allergic disease. *Adv. Exp. Med. Biol.* 716, 123–142.
- Ong, P.Y., Ohtake, T., Brandt, C., Strickland, I., Boguniewicz, M., Ganz, T., Gallo, R.L., and Leung, D.Y.M. (2002). Endogenous antimicrobial peptides and skin infections in atopic dermatitis. *N. Engl. J. Med.* 347, 1151–1160.
- Palmer, C.N.A., Irvine, A.D., Terron-Kwiatkowski, A., Zhao, Y., Liao, H., Lee, S.P., Goudie, D.R., Sandilands, A., Campbell, L.E., Smith, F.J.D., et al. (2006). Common loss-of-function variants of the epidermal barrier protein filaggrin are a major predisposing factor for atopic dermatitis. *Nat. Genet.* 38, 441–446.
- Payne, C.D., Ray, T.L., and Downing, D.T. (1996). Cholesterol Sulfate Protects *Candida albicans* from Inhibition by Sphingosine in Vitro. *J. Invest. Dermatol.* 106, 549–552.
- Perry, D.K., and Hannun, Y.A. (1998). The role of ceramide in cell signaling. *Biochim. Biophys. Acta* 1436, 233–243.
- Pewzner-Jung, Y., Ben-Dor, S., and Futerman, A.H. (2006). When do Lasses (longevity assurance genes) become CerS (ceramide synthases)? Insights into the regulation of ceramide synthesis. *J. Biol. Chem.* 281, 25001–25005.
- Potten, C.S., Saffhill, R., and Maibach, H.I. (1987). Measurement of the transit time for cells through the epidermis and stratum corneum of the mouse and guinea-pig. *Cell Tissue Kinet.* 20, 461–472.
- Pruett, S.T., Bushnev, A., Hagedorn, K., Adiga, M., Haynes, C.A., Sullards, M.C., Liotta, D.C., and Merrill, A.H. (2008). Biodiversity of sphingoid bases (“sphingosines”) and related amino alcohols. *J. Lipid Res.* 49, 1621–1639.
- Rabionet, M. (2011). Ceramide Synthase 3 and its Essential Role in Skin Barrier Function and Male Fertility.
- Rabionet, M., van der Spoel, A.C., Chuang, C.C., von Tumpling-Radosta, B., Litjens, M., Bouwmeester, D., Hellbusch, C.C., Korner, C., Wiegandt, H., Gorgas, K., et al. (2008). Male germ cells require polyenoic sphingolipids with complex glycosylation for completion of meiosis: a link to ceramide synthase-3. *J. Biol. Chem.* 283, 13357–13369.
- Rabionet, M., Bayerle, A., Marsching, C., Jennemann, R., Grone, H.J., Yildiz, Y., Wachten, D., Shaw, W., Shayman, J.A., and Sandhoff, R. (2013). 1-O-Acylceramides are natural components of human and mouse epidermis. *J. Lipid Res.* 1–34.
- Rabionet, M., Gorgas, K., and Sandhoff, R. (2014). Ceramide synthesis in the epidermis. *Biochim. Biophys. Acta* 1841, 422–434.

- Radner, F., Marrakchi, S., Kirchmeier, P., Kim, G., Ribierre, F., Kamoun, B., Abid, L., Leipoldt, M., Turki, H., Schempp, W., et al. (2013). Mutations in CERS3 cause autosomal recessive congenital ichthyosis in humans. *PLoS Genet.* 9, e1003536.
- Raffaghello, L., Marimpietri, D., Pagnan, G., Pastorino, F., Cosimo, E., Brignole, C., Ponzoni, M., and Montaldo, P.G. (2003). Anti-GD2 monoclonal antibody immunotherapy: a promising strategy in the prevention of neuroblastoma relapse. *Cancer Lett.* 197, 205–209.
- Ramesh Panchagnula *, Pramod Sridhar Salve, Narisetty Sunil Thomas, Amit Kumar Jain, P.R. (2001). Transdermal delivery of naloxone: effect of water, propylene glycol, ethanol and their binary combinations on permeation through rat skin. *Int. J. Pharm.* 219, 95–105.
- Reines, I., Kietzmann, M., Mischke, R., Tschernig, T., Luth, A., Kleuser, B., and Baumer, W. (2009). Topical application of sphingosine-1-phosphate and FTY720 attenuate allergic contact dermatitis reaction through inhibition of dendritic cell migration. *J. Invest. Dermatol.* 129, 1954–1962.
- Riebeling, C., Allegood, J.C., Wang, E., Merrill, A.H., and Futerman, A.H. (2003). Two mammalian longevity assurance gene (LAG1) family members, *trh1* and *trh4*, regulate dihydroceramide synthesis using different fatty acyl-CoA donors. *J. Biol. Chem.* 278, 43452–43459.
- Robinson, B.S., Johnson, D.W., and Poulos, A. (1992). Novel molecular species of sphingomyelin containing 2-hydroxylated polyenoic very-long-chain fatty acids in mammalian testes and spermatozoa. *J. Biol. Chem.* 267, 1746–1751.
- Röse, L., Schneider, C., Stock, C., Zollner, T.M., and Döcke, W.-D. (2012). Extended DNFB-induced contact hypersensitivity models display characteristics of chronic inflammatory dermatoses. *Exp. Dermatol.* 21, 25–31.
- Rosen, H., Gonzalez-Cabrera, P.J., Sanna, M.G., and Brown, S. (2009). Sphingosine 1-phosphate receptor signaling. *Annu. Rev. Biochem.* 78, 743–768.
- Saeedi, R., Li, M., and Frohlich, J. (2014). A review on lecithin:cholesterol acyltransferase deficiency. *Clin. Biochem.*
- Saigusa, D., Shiba, K., Inoue, A., Hama, K., Okutani, M., Iida, N., Saito, M., Suzuki, K., Kaneko, T., Suzuki, N., et al. (2012). Simultaneous quantitation of sphingoid bases and their phosphates in biological samples by liquid chromatography/electrospray ionization tandem mass spectrometry. *Anal. Bioanal. Chem.* 403, 1897–1905.
- Sandhoff, R. (2010). Very long chain sphingolipids: tissue expression, function and synthesis. *FEBS Lett.* 584, 1907–1913.
- Sandhoff, R., Geyer, R., Jennemann, R., Paret, C., Kiss, E., Yamashita, T., Gorgas, K., Sijmonsma, T.P., Iwamori, M., Finaz, C., et al. (2005). Novel class of glycosphingolipids involved in male fertility. *J. Biol. Chem.* 280, 27310–27318.
- Sands, M.S. (2013). Farber disease: Understanding a fatal childhood disorder and dissecting ceramide biology. *EMBO Mol. Med.* 5, 799–801.

- Sassa, T., Ohno, Y., Suzuki, S., Nomura, T., Nishioka, C., Kashiwagi, T., Hirayama, T., Akiyama, M., Taguchi, R., Shimizu, H., et al. (2013). Impaired epidermal permeability barrier in mice lacking *elov11*, the gene responsible for very-long-chain fatty acid production. *Mol. Cell Biol.* *33*, 2787–2796.
- Sato, J., Denda, M., Nakanishi, J., Nomura, J., and Koyama, J. (1998). Cholesterol sulfate inhibits proteases that are involved in desquamation of stratum corneum. *J. Invest. Dermatol.* *111*, 189–193.
- Scherer, M., Leuthäuser-Jaschinski, K., Ecker, J., Schmitz, G., and Liebisch, G. (2010). A rapid and quantitative LC-MS/MS method to profile sphingolipids. *J. Lipid Res.* *51*, 2001–2011.
- Schmidt, H., Schmidt, R., and Geisslinger, G. (2006). LC-MS/MS-analysis of sphingosine-1-phosphate and related compounds in plasma samples. *Prostaglandins Other Lipid Mediat.* *81*, 162–170.
- Schnaar, R.L. (1991). Glycosphingolipids in cell surface recognition. *Glycobiology* *1*, 477–485.
- Schorling, S., Vallée, B., Barz, W.P., Riezman, H., and Oesterhelt, D. (2001). Lag1p and Lac1p are essential for the Acyl-CoA-dependent ceramide synthase reaction in *Saccharomyces cerevisiae*. *Mol. Biol. Cell* *12*, 3417–3427.
- Seidler, J., Zinn, N., Haaf, E., Boehm, M.E., Winter, D., Schlosser, A., and Lehmann, W.D. (2011). Metal ion-mobilizing additives for comprehensive detection of femtomole amounts of phosphopeptides by reversed phase LC-MS. *Amino Acids* *41*, 311–320.
- Shaner, R.L., Allegood, J.C., Park, H., Wang, E., Kelly, S., Haynes, C.A., Sullards, M.C., and Merrill, A.H. (2009). Quantitative analysis of sphingolipids for lipidomics using triple quadrupole and quadrupole linear ion trap mass spectrometers. *J. Lipid Res.* *50*, 1692–1707.
- Shayman, J., Kelly, R., Kollmeyer, J., He, Y., and Abe, A. (2011). Group XV phospholipase A₂, a lysosomal phospholipase A₂. *Prog. Lipid Res.* *50*, 1–13.
- Shayman, J.A., Abe, A., and Hiraoka, M. (2004). A turn in the road: How studies on the pharmacology of glucosylceramide synthase inhibitors led to the identification of a lysosomal phospholipase A₂ with ceramide transacylase activity. *Glycoconj. J.* *20*, 25–32.
- Singh, A., Verma, R., Murari, A., and Agrawal, A. (2014). Oral candidiasis: An overview. *J. Oral Maxillofac. Pathol.* *18*, S81–S85.
- Soley, J.T. (1994). Centriole development and formation of the flagellum during spermiogenesis in the ostrich (*Struthio camelus*). *J. Anat.* *185* (Pt 2), 301–313.
- Song, W.C., Sarrias, M.R., and Lambris, J.D. (2000). Complement and innate immunity. *Immunopharmacology* *49*, 187–198.
- Sorger, D., and Daum, G. (2002). Synthesis of triacylglycerols by the acyl-coenzyme A:diacyl-glycerol acyltransferase Dga1p in lipid particles of the yeast *Saccharomyces cerevisiae*. *J. Bacteriol.* *184*, 519–524.

- Spiegel, S., and Kolesnick, R. (2002). Sphingosine 1-phosphate as a therapeutic agent. *Leukemia* 16, 1596–1602.
- Spiegel, S., and Milstien, S. (2011). The outs and the ins of sphingosine-1-phosphate in immunity. *Nat. Rev. Immunol.* 11, 403–415.
- Sprong, H., Kruithof, B., Leijendekker, R., Slot, J.W., van Meer, G., and van der Sluijs, P. (1998). UDP-galactose:ceramide galactosyltransferase is a class I integral membrane protein of the endoplasmic reticulum. *J. Biol. Chem.* 273, 25880–25888.
- Steinert, P.M., Candi, E., Kartasova, T., and Marekov, L. (1998). Small proline-rich proteins are cross-bridging proteins in the cornified cell envelopes of stratified squamous epithelia. *J. Struct. Biol.* 122, 76–85.
- Steinman, R.M. (2007). Dendritic cells: understanding immunogenicity. *Eur. J. Immunol.* 37 *Suppl 1*, S53–S60.
- Stewart, M.E., and Downing, D.T. (1995). Free sphingosines of human skin include 6-hydroxysphingosine and unusually long-chain dihydrosphingosines. *J. Invest. Dermatol.* 105, 613–618.
- Stone, S.J., Myers, H.M., Watkins, S.M., Brown, B.E., Feingold, K.R., Elias, P.M., and Farese, R. V (2004). Lipopenia and skin barrier abnormalities in DGAT2-deficient mice. *J. Biol. Chem.* 279, 11767–11776.
- Strum, J.C., Ghosh, S., and Bell, R.M. (1997). Lipid second messengers. A role in cell growth regulation and cell cycle progression. *Adv. Exp. Med. Biol.* 407, 421–431.
- Subbaiah, P., Horvath, P., and Achar, S.B. (2006). Regulation of the activity and fatty acid specificity of lecithin-cholesterol acyltransferase by sphingomyelin and its metabolites, ceramide and ceramide phosphate. *Biochemistry* 45, 5029–5038.
- Subramanian, P., Stahelin, R. V, Szulc, Z., Bielawska, A., Cho, W., and Chalfant, C.E. (2005). Ceramide 1-phosphate acts as a positive allosteric activator of group IVA cytosolic phospholipase A2 alpha and enhances the interaction of the enzyme with phosphatidylcholine. *J. Biol. Chem.* 280, 17601–17607.
- Tegelenbosch, R.A., and de Rooij, D.G. (1993). A quantitative study of spermatogonial multiplication and stem cell renewal in the C3H/101 F1 hybrid mouse. *Mutat. Res.* 290, 193–200.
- Thudichum, J.L.W. (1884). A treatise on the chemical constitution of the brain.
- Tidhar, R., and Futerman, A.H. (2013). The complexity of sphingolipid biosynthesis in the endoplasmic reticulum. *Biochim. Biophys. Acta* 1833, 2511–2518.
- Turchetto-Zolet, A.C., Maraschin, F.S., de Moraes, G.L., Cagliari, A., Andrade, C.M.B., Margis-Pinheiro, M., and Margis, R. (2011). Evolutionary view of acyl-CoA diacylglycerol acyltransferase (DGAT), a key enzyme in neutral lipid biosynthesis. *BMC Evol. Biol.* 11, 263.

- Turkish, A., and Sturley, S.L. (2007). Regulation of triglyceride metabolism. I. Eukaryotic neutral lipid synthesis: “Many ways to skin ACAT or a DGAT”. *Am. J. Physiol. Gastrointest. Liver Physiol.* *292*, G953–G957.
- Turkish, A.R., Henneberry, A.L., Cromley, D., Padamsee, M., Oelkers, P., Bazzi, H., Christiano, A.M., Billheimer, J.T., and Sturley, S.L. (2005). Identification of two novel human acyl-CoA wax alcohol acyltransferases: members of the diacylglycerol acyltransferase 2 (DGAT2) gene superfamily. *J. Biol. Chem.* *280*, 14755–14764.
- Uchida, Y., and Hamanaka, S. (2006). Stratum Corneum Ceramides: Function, Origins, and Therapeutic Applications. In *Skin Barrier*, pp. 43–64.
- Uchida, Y., Hara, M., Nishio, H., Sidransky, E., Inoue, S., Otsuka, F., Suzuki, A., Elias, P.M., Holleran, W.M., and Hamanaka, S. (2000). Epidermal sphingomyelins are precursors for selected stratum corneum ceramides. *J. Lipid Res.* *41*, 2071–2082.
- Unanue, E.R. (1997). Inter-relationship among macrophages, natural killer cells and neutrophils in early stages of *Listeria* resistance. *Curr. Opin. Immunol.* *9*, 35–43.
- Vallée, B., and Riezman, H. (2005). Lip1p: a novel subunit of acyl-CoA ceramide synthase. *EMBO J.* *24*, 730–741.
- Vasireddy, V., Uchida, Y., Salem, N., Kim, S.Y., Mandal, M.N.A., Reddy, G.B., Bodepudi, R., Alderson, N.L., Brown, J.C., Hama, H., et al. (2007). Loss of functional ELOVL4 depletes very long-chain fatty acids (> or =C28) and the unique omega-O-acylceramides in skin leading to neonatal death. *Hum. Mol. Genet.* *16*, 471–482.
- Veerman, E.C.I., Valentijn-Benz, M., van’t Hof, W., Nazmi, K., van Marle, J., and Amerongen, A.V.N. (2010). Phytosphingosine kills *Candida albicans* by disrupting its cell membrane. *Biol. Chem.* *391*, 65–71.
- Venkataraman, K., Riebeling, C., Bodennec, J., Riezman, H., Allegood, J.C., Sullards, M.C., Merrill, A.H., and Futerman, A.H. (2002). Upstream of growth and differentiation factor 1 (*uog1*), a mammalian homolog of the yeast longevity assurance gene 1 (*LAG1*), regulates N-stearoyl-sphinganine (C18-(dihydro)ceramide) synthesis in a fumonisin B1-independent manner in mammalian cells. *J. Biol. Chem.* *277*, 35642–35649.
- Vielhaber, G., Pfeiffer, S., Brade, L., Lindner, B., Goldmann, T., Vollmer, E., Hintze, U., Wittern, K.P., and Wepf, R. (2001). Localization of ceramide and glucosylceramide in human epidermis by immunogold electron microscopy. *J. Invest. Dermatol.* *117*, 1126–1136.
- Voynova, N.S., Vionnet, C., Ejsing, C.S., and Conzelmann, A. (2012). A novel pathway of ceramide metabolism in *Saccharomyces cerevisiae*. *Biochem. J.* *447*, 103–114.
- Walzer, T., Chiossone, L., Chaix, J., Calver, A., Carozzo, C., Garrigue-Antar, L., Jacques, Y., Baratin, M., Tomasello, E., and Vivier, E. (2007). Natural killer cell trafficking in vivo requires a dedicated sphingosine 1-phosphate receptor. *Nat. Immunol.* *8*, 1337–1344.
- Wang, A., Johnson, D.G., and MacLeod, M.C. (2001). Molecular cloning and characterization of a novel mouse epidermal differentiation gene and its promoter. *Genomics* *73*, 284–290.

- Watt, F.M. (2002). The stem cell compartment in human interfollicular epidermis. *J. Dermatol. Sci.* 28, 173–180.
- Weerheim, A., and Ponc, M. (2001). Determination of stratum corneum lipid profile by tape stripping in combination with high-performance thin-layer chromatography. *Arch. Dermatol. Res.* 293, 191–199.
- Weigert, A., Weis, N., and Brüne, B. (2009). Regulation of macrophage function by sphingosine-1-phosphate. *Immunobiology* 214, 748–760.
- Weinberg, A., Krisanaprakornkit, S., and Dale, B.A. (1998). Epithelial antimicrobial peptides: review and significance for oral applications. *Crit. Rev. Oral Biol. Med.* 9, 399–414.
- Wertz, P.W. (1992). Epidermal lipids. *Semin. Dermatol.* 11, 106–113.
- Wertz, P.W., and Downing, D.T. (1990). Free Sphingosine in Human Epidermis. *J. Invest. Dermatol.* 94, 159–161.
- Wertz, P.W., Cox, P.S., Squier, C.A., and Downing, D.T. (1986). Lipids of epidermis and keratinized and non-keratinized oral epithelia. *Comp. Biochem. Physiol. Part B* 83, 529–531.
- Westerberg, R., Tvrdik, P., Undén, A.-B., Månsson, J.-E., Norlén, L., Jakobsson, A., Holleran, W.H., Elias, P.M., Asadi, A., Flodby, P., et al. (2004a). Role for ELOVL3 and fatty acid chain length in development of hair and skin function. *J. Biol. Chem.* 279, 5621–5629.
- Westerberg, R., Tvrdik, P., Uden, A.B., Mansson, J.E., Norlen, L., Jakobsson, A., Holleran, W.H., Elias, P.M., Asadi, A., Flodby, P., et al. (2004b). Role for ELOVL3 and fatty acid chain length in development of hair and skin function. *J. Biol. Chem.* 279, 5621–5629.
- Westwick, J.K., Bielawska, A.E., Dbaibo, G., Hannun, Y.A., and Brenner, D.A. (1995). Ceramide activates the stress-activated protein kinases. *J. Biol. Chem.* 270, 22689–22692.
- Winter, D., Seidler, J., Ziv, Y., Shiloh, Y., and Lehmann, W.D. (2008). Citrate Boosts the Performance of Phosphopeptide Analysis by UPLC-ESI-MS/MS. *J. Proteome Res.* 8, 418–424.
- Wong, P., Colucci-Guyon, E., Takahashi, K., Gu, C., Babinet, C., and Coulombe, P.A. (2000). Introducing a null mutation in the mouse K6alpha and K6beta genes reveals their essential structural role in the oral mucosa. *J. Cell Biol.* 150, 921–928.
- Yang, J., Brown, M.S., Liang, G., Grishin, N. V, and Goldstein, J.L. (2008). Identification of the acyltransferase that octanoylates ghrelin, an appetite-stimulating peptide hormone. *Cell* 132, 387–396.
- Yasuhiro, M., Hirofumi, M., Kyoko, S., Hirotoshi, K., Chiba, K., and Sugahara, K. (2007). Migration of CD4 T Cells and Dendritic Cells toward Sphingosine 1-Phosphate (S1P) Is Mediated by Different Receptor Subtypes: S1P Regulates the Functions of Murine Mature Dendritic Cells via S1P Receptor Type 3. *J. Immunol.* 178, 3437–3446.
- Yen, C.-L.E., and Farese, R. V (2003). MGAT2, a monoacylglycerol acyltransferase expressed in the small intestine. *J. Biol. Chem.* 278, 18532–18537.

Yen, C.-L.E., Stone, S.J., Cases, S., Zhou, P., and Farese, R. V (2002). Identification of a gene encoding MGAT1, a monoacylglycerol acyltransferase. *Proc. Natl. Acad. Sci. U. S. A.* *99*, 8512–8517.

Yen, C.-L.E., Brown, C.H., Monetti, M., and Farese, R. V (2005). A human skin multifunctional O-acyltransferase that catalyzes the synthesis of acylglycerols, waxes, and retinyl esters. *J. Lipid Res.* *46*, 2388–2397.

Yen, C.-L.E., Stone, S.J., Koliwad, S., Harris, C., and Farese, R. V (2008). Thematic review series: glycerolipids. DGAT enzymes and triacylglycerol biosynthesis. *J. Lipid Res.* *49*, 2283–2301.

Yoo, H.H., Son, J., and Kim, D.H. (2006). Liquid chromatography-tandem mass spectrometric determination of ceramides and related lipid species in cellular extracts. *J. Chromatography B* *843*, 327–333.

Youm, Y.-H., Kanneganti, T.-D., Vandanmagsar, B., Zhu, X., Ravussin, A., Adijiang, A., Owen, J.S., Thomas, M.J., Francis, J., Parks, J.S., et al. (2012). The Nlrp3 inflammasome promotes age-related thymic demise and immunosenescence. *Cell Rep.* *1*, 56–68.

Zhai, L., Chaturvedi, D., and Cumberledge, S. (2004). *Drosophila* wnt-1 undergoes a hydrophobic modification and is targeted to lipid rafts, a process that requires porcupine. *J. Biol. Chem.* *279*, 33220–33227.

Zhang, J.-H. (1999). A Simple Statistical Parameter for Use in Evaluation and Validation of High Throughput Screening Assays. *J. Biomol. Screen.* *4*, 67–73.

Zhang, H., Desai, N.N., Olivera, A., Seki, T., Brooker, G., and Spiegel, S. (1991). Sphingosine-1-phosphate, a novel lipid, involved in cellular proliferation. *J. Cell Biol.* *114*, 155–167.

Zuo, Y., Zhuang, D.Z., Han, R., Isaac, G., Tobin, J.J., McKee, M., Welti, R., Brissette, J.L., Fitzgerald, M.L., and Freeman, M.W. (2008). ABCA12 maintains the epidermal lipid permeability barrier by facilitating formation of ceramide linoleic esters. *J. Biol. Chem.* *283*, 36624–36635.

VI. Appendix

List of figures

Figure 1 Structure of major sphingolipid classes.	2
Figure 2 <i>De novo</i> ceramide synthesis, recycling and processing to higher SLs.....	4
Figure 3 <i>De novo</i> and salvage (dihydro)ceramide synthesis catalyzed by the ceramide synthases..	5
Figure 4 Plasmid map from mCerS3-EGFP.	19
Figure 5 The epidermal structure..	35
Figure 6 Acyl FA chain length in sphingolipids.	37
Figure 7 Major epidermal ceramide subclasses distinguished by acyl FA chain length and hydroxylation.....	39
Figure 8 Synthesis of LC-, VLC- and ULC-CoAs by elongation cycle of FAs.....	41
Figure 9 Chromatogram of non-phosphorylated sphingoid bases without and with CSH column. ...	50
Figure 10 Chromatogram of phosphorylated sphingoid bases without and with CSH column.	51
Figure 11 fragmentation patterns of standard substances.....	53
Figure 12 Calibration curves of available unphosphorylated standard substances.	56
Figure 13 Calibration curves of available standard substances.....	57
Figure 14 Calibration curves of available phosphorylated standard substances.	58
Figure 15 Comparisons of data derived by own LC-MS/MS method in mg wet weight or per μ l with that published in literature in the same units	61
Figure 16 Quantification of free and phosphorylated sphingoid bases as well as ceramide-1-phosphates in skin of CerS3 mutant mice	62
Figure 17 Quantification of sphingoid bases in constitutive keratinocyte specific Ugcg mutant mice..	64
Figure 18 Quantification of free and phosphorylated sphingoid bases in epithelium of tongue.....	65
Figure 19 CD45 staining in epidermis of CerS3 mutant mice.	68
Figure 20 Infection assay..	71
Figure 21 Ceramides are branching points of SL pathways.	77
Figure 22 Structure of 1-O-acylceramides..	79
Figure 23 Affected pathways by FD (Sands 2013).	81
Figure 24 Product ion spectra of protonated 1-O-acylceramides ($[M+H]^+$) from epidermal lipid extract of CerS3- deficient mice.....	83
Figure 25 RP chromatography of 1-O-acylceramides with a C17-So backbone.....	85
Figure 26 Correlation of occurrence of 1-O-acylceramides with establishment of water permeability barrier.	86

Figure 27 Quantification of 1-O-acylceramide levels in the epidermis of LPLA2 -deficient, keratinocyte-specific GlcCer-S-deficient, nGlcCerase-deficient, and corresponding control mice.....	88
Figure 28 Detailed analysis of epidermal 1-O-acylceramides from neutral glucosylceramidase-deficient mice.	89
Figure 29 Detailed analysis of epidermal 1-O-acylceramides from DGAT2-deficient mice.....	91
Figure 30 Quantification of 1-O-Acylceramides in LCAT mutant mice.	93
Figure 31 Sums of 1-Oacylceramides in mutant mice models.	95
Figure 32 Total amount of sphingoid bases in mutant mouse models.	96
Figure 33 1-Oacylceramide levels of Farber mutant spleen (hom) and controls (wt and het) sorted after 1-O-acyl moiety length.....	98
Figure 34 1-Oacylceramide (sorted according the anchor lengths) levels of Farber mutant spleen (hom) and controls (wt and het).	98
Figure 35 1-Oacylceramide levels of Farber mutant thymus (hom) and controls (wt and het).....	99
Figure 36 1-O-acylceramide levels of Farber mutant heart and kidney (hom) and controls (wt and het).	99
Figure 37 Free Ceramide levels in organs of Farber mutant and control mice.	100
Figure 38 1-O-acylceramide levels in BL6 control epidermis samples.	101
Figure 39 Testis structure and spermatogenesis.....	109
Figure 40 GSL structures expressed in mouse testis.	112
Figure 41 Cell lines transfected with CerS3.....	115
Figure 42 Cers3 (D2) staining in skin.Cers3 in red, Dapi in blue.	117
Figure 43 CerS3 expression in oral cavities and tongue..	119
Figure 44 CerS3 expression in control and mutant CerS3-depleted testis.	122
Figure 45 Aberrant expression of Piwil1-associated chromatoid body (green) in CerS3 deficient testis (A' earlier stage and A'' and later stage) as compared to endogenous expression in control (A). Lack of colocalization of CerS3 (red) in autophagosomes as shown with Lc3 (green) immunostaining (B). Scale bar: 30 μ m.).	124
Figure 46 possible pathways leading to 1-O-Acyl-Cer formation.	131

List of tables

Table 1 Buffers for genotyping and western blot.....	9
Table 2 Buffers for ICH and IF.....	10
Table 3 Buffers for epidermis treatment.....	11
Table 4 List of mouse lines.....	12
Table 5 List of primers.....	12
Table 6 List of primary and secondary antibodies.....	13
Table 7 Media for cell culture.....	14
Table 8 List of kits and standards.....	15
Table 9 List of instrumentations.....	16
Table 10 UPLC-gradient elution of sphingolipids for detection by tandem mass spectrometry.....	27
Table 11 Multiple SRM transitions (MRM) used for detection and quantification of 1-O-acylceramides.....	29
Table 12 LC Parameters for sphingoid base quantification.....	30
Table 13 Gradient for sphingoid base quantification.....	30
Table 14 Tissue distribution and substrate specificity of the Elovl proteins.....	40
Table 15 Tissue distribution and substrate specificity of the CerS proteins.....	43
Table 16 LC and MS conditions for measurement of sphingoid bases.....	52
Table 17 Optimized collision energies and of major transitions of phosphorylated and free sphingoid bases.....	54
Table 18 List of calculated relative response factors (rRFs).....	55
Table 19 LOD and LOQ for quantification of sphingoid bases.....	59
Table 20 Z- Factor of unphosphorylated sphingoid bases.....	60
Table 21 Z-factor of phosphorylated sphingoid bases and ceramides.....	60

Acknowledgements

Herewith I would like to acknowledge everyone who supported me during my PhD.

First, I would like to express my gratitude towards my supervisor, Prof. XX, for his inspiring guidance and his encouragement.

Furthermore, I would like to thank my examination committee, especially Prof. XX for being my first supervisor, as well as Prof. XX and Prof. XX.

Most especially I would like to thank Prof. Dr. XX for her key suggestions and immense contribution to this work. Her constant strive for work perfectly done, as well as her impassionate perspective of life and science have been most inspiring and encouraging.

I also would like to acknowledge the work of XX regarding the generation of the CerS3 and Ugcg deficient mice.

Additionally, I am very grateful to my collaboration partners Prof. Dr. XX and XX from the Department of Medical Microbiology and Hygiene of University of Heidelberg.

Additionally, I would like to thank Prof. X and for kindly supporting our analysis with samples of DGAT2 mice, Prof. X for samples of LCAT mice, Prof. X for samples of Gb2a mice, Prof. X for samples of Asah mice and finally to Prof. X for supplying us with samples of LPLA2 mice.

I would like to express my greatest thanks to XX, XX and XX for their technical expertise and important contribution to this work. Also I am thankful for the valuable technical assistance.

Curriculum Vitae

Zur Person

Aline Bayerle
geboren 30.06.1985
in Mainz

Anschrift: Steubenstr. 22
69121 Heidelberg
Deutschland

Mail: a.bayerle@dkfz-heidelberg.de



SCHLÜSSELQUALIFIKATIONEN

- Hochdruckflüssigkeitschromatographie und Massenspektrometrie
- Analytische Methodik in Biochemie und Umweltchemie

AUSBILDUNG

02/2011 – 12/2014	<p>PhD am Deutschen Krebsforschungszentrum, Heidelberg Thema: Funktionen der Ceramidsynthase 3 und der sehr langkettigen Sphingolipide beim Aufbau der Epidermis und ihrer Wasserpermeabilitätsbarriere Schwerpunkte: UPLC-MS/MS, Lipidomics, Immunohistochemie, biomolekulare Methoden, Pathobiochemie</p>
04/2004 - 12/2010	<p>Studium der biomedizinischen Chemie an der Johannes Gutenberg-Universität Mainz Hauptfächer: Analytische Chemie, Biophysikalische Chemie, organische Chemie, Biochemie Abschluss: Diplom Chemiker; Gesamtnote: gut</p>
04/2010 - 12/2010	<p>Diplomarbeit unter Mitwirkung in einer Feldmesskampagne in Finnland (HUMPPA Kampagne des MPI für Chemie; Mainz) im Fach Analytische Chemie Thema: Untersuchungen zur oxidativen Alterung von sekundärem organischem Aerosol in der Atmosphäre mittels HPLC-ESI-IT/MS Schwerpunkte: organische Spurenanalytik, atmosphärische Aerosole; ESI-MS/MS, HPLC, Umweltchemie Note: 1,0</p>
09/2008 - 02/2009	<p>Auslandssemester an der „University of Aberdeen“, Schottland Thema: “Mercury speciation of Thimerosal in blood by using HPLC-ICPMS/ESI-MS”</p>
09/2007	<p>Vordiplom in Chemie; Gesamtnote: sehr gut</p>

DIDAKTISCHE FÄHIGKEITEN & ENGAGEMENT

2013 - 2014	Projektanleitung von Bachelor- und Masterstudenten am DKFZ
2011 - 2014	Betreuung von Studentenpraktika an der Hochschule Mannheim und der Universität Mainz
2005 - 2011	Wissenschaftlicher Mitarbeiter an der Johannes Gutenberg Universität Mainz als Mentorin beim Ada Lovelace Projekt, zur Förderung von Frauen in Naturwissenschaften Tätigkeitsbereich: Planung und Durchführung von wöchentlichen Workshops für Schüler/innen, Öffentlichkeitsarbeit auf Tagungen und Messen, Teilnahme an Seminaren zur Erweiterung der eigenen didaktischen und kommunikativen Fähigkeiten.
5.07.2010 - 14.08.2010	Organisation und Teilnahme an einer internationalen Messkampagne des Max-Planck-Instituts für Chemie in Mainz (HUMPPA; <i>Hyytiälä United Measurements of Photochemistry and Particles in Air</i>) in Hyytiälä, Finnland im Rahmen der Diplomarbeit
2007 - 2010	Leitung von wöchentlichen Förder-AG's im Rahmen der Ganztagschule an der Maria-Ward Schule und dem Gymnasium Gonsenheim, Mainz.
26.02.2007 - 27.04.2007	Werksstudent in der Abteilung Aus- und Weiterbildung bei der Boehringer Ingelheim Pharma GmbH & Co. KG, Ingelheim. Tätigkeitsbereich: Betreuung von Auszubildenden und Unterstützung in der Durchführung von Praktika und Seminaren.
17.06.2002 - 28.06.2002	Schulpraktikum als Chemielaborantin bei der Boehringer Ingelheim Pharma GmbH & Co. KG, Ingelheim (Abteilung Qualitätssicherung).

SPRACHKENNTNISSE

Englisch	fließend in Wort und Schrift
Französisch	Grundkenntnisse

Heidelberg, 18. Dezember 2014

